

UNIVERSIDAD DE CANTABRIA



ESCUELA DE DOCTORADO DE LA UNIVERSIDAD DE CANTABRIA
DOCTORADO EN INGENIERÍA DE COSTAS, HIDROBIOLOGÍA Y
GESTIÓN DE SISTEMAS ACUÁTICOS (IH2O)

TESIS DOCTORAL

SOLUCIONES BASADAS EN LA NATURALEZA PARA
ACELERAR LA RECUPERACIÓN DE PLAYAS

PhD THESIS

NATURE-BASED SOLUTIONS TO ENHANCE
BEACH RECOVERY

Presentada por: **ERICA PELLÓN DE PABLO**

Dirigida por: **Prof. ERNESTO MAURICIO GONZÁLEZ RODRÍGUEZ**
Prof. RAÚL MEDINA SANTAMARÍA

Santander, Septiembre de 2023

*A mis padres,
vosotros me habéis traído hasta aquí.*

*"Hard times create strong men.
Strong men create good times.
Good times create weak men.
And, weak men create hard times."*

G. Michael Hopf

AGRADECIMIENTOS/ ACKNOWLEDGEMENTS

El desarrollo de esta tesis ha sido un camino apasionante lleno de aprendizajes. Sois muchos los que me habéis acompañado en la travesía, pero merecen especial mención Mauricio González y Raúl Medina, mis directores. Solo a vosotros tengo que agradecerlos la oportunidad de realizar mi tesis en IHCantabria junto a los mejores. Gracias por vuestra confianza en mí para llevar a cabo esta investigación y desarrollar gran parte de los trabajos previstos en el proyecto Beach-ART (cuya financiación ha permitido realizar esta tesis). Todos los conocimientos y experiencia que me habéis transmitido me han permitido evolucionar profesionalmente y parecerme un poquito más a vosotros. Gracias por vuestra generosidad, vuestras orientaciones y vuestro apoyo. Espero haber estado a la altura y haber incorporado todos los conocimientos que me habéis transmitido durante estos años.

Esta tesis ha sido un largo recorrido que no podría haber hecho sin todos mis compañeros del grupo de Ingeniería y Gestión de la Costa. Todos vosotros me habéis apoyado en esta aventura, tanto los que continuáis en IHCantabria desde el inicio, como los que habéis seguido vuestro camino en otros lugares, y los que habéis llegado más recientemente, todos habéis aportado vuestro granito de arena a esta investigación. No puedo dejar de mencionar algunos nombres de aquellos cuyos temas de investigación están más ligados a esta tesis: Iñigo Aniel-Quiroga, Paula Gomes, Omar Gutiérrez, Laura Ribas, Roland Garnier, Lara Ruiz, Jara Martínez, Camilo Jaramillo, Verónica Cánovas. Gracias a todos por los conocimientos aportados a esta investigación.

Tampoco me olvido del resto de compañeros de IHCantabria, ya que todos ellos han aportado. Desde buenos ratos y palabras amables a diario, hasta conocimientos en ámbitos muy diversos: Tecnología de la información, Laboratorio de hidráulica, costas y offshore, Laboratorio de hidrobiología, Clima marino y cambio climático, Ecosistemas litorales, entre

AGRADECIMIENTOS/ACKNOWLEDGEMENTS

otros. Esta tesis trata de unir los conocimientos en todos esos ámbitos, espero que os guste el resultado.

Merecen una especial mención y reconocimiento todos los compañeros del Laboratorio de hidráulica, costas y offshore. Es mucho lo que he aprendido con vosotros tras tres ensayos en dos instalaciones diferentes (COCoTsu y TOD). Muchas gracias por vuestra paciencia para explicarme una y mil veces el funcionamiento de los controladores y sensores. Resulta impresionante vuestra capacidad para resolver cualquier imprevisto y vuestra habilidad para hacer realidad cualquier cosa que os pida un investigador. Ya sabemos que el papel lo aguanta todo, pero el laboratorio es el mundo real y he podido comprobar con mis propias manos la dificultad que tiene el trabajo que realizáis. También quiero agradecer a Mónica Pedraza y a Mariana Roldán por su inestimable ayuda durante los ensayos realizados en el TOD. Sin vosotras no habría podido realizar esas largas jornadas en las que simulábamos dos ciclos de marea completos al día. Gracias por vuestro esfuerzo. Y por supuesto, un infinito agradecimiento a Cesar Vidal por todos los conocimientos sobre ensayos de laboratorio que me ha transmitido. Sin ti esta tesis no habría sido la que es. Muchas gracias por estar siempre dispuesto a ayudarme y resolver cualquier duda.

Patricio Poulet, tu predisposición para colaborar aportando el máximo posible a la investigación de costas es inestimable. Mi más sincero agradecimiento por todos los datos de campo que nos has aportado desde la Demarcación de Costas Andalucía Atlántico y por tu confianza en nosotros a la hora de probar la técnica del scraping (reperfilado) en una ubicación real. Si el mundo tuviera más gestores como tú avanzaríamos más rápido hacia un futuro mejor.

Gracias a los voluntarios (Sergio Gómez, Rosana de Pablo y Pedro Pellón) que me ayudaron en las campañas de El Sardinero y Somo sin quejarse por los madrugones a la hora de bajamar, incluso al amanecer cuando la playa aún estaba vacía. No os pago lo suficiente. Una parte de esta tesis es vuestra.

Muchas gracias a Imen Turki por darme la oportunidad de realizar mi estancia de investigación en colaboración con ella y con su equipo (Antoine Soloy, and Ernesto Tonatiuh) del French National Centre for Scientific Research (CNRS), Rouen University (France). En especial, gracias a Antoine Soloy por su tiempo y todo el conocimiento intercambiado. Espero que esta colaboración se extienda por muchos años más.

No puedo dejar de agradecer a Laura Ribas de Almeida por todo el conocimiento sobre dunas. Sin ti esta tesis habría tardado mucho más en ver la luz.

También aprecio la paciencia de los tribunales de las jornadas doctorado que año tras año han leído cada uno de los documentos entregados y han sabido aconsejarme sabiamente para progresar tanto en el desarrollo de la tesis como en el cumplimiento de los requisitos académicos.

Gracias a mis profesores, porque sin vosotros nunca habría llegado hasta aquí.

Tan importante como los conocimientos adquiridos a lo largo de una vida, que me han permitido desarrollar esta tesis, son los buenos ratos que he disfrutado con mi familia y amigos. Gracias a mis tíos, primos, abuelos y familia política por apoyarme. Espero que disfrutéis de este documento tanto como sé que lo habrían hecho los que ya no están. También agradezco a todos mis amigos de Asnem, Locus pocus, Uni y Fantasmas por haber sido capaces de soportar mis quejas cuando la tesis se cruzaba. Paula, Marina, Soraya, Rocío, Pablo, Laura, Rubén, Álvaro, Águeda, Tamara, Íñigo, Mar, Ángela, Henar, Desi, Dani, y un largo etcétera (sois muchos y siempre queda alguien sin poner) muchas gracias a todos. Vosotros habéis hecho posible que pudiera desconectar de vez en cuando y ver que el mundo es más grande que la tesis. Muchas gracias por estar ahí y por todas las veces que me preguntasteis “*¿cómo vas con la tesis?*” a pesar de que probablemente ni vosotros ni yo entendiésemos aún cual iba a ser el producto final.

Y como lo mejor siempre se deja para el final, solo me queda agradecer a mis padres y a mi marido Sergio por vuestro apoyo incondicional, vuestra paciencia y vuestra ayuda siempre que lo he necesitado. ¡Hasta campañas de campo habéis hecho! Muchas gracias a Sergio por ser el primer revisor de cada uno de los infinitos documentos que he escrito. Muchísimas gracias a mi padre y a Sergio por los millones de veces que me habéis preguntado: “*y ¿cuándo vas a acabar la tesis?*”, los cuatro sabemos que de no ser por vuestra insistencia nunca lo habría logrado. Y qué decir de mi madre que ha aportado calma en toda esta locura. Os quiero mucho, sois los mejores. Gracias por impulsarme día tras día.

LIST OF CONTENTS

AGRADECIMIENTOS/ ACKNOWLEDGEMENTS.....	vii
LIST OF CONTENTS	xi
LIST OF FIGURES	xvii
LIST OF TABLES	xxix
ABBREVIATIONS	xxxi
SYMBOLS	xxxiii
RESUMEN EN ESPAÑOL	xxxvii
1. Introducción	xxxvii
2. Acreción natural en playas.....	xli
2.1. Áreas de estudio de las campañas de campo.....	xlii
2.2. Resultados	xliv
2.3. Discusión.....	lii
3. Arado de playas.....	liv
3.1. Descripción de los experimentos de laboratorio	lv
3.2. Evaluación de la efectividad del arado	lvii
3.3. Evolución de las formas del lecho	lxiii
4. Reperfilado de playas.....	lxxi
4.1. Descripción de los experimentos de laboratorio	lxxii

LIST OF CONTENTS

4.2.	Resultados	lxxvi
4.3.	Campañas de campo.....	lxxxii
4.4.	Discusión	lxxxv
5.	Metodología para la aplicación de técnicas de recuperación asistida de playas.....	lxxxvi
5.1.	Metodología	lxxxvii
5.2.	Discusiónxc
6.	Conclusiones.....	.xcii
7.	Futuras líneas de investigación.....	.xcviii
 CHAPTER 1 INTRODUCTION AND SCOPE		1
1.1.	Introduction and motivation.....	1
1.2.	Research questions	3
1.3.	Objectives.....	3
1.4.	Thesis outline	4
 CHAPTER 2 BACKGROUND AND LITERATURE REVIEW		7
2.1.	Introduction.....	7
2.2.	Sand accretion	9
2.3.	Bedforms	12
2.4.	Nature-based solution (NBS)	14
2.5.	Nature assisted beach enhancement (NABE)	15
2.5.1.	Beach scraping	15
2.5.2.	Beach ploughing.....	18
2.6.	Physical experiments.....	19
2.7.	Conclusions	19
 CHAPTER 3 NATURAL BEACH ACCRETION		21
3.1.	Introduction.....	21
3.2.	Field survey Study sites.....	22

3.2.1.	Cádiz	25
3.2.2.	Santander.....	28
3.2.3.	Somo.....	32
3.3.	Methods	34
3.3.1.	Measurement with RTK-GPS	35
3.3.2.	Measurement with distancemeter	36
3.4.	Results	38
3.4.1.	Cádiz	40
3.4.2.	Santander.....	44
3.4.3.	Somo.....	48
3.4.4.	Influence of the hydrodynamic parameters on beach accretion.....	52
3.5.	Discussion.....	56
3.6.	Conclusions	59
CHAPTER 4	BEACH PLOUGHING	61
4.1.	Introduction.....	61
4.2.	Laboratory facilities and setup	62
4.2.1.	Morphology	63
4.2.2.	Instrumentation.....	65
4.2.3.	Hydrodynamics.....	66
4.3.	Ploughing performance	67
4.3.1.	Morphology	67
4.3.2.	Hydrodynamics.....	69
4.3.3.	Sediment dynamics.....	76
4.3.4.	Sediment balance	79
4.3.5.	Discussion	80
4.4.	Bedforms evolution	84
4.4.1.	Methodology.....	84

LIST OF CONTENTS

4.4.2.	Ploughed subchannel morphology.....	87
4.4.3.	Hydromorphodynamic effects of ploughing	94
4.4.4.	Discussion	105
4.5.	Conclusions	108
CHAPTER 5	BEACH SCRAPING.....	113
5.1.	Introduction.....	113
5.2.	Laboratory experiments description / methods	114
5.2.1.	Scaling design	114
5.2.2.	Experimental setup	122
5.3.	Results	127
5.3.1.	Beach berm formation	128
5.3.2.	Dry beach widening and accreted berm characteristics	130
5.3.3.	Accreted volume	132
5.4.	Field campaign.....	136
5.5.	Discussion.....	141
5.6.	Conclusions	145
CHAPTER 6	METHODOLOGY FOR THE APPLICATION OF NATURE ASSISTED BEACH ENHANCEMENT TECHNIQUES	149
6.1.	Introduction.....	149
6.2.	Methodology	150
6.2.1.	Decision tree.....	151
6.2.2.	When to perform a NABE technique or not	153
6.2.3.	Design of NABE actions	154
6.3.	Discussion	160
6.4.	Conclusions	162
CHAPTER 7	CONCLUSIONS AND FUTURE RESEARCH	165
7.1.	Conclusions	165

LIST OF CONTENTS

7.2. Future research	174
7.3. Financial support.....	178
REFERENCES	181
APPENDICES	1
Appendix I Methodology for field surveys on beach accretion.....	AI.1
Appendix II Foredune conceptual model and design characteristics	AII.1

LIST OF FIGURES

- Figura 1 Técnicas de recuperación asistida analizadas en esta tesis. Izquierda: Reperfilado de playas aplicado en Gold Coast 1965 (Australia). Fuente: Carley et al. (2010). Derecha: Arado de playas aplicado en Laida 2015 (España).....xxxix
- Figura 2 Localización de las playas en las que se han realizado campañas de campo.....xlii
- Figura 3 Ubicación de los perfiles medidos en cada una de las playas. Izquierda: Playa de Fuentebravía. Centro: Playas de El Sardinero. Derecha: Playas de Somo y Loredo.....xliv
- Figura 4 Evolución del perfil de playa en Fuentebravía (playa seca y zona intermareal). Cota referida al nivel medio del mar local en Fuentebravía.xlvii
- Figura 5 Variables hidrodinámicas y morfológicas medidas en la playa de Fuentebravía. En el panel superior: las áreas sombreadas en gris se refieren a condiciones de tormenta, donde la altura de ola significante está por encima del nivel de excedencia del 5% durante un mínimo de un ciclo de marea; las líneas discontinuas verticales son las fechas de las campañas de campo y los círculos rojos indican el valor de Ω_∞ en la pleamar anterior a cada campaña.....xlviii
- Figura 6 Relación entre la elevación de la cresta de la berma y el TWL superado el 1% del tiempo en un mes (de marea viva a marea viva). El ascenso (+) o descenso (-) del nivel de la berma está relacionado con el porcentaje del tiempo en el que el nivel de la berma previo es superado por el agua.li
- Figura 7 Fotografía del arado en la instalación experimental. Las paredes laterales del tramo de ensayos del canal COCoTsu están hechas de vidrio. La imagen muestra la geometría de arado inicial de cada ensayo antes de su inundación con agua.lvi

LIST OF FIGURES

Figura 8 Evolución de la altura de ola significante a lo largo de ambos subcanales para cada ensayo con diferentes niveles de agua (ver leyenda). Los valores del lado natural se muestran con línea discontinua y marcadores vacíos. Los valores del lado arado se muestran con línea continua y marcadores sólidos. El diagrama en la parte inferior muestra un perfil de la batimetría arada como referencia de la ubicación de cada sensor	lix
Figura 9 Transporte de sedimento transversal de la costa por unidad de ancho. Los valores positivos indican acreción. Las áreas sombreadas en gris indican una desviación estándar del valor medio (la línea negra gruesa). Las líneas grises claras son los resultados de cada ensayo de laboratorio con diferentes niveles de agua. El diagrama en la parte inferior muestra un perfil de la batimetría arada como referencia de la ubicación de las crestas y surcos.....	lx
Figura 10 Volúmenes de sedimento movilizados. Los valores positivos indican acumulación de arena y los valores negativos indican erosión y movilización hacia la costa (acrección). Izquierda: Volúmenes de sedimento acumulados (rojo), erosionados (azul) y netos (*). Derecha: Comparación del volumen neto de sedimento en acreción (erosionado del área de arena) en ambos lados (cada punto corresponde a un par de asteriscos en el panel izquierdo).	lxii
Figura 11 Serie temporal de datos SCP para el Test A y el Test B. De 9.5 a 10.3 m, no hay datos ya que el marco de la ventana de vidrio (ver Figura 7) impide la medición de la superficie de la arena. La línea discontinua indica la ubicación estimada del límite de avance del arado hasta alcanzar el umbral del cajón, cuando la arena comienza a caer directamente en el cajón de captura de sedimento.....	lxiv
Figura 12 Evolución morfológica del arado. Las dos figuras de la derecha comparten leyenda.....	lxvi
Figura 13 Rugosidad del fondo arenoso calculada a partir de imágenes y batimetrías 3D con escáner láser para cada ensayo de laboratorio.....	lxvii
Figura 14 Altura de ola significante al final del área de estudio, en el extremo opuesto a los generadores de oleaje. Los círculos muestran los resultados del lado natural y los diamantes los resultados del lado arado.....	lxviii
Figura 15 Peso acumulado del sedimento transportado en forma de acreción y capturado en el cajón desde el inicio de los ensayos.....	lxix

Figura 16	Tanque de oleaje direccional (TOD) durante los ensayos.....	lxxv
Figura 17	Evolución del perfil de playa hasta alcanzar la máxima acreción en el frente de playa. Las técnicas de recuperación asistida se describen en la Tabla 2 (ver acrónimos). Cada panel indica el número de ciclos de marea que fueron necesarios para alcanzar la acreción máxima.....	lxxvii
Figura 18	Cota de la berma y avance de la línea de costa alcanzados en el momento de máxima acreción. Las líneas discontinuas se muestran como referencia de las características de la berma formada bajo condiciones naturales. Los marcadores vacíos indican las características de la berma creada artificialmente por el reperfilado L2BF.....	lxxviii
Figura 19	Volumen de acreción en la berma. La barra del Canal 4 muestra los volúmenes de sedimento movilizados manualmente por el reperfilado (relleno blanco con líneas descendentes) y por acción de las olas (relleno morado). La barra del Canal 6 representa todo el volumen movilizado por la acción del oleaje, incluido el volumen de sedimento en la berma (relleno azul) y el volumen de sedimento que llenó parcialmente el área de préstamo (relleno blanco con cruz azul).	lxxx
Figura 20	Motoraillas realizando el reperfilado de la playa de Fuentebravía.	lxxxii
Figura 21	Área reperfilada (rojo: área de préstamo, verde: área de vertido) y localización de los perfiles medidos	lxxxiii
Figura 22	Comparativa de la evolución de los perfiles P2 (natural) y P4 (reperfilado).	lxxxiv
Figura 23	Metodología para la aplicación de técnicas NABE.	lxxxvii
Figura 24	Árbol de decisión para escoger la técnica NABE más apropiada para cada playa.....	lxxxviii
Figura 25	Esquema de las tres componentes que producen un aumento de la acreción al aplicar el arado.	xci
Figure 2.1	Beach profile scheme and nomenclature.....	8
Figure 2.2	Four behavioural modes of berm recovery and decision tree depending on dimensionless fall velocity Ω , swash exceedance of berm crest and ocean water level. Storm conditions refer to significant wave heights above the 5% exceedance level for a	

LIST OF FIGURES

minimum duration of one tidal cycle during which $\Omega > 4$. $\bar{\Omega}$ is the average dimensionless fall velocity, and MHWS is the mean high water springs. Adapted from Phillips et al. (2019).	10
Figure 2.3 Superposition of bedforms at El Puntal beach, Cantabria, Spain. Images were taken in September 2020. Top: Shore parallel intertidal bar (low-amplitude ridge). Bottom: The image was taken from the middle of the bar on the image of the top pointing to the dry beach. Megaripples ($\lambda \sim 1.5$ m) with ripples ($\lambda \sim 0.1$ m) over them.....	11
Figure 2.4 Occurrence of bedforms according to their geometric characteristics.....	13
Figure 2.5 Examples of beach scraping. Source: Carley et al. (2010).....	16
Figure 2.6 Beach scraping concept. Source: Carley et al. (2010).	17
Figure 2.7 Mechanical ploughing being performed at Laida beach during low tide in the summer of 2015.	18
Figure 3.1 Location of the field survey sites.....	23
Figure 3.2 Fuentebravía beach location and surrounding elements that influence the morphodynamics.....	25
Figure 3.3 Location of measured profiles at Fuentebravía beach.....	26
Figure 3.4 Wave characteristics extracted from GOW database at Cádiz bay. Grey-shaded areas indicate storm conditions, where significant wave is above the 5% exceedance level with a minimum duration of one tidal cycle and $\Omega > 4$. Vertical dashed lines are the dates of the field surveys and red circles indicate the wave characteristics at the high tide previous to each survey.....	27
Figure 3.5 Santander and Somo study areas' location and surrounding elements that influence the morphodynamics.....	29
Figure 3.6 Wave characteristics extracted from the GOW database in front of El Sardinero beaches. Grey-shaded areas indicate storm conditions, where significant wave is above the 5% exceedance level with a minimum duration of one tidal cycle and $\Omega > 4$. Vertical dashed lines are the dates of the field surveys and red circles indicate the wave characteristics at the high tide previous to each survey.	30

- Figure 3.7 Location of measured profiles at El Sardinero I and II beaches..... 31
- Figure 3.8 Location of measured profiles at Somo and Loredo beaches..... 32
- Figure 3.9 Wave characteristics extracted from the GOW database in front of Somo and Loredo beaches. Grey-shaded areas indicate storm conditions, where significant wave is above the 5% exceedance level with a minimum duration of one tidal cycle and $\Omega > 4$. Vertical dashed lines are the dates of the field surveys and red circles indicate the wave characteristics at the high tide previous to each survey..... 33
- Figure 3.10 Field survey at El Sardinero beach employing RTK-GPS device. 35
- Figure 3.11 Example of profile definition (Somo P1). Left: Origin at the joint between the stone tiles of the upper stair at the entrance to the beach. Right: Orientation definition by the alignment of the streetlight and the ridge of the roof. 36
- Figure 3.12 Measurement procedure for obtaining each profile point. On the left the surveyor S1 with the distancemeter device on the top of the walking stick, and at the right the other surveyor S2 with the target at the top of the walking stick. Both walking sticks were set to the same height. 37
- Figure 3.13 Validation of distancemeter measurements with RTK-GPS. 38
- Figure 3.14 Beach profile evolution at Fuentebravíá (dry beach and intertidal zone). Elevation referred to the local mean sea level of Fuentebravíá. 42
- Figure 3.15 Hydrodynamic and morphologic variables measured at Fuentebravíá beach. In the upper panel: grey shaded areas refer to storm conditions, where significant wave heights are above the 5% exceedance level for a minimum duration of one tidal cycle; vertical dashed lines are the dates of the field surveys and red circles indicate the Ω_∞ at the high tide previous to each survey..... 43
- Figure 3.16 Beach profile evolution at El Sardinero I (dry beach and intertidal zone). Elevation referred to the local mean sea level of Santander. 45
- Figure 3.17 Beach profile evolution at El Sardinero II (dry beach and intertidal zone). Elevation referred to the local mean sea level of Santander. 46
- Figure 3.18 Hydrodynamic and morphologic variables measured at El Sardinero beach. In the upper panel: grey shaded areas refer to storm conditions, where significant wave heights are above the 5% exceedance level for a minimum duration of one tidal cycle;

LIST OF FIGURES

vertical dashed lines are the dates of the field surveys and red circles indicate the Ω_{∞} at the high tide previous to each survey.....	47
Figure 3.19 Beach profile evolution at Somo and Loredo (dry beach and intertidal zone). Elevation referred to the local mean sea level of Somo.	49
Figure 3.20 Hydrodynamic and morphologic variables measured at Somo and Loredo beaches. In the upper panel: grey shaded areas refer to storm conditions, where significant wave heights are above the 5% exceedance level for a minimum duration of one tidal cycle; vertical dashed lines are the dates of the field surveys and red circles indicate the Ω_{∞} at the high tide previous to each survey.....	50
Figure 3.21 Examples of spring-neap-spring tide evolution of the beach profile P1 of Fuentebravía.....	52
Figure 3.22 Relation between the berm crest elevation and the TWL exceeded 1% of the time in one month (from spring tide to spring tide). Berm level growth (+) or descent (-) is related to the time of exceedance of the previous berm level.	54
Figure 3.23 Relation of the average value of the standardized equilibrium dimensionless fall velocity parameter ($std(\Omega_{\infty})$) in one month (from spring to spring tide) and the daily rate of accreted volume. Shoreline progradation (+) achieved and time of $\Omega_{\infty} < \bar{\Omega}$	55
Figure 4.1 Photograph of the plough and sandy area at the experimental facility. The sidewalls of the test section of the COCoTsu channel are made of glass. The image shows the initial ploughed geometry of each test before water inundation.....	63
Figure 4.2 Cross-sectional sketch of the longitudinal profile of the COCoTsu showing the experimental setup. The water levels correspond to the two tests of the Set of experiments 2. The vertical scale is 10 times the horizontal scale.	64
Figure 4.3 The COCoTsu longitudinally split into two channels showing the instrumental layout of each side. Top: Natural geometry side. Bottom: Ploughed geometry side. The vertical scale is 4 times the horizontal scale.....	65
Figure 4.4 Longitudinal profiles extracted from the 3D sandy bottom at three moments in time: (1) dry before: just after manually rebuilding the initial bathymetric geometry, (2) wet before: after slowly raising the water level to the test level, and (3) after 1 h: at the end of the test wave simulation. The test run had a water level of 0.85 m.....	67

- Figure 4.5 Statistical analysis (box plots) of the sandy bottom roughness computed from 3D bathymetry for each laboratory test at three different moments in time: (1) dry before: just after manually rebuilding the initial bathymetric geometry, (2) wet before: after slowly raising the water level to the test level, and (3) after 1 h: at the end of the test wave simulation. Left: Roughness parameter k_o . Right: Rugosity parameter k_R 69
- Figure 4.6 Significant wave height evolution along both sub-channels for each test with different water levels (see the legend). Natural beach side values are shown with a dashed line and empty markers. Ploughed side values are shown with a continuous line and solid markers. The diagram on the bottom shows a profile of the ploughed bathymetry for reference to each sensor location. 70
- Figure 4.7 Wave-energy dissipation rate comparison for the natural and ploughed sides. The dots on the black line indicate the same dissipation on both sides. The dots in the top-left area indicate that the ploughed side dissipation is larger, and the dots in the bottom-right area indicate that the natural side dissipation is larger. 71
- Figure 4.8 Wave energy spectrum at generation (WG1) and each pair of sensors at the same longitudinal position in the channel. The top-left panel corresponds to the offshore end of the sandy area, and the bottom-right panel corresponds to the onshore end (see the position of each sensor in Figure 4.3). 72
- Figure 4.9 The top left panel shows the percentage of wave dissipation (positive dissipation, negative energy increase) for each frequency and water level on the natural side (see equation (4.3)). The other panels correspond to each frequency window identified in the first panel (A, B, C, D, and E). Each panel shows a comparison of the integrated energy (in the indicated windows) for WG1, WG10, and WG16 for each water level tested. Note the different scales of the vertical axes. 74
- Figure 4.10 Extra energy dissipation on the ploughed side at each frequency of the spectrum (see equation (4.4)). Positive values indicate that the energy on the ploughed side (WG10) is lower than the energy on the natural side (WG16). The shaded grey areas indicate one standard deviation from the mean value. 75
- Figure 4.11 Cross-shore current analysis for each water level tested. Sensors ADV1 and 2 are located on the ploughed side, and sensors ADV3 and 4 are located on the natural side (the position of each sensor is shown in Figure 4.3). Positive values of the mean velocity are given onshore. 76

LIST OF FIGURES

Figure 4.12 Cross-shore sediment transport per unit width (see equation (4.5)). Positive values indicate accretion. The shaded grey areas indicate one standard deviation from the mean value (the thick black line). The light grey lines are the results for each laboratory test with different water levels. The diagram on the bottom shows a profile of the ploughed bathymetry for reference of ridges and furrows location.....	77
Figure 4.13 Statistical analysis (box plots) of the suspended sediment concentration time series obtained from OBS data for each laboratory test (the position of each sensor is shown in Figure 4.3).....	78
Figure 4.14 Mobilized sediment volumes. Positive values indicate sand accumulation, and negative values indicate sand erosion and onshore mobilization (accretion). Left: Accumulated (red), eroded (blue) and net (*) sediment volumes. Right: Comparison of the net sediment volume accreted (eroded from the sandy area) on both sides (each dot corresponds to a couple of asterisks in the left panel).	80
Figure 4.15 Side-channel images after fisheye correction and rectification.....	84
Figure 4.16 3D visualization of the spatial and temporal evolution of the bottom profile during Test A.	85
Figure 4.17 Top: Fast Fourier transformation of the SCP signal and wavelength filtering to split the spectra into two components, PC and RC. Bottom: Bathymetry (SCP) separation into two components, PC and RC, by inverse fast Fourier transformation of the spectra of the upper panel.	86
Figure 4.18 SCP data time series for Test A and Test B. From 9.5 to 10.3 m, there are no data as the frame of the glass window (see Figure 4.15) prevents the measurement of the sand surface. The dashed line indicates the estimated location of the onshore boundary of the plough up to the trap box threshold, when the sand begins to fall directly into the trap box.	88
Figure 4.19 Evolution of the ploughing (PC) height for each laboratory test.....	89
Figure 4.20 Wavelength time evolution of the ploughing (PC) for each laboratory test.....	90
Figure 4.21 Sketch of a cross-shore section of a ploughed bedform. Sign criteria adopted for the characterization of the stoss and slip face slopes and the ridge area.	90

Figure 4.22 Evolution of the slope of the slip and stoss face of the ploughing for each laboratory test	91
Figure 4.23 Evolution of the onshore migration velocity of the ploughing for each laboratory test	92
Figure 4.24 Ridge area evolution for both tests and ridges 1 to 4. The lines show the fitting result of an exponential curve of equation (4.10) to the data of each test.	93
Figure 4.25 Sandy bottom roughness computed from images and laser scanner 3D bathymetry for each laboratory test.....	95
Figure 4.26 Significant wave height at the onshore end of the study area (see sensor location in Figure 4.3). Circle markers refer to WG16 on the natural control side, and diamond markers refer to WG10 on the ploughed side.	96
Figure 4.27 Wave energy spectrum at generation (WG1) and the onshore end of the sandy area on the natural control side (WG16) and ploughed side (WG10). The plots on the left show the spectrum for Test A and the plots on the right for Test B. Each plot corresponds to one hour of simulated waves, from the 1 st hour in the upper panels to the 4 th hour in the lower panels.....	97
Figure 4.28 Wave energy dissipation for each wave frequency and hour of the experiment. Positive values (red and yellow colour) correspond to less energy than the one at generation. Negative values (blue colour) correspond to more energy than the one at generation. Panels on the left show the results for Test A and on the right for Test B. Upper panels correspond to the natural control side, and lower panels correspond to the ploughed side.	98
Figure 4.29 Extra energy dissipation produced on the ploughed side compared to the natural side for each test and frequency of the spectrum (see equation (4.13)). Positive values indicate that the energy on the ploughed side (WG10) is lower than the energy on the natural side (WG16). The black thick continuous line indicates the average value for the four hours analysed. Discontinuous grey lines indicate one standard deviation from the mean value	100
Figure 4.30 Cross-shore currents measured by ADV sensors at the onshore end of the sandy area. Positive values indicate onshore directed currents. See the location of each sensor in Figure 4.3.	101

LIST OF FIGURES

Figure 4.31 Statistical analysis (box plots) of the suspended sediment concentration measured by OBS sensors (see location in Figure 4.3).	102
Figure 4.32 Sediment transport produced by the migration of the plough.	103
Figure 4.33 Cumulative weight of the sediment accreted since the beginning of each test.....	105
Figure 4.34 Ridge 5 time and spatial evolution for Test A. Bold lines represent each hour. Thin lines every 10 min.....	106
Figure 5.1 Directional Wave Tank (TOD) during the experiments.....	123
Figure 5.2 Setup, initial profile, and maximum accretion achieved for Test B at prototype scale. h^* is the depth of closure for test waves.....	124
Figure 5.3 NABE techniques applied to each channel and Test. Borrow and filling locations for scraped channels (3 to 6) and ploughing extent (channel 1).	126
Figure 5.4 Ploughing. Left: Zoom of a profile of the ploughing performed in Channel 1. Centre: Picture of ploughing being conducted at the model at a reduced scale. Right: Example of ploughing at prototype scale at Laida beach (Source: Gainza et al., 2019).....	127
Figure 5.5 Profile evolution up to the maximum accretion achieved at the beachfront. Each graph indicates the number of tidal cycles that were necessary to achieve the maximum accretion.....	129
Figure 5.6 Berm height and shoreline progradation achieved at maximum accretion. Dashed lines are plotted as a reference of the natural behaviour of the beach. The empty marker indicates the characteristics of the artificial berm created by scraping Channel 4.....	131
Figure 5.7 Swash zone slope and shoreline progradation achieved at maximum accretion. Dashed lines are plotted as a reference of the natural behaviour of the beach. Empty markers indicate the characteristics of the berm created artificially by scraping Channel 4.....	132
Figure 5.8 Maximum accreted volume on the berm. The bar for Channel 4 shows the volumes of sediment manually mobilized by scraping (white fill with purple descending lines legend on top of purple bars) and by wave action (purple fill) filling	

the berm. The bar for Channel 6 represents all the volume mobilized by wave action, including the volume of sediment on the berm (blue fill) and the volume of sediment that filled the borrow area partially next to the high tide level (white fill with blue cross-squared legend on top of blue bars).	135
Figure 5.9 Scrappers performing beach scraping at Fuentebavía beach.....	136
Figure 5.10 Beach scraping extent (red colour: borrow area, green colour: filling area) and location of the surveyed profiles at Fuentebavía beach.	137
Figure 5.11 Scrapped beach profile evolution at Fuentebavía.	138
Figure 5.12 Comparative of scraped (Profile 4) and natural (Profile 2) beach profiles evolution.....	140
Figure 5.13 Non-optimal design scheme of the L2BF filling area.	143
Figure 6.1 Methodology for the application of NABE techniques.	150
Figure 6.2 Decision tree to choose the best NABE option for a beach.	152
Figure 6.3 Natural accretion volume estimation scheme.	156
Figure 6.4 Scheme of the procedure to compute $TWL_{1\%}$	159
Figure 6.5 Scheme of the three components that enhance onshore sediment transport when ploughing is applied.	161
Figure AII.1 Cross-shore profile scheme of the beach and foredune morphometric parameters. Extracted from Pellón et al. (2020).	AII.3
Figure AII.2 Relationship between foredune toe level and the 10-year return period of total water level (TWL_10y). Extracted from Pellón et al. (2020).	AII.4
Figure AII.3 Relationship between aeolian drift potential depending on the wind angle in relation to the coastline ($DP\alpha$) and mean foredune volume for each study area. Extracted from Pellón et al. (2020).	AII.5
Figure AII.4 Relationship between the 10-year return period of total water level (TWL_10y) and mean foredune volume for each study area. Extracted from Pellón et al. (2020).	AII.6

LIST OF FIGURES

Figure AII.5 Foredune development in a system dominated by aeolian dynamics.
Extracted from Pellón et al. (2020) AII.8

Figure AII.6 Foredune development considering both marine and aeolian dynamics.
Extracted from Pellón et al. (2020) AII.9

Figure AII.7 Foredune development considering both marine and aeolian dynamics, but
where the marine dynamics are not as energetic as to produce a beach width larger
than the critical fetch. Extracted from Pellón et al. (2020) AII.9

LIST OF TABLES

Tabla 1	Dinámicas marinas simuladas en escala prototipo y modelo.....	lxxv
Tabla 2	Características de las técnicas NABE ensayadas en cada canal.....	lxxvi
Tabla 3	Características morfométricas del arado y ripples.....	xciv
Table 3.1	Coordinates that define the beach profiles measured at Fuentebravía beach. ETRS89-UTM30N coordinate system.....	28
Table 3.2	Coordinates that define the beach profiles measured at El Sardinero I and II beaches. ETRS89-UTM30N coordinate system.....	31
Table 3.3	Coordinates that define the beach profiles measured at Somo and Loredo beaches. ETRS89-UTM30N coordinate system.....	34
Table 5.1	Prototype, target and physical model variables and scales for sediment and water. (1) Known values; (2) Target values obtained from Froude, Shields and Reynolds numbers similarities; (3) Final model sediment variables and scales used in the physical experiments.....	121
Table 5.2	Prototype and model marine dynamics simulated.....	124
Table 5.3	Characteristics of the NABE technique conducted in each channel.....	125
Table 5.4	Coordinates that define the beach profiles measured at Fuentebravía beach. ETRS89-UTM30N coordinate system.....	137
Table 7.1	Morphometric characteristics of ploughing and rippling.....	168

ABBREVIATIONS

- ADV – Acoustic Doppler Velocimeter
- COCoTsu – Wave Current Tsunami Channel (Canal de Oleaje Corriente Tsunami)
- GOS – Global Ocean Surge database
- GOT – Global Ocean Tide database
- GOW – Global Ocean Waves database
- L2B – Lower intertidal To intertidal Bar
- L2BF – Lower intertidal To BeachFront
- L2D – Lower intertidal To Dune
- MHWS – Mean High Water Spring
- NABE – Nature Assisted Beach Enhancement
- NAT – Natural
- NBS – Nature-Based Solutions
- OBS – Optical Backscatter Sensor
- OWL – Ocean Water Level
- PC – Plough Component
- RC – Ripple Component
- RTK-GPS – Real-Time Kinematic Global Positioning System
- SCP – Slope-Corrected Profile
- SSC – Suspended sediment concentration
- TOD – Directional Wave Tank (Tanque de Oleaje Direccional)
- TWL – Total Water Level
- U2D – Upper intertidal To Dune
- WG – Wave Gauge

SYMBOLS

A	Flow regime parameter
A, B	Fitting parameters of the ridge area
A_a	Geometric area measured by the laser scanner
A_b	Bottom orbital excursion
A_r	3D surface area of the sandy bottom
C_g	Wave group velocity in shallow water
dt	Sampling rate of the ADV sensor
d_{50}	Median sediment grain size
Dir	Wave direction
$DP\alpha$	Aeolian drift potential depending on the angle of the shoreline
$D(x)$	Wave-energy-flux dissipation per unit water volume cross-shore
E	Wave energy per unit area
f_w	Wave friction factor
F_g	Gravitatory forces
F_i	Inertial forces
F_n	Froude number
g	Gravity acceleration
h	Water depth
h_{mid}	Water depth at the midpoint between the free surface sensors
H	Height of bedforms
H_{rms}	Root-mean-squared wave height
H_s	Significant wave height
HT	High tide level

SYMBOLS

H_0	Deep-water wave height
k_σ	Roughness parameter
k_R	Rugosity parameter
k_s	Nikuradse equivalent sand grain roughness
L	Length
LT	Low tide level
L_0	Deep-water wavelength
m_0	Zero-order momentum
M_m	Magnitude in the model
M_p	Magnitude in the prototype
$M_{r, \text{bedform}}$	Migration rate of the bedform
p	Solid fraction
p_h	Porosity
Q	Net time-averaged cross-shore sediment transport
Q_{bedform}	Bedform sediment transport
$Q(x_i)$	Integral volume of sediment transport at position x_i
Re^*	Grain Reynolds number
R_o	Rouse number
R_2	Runup
SP_{HT}	Shoreline position at high tide
$S(f)$	Water surface elevation power spectrum
t	Time in hours
$\tan\beta$	Bed gradient
T	Time magnitude
T_p	Sea state peak period
$TWL_{1\%}$	Total Water Level exceeded 1% computed monthly
TWL_{10y}	10-year return period of Total Water Level
u^*	Bottom friction velocity
U_δ	Oscillatory velocity amplitude on top of the bottom boundary layer
$V_{\text{accretion}}$	Accretion volume
V_{erosion}	Erosion volume

V_i	Volume of sand on the cell i
$Z_{bedform}$	Bed elevation of the PC data
Z_i	Representative elevation of the cell i
$Z_{i,after}$	Surface elevation of the cell after the experiment
$Z_{i,before}$	Surface elevation of the cell before the wave action
β_s	Swash zone slope
Δ	Sediment relative submerged density
Δz	Difference in the bed elevation averaged over the width of the channel between the initial and final measured bathymetries
Δt	Time difference between measured bathymetries
$\eta_{bedform}$	Height of the ploughed bedforms
$\bar{\eta}$	Setup
θ	Shields number
κ	von Karman constant
λ	Wavelength of bedforms
λ_d	Sediment grain size scale
λ_F	Froude scale
λ_g	Gravity acceleration scale
λ_l	Length scale
λ_M	Scale of a magnitude M
λ_{Re^*}	Grain Reinolds scale
λ_{Ro}	Rouse scale
λ_t	Time scale
λ_v	Velocity scale
λ_Δ	Sediment relative submerged density scale
λ_θ	Shields scale
λ_ν	Fluid kinematic viscosity scale
λ_w	Fall velocity of the grains scale
μ_i	Mean value of the results for the magnitude/characteristic i measured on the seven tests/over the time series of results
ν	Water kinematic viscosity

SYMBOLS

ρ_s	Sediment grain density
ρ_w	Water density
σ_i	Standard deviation of the results for the magnitude/characteristic i measured on the seven tests/over the time series of results
σ_z	Standard deviation of the points of the surface
τ_0	Bed shear stress
Φ, D	Wright parameters
Ω	Dimensionless fall velocity or Dean number
$\bar{\Omega}$	Mean dimensionless fall velocity
Ω_∞	Equilibrium dimensionless fall velocity
w	Fall velocity of grains

RESUMEN EN ESPAÑOL*

1. INTRODUCCIÓN

Las áreas costeras son las regiones más pobladas de la Tierra. Un diez por ciento de la población mundial vive en zonas cercanas a la costa a menos de 10 metros sobre el nivel del mar. Gran parte de estas zonas costeras habitadas están protegidas por playas. Las dinámicas marinas golpean continuamente la línea de costa, y las playas actúan como una defensa flexible que modifica su morfología de acuerdo con estas dinámicas. Las playas y dunas constituyen una reserva de sedimentos para la erosión y conforman un ecosistema único que es el hábitat de innumerables especies. El mantenimiento de una playa en buen estado es fundamental para la sostenibilidad de esas áreas. La duna se recupera y crece gracias a la arena que sopla el viento desde la playa seca. Muchos mamíferos, aves, plantas, macro y microinvertebrados no pueden vivir en una zona costera si la playa desaparece periódicamente. Además, desde hace siglos, las playas son espacios recreativos muy demandados por turistas y población local.

Las playas ofrecen muchos servicios ecosistémicos que pueden impulsar la economía de los municipios costeros. Protegen las áreas costeras de la erosión e inundaciones, proporcionan espacios para actividades recreativas como por ejemplo tomar el sol, nadar, pasear, hacer surf, kitesurf, vóley playa entre otros. Además, aparte de ser una importante fuente de recursos como peces, mariscos y algas medicinales, son fundamentales para la supervivencia de otras especies (que no viven en la playa), ya que las playas constituyen áreas de anidación para tortugas y espacios de reproducción para muchas aves. Estos son

* Este resumen en castellano es una versión reducida del contenido total de la tesis. Si bien contiene los fundamentos, resultados y conclusiones principales, se remite al lector a la versión en inglés para una información más detallada.

RESUMEN EN ESPAÑOL

solo unos pocos ejemplos de los servicios ecosistémicos que las playas pueden proporcionar, lo que justifica la necesidad de garantizar la sostenibilidad de estas áreas.

El ancho de la playa cambia periódicamente a lo largo del año. Normalmente, las playas alcanzan su máxima amplitud en octubre (Aubrey, 1979), justo antes del comienzo de las tormentas de invierno. Durante el invierno, la playa se erosiona rápidamente, reduciendo su anchura después de cada temporal marino. En primavera, el ancho de la playa es mínimo, y a veces el clima invernal es tan duro que la playa seca desaparece y la duna también se erosiona. Las condiciones de calma habituales durante la primavera y el verano hacen que la playa se recupere. Durante estos meses, la arena vuelve lentamente de las áreas sumergidas a la playa emergida en un proceso natural llamado acreción. Análogamente, la duna se recupera lentamente mediante procesos eólicos en los que el viento transporta la arena desde la playa seca (una vez ha comenzado su recuperación) hasta el pie de la duna. Sin embargo, a veces estos meses no son suficientes para lograr una recuperación completa. Como resultado, la playa y la duna están menos preparadas para el impacto de los siguientes temporales de invierno, lo que puede producir un retroceso permanente de la línea de costa y frecuentes inundaciones de pueblos o instalaciones costeras.

Aunque las oscilaciones estacionales de la línea de costa son ampliamente conocidas y la erosión es un fenómeno estudiado en profundidad, los procesos de acreción aún son poco comprendidos y las dinámicas marinas que desencadenan la recuperación de las playas siguen siendo objeto de investigación. Estudios previos señalan la importancia de las mareas para la migración de las barras de arena hacia la costa hasta que se unen a la parte frontal de la playa formando y extendiendo la berma de verano. Otros autores indican que las formas del lecho marino más pequeñas, como por ejemplo los ripples, pueden migrar hacia la costa produciendo un efecto en la acreción. Por esta razón, la presente tesis se enfoca en el análisis de la acreción en playas meso/macro-mareales, un campo que aún está poco estudiado.

Históricamente, la erosión y las inundaciones costeras se combatían con costosas infraestructuras artificiales grises como rompeolas, diques o muros costeros. A medida que la concienciación social ha ido en aumento, soluciones ecológicas como la regeneración de playas generalizaron su uso y nacieron las Soluciones basadas en la Naturaleza (SbN). Las SbN buscan soluciones sostenibles en las que las acciones humanas trabajen mano a mano con la naturaleza para lograr el efecto deseado. Cuando se habla de acreción en playas, este tipo de acciones se denominan técnicas de recuperación asistida (Nature Assisted Beach Enhancement, NABE), y tienen como objetivo acelerar los procesos naturales de acreción a

base de acciones con reducido impacto ambiental. En esta tesis se analizan dos técnicas NABE: (1) reperfilado de playas, y (2) arado de playas.

El reperfilado de playas es una técnica bastante extendida pero pocos estudios científicos han cuantificado su efectividad (Carley et al., 2010; Figura 1) ni han propuesto metodologías para su diseño. Esta técnica consiste en retirar mecánicamente una capa de arena de la zona intermareal y verterla en el frente de playa (ampliando la playa seca) o en la duna. A pesar de que esta técnica solo se ha utilizado para combatir la erosión, en este documento se analiza si el reperfilado de playas permite aumentar el ancho de playa seca disponible para el turismo desde principios de primavera.

El arado de playas es una técnica innovadora que solo se ha aplicado una vez antes (en la playa de Laida en 2015; Gainza et al., 2019; Figura 1). Esta técnica consiste en arar mecánicamente la zona intermareal de una playa durante la bajamar. Aunque no mueve arena directamente de la zona más baja a la superior, se prevé que acelere la acreción natural.



Figura 1 Técnicas de recuperación asistida analizadas en esta tesis. Izquierda: Reperfilado de playas aplicado en Gold Coast 1965 (Australia). Fuente: Carley et al. (2010). Derecha: Arado de playas aplicado en Laida 2015 (España).

La presente tesis incluye campañas de campo y experimentos de laboratorio (a escala real y reducida) en los que se analiza la acreción en ambientes meso/macro-mareales y se cuantifica el efecto del reperfilado y el arado de playas con el objetivo de proponer técnicas eficientes, sostenibles e innovadoras capaces de mejorar las condiciones de las playas con fines turísticos y para combatir la erosión y las inundaciones producidas durante el invierno.

RESUMEN EN ESPAÑOL

Preguntas de investigación

Esta tesis responde a las siguientes preguntas de investigación:

- ¿Cuál es el efecto cualitativo de las dinámicas marinas en la acreción de playas en un ambiente meso/macro-mareal?
- ¿Es posible acelerar las tasas naturales de acreción de playas con técnicas NABE?
- ¿El reperfilado de playas mejora las tasas naturales de acreción de playas?
- ¿Se puede utilizar el reperfilado de playas para aumentar el ancho de la playa seca a principios del verano?
- ¿Es el arado de playas una técnica efectiva para acelerar la acreción de playas en entornos meso/macro-mareales?
- ¿Qué técnica NABE es la más adecuada para acelerar la acreción en una playa meso/macro-mareal en particular?

Objetivos

El objetivo general de esta tesis es el análisis de la efectividad de dos **Soluciones Basadas en la Naturaleza para acelerar la recuperación de playas**.

Para lograr este objetivo, se proponen los siguientes objetivos específicos:

- OB1. Mejorar el conocimiento de la acreción en playas meso/macro-mareales, considerando la influencia de las dinámicas marinas.
- OB2. Realizar campañas de campo en playas meso/macro-mareales que abarquen la recuperación completa durante la temporada de verano.
- OB3. Realizar experimentos de laboratorio que permitan el análisis de las técnicas NABE en condiciones controladas.
- OB4. Analizar si las técnicas de reperfilado y/o arado de playas producen un aumento de la playa seca utilizable para fines turísticos.
- OB5. Analizar si las técnicas de reperfilado y/o arado de playas aumentan el volumen de arena acumulada al final del verano que estará disponible como reserva de sedimentos (en la playa seca y la duna) para combatir la erosión y las inundaciones durante el invierno.
- OB6. Evaluar la efectividad de las técnicas de recuperación asistida para acelerar la recuperación de playas en ambientes meso/macro-mareales.

OB7. Desarrollar una metodología que ayude a los gestores de la costa a determinar qué técnica es la más adecuada para su playa, incluyendo pautas para el diseño de las acciones seleccionadas.

Los objetivos OB1 y OB2 se abordan en el apartado 2 (chapter 3), el cual analiza la recuperación natural de playas meso/macro-mareales durante el verano. El apartado 3 (chapter 4) se centra en la parte relativa al arado de playas de los objetivos OB3, OB4, OB5 y OB6, mientras que el apartado 4 (chapter 5) cumple con el resto de pretensiones de estos objetivos al incluir los resultados sobre el reperfilado de playas y una comparación entre las técnicas NABE analizadas. Finalmente, el apartado 5 (chapter 6) responde al objetivo OB7, incluyendo la metodología mencionada anteriormente.

2. ACRECIÓN NATURAL EN PLAYAS

Esta sección explora el fenómeno de acreción en playas meso/macro-mareales, el cual es fundamental para la recuperación de playas, pero aún no está bien estudiado en la literatura. Las tasas de acreción dependen de varios factores como la geometría del perfil de la playa, las características del sedimento, las formas del lecho y las dinámicas marinas, incluyendo altura, período y dirección del oleaje, la marea y las corrientes. Sin embargo, medir la acreción es costoso, ya que es un proceso lento y requiere tomar datos durante semanas o meses. Los modelos numéricos no son capaces de reproducir la acreción adecuadamente sin una calibración previa con datos de campo para cada ubicación específica. La complejidad de las interacciones entre el oleaje y la marea dificulta aún más la comprensión de los procesos de acreción. Además, mientras que la erosión causa un problema evidente de retroceso costero, la acreción únicamente es un problema cuando no logra recuperar toda la arena perdida durante los episodios de erosión. Este aspecto no es fácil de medir, lo que ha llevado a que la investigación sobre acreción sea menos prioritaria.

La descripción cuantitativa y cualitativa de la evolución de las playas durante la época estival es fundamental para evaluar la resiliencia de la playa y para el diseño de acciones. Las Soluciones basadas en la Naturaleza (SbN) analizadas en esta tesis fueron concebidas para ser aplicadas en playas meso/macro-mareales, por lo tanto, este capítulo se enfoca en este tipo de playas, donde el arado y el reperfilado pueden aplicarse por medios terrestres durante la marea baja.

En este apartado, se analiza la acreción utilizando datos de campañas de campo en tres sitios de estudio. Se describe por primera vez la formación de la berma a lo largo de

una temporada de verano completa en una playa meso/macro-mareal, de arena fina y con pendiente suave. Las dinámicas marinas incidentes también se tienen en cuenta en el análisis. Por lo tanto, aquí se abordan los objetivos OB1 y OB2 de la tesis. El apartado 2.1 presenta la ubicación y características de los sitios de estudio y describe las campañas. El apartado 2.2 analiza los resultados, y el apartado 2.3 incluye la discusión.

2.1. Áreas de estudio de las campañas de campo

Este estudio se centra en playas meso/macro-mareales expuestas a condiciones marinas severas durante el invierno y a olas suaves durante el verano. Las diferencias en la altura de ola entre el invierno y el verano provocan la acreción de arena durante el verano. Se seleccionaron tres sitios de estudio en la costa atlántica de España: Cádiz (playa de Fuentebravía), Santander (playas de El Sardinero I y II) y Somo (playas de Somo y Loredo). La ubicación de estas playas puede verse en la Figura 2.



Figura 2 Localización de las playas en las que se han realizado campañas de campo.

Para cada sitio de estudio, se realizaron mediciones periódicas de la elevación de la arena a lo largo de un conjunto de perfiles de playa, midiendo desde la playa seca hasta el límite de la marea baja. Estas campañas se utilizaron para analizar la acreción en cada playa durante la época estival. Además, se consideraron las características de las olas y mareas durante el período de estudio, que fueron obtenidas de bases de datos de reanálisis. Estos

datos permitieron analizar la influencia de las dinámicas marinas en los procesos de acreción.

La playa de Fuentebravía, ubicada en Puerto de Santa María, Cádiz, es una playa encajada, limitada por dos espigones, uno al noroeste en el límite entre la Base Naval de la OTAN en Rota y el área pública (construido en 1993), y otro al sureste frente a Punta Bermeja (construido en 2014). La playa tiene una longitud de 630 m y un ancho medio de 48 m. En invierno, la altura de ola significante oscila entre 1 y 2.8 m, con un período alrededor de 12 s y dirección WSW. En verano, la altura de ola varía entre 0.2 y 0.9 m, con un período de alrededor de 5 s y dirección W. Se realizaron 13 campañas de campo desde mayo hasta octubre de 2021, midiendo la evolución de la playa en 4 perfiles (Figura 3), en los que se ha analizado la acreción de la playa durante toda la época estival. Además, estas campañas también sirvieron para analizar el efecto del reperfilado de playas. El reperfilado se realizó el 12 de mayo de 2021 en la parte central de la playa de Fuentebravía. Las medidas realizadas y los resultados obtenidos relativos al reperfilado se muestran en el apartado 4.3. Los datos fueron obtenidos mediante un dispositivo RTK-GPS de alta precisión gracias a la colaboración con la Demarcación de Costas Andalucía Atlántico (Ministerio para la Transición Ecológica y el Reto Demográfico).

La playa de El Sardinero en Santander, Cantabria, es una playa en equilibrio estático limitada al norte por Cabo Menor y al sur por un fondo rocoso. La playa está dividida en dos durante la marea alta debido a la presencia del cabo de Piquío. El Sardinero I se encuentra al sur de Piquío y El Sardinero II al norte. En invierno, las olas incidentes tienen alturas de 5 m, período superior a 10 s y provienen del NW. En verano, la altura ola varía entre 0.2 y 2.2 m, con un período entre 5 y 13 s y provienen del NW a NE. Se realizaron 7 campañas de campo desde abril hasta septiembre de 2019 en 7 perfiles repartidos entre ambas playas (ver localización en Figura 3). Los datos se recogieron mediante distanciómetro láser, y fueron validados con los datos de una campaña RTK-GPS.

Las playas de Loredo, Somo y El Puntal en Somo, Cantabria, son parte del mismo arenal que se extiende desde los alrededores de la isla de Santa Marina hasta el canal de navegación que permite el acceso a la bahía de Santander. En invierno, las olas incidentes en Somo y Loredo tienen alturas de 4.5 m, período superior a 10 s y provienen del NW. En verano, la altura de ola varía entre 0.2 y 2.5 m, con un período entre 5 y 13 s y provienen del NW a NE. Se realizaron 7 campañas de campo (empleando distanciómetro láser) desde mayo hasta septiembre de 2019 en 4 perfiles (ver ubicación en Figura 3).

RESUMEN EN ESPAÑOL

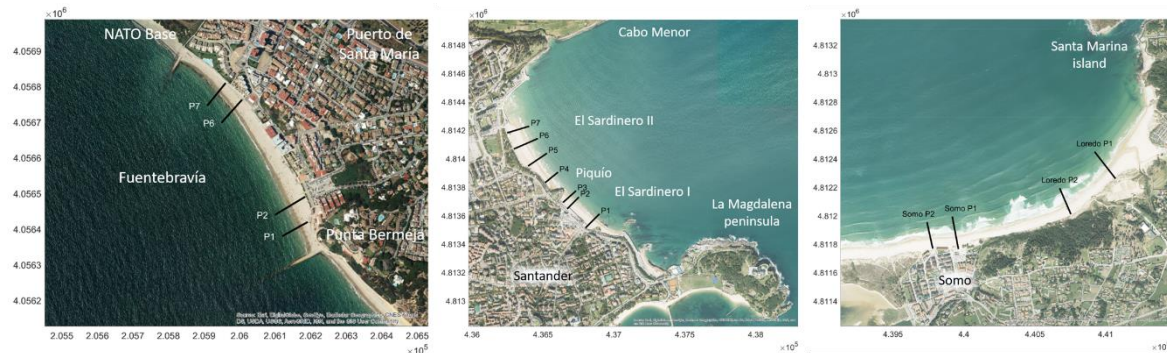


Figura 3 Ubicación de los perfiles medidos en cada una de las playas. Izquierda: Playa de Fuentebravía. Centro: Playas de El Sardinero. Derecha: Playas de Somo y Loredo.

2.2. Resultados

Los datos recopilados en las campañas de campo se referenciaron respecto al nivel medio del mar local de cada sitio de estudio. Posteriormente se analizó la evolución del perfil de la playa durante toda la temporada estival. Jensen et al. (2009) observaron que durante la vaciante de marea, el perfil de la playa permanecía en equilibrio, mientras que durante la llenante de marea la berma migraba tierra adentro hasta estabilizarse al alcanzar la pleamar. Por lo tanto, la geometría de los perfiles medidos en bajamar debe ser representativa de la acumulación lograda hasta la pleamar anterior. En consecuencia, los perfiles medidos se han representado junto con el nivel del agua del océano (OWL) en la pleamar anterior a cada campaña (línea discontinua) y la posición de la línea de costa (intersección entre el OWL en la pleamar anterior y el perfil medido, círculo). Ambas referencias se han representado con el mismo color que el perfil.

Los datos de las campañas se procesaron para obtener los siguientes parámetros morfológicos:

- Progradación de la línea de costa: es la posición de la línea de costa calculada al nivel la pleamar viva media (MHWS). La posición de la línea de costa en la primera campaña se tomó como referencia. Este parámetro es indicativo de la ganancia de playa seca lograda (protección costera extra y espacio para el turismo).
- Volumen de acreción: Es el volumen de arena acumulado en la berma tomando como referencia la primera campaña de campo. Sólo se han considerado áreas de acumulación. La berma se extiende desde la playa seca hasta el punto nodal en la zona intermareal descrito por Phillips et al. (2019).

- Pendiente: Es la pendiente del frente de playa al nivel de la pleamar anterior a cada campaña.
- Cota de la berma: La cresta de la berma se identificó manualmente como el punto más alto alrededor del cambio máximo de pendiente entre el nivel de pleamar y la playa seca. Si un perfil presenta dos bermas, se seleccionó la más cercana al mar, ya que es la nueva berma formada durante los ciclos de marea anteriores.

Todos esos parámetros morfológicos se han representado junto a los siguientes parámetros hidrodinámicos:

- Parámetro adimensional de caída de grano (Dean, 1973): $\Omega = \frac{H_s}{wT_p}$ calculada como una función de la altura de ola significante (H_s), el período pico (T_p) y la velocidad de caída de grano (w ; Hallermeier, 1981). El parámetro adimensional de caída de grano medio $\bar{\Omega}$ de cada sitio de estudio se calculó como el promedio de los valores horarios de Ω durante todo el año en el que se realizaron campañas (representado con línea discontinua).
- Parámetro adimensional de caída de grano de equilibrio: Ω_∞ propuesto por Wright et al. (1985) se calculó considerando $\Phi = 5$ días y $D = 30$ días como sugieren los autores. Este parámetro tiene en cuenta los estados morfodinámicos de la playa en días anteriores y realiza una media ponderada considerada como memoria de playa.
- Nivel del agua del océano (OWL): se obtuvo sumando las series temporales de marea astronómica y meteorológica extraídas de las bases de datos GOT y GOS, respectivamente.
- Nivel de agua total (TWL): se obtuvo como el OWL más el runup de la ola (R_2), obtenido con la formulación de Stockdon et al. (2006).
- Nivel de pleamar viva media (MHWS): se calculó para la serie temporal de marea astronómica y se representa con línea discontinua.

En los siguientes subapartados se analizan los resultados para cada sitio de estudio. Posteriormente se evalúan las relaciones entre las variables hidrodinámicas y los parámetros morfológicos.

RESUMEN EN ESPAÑOL

Cádiz

La Figura 4 muestra la evolución de la playa de Fuentebravía durante el verano de 2021 a través de trece campañas de campo. Los cuatro perfiles analizados muestran un comportamiento similar, con una significativa acumulación de arena a partir de mediados de mayo. La playa se recupera gradualmente desde mayo hasta septiembre, formando una nueva playa seca a medida que la berma recupera su arena. Durante este período, predomina la progradación de la línea de costa, aunque se observan algunos cambios en el nivel de la berma. En octubre, la berma se eleva, aumentando la altura de la playa seca y el volumen acumulado.

La Figura 5 muestra más claramente la acreción producida desde mediados de mayo hasta octubre, con tasas de acreción diferentes entre los perfiles. El perfil 1 experimentó la mayor acumulación y progradación de la línea de costa, mientras que el perfil 7 la menor. Esto indica una rotación en sentido horario de la playa de Fuentebravía durante el estudio, coincidiendo con un cambio en la dirección de las olas incidentes, de 260°N en invierno a 270°N en verano. La tasa de acreción fue suficiente para evitar la erosión de los perfiles 6 y 7 a pesar de que estaban cediendo arena longitudinalmente por el efecto de la rotación.

La progradación de la línea de costa (segundo panel de la Figura 5) se midió al nivel de MHWS = 1.36 m. La tasa de avance fue de ~5 m/mes para los perfiles 1 y 2, y ~2 m/mes para los perfiles 6 y 7. Se observa un retroceso de la línea de costa en la segunda mitad de julio, a pesar de que el volumen acumulado aumenta, debido a cambios en la elevación de la cresta de la berma y en el nivel de pleamar por el ciclo de mareas vivas-muertas. En septiembre y octubre el avance se ralentiza hasta una tasa de 2.5 m/mes para los perfiles 1 y 2 y de 0.5 m/mes para los perfiles 6 y 7.

Por otro lado, las tasas medias de acreción (tercer panel de la Figura 5) para los perfiles 1 y 2 fueron de 6 m³/mes entre mayo y septiembre y posteriormente se incrementaron a 15 m³/mes en octubre (2.5 veces mayor). Nótese que en octubre el avance de la línea de costa es menor, pero el volumen acumulado es superior debido al marcado ascenso de la cota de la berma. En los perfiles 6 y 7 el comportamiento es el mismo, pero con tasas de acreción inferiores debidas al mencionado giro de la playa.

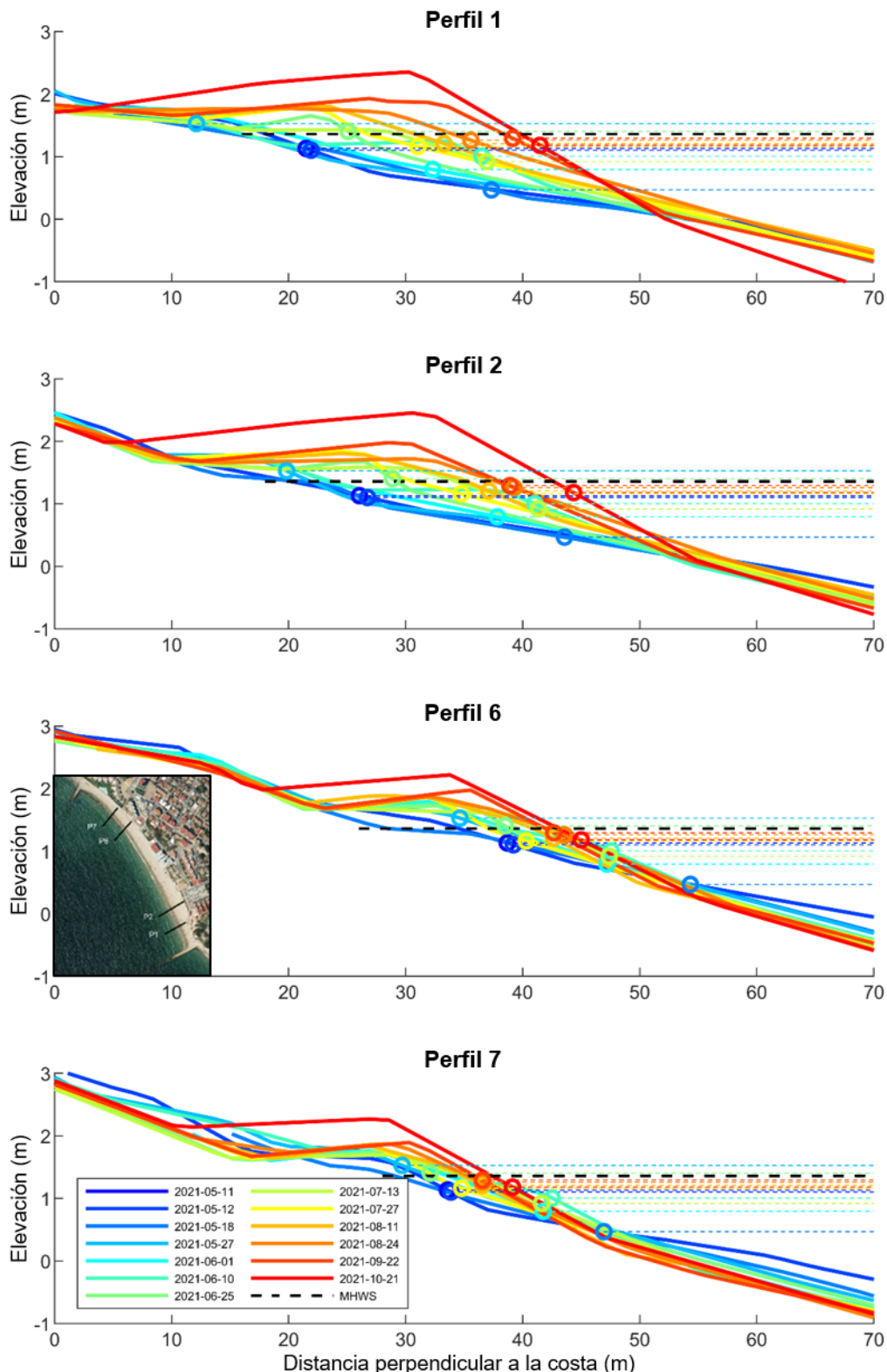


Figura 4 Evolución del perfil de playa en Fuentebravíá (playa seca y zona intermareal). Cota referida al nivel medio del mar local en Fuentebravíá.

RESUMEN EN ESPAÑOL

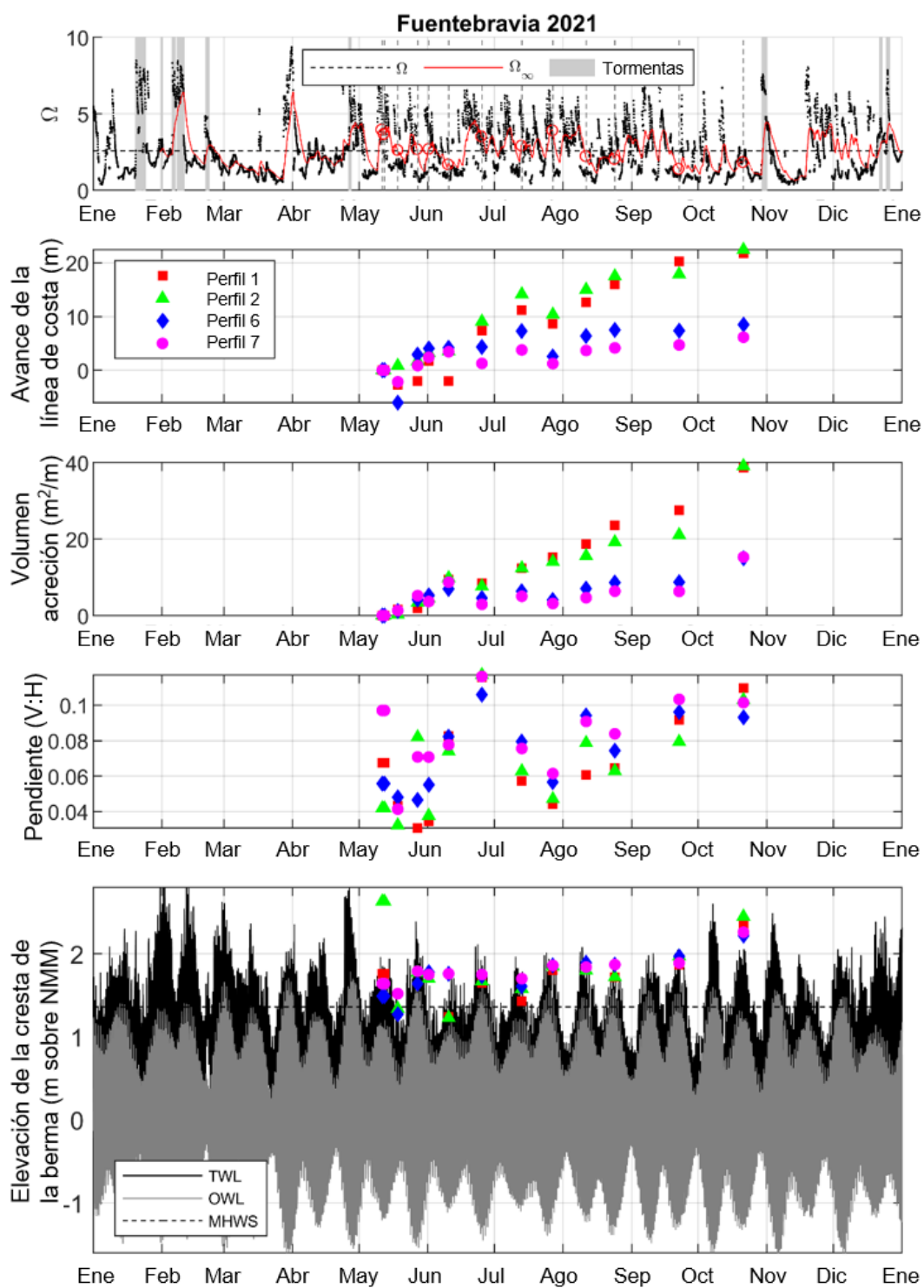


Figura 5 Variables hidrodinámicas y morfológicas medidas en la playa de Fuentebravia. En el panel superior: las áreas sombreadas en gris se refieren a condiciones de tormenta, donde la altura de ola significante está por encima del nivel de excedencia del 5% durante un mínimo de un ciclo de marea; las líneas discontinuas verticales son las fechas de las campañas de campo y los círculos rojos indican el valor de Ω_∞ en la pleamar anterior a cada campaña.

La pendiente de la playa (cuarto panel de la Figura 5) es altamente variable durante los primeros meses analizados debido a los diferentes momentos del ciclo de mareas vivas-muertas en los que se realizó cada campaña. Las tres últimas campañas se realizaron durante la marea viva mensual más grande, y muestran el incremento progresivo de la pendiente descrito por Phillips et al. (2019), indicativo de la finalización del período de recuperación de la playa.

La cota de la cresta de la berma (panel inferior de la Figura 5) fluctúa, dependiendo del TWL en el momento de la campaña de campo. Las campañas realizadas durante las mareas muertas muestran cotas de la cresta que pueden ser inferiores al MHWS. Phillips et al. (2019) describió este fenómeno como el proceso de formación de la berma. Durante las mareas muertas se genera una nueva berma con cota baja, la cual va elevándose progresivamente a medida que el rango de marea aumenta. Durante las mareas vivas la berma alcanza su máxima cota y queda estabilizada en el frente de playa como una prolongación de la berma del mes anterior. Por tanto, la morfología de la berma medida entre mareas vivas es compleja, mostrando aparentes retrocesos y avances de la línea de costa que no son permanentes. Los datos medidos durante las mareas vivas muestran una cota de la berma bastante uniforme en el tiempo y el espacio, con leves descensos hasta que la cota de la berma se sobrepasa por el TWL. Cuando esto ocurre, el agua sobrepasa la cresta de la berma y se produce una elevación de la misma, acumulándose la arena en capas sobre la berma anterior. El mayor evento de este tipo ocurrió en octubre, cuando la berma se elevó 0.35 m. Este evento estuvo asociado a: (1) un aumento en el periodo del oleaje, el cual produjo un aumento en el runup (y por tanto en el TWL) y un descenso en Ω , y (2) la ocurrencia de mareas vivas equinocciales con mayor rango de marea y aumentando aún más el TWL.

Santander

Durante el verano de 2019, se analizó la evolución de la playa de El Sardinero mediante siete campañas de campo con periodicidad mensual, de abril a septiembre. Se midieron tres perfiles en El Sardinero I y cuatro en El Sardinero II. La berma de verano comenzó a formarse en mayo, con el frente de playa progradando y desplazándose paralelamente a sí mismo hasta inicios de agosto. La tasa de avance fue de 5 m/mes en El Sardinero I y 4 m/mes en El Sardinero II. La elevación de la cresta de la berma se mantuvo constante en este período, y se elevó 0.4 m en octubre. Se observó un gradiente en la cota de la berma, siendo menor en El Sardinero II, posiblemente debido al efecto protector del Cabo Menor.

RESUMEN EN ESPAÑOL

La tasa de acreción fue constante de abril a inicios de agosto, con tasas de 9.5 m³/mes en El Sardinero I y 6 m³/mes en El Sardinero II. En agosto no se produjo acreción y algunos perfiles llegan a erosionarse levemente. Esta falta de acreción en agosto no pudo ser explicada por eventos específicos. Finalmente, en septiembre la tasa de acreción aumenta de nuevo a 11 m³/mes en El Sardinero I y 5 m³/mes en El Sardinero II.

Somo

Se realizaron siete campañas de campo entre mayo y septiembre de 2019 en las playas de Somo y Loredo, midiendo cuatro perfiles de playa (dos en cada playa). Las pendientes en estas playas son más suaves debido a la exposición directa a los grandes oleajes del NE y N del Mar Cantábrico. Estas playas suelen presentar formas rítmicas, lo cual probablemente sea la causa de las irregularidades espaciales en los perfiles.

La recuperación de la playa no comenzó hasta junio, cuando la altura de ola se redujo por debajo de 0.8 m. Probablemente, pequeñas tormentas de primavera, junto a la mayor exposición de estas playas, retrasaron el inicio de la recuperación. La progradación promedio de la línea de costa fue de 5.2 m/mes y la acreción promedio de 8 m³/mes. Estas tasas fueron uniformes a lo largo de todo el periodo estudiado.

La cresta de la berma de verano no se evidenció claramente hasta julio, y desde entonces aumentó de cota cada mes hasta septiembre (desde 2.1 m hasta 2.8 m). La mayor subida de la berma fue de 0.26 m en septiembre debido a mareas vivas equinocciales y un mayor período de olas que incrementaron el TWL.

Influencia de los parámetros hidrodinámicos en la acreción de la playa

Las mareas vivas ocurren cuando la Tierra, la Luna y el Sol se alinean, sucediendo dos veces al mes durante las lunas nuevas y llenas. Las dos mareas vivas mensuales pueden presentar grandes diferencias en el rango de marea. Las mediciones en la playa de Fuentebravía durante los meses de junio y julio de 2021 son ejemplos de estas variaciones, con un rango de marea en torno a 2.1 m coincidiendo con la luna nueva, y de 2.9 m con la luna llena. El rango de marea fue de 1.5 m en las mareas muertas. El análisis de las campañas de campo realizadas en estas fechas ha permitido verificar la complejidad de la morfología de la berma en los periodos entre mareas vivas (que siguen el patrón de formación de la berma descrito por Phillips et al. (2019) mencionado anteriormente) y la relevancia que tienen las diferencias del rango de marea entre unas mareas y otras. Por ello, se han seleccionado los datos de las campañas de campo realizadas durante la marea viva

más grande mensual, la cual es representativa de la acreción ocurrida durante ese mes, ya que es durante las mareas vivas cuando la arena recuperada se estabiliza en la berma.

Las mediciones mensuales de la elevación de la cresta de la berma (alrededor de las mareas vivas) muestran una alta correlación con el nivel del mar total superado en un 1% el mes anterior ($TWL_{1\%}$; Figura 6). El error entre ambas variables es de 0.12 m, lo que indica que la elevación de la cresta de la berma puede predecirse con la serie temporal de TWL.

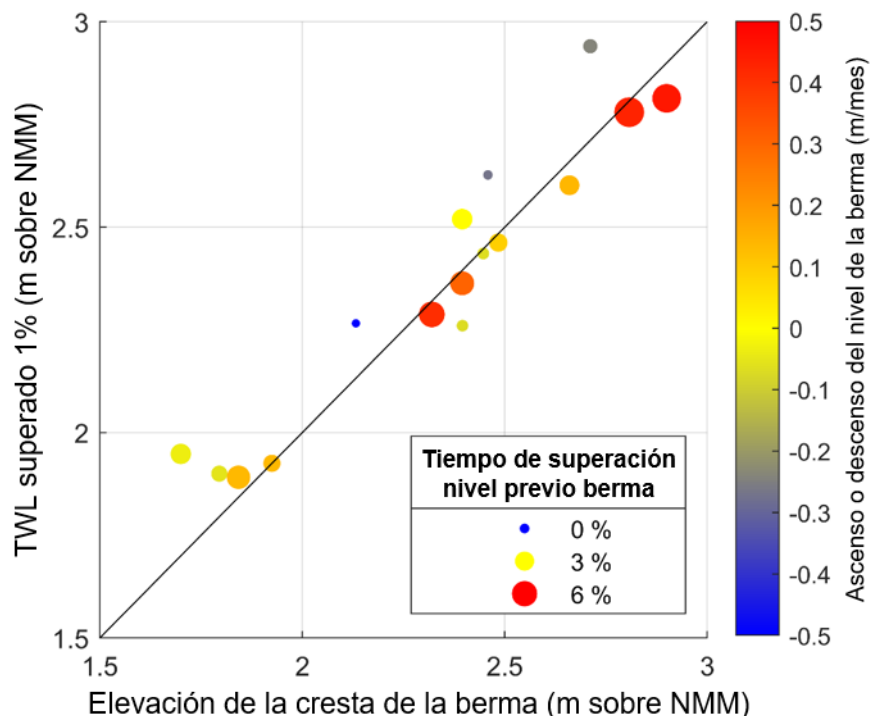


Figura 6 Relación entre la elevación de la cresta de la berma y el TWL superado el 1% del tiempo en un mes (de marea viva a marea viva). El ascenso (+) o descenso (-) del nivel de la berma está relacionado con el porcentaje del tiempo en el que el nivel de la berma previo es superado por el agua.

Además, el tamaño y el color de los puntos en la Figura 6 indican el porcentaje de tiempo en el que el nivel de la cresta de la berma fue superado y el ascenso o descenso de la cresta de la berma desde la observación anterior hasta la actual, respectivamente. La mayoría de los meses, la cresta de la berma se eleva o mantiene su nivel, como indican los puntos rojos y amarillos. Solo tres observaciones corresponden a eventos en los que la cresta de la berma disminuye (color azul). Los puntos rojizos son más grandes, lo que significa que el nivel de la cresta de la berma fue superado un mayor porcentaje de tiempo durante el último mes. En cambio, los puntos más pequeños (menos del 2% del tiempo de

superación de TWL) son azules o amarillos, lo que indica que en esos casos la berma no se elevó e incluso redujo su cota. En resumen, se necesita un mínimo del 3% del tiempo de superación del TWL sobre la cresta de la berma para observar una elevación de la cota en la próxima marea viva.

Es ampliamente conocido que la acreción en la playa se produce cuando el parámetro adimensional de caída del grano (Ω) es pequeño. Wright et al. (1985) encontraron que el promedio ponderado de los valores anteriores de Ω (Ω_∞ , parámetro adimensional de caída de grano de equilibrio) era el mejor descriptor del estado de la playa. Se ha analizado la relación entre cada uno de estos dos parámetros y la acreción producida mensualmente. En general, cuanto menor es Ω_∞ (y también Ω), la acreción producida es mayor, aunque la relación obtenida es débil y cuatro observaciones no siguen la tendencia general.

2.3. Discusión

Se ha analizado la recuperación natural de tres playas meso/macro-mareales durante toda una temporada de verano. Se utilizaron GPS de alta precisión (RTK-GPS) y distanciómetros (El Sardinero, Somo y Loredo) para medir las playas. Las mediciones de los distanciómetros fueron validadas con RTK-GPS, demostrando que el error cuadrático medio vertical de los datos de los distanciómetros fue de 0.09 m. Ward et al. (2021) también obtuvieron buenos resultados con técnicas poco costosas. Esto demuestra que técnicas sencillas y económicas también son fuentes válidas de datos, con la ventaja de no requerir equipo costoso ni personal cualificado.

La mayoría de los estudios de acreción se centran en la formación de barras intermareales o sumergidas y en sus tasas de migración hacia la costa. Son pocos los estudios que han analizado la evolución de la berma de la playa y el ensanchamiento de la playa seca debido a los procesos de acreción. Strahler (1966) y Thom y Hall (1991) fueron de los primeros que analizaron la formación y el crecimiento de la berma de playa. Jensen et al. (2009) estudiaron una playa de arena fina, pendiente suave, micro-mareal, y observaron que “durante la llenante de marea y bajo niveles de marea crecientes, la berma se transforma en barra intermareal y migra hacia la costa, hasta que finalmente se estabiliza en la parte más alta del frente de playa, incrementando la cota de la berma preexistente”. Este proceso es el mismo que fue observado en la playa de Fuentebravía en un entorno meso-mareal.

Recientemente, Phillips et al. (2019) propusieron cuatro modos de acreción basados en la morfología de la berma de una playa micro-mareal. En nuestro estudio, el retroceso

de la costa solo se observó en campañas intermedias entre mareas vivas, por lo que se cree que los modos propuestos por Phillips et al. (2019) que producen erosión solo se producen un número reducido de días al mes y por tanto no resultan dominantes de forma mensual. En cuanto a la relación con las dinámicas marinas, en este estudio la cota de la berma solo se eleva si el TWL es excedido un 3% del tiempo durante el mes previo (no con cualquier excedencia como en Phillips et al. (2019)).

En concordancia con los estudios de Jensen et al. (2009), Phillips et al. (2019) y Strahler (1966), en esta tesis también se ha observado que la cota máxima de la berma se alcanza durante la marea viva más grande de cada mes. Es en este momento de marea máxima mensual cuando la berma alcanza su máxima altura y el volumen de arena recuperado se estabiliza en la berma, por lo que se considera esta fecha como representativa de la acreción producida cada mes. Por tanto, se sugiere la elección de este día para la realización de campañas de campo de seguimiento de la acreción en playas. Esto permite minimizar el esfuerzo necesario para medir la recuperación completa de la playa durante el verano.

En el estudio realizado por Phillips et al. (2019) la tasa de acreción fue tres veces mayor en la fase final de la recuperación, cuando la berma creció en altura. Este resultado coincide con los hallazgos en nuestras playas meso/macro-mareales, donde las tasas de acreción fueron hasta 2.5 veces mayores durante el último mes cuando la berma se elevó. Al final de la temporada de verano, la concomitancia de mareas vivas equinocciales y períodos de ola más grandes produce un aumento en el nivel del mar total (TWL), lo que lleva a que las olas sobrepasen la cresta de la berma y se produzca un crecimiento en altura de la misma.

La cota máxima de la cresta de la berma (alcanzada durante la marea viva más alta cada mes) está correlacionada con el nivel del mar total que es excedido el 1% del tiempo durante el mes anterior ($TWL_{1\%}$). Esto significa que la elevación de la cresta de la berma puede predecirse si se conocen las dinámicas marinas, sin necesidad de campañas de campo previas. Esto es útil para el diseño de técnicas de recuperación asistida (NABE). Por ejemplo, la técnica de reperfilado de playas propone crear una berma de verano con arena tomada de la zona intermareal. El diseño de la geometría de la berma requiere la predicción del nivel de cresta y el volumen de la berma más adecuado para cada sitio de estudio.

El uso del parámetro adimensional de caída de grano (Ω) para analizar el estado de la playa y, por lo tanto, su acreción o erosión, está ampliamente extendido. Wright et al. (1985) propusieron un nuevo parámetro (Ω_∞ , parámetro adimensional de caída de grano

RESUMEN EN ESPAÑOL

de equilibrio). Este parámetro explica mejor que el anterior el estado de una playa, pero en nuestro estudio no pudo predecir con precisión la tasa de acreción.

En nuestro estudio, encontramos que la acreción se produce cuando Ω_∞ está por debajo de $\bar{\Omega}$ (como se esperaba), pero también puede ocurrir en meses con un Ω_∞ promedio mayor que $\bar{\Omega}$. Esto coincide con las observaciones de Phillips et al. (2019), donde la acreción se produjo cuando $\Omega < \bar{\Omega}$, pero también si $\Omega > \bar{\Omega}$, siempre que haya condiciones sin tormentas y que OWL < MHWS (aunque esta última condición no se cumplió en nuestras observaciones). En general, cuanto menor sea Ω_∞ (o Ω), mayor será la tasa de acreción, pero hubo algunas excepciones. Estos resultados sugieren que tanto Ω como Ω_∞ podrían servir como indicadores de acreción (la acreción es clara cuando $\Omega < \bar{\Omega}$), aunque la relación obtenida es débil. Por tanto, otros parámetros pueden ser importantes para comprender la acreción de la playa y se requiere de más investigaciones para arrojar luz sobre este campo.

3. ARADO DE PLAYAS

Monge-Ganuzas et al. (2017) probaron una nueva técnica en la playa de Laida (norte de España) que consiste en arar mecánicamente el área intermareal de la playa. En su trabajo, concibieron el arado como una técnica poco invasiva para ayudar a la acreción y conseguir una playa más ancha a principios del verano, mejorando el potencial recreativo de la playa. La playa de Laida fue arada 22 veces durante el verano de 2015, de julio a septiembre. Los surcos generados por el arado tenían una longitud de 1.42 m y una altura de 0.27 m (ver Figura 1). El análisis de las batimetrías mostró que el arado aceleró la migración natural de la barra hacia la costa (Gainza et al., 2019), obteniendo resultados prometedores para conseguir un mayor ancho de playa durante el verano.

En esta tesis, se analiza el comportamiento morfológico de las formas del lecho creadas artificialmente. Los surcos y crestas se crean mecánicamente arando la zona intermareal paralelamente a la línea de costa (Monge-Ganuzas et al., 2017). En esta innovadora técnica de recuperación asistida por la naturaleza, la altura de los surcos es claramente mayor que la de las formas del lecho formadas naturalmente para esta longitud de onda; por lo tanto, la rugosidad del fondo inducida es mayor, aunque se reduce progresivamente a medida que el arado se suaviza por la acción de las olas. En esta tesis, por primera vez, se analiza bajo condiciones controladas de laboratorio la efectividad del arado para acelerar la acreción, así como la atenuación y la migración de las formas.

En este apartado, se analizan detalladamente los resultados de los experimentos de laboratorio para confirmar la efectividad del arado y su aplicabilidad. Aquí se abordan los objetivos OB3, OB4, OB5 y OB6 de la tesis en su faceta relativa al arado. Adicionalmente, en el apartado 4 se incluye un análisis comparativo entre las técnicas del arado y reperfilado, complementando los hallazgos de este apartado para cumplir con los objetivos mencionados. El apartado 3.1 describe los ensayos de laboratorio realizados. El apartado 3.2 analiza la efectividad del arado, incluyendo los resultados relacionados con la morfología, la hidrodinámica, la dinámica sedimentaria y el balance sedimentario. El apartado 3.3 contiene un análisis detallado de la evolución del arado y de las formas del lecho, incluyendo la metodología y los resultados de los experimentos de laboratorio de mayor duración. Finalmente, la discusión de los resultados se incluye al final de los apartados 3.2 y 3.3. La novedad de este trabajo radica en que, por primera vez, la técnica de arado se analiza bajo condiciones controladas de laboratorio.

3.1. Descripción de los experimentos de laboratorio

Los experimentos se realizaron en el Canal de Oleaje-Corriente-Tsunami (COCoTsu) en las instalaciones de IHCantabria en Cantabria, España. El canal tiene una longitud de 56 m, 2 m de ancho y 2.5 m de alto, con paredes laterales de vidrio. Los experimentos se llevaron a cabo a escala prototipo (1:1) en este canal, que se dividió longitudinalmente en dos subcanales iguales de 1 m de ancho cada uno. Un subcanal se usó para simular la evolución morfodinámica de un área intermareal arada (Figura 7), mientras que el otro se mantuvo como control, representando una geometría intermareal natural. Se realizaron dos conjuntos de simulaciones:

- Conjunto 1: Siete ensayos con una duración de 1 hora cada uno, con diferentes niveles de agua y el mismo oleaje que genera acreción. Los resultados de este conjunto de experimentos se describen en el apartado 3.2 "Evaluación de la efectividad del arado".
- Conjunto 2: Dos ensayos con una duración de 4 horas cada uno, con diferentes niveles de agua y el mismo oleaje que genera acreción. La duración de este conjunto de experimentos se determinó después de simular una prueba de 7 h de duración. Los resultados indicaron que las características de las formas del lecho no cambian después de 4 horas, y la geometría arada ya no puede distinguirse (como se demuestra en los apartados siguientes). Los resultados de este conjunto de experimentos se describen en el apartado 3.3 "Evolución de las formas del lecho".

RESUMEN EN ESPAÑOL

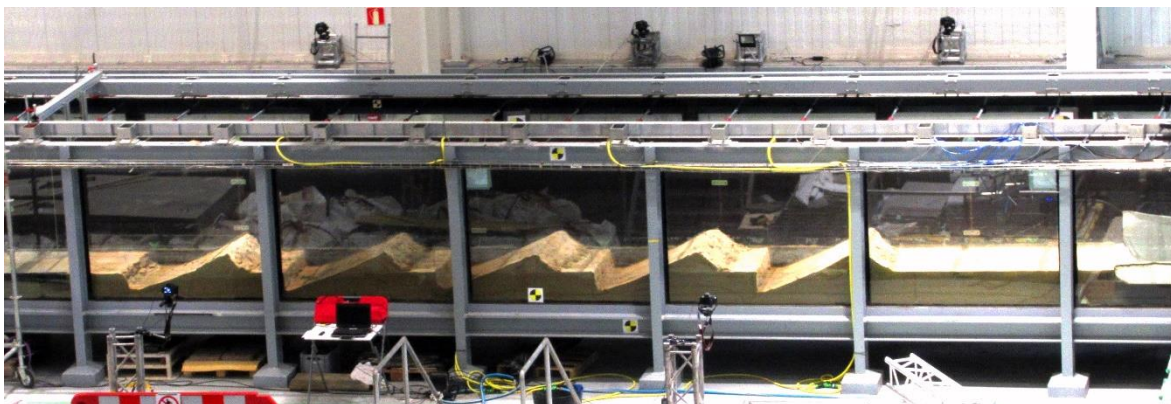


Figura 7 Fotografía del arado en la instalación experimental. Las paredes laterales del tramo de ensayos del canal COCoTsu están hechas de vidrio. La imagen muestra la geometría de arado inicial de cada ensayo antes de su inundación con agua.

Se construyó a escala prototipo (1:1) un tramo de un área intermareal en el canal COCoTsu, formado por una rampa de hormigón y una sección de arena móvil. La rampa estaba formada por una parte permanente y otra ad-hoc construida para estos experimentos. La parte permanente consistía en una rampa de hormigón de 4.7 m de longitud con una pendiente de 1/13.55 que comenzaba a 11 m del generador de oleaje. A continuación, sobre el fondo permanente elevado se colocó otra rampa de hormigón de 12 m de longitud con una pendiente de 1/30 en la primera mitad y 1/60 en la segunda mitad. La parte final de 0.3 m de hormigón incluía una transición redondeada para evitar saltos bruscos en el inicio del área de arena. El área de ensayo era un relleno de arena de 10 m de longitud con una pendiente de 1/100. La parte superior de la arena alcanzaba 0.75 m sobre el fondo del canal. Se utilizó arena natural con un tamaño de partícula $D_{50} = 0.318$ mm y una densidad $\rho_s = 2580$ kg/m³. La pendiente era suave ($\tan\beta = 0.01$), típica del área intermareal de una playa de arena fina-media expuesta a oleaje energético. Un cajón colocado en el extremo opuesto al generador de oleaje capturaba la arena transportada hacia la costa por la acreción. En el extremo del canal, se instalaron disipadores para evitar la reflexión del oleaje.

El canal se dividió longitudinalmente en dos subcanales iguales de 1 m de ancho usando paneles unidos unos a otros que actuaban como una pared delgada. La separación se extendía desde el inicio de la rampa de hormigón hasta los disipadores de olas, por lo que la hidrodinámica y la morfodinámica eran completamente independientes en ambos lados. Uno de los canales se utilizó para simular las condiciones de una playa natural como referencia. El otro canal incluía la misma geometría básica con 5 surcos y crestas cavadas transversalmente sobre la zona de arena. La geometría de arado fue la misma para todos los ensayos, con una longitud de onda de 1.6 m y una amplitud de 0.25 m, correspondiente

a las dimensiones del arado que puede realizar un tractor. Esta geometría inicial, natural y arada, fue reconstruida al inicio de cada ensayo en ambos subcanales. En cada subcanal se instaló un cajón de 2 m de largo, cubriendo todo el ancho del subcanal para asegurar que se capturara todo el sedimento representativo de la acreción producida en cada lado.

Se utilizó un láser escáner de alta resolución para medir la geometría del fondo de arena antes y después de cada ensayo. La elevación de la superficie del agua se midió continuamente a 50 Hz mediante 16 sensores capacitivos de oleaje (WGs). Las corrientes se midieron con 4 velocímetros acústicos Doppler (ADV) ubicados en el extremo más alejado de los generadores de oleaje sobre área de arena (2 en cada subcanal). El transporte de sedimentos en suspensión se midió con 2 sensores ópticos de retrodispersión (OBS) ubicados justo debajo de los ADV (1 en cada subcanal). En el Conjunto 2 de ensayos se agregó más instrumentación: dos cámaras sincronizadas entre sí para tomar imágenes simultáneas cada 5 minutos del fondo de arena en el lado arado a través de la pared de cristal, y el sedimento capturado en los cajones fue extraído y pesado tras 1 h, 2 h, y 4 h de ensayo.

Las características del oleaje fueron las mismas para todos los ensayos en ambos conjuntos de experimentos. Se simuló un oleaje irregular con altura de ola significante $H_s = 0.3$ m, período de pico $T_p = 7$ s y espectro JONSWAP ($\gamma = 3.3$) con absorción activa para evitar oleaje reflejado. El parámetro adimensional de caída de grano $\Omega = H_s/(w \cdot T_p) = 1.08$ corresponde a un estado morfodinámico reflejante según Wright y Short, (1984). Según la metodología de Kraus et al. (1991) la acreción es muy probable para este oleaje. En el Conjunto 1, se realizaron siete ensayos con diferentes niveles de agua (0.75 m, 0.8 m, 0.85 m, 0.9 m, 1 m, 1.1 m, y 1.2 m sobre el fondo del canal junto a los generadores de oleaje), los cuales se mantuvieron constantes durante 1 h que duró cada ensayo. En el Conjunto 2, se realizaron dos ensayos con nivel de agua constante de 0.85 m para el Test A y 1.2 m para el Test B. La duración fue de 4 h cada ensayo, con pausas cada 1 h que permitieron medir la acumulación de sedimentos y la geometría del fondo.

3.2. Evaluación de la efectividad del arado

Esta sección muestra el análisis realizado para caracterizar la morfología, hidrodinámica, dinámica sedimentaria y balance de sedimentos del área de estudio para los siete ensayos realizados en el conjunto de experimentos 1. Se ha llevado a cabo un análisis estadístico de los resultados para la mayoría de las magnitudes analizadas. Los valores individuales de cada uno de los siete ensayos se agruparon como $\mu_i \pm \sigma_i$, donde μ_i

RESUMEN EN ESPAÑOL

es el valor medio de los resultados para la magnitud i medida en los siete ensayos y σ_i es la desviación estándar de esas mismas siete mediciones (una para cada nivel de agua).

Morfología

Las mediciones del fondo de arena realizadas mediante escáner láser permitieron analizar la evolución de la geometría natural y arada. Tras la acción de 1 h de olas simuladas, aparecieron ripples en el lado natural y el arado se suavizó. El sedimento erosionado de las crestas fue transportado hacia la costa y una parte del mismo se depositó en los surcos, rellenándolos parcialmente. En las zonas planas formadas en la parte superior de las crestas del arado aparecieron ripples.

Se calculó la rugosidad del fondo arenoso para cuantificar el impacto de las formas del lecho en la hidrodinámica y la evolución morfológica. La rugosidad se calculó como $k_\sigma = 4 \sigma_z$, donde σ_z es la desviación estándar de los puntos de la superficie respecto al fondo inicial con pendiente uniforme 1/100, medido en m. En el lado natural $k_\sigma = 0.029$ m al inicio de los ensayos (debido a pequeñas irregularidades producidas al colocar la arena manualmente con pendiente 1/100), y posteriormente aumenta a 0.047 m por la aparición de ripples. En el lado arado, la rugosidad inicial roza 0.4 m, ya que tiene en cuenta la geometría de los surcos y crestas. Tras la acción del oleaje el arado se suaviza y la rugosidad se reduce a 0.168 m, demostrando que los surcos y crestas aún son pronunciados después de 1 h de acción del oleaje. Por tanto, la rugosidad en el lado arado es 3.57 veces mayor al final de los ensayos independientemente del nivel de agua simulado.

Hidrodinámica

Los sensores de superficie libre (WG) se instalaron distribuidos sobre la zona de arena por parejas, uno en el lado natural y su correspondiente en el lado arado. Se obtuvo la altura de ola significante (H_s) de cada uno de ellos, y para cada nivel del agua ensayado (Figura 8). Además, se midió H_s en las proximidades de los generadores de oleaje, resultando 0.29 ± 0.01 m. La Figura 8 muestra que la altura de ola al inicio de la zona de arena disminuye a medida que el nivel de agua es menor, debido a una mayor rotura del oleaje sobre la rampa de hormigón. Las olas continúan rompiendo sobre el fondo de arena. Al inicio de la zona de estudio el oleaje en ambos lados es muy similar, mientras que al final de la misma la altura de ola del lado arado es inferior para todos los niveles ensayados. Comparando la altura de ola al inicio y al final de los 10 m de arena se obtiene una reducción de 0.059 ± 0.007 m en el lado natural y de 0.071 ± 0.008 m en el lado arado. Esto evidencia que el arado produce una mayor disipación del oleaje y que esta disipación es muy similar para

todos los niveles de agua. Como resultado, las olas son un $11.08 \pm 7.75\%$ más pequeñas al final del lado arado comparadas con el lado natural.

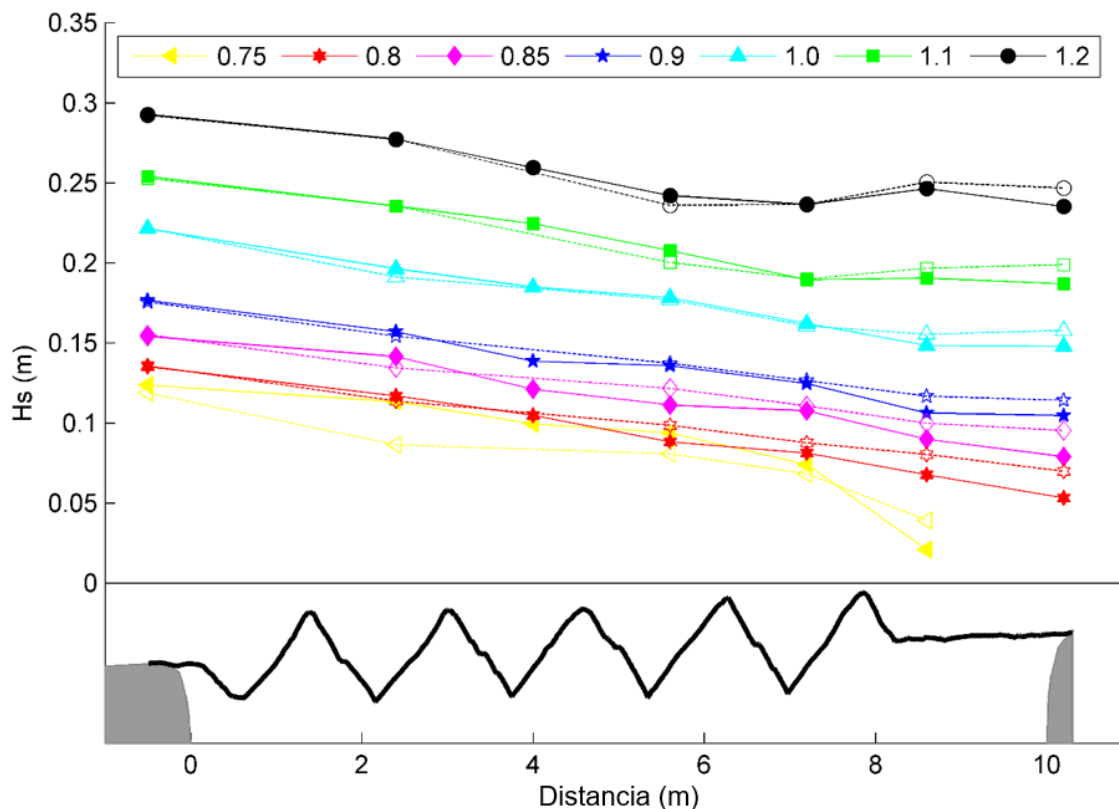


Figura 8 Evolución de la altura de ola significante a lo largo de ambos subcanales para cada ensayo con diferentes niveles de agua (ver leyenda). Los valores del lado natural se muestran con línea discontinua y marcadores vacíos. Los valores del lado arado se muestran con línea continua y marcadores sólidos. El diagrama en la parte inferior muestra un perfil de la batimetría arada como referencia de la ubicación de cada sensor.

Se realizó el análisis espectral de las series de oleaje medidas en cada uno de los sensores, y se observó que el arado produce una mayor disipación del oleaje en todas las frecuencias por encima de 0.03 Hz. Esta disipación llega a ser un 45% superior a la producida naturalmente para frecuencias entre 0.055 y 0.175 Hz, coincidiendo con la frecuencia del oleaje generado (0.143 Hz; periodo 7 s).

El análisis de los datos recogidos por los sensores ADV mostró que la corriente media en el lado arado es más fuerte cuando está dirigida hacia la costa y más débil cuando está dirigida hacia el mar. Esto indica que el arado favorece las corrientes hacia la costa, las cuales facilitan la acreción.

RESUMEN EN ESPAÑOL

Dinámica sedimentaria

Se ha calculado el transporte de sedimento transversal a la costa en base a los datos de batimetría inicial y final de cada ensayo mediante la ecuación de Exner. La Figura 9 muestra los resultados obtenidos para el lado natural y arado (nótese que la escala vertical es diferente para ambos). Se han promediado los resultados individuales para observar la tendencia. En el lado arado puede verse que las crestas se erosionan (Q aumenta) y parte de ese sedimento se deposita en los surcos (Q disminuye), quedando una parte del sedimento erosionado en cada cresta en suspensión (el mínimo Q en cada surco es superior al anterior y por tanto el transporte en suspensión va en aumento). La acreción predomina en ambos lados, alcanzándose un transporte hacia la costa en el extremo más alejado de los generadores de oleaje de $Q = 3.44 \times 10^{-6} \text{ m}^2/\text{s}$ en el lado natural y $Q = 9.96 \times 10^{-6} \text{ m}^2/\text{s}$ en el lado arado, 2.9 veces mayor.

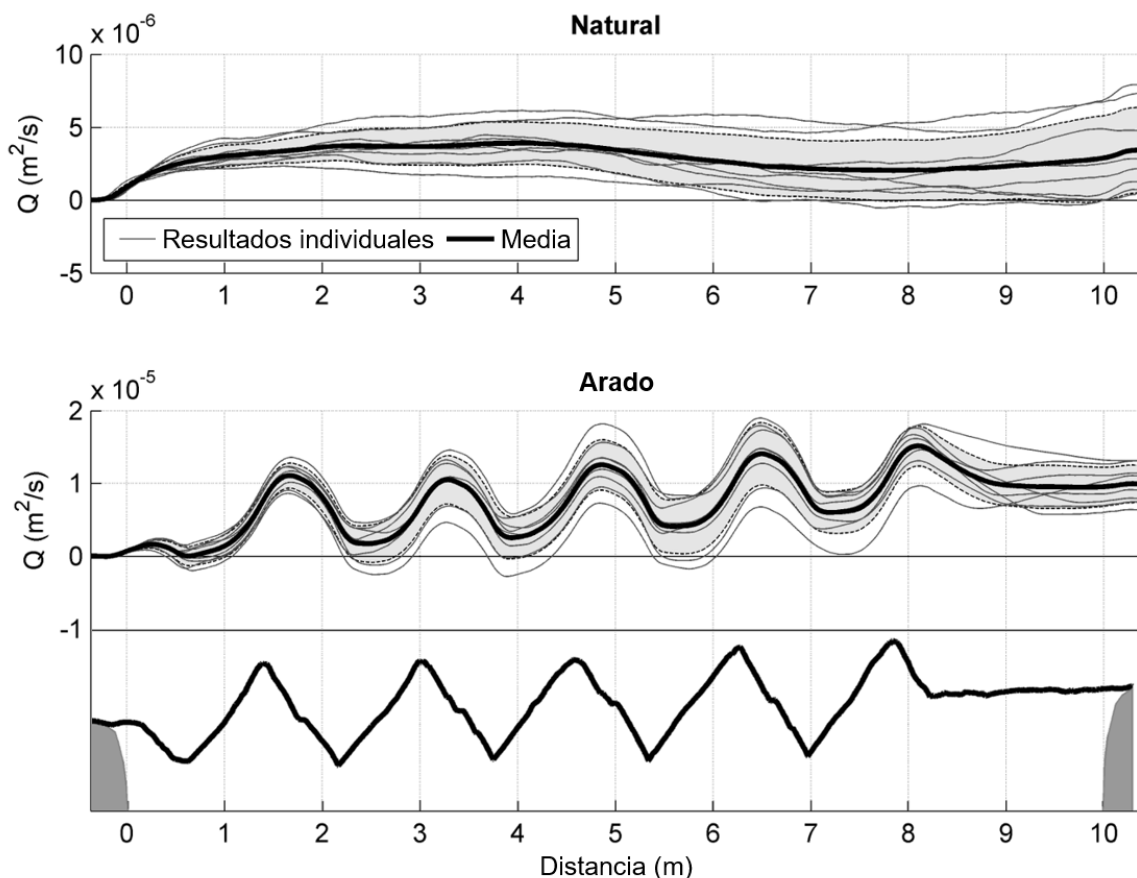


Figura 9 Transporte de sedimento transversal de la costa por unidad de ancho. Los valores positivos indican acreción. Las áreas sombreadas en gris indican una desviación estándar del valor medio (la línea negra gruesa). Las líneas grises claras son los resultados de cada ensayo de laboratorio con diferentes niveles de agua. El diagrama en la parte inferior muestra un perfil de la batimetría arada como referencia de la ubicación de las crestas y surcos.

Los sensores OBS midieron la concentración de sedimento en suspensión a 0.05 m sobre el fondo de arena. Los datos se analizaron estadísticamente y se obtuvo el valor mediana en cada ensayo. Los resultados muestran que el valor mediana es un 8.98% mayor en el lado arado para el ensayo con nivel de agua de 0.85 m, 46.33% para 1 m, 48.92% para 1.1 m, y 36.09% para 1.2 m. En el caso del ensayo con nivel de 0.9 m, la concentración de sedimento en suspensión en el lado arado fue un 2.44% menor. Esta mayor concentración de sedimento en suspensión en el lado arado era claramente visible como una mayor turbidez en toda la columna de agua desde el inicio de cada ensayo.

Balance de sedimentos

Como se ha mencionado anteriormente, la zona arenosa de estudio presenta zona de erosión y zonas de acreción. Se calculó el volumen de sedimentos erosionados y acumulados a partir de la diferencia entre las batimetrías final e inicial de cada ensayo. La Figura 10 muestra los resultados obtenidos para el lado natural y el lado arado. Puede apreciarse que el volumen de sedimento movilizado en el arado es superior, debido a la erosión de las crestas y relleno de los surcos. En el lado natural los volúmenes responden a la formación de ripples.

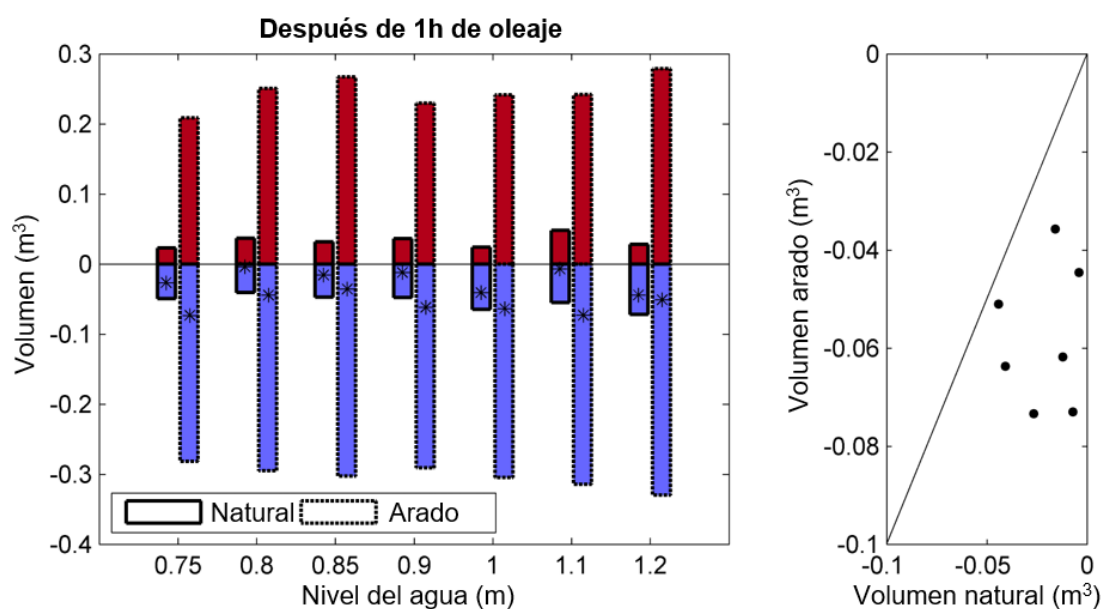


Figura 10 Volúmenes de sedimento movilizados. Los valores positivos indican acumulación de arena y los valores negativos indican erosión y movilización hacia la costa (acreción). Izquierdo: Volúmenes de sedimento acumulados (rojo), erosionados (azul) y netos (*). Derecha: Comparación del volumen neto de sedimento en acreción (erosionado del área de arena) en ambos lados (cada punto corresponde a un par de asteriscos en el panel izquierdo).

RESUMEN EN ESPAÑOL

La Figura 10 también muestra el balance de sedimento con un asterisco. En todos los casos predomina la erosión, indicando que ese volumen de arena se ha desplazado hacia la costa en forma de acreción. La figura de la derecha muestra una comparativa entre la acreción producida en el lado natural y el arado, resultando evidente que el lado arado produce mayor acreción en todos los ensayos realizados.

Discusión

Los ensayos de laboratorio descritos muestran el efecto generado por la creación de 5 surcos y crestas aradas en la zona intermareal. Estas formas generaron una rugosidad del fondo 3.57 veces superior (tras 1 h de oleaje) a la rugosidad de la zona intermareal de una playa natural. Los efectos del arado incluyen: (1) una reducción de la altura de ola significante que alcanza un $11.08 \pm 7.75\%$ en el extremo más cercano a la costa del lado arado, (2) una reducción de la energía del oleaje con frecuencias superiores a 0.03 Hz, (3) un transporte de sedimento total hacia la costa 2.9 veces superior, y (4) una concentración de sedimento en suspensión hasta un 49% superior, lo que unido a unas corrientes más tendentes a dirigirse hacia la costa puede facilitar el aumento del transporte de sedimento en suspensión hacia la costa. En conjunto, estos resultados demuestran que la técnica del arado es efectiva para acelerar la acreción natural en playas.

La disipación por fricción podría desempeñar un papel importante en la efectividad del arado. La altura de la ola incidente y el gradiente del fondo son los mismos para las geometrías natural y arada, pero la rugosidad del fondo es claramente mayor cuando se aplica el arado. Poate et al. (2018) encontraron que la importancia de la disipación por fricción (relativa a la disipación total producida) aumenta con un gradiente del fondo decreciente ($\tan\beta < 0.02$), una altura de ola pequeña ($H_0 < 0.5$ m) y una rugosidad del lecho creciente, donde la fricción puede representar ~20% de la disipación total de energía del oleaje. En este experimento, el gradiente del lecho es muy bajo ($\tan\beta = 0.01$) y la altura de ola es pequeña ($H_0 = 0.3$ m). La principal diferencia entre los lados natural y arado es la rugosidad del lecho, la cual después de 1 h bajo la acción del oleaje sigue siendo 3.57 veces mayor en el lado arado. Esto explica que la disipación del oleaje sea mayor aplicando el arado.

Gainza et al. (2019) propusieron la rugosidad del lecho como un posible mecanismo que provoca la aceleración de la acreción al emplear el arado. También afirmaron que los cambios en la porosidad de la arena, debido a la descompactación producida al arar la playa, podrían acelerar el transporte de sedimentos. Dados los valores habituales de porosidad en las playas naturales, el efecto sobre el transporte es muy bajo. Además, en los

ensayos de laboratorio, la descompactación medida se redujo a un 2.69% y, por lo tanto, los cambios de porosidad son insignificantes.

La mayor disipación del oleaje producida por el arado genera que el parámetro adimensional de caída del grano Ω se reduzca, conduciendo a estados morfodinámicos más reflejantes. Esto conduce a pensar que la repetición del arado en cada bajamar producirá un incremento en la acreción, ya que la playa intentará adoptar una forma más reflejante que sin el arado (con mayor anchura de la playa seca). Para ello, el arado debe ser aplicado únicamente en las fechas en que se prevea la incidencia de oleaje de calma (que produce acreción). Se requieren más investigaciones bajo un rango más amplio de condiciones de oleaje para determinar con mayor precisión los límites en los que el arado continúa siendo efectivo.

La técnica del arado de playas afecta únicamente al transporte de sedimento transversal producido estacionalmente. El arado es una solución respetuosa con la naturaleza aplicable a playas encajadas o costas en equilibrio dinámico. En playas en desequilibrio, el arado puede aplicarse para paliar los efectos de las variaciones estacionales, pero los problemas de erosión o acreción a largo plazo deben ser tratados separadamente (ej. mediante regeneraciones o bypass de arena). El uso apropiado de la técnica del arado permite conseguir playas más anchas al inicio de la temporada turística.

3.3. Evolución de las formas del lecho

Este apartado describe la metodología utilizada para procesar y extraer datos de las cámaras laterales que tomaron fotos del subcanal arado durante el conjunto de ensayos 2 (compuesto por dos ensayos de 4 h de duración). A continuación, se analiza la evolución morfológica del arado a partir de dichos datos y finalmente se evalúan los efectos del arado en la hidromorfodinámica comparando las mediciones de todos los sensores en los lados natural y arado.

Metodología

Para obtener datos a partir de las imágenes se siguió el siguiente procedimiento. Se extrajo la línea de contorno de la superficie de arena de cada una de las imágenes (cada 5 minutos). Se aplicó una corrección del efecto ojo de pez y luego se rectificaron los datos para transformar la posición de píxeles a coordenadas reales a lo largo del canal. Los datos extraídos de las imágenes se validaron con datos de escáner láser, mostrando una buena concordancia. Con esto se obtuvieron perfiles que muestran la evolución morfológica.

RESUMEN EN ESPAÑOL

El área de arena tenía una pendiente inicial uniforme de 1/100. Esta pendiente se sustrajo de los datos para obtener la geometría del arado (crestas y surcos), y el resultado se denominó perfil de pendiente corregida (SCP). La Figura 11 muestra los datos SCP, donde se observa el amortiguamiento del arado y su migración hacia la costa. Las crestas se representan con color rojo y amarillo, los surcos en azul y las áreas blancas no presentan ni erosión ni acumulación. Se formaron ripples sobre las crestas del arado que migraban más rápidamente hacia la costa. Tras las 4 h de ensayo el arado ya no puede identificarse, corroborando la adecuación de la duración elegida para los experimentos.

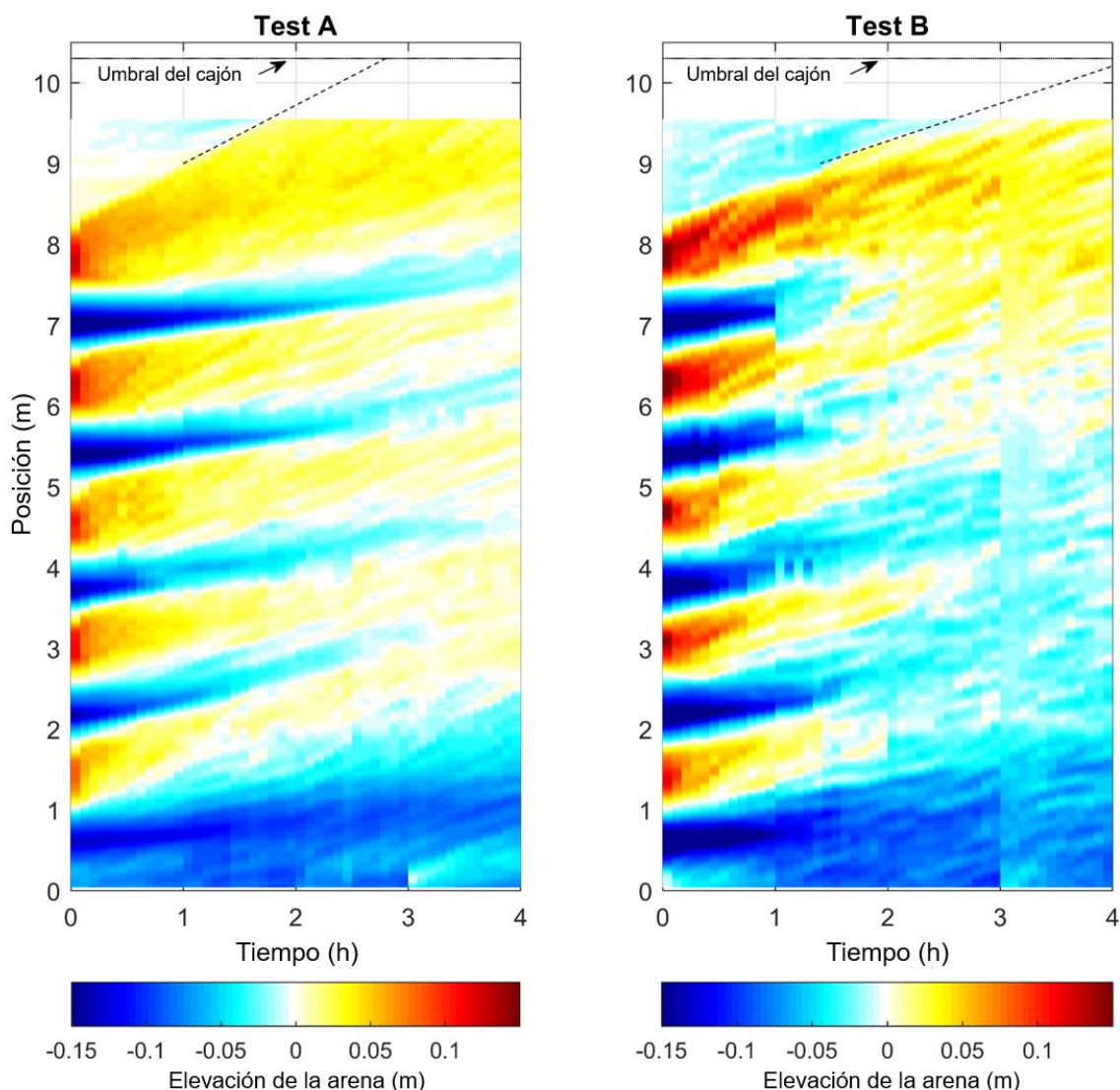


Figura 11 Serie temporal de datos SCP para el Test A y el Test B. De 9.5 a 10.3 m, no hay datos ya que el marco de la ventana de vidrio (ver Figura 7) impide la medición de la superficie de la arena. La línea discontinua indica la ubicación estimada del límite de avance del arado hasta alcanzar el umbral del cajón, cuando la arena comienza a caer directamente en el cajón de captura de sedimento.

Para obtener datos de la morfología de las formas del lecho se descartaron los extremos del canal por presentar efectos de contorno, quedándose únicamente con los datos SCP desde 2 a 8.5 m a lo largo del canal. A continuación, se realizó un análisis espectral de dicho recorte de los datos SCP y se separaron dos componentes por sus frecuencias tomando una longitud de onda de 0.4 m como punto de corte. Las frecuencias superiores contienen la componente del arado y otras formas de longitud de onda superior a 0.4 m (PC) y las frecuencias inferiores contienen la componente de los ripples (RC). La morfología de cada componente se analiza de forma separada a continuación.

Evolución morfológica del canal arado

En este apartado se analiza la altura, longitud de onda y velocidad de migración del arado (PC) y los ripples (RC) del subcanal arado. Para la componente del arado (PC) también se analizan las pendientes de barlomar y sotamar (de cara al mar y de cara a la costa respectivamente) y el área de las crestas. Como se muestra a continuación, casi todas las variables medidas para el arado presentan una evolución a lo largo de las 4 h de ensayo, mientras que los ripples se comportan de forma uniforme durante todo el periodo de estudio. Cuando no se obtuvo una evolución temporal compleja, los resultados se resumen en el formato $\mu_i \pm \sigma_i$, donde μ_i es el valor promedio en el tiempo de la característica i y σ_i es su desviación estándar.

La caracterización morfométrica del arado fue la siguiente:

- La longitud de onda resultó de 1.62 ± 0.05 m en los dos ensayos, y fue constante durante las 4 h de cada ensayo. El arado fue imposible de identificar tras 2 h de ensayo para el Test B.
- La altura inicial del arado fue de aproximadamente 0.3 m y disminuyó exponencialmente con el tiempo (ver Figura 12), reduciéndose a 0.12 m tras 1 h y por debajo de 0.06 m tras 2 h de acción del oleaje.
- Las pendientes (ver paneles derechos de la Figura 12) de sotamar y barlomar en las crestas aradas manualmente fueron de 34 y 23 grados, respectivamente, disminuyendo a 5 grados a las 3 h (posteriormente se mantienen alrededor de este valor).
- La velocidad de migración hacia la costa fue de 0.18 m/h para el Test A y de 0.25 m/h para el Test B durante la primera hora, disminuyendo a medida que transcurría el tiempo.
- El área inicial de las crestas aradas manualmente fue de 0.075 m^2 , disminuyendo exponencialmente a 0.006 m^2 después de 2 h (ver Figura 12).

RESUMEN EN ESPAÑOL

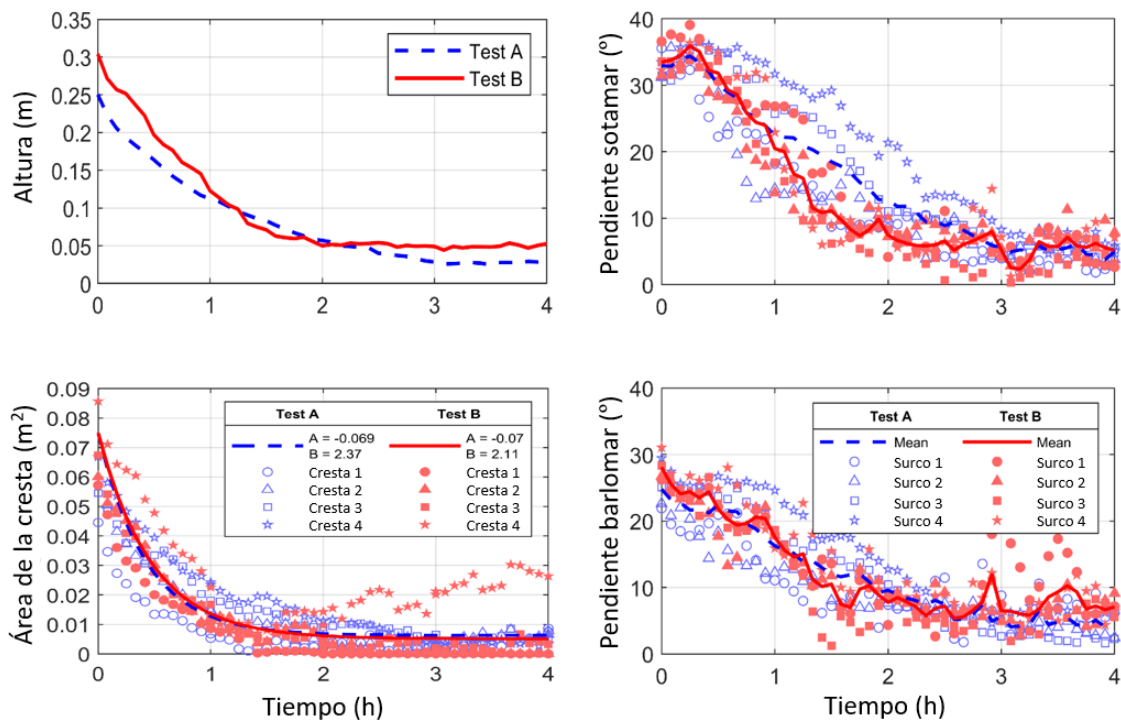


Figura 12 Evolución morfológica del arado. Las dos figuras de la derecha comparten leyenda.

Las características morfométricas de los ripples fueron las siguientes:

- Longitud de onda de 0.28 ± 0.01 m constante durante la duración del experimento.
- Altura de 0.011 ± 0.003 m para en Test A y 0.016 ± 0.004 m para el Test B.
- Velocidad de migración hacia la costa de 0.36 ± 0.15 m/h para el Test A y 0.33 ± 0.11 m/h para el Test B. Los ripples se formaron sobre las crestas del arado y migraron hacia la costa más rápidamente que las formas del arado.

Efectos del arado en la hidromorfodinámica

El arado modifica la morfología del perfil de la playa, lo que produce un efecto directo sobre la rugosidad del fondo, la propagación del oleaje y el transporte de sedimentos. Estos efectos se cuantifican en este apartado y se comparan con los de la geometría de natural empleada como control.

La rugosidad del fondo de arena se calculó a partir de datos de imágenes del lado arado cada 5 minutos. Estos resultados fueron validados con valores de rugosidad

obtenidos a partir de batimetrías de escáner láser del lado arado y comparados con el lado natural. La rugosidad se calculó como $k_\sigma = 4 \sigma_z$, donde σ_z es la desviación estándar de los puntos de la superficie respecto al fondo inicial con pendiente uniforme 1/100, medido en m. Los resultados (Figura 13) mostraron que la rugosidad disminuyó progresivamente debido a la acción del oleaje. Al comienzo, k_σ alcanzó 0.4 m, pero en solo 1 hora, más del 50% de la rugosidad generada artificialmente por el arado se perdió. La velocidad de suavizado disminuyó con el tiempo y la rugosidad se mantuvo casi constante ($k_\sigma \approx 0.11$ m para el Test A y $k_\sigma \approx 0.13$ m para el Test B) a partir de la segunda hora. La rugosidad en el lado natural aumentó al inicio, con la aparición de los ripples, pero se mantuvo siempre menor que en el lado arado. Al final de las 4 horas de olas, el arado aún presentaba rugosidad adicional en el fondo que podría afectar la propagación de las olas.

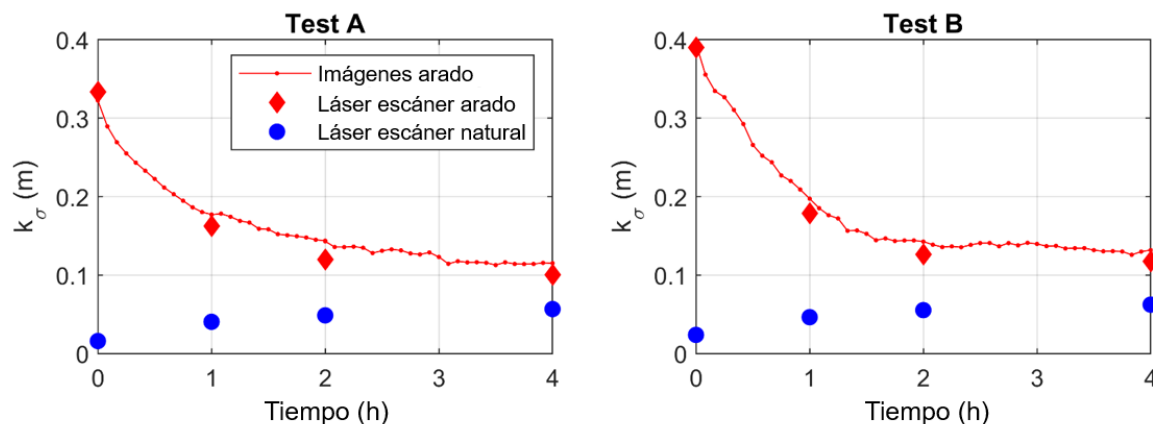


Figura 13 Rrugosidad del fondo arenoso calculada a partir de imágenes y batimetrías 3D con escáner láser para cada ensayo de laboratorio.

Se analizaron los datos de dos sensores de nivel (WG) localizados en el extremo más hacia la costa del área de arena, uno en cada subcanal. Se obtuvo la altura significante (H_s) en cada uno de ellos, y para cada hora de ensayo. Los resultados se han representado en la Figura 14 y muestran que en el lado arado la H_s siempre fue menor que en el lado natural, evidenciando la mayor disipación del oleaje producida por las crestas. La altura de ola medida junto a los generadores de oleaje fue de 0.3 m en ambos ensayos, por lo que en el Test A se produjo más disipación debido al menor nivel de agua que generó una mayor rotura del oleaje por fondo. Además, la reducción de la altura de ola en el lado arado fue mayor durante la primera hora, reduciéndose progresivamente a medida que los surcos y crestas se suavizaban. Esto revela que la rugosidad del fondo generada por el arado es la principal responsable de la mayor disipación del oleaje producida con esta técnica.

RESUMEN EN ESPAÑOL

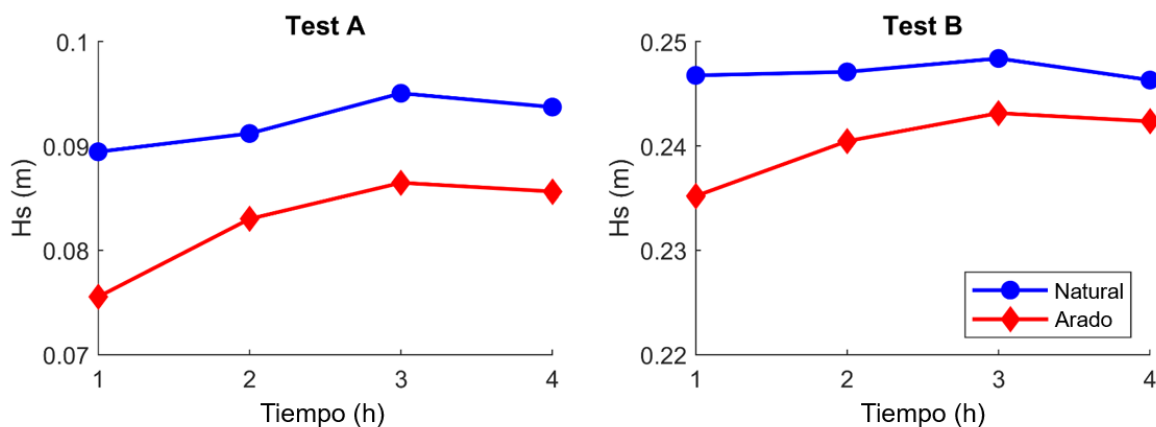


Figura 14 Altura de ola significante al final del área de estudio, en el extremo opuesto a los generadores de oleaje. Los círculos muestran los resultados del lado natural y los diamantes los resultados del lado arado.

La concentración de sedimento en suspensión (SSC) se midió a partir de los datos de los sensores OBS. En el Test A los valores de SSC fueron similares en ambos subcanales, mientras que en el Test B el SSC fue más alto en el lado arado durante la primera hora y luego disminuyó en las horas siguientes.

La migración de las formas del lecho genera un transporte de sedimento en la dirección en la que migran, en este caso hacia la costa, favoreciendo la acreción. Se ha calculado el transporte producido por el arado y los ripples en base a su velocidad de migración, su altura y las características de la arena. Los resultados revelan un transporte generado por la migración del arado de $Q_{\text{plough}} = 38 \text{ kg m}^{-1} \text{ h}^{-1}$ para el Test A y de $Q_{\text{plough}} = 61 \text{ kg m}^{-1} \text{ h}^{-1}$ para el Test B al inicio de los ensayos, el cual se reduce progresivamente a medida que las formas se atenúan, siendo este transporte inferior a $14 \text{ kg m}^{-1} \text{ h}^{-1}$ después de 1 h y menor que $9 \text{ kg m}^{-1} \text{ h}^{-1}$ tras 2 h. En el caso de los ripples, su migración generó un transporte $Q_{\text{ripples}} = 3.32 \text{ kg m}^{-1} \text{ h}^{-1}$ para el Test A y $Q_{\text{ripples}} = 4.43 \text{ kg m}^{-1} \text{ h}^{-1}$ para el Test B. Estos valores son inferiores a los calculados para el arado al inicio de los ensayos, pero se igualan durante la cuarta hora, soportando la hipótesis de Venditti et al. (2005) de que la tasa de transporte es invariantes a la escala si el tamaño y velocidad de migración de las formas son proporcionales (las formas pequeñas migran más deprisa). Los ripples migraron más rápido que el arado, sobre las crestas, ayudando a la migración del arado.

La acreción se midió tras 1 h, 2 h y 4 h de ensayo mediante la retirada y pesaje del sedimento capturado en los cajones colocados a sotavento de la zona de estudio. La Figura 15 muestra los resultados obtenidos. La tasa de acreción obtenida para las primeras 3 h del Test A fueron de 12.68 kg/h en el lado natural y de 17.79 kg/h en el lado arado, mientras

que el Test B se obtuvieron tasas de acreción de 20.76 kg/h en el lado natural y 22.64 kg/h en el lado arado durante la primera hora. En ambos ensayos se obtuvo mayor volumen de arena en el lado arado (40.30% más en el Test A y 30.85% más en el Test B). Esto prueba la efectividad de la técnica del arado a la hora de aumentar la acreción natural en playas.

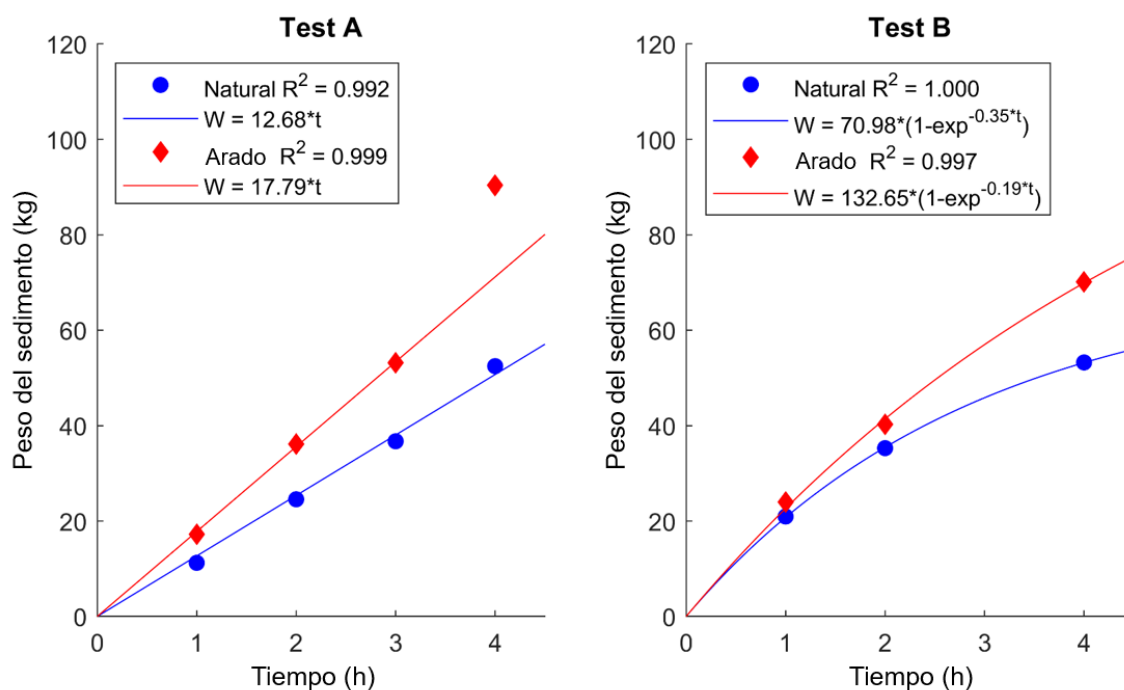


Figura 15 Peso acumulado del sedimento transportado en forma de acreción y capturado en el cajón desde el inicio de los ensayos.

Discusión

El arado artificial simulado en laboratorio tenía una longitud de onda de 1.62 m, una altura inicial de 0.3 m y migró hacia la costa a una velocidad de aproximadamente 0.2 m/h. La altura del arado se redujo con el tiempo debido a la acción del oleaje sobre las crestas, alcanzando una altura de 0.06 m en la segunda hora, que corresponde a la altura de equilibrio teórica para su longitud de onda, manteniéndose así hasta el final de los ensayos tras 4 h.

Sobre las crestas del arado aparecieron ripples con longitud de onda de 0.28 m, altura de 0.011 m y velocidad de migración hacia la costa de 0.36 m/h para Test A y 0.016 m (más alto) y 0.33 m/h (más lento) respectivamente para Test B, apoyando la idea de que cuanto más grandes las formas, más lento migran (Venditti et al., 2005). Además, el arado es mayor que los ripples y también migró más lentamente. Esta migración más rápida de los ripples

RESUMEN EN ESPAÑOL

sobre el arado permitió su contribución a la migración de la forma del lecho anfitriona. Reesink y Bridge (2007) identificaron este fenómeno, en el que formas del lecho más pequeñas ascienden por el lado de barlomar de la forma del lecho anfitriona y se avalanchan sobre el lado de sotamar, contribuyendo con sedimento a la migración de la forma del lecho anfitriona.

El transporte de sedimentos producido por la migración hacia la costa del arado y los ripples se calculó utilizando la ecuación de Huntley et al. (1991). Los ripples generaron una tasa de transporte constante de aproximadamente $4 \text{ kg m}^{-1} \text{ h}^{-1}$, mientras que el arado produjo una tasa de transporte de aproximadamente un orden de magnitud mayor al inicio, disminuyendo hasta que en la cuarta hora ambas tasas se igualaron. En la cuarta hora la altura del arado se redujo hasta la altura de equilibrio que corresponde a su longitud, y el transporte generado se vuelve invariante con la escala de las formas, tal y como propusieron Venditti et al. (2005).

Los resultados demuestran que el arado acelera la acreción de playas mediante dos mecanismos: aumentando la rugosidad hidráulica del fondo y la migración de las formas del lecho. Ambos mecanismos han sido propuestos previamente por otros autores y medidos en este estudio por primera vez. Guerrero et al. (2021) destacó la importancia de la migración de los ripples hacia la costa para la recuperación de la playa y apoyó su idea en el trabajo desarrollado por otros autores (Allen, 1968; Middleton and Southard, 1984; Reesink and Bridge, 2007; Venditti et al., 2005). Por otro lado, Gallagher et al. (1998b) analizó el efecto de las formas del lecho en la hidrodinámica a través de la modificación de la rugosidad hidráulica del fondo. Este efecto ha sido investigado por muchos autores (Dalrymple et al., 1978; Garcez Faria et al., 1998), y algunos de ellos afirmaron que las formas del lecho contribuyen a la hidrodinámica de la capa límite del fondo y al transporte de sedimentos (Miles et al., 2014). Juntos, ambos mecanismos naturales reforzaron la idea de Hunt y F.G.S. (1904) de que las formas del lecho son un factor importante para la erosión y recuperación de las playas. Además, en este caso particular de arado generado artificialmente, el movimiento del sedimento realizado por el tractor en cada marea baja también contribuye a la acumulación de sedimentos, por lo que se recomienda mover la arena de los surcos (en el lado del mar), hacia las crestas (en el lado de tierra).

4. REPERFILADO DE PLAYAS

El reperfilado de playas (Bruun, 1983) nació como una técnica de ingeniería respetuosa con la naturaleza para redistribuir arena en el perfil de la playa con el fin de aumentar la protección costera. Esta técnica evita la problemática necesidad de encontrar fuentes de arena para la regeneración de playas con cambios estacionales pero sin pérdidas de sedimento. El reperfilado de playas consiste en retirar mecánicamente una capa delgada (~0.3 m) de arena de la parte inferior de la zona intermareal y colocar la arena obtenida en la parte superior del perfil de la playa (para construir una duna o en el frente de playa). Tiene un efecto directo de remodelar la geometría del perfil de la playa, lo que automáticamente puede resultar en una playa seca más ancha (si se coloca la arena en el frente de playa). Esta técnica se utiliza frecuentemente en las costas australianas (Carley et al., 2010), donde se conoce como técnica de recuperación asistida (NABE, por sus siglas en inglés). Este nombre destaca un segundo efecto interesante de esta técnica: acelera los procesos naturales de acreción en las playas (Smutz et al., 1980), logrando una mayor protección costera con un menor impacto ambiental.

Dependiendo de la ubicación de las áreas de préstamo y relleno de arena, el reperfilado de playas presenta múltiples posibilidades. El objetivo de este apartado es determinar la técnica NABE más adecuada para acelerar la recuperación natural de la playa. Para lograr este objetivo, presentamos un análisis comparativo del efecto del reperfilado y el arado (ver apartado 3 para más detalles) basado en experimentos de laboratorio a escala reducida. Además, durante el verano de 2021 se probó el reperfilado en la playa de Fuentebraví, retirando la arena de la parte baja del área intermareal y llenando el frente de playa. Toda la información recopilada durante las campañas de campo se analiza aquí y se compara con los resultados del modelo físico.

Los ensayos a escala reducida consideraron el efecto simultáneo del oleaje y las mareas. Hasta donde llega el conocimiento de los autores, esta es la primera vez que se evalúa el reperfilado de playas bajo estas condiciones en laboratorio, lo que permite la validación de la hipótesis de Carley et al. (2010) y Smutz et al. (1980) que afirman que el reperfilado acelera la acreción. Aunque este apartado se centra en el reperfilado de playas, también se compara la efectividad del reperfilado con el comportamiento natural y con arado. Por lo tanto, este apartado (en combinación con el apartado 3) aborda los objetivos OB3, OB4, OB5 y OB6 de esta tesis. Este apartado 4 está estructurado de la siguiente manera: los experimentos de laboratorio se describen en el apartado 4.1 y los resultados se muestran en el apartado 4.2. Los estudios de campo realizados en la playa de Fuentebraví (Cádiz)

incluyendo el reperfilado se presentan y analizan en el apartado 4.3. Finalmente, la discusión de los resultados se detalla en el apartado 4.4.

4.1. Descripción de los experimentos de laboratorio

Los ensayos de laboratorio a escala reducida se realizaron en el Tanque de Oleaje Direccional (TOD) en las instalaciones de IHCantabria. El perfil de playa se reprodujo con sedimento sintético de baja densidad para reducir los efectos de escala en los procesos de transporte de sedimento. Ambas técnicas, el reperfilado y el arado, se analizaron bajo tres condiciones diferentes de oleaje (todas ellas generan acreción), incluyendo la simulación simultánea de mareas. En este apartado, se describe el cálculo de la escala y la configuración experimental utilizada.

Cálculo de la escala

El modelado de laboratorio a escala reducida con lecho móvil sigue siendo un desafío actualmente. Aún no se conocen metodologías que permitan reproducir todos los parámetros adimensionales que determinan la hidrodinámica costera y el transporte de sedimentos en modelo físico a escala reducida. El estado del arte recoge dos enfoques: el uso de sedimento real con la misma densidad que en la naturaleza, y el uso de sedimento sintético de baja densidad. El sedimento real hace que los efectos de escala sean inevitables. En esta tesis se presentan relaciones para lograr la similitud de 4 de los 5 parámetros adimensionales que serían necesarios, y se discute las implicaciones que tiene la falta de similitud del último parámetro requerido. Los parámetros adimensionales considerados y las ecuaciones resultantes se describen a continuación.

El número de Froude es la relación entre las fuerzas iniciales y gravitacionales. La similitud del número de Froude en el flujo del prototipo y el modelo implica que las escalas de tiempo (λ_t) y velocidad (λ_v) pueden expresarse en función de la escala de longitudes (λ_l) mediante la ecuación (1):

$$\lambda_t = \lambda_v = \sqrt{\lambda_l} \quad (1)$$

Para asegurar la similitud del transporte por fondo del sedimento expuesto al oleaje y corrientes se emplean: el número de Shields y el número de Reynolds de grano.

El número de Shields controla el inicio del movimiento del sedimento. Su similitud en prototipo y modelo arroja la siguiente relación (ecuación (2)) entre la escala de tamaño de grano de las partículas (λ_d), la escala de densidad relativa sumergida (λ_Δ), y la escala de longitudes.

$$\lambda_d = \frac{\lambda_l}{\lambda_\Delta^{2.083}} \quad (2)$$

El número de Reynolds de grano controla la forma de la capa límite del fondo. La similitud de este parámetro implica la relación de la ecuación (3) que involucra la escala del tamaño de grano, la escala de la viscosidad cinemática del agua (λ_v), y la escala de longitudes.

$$\lambda_d = \lambda_v^{0.794} \lambda_l^{-0.19} \quad (3)$$

Asumiendo que el fluido empleado en los experimentos es agua, los únicos parámetros que se pueden variar son el tamaño y densidad del sedimento. Las ecuaciones (2) y (3) permiten determinar ambos parámetros una vez escogida la escala de longitudes.

En la zona de rompientes el transporte en suspensión cobra gran importancia. El parámetro adimensional de caída de grano, Ω , (Dean, 1973; Gourlay, 1968) involucra la altura de ola (H_s), su periodo (T_p), y la velocidad de caída de las partículas de sedimento (w), que son las variables fundamentales involucradas en el transporte en suspensión. Por ello este parámetro adimensional se considera adecuado para el escalado de los procesos en la zona de rompientes.

Por último, el número de Rouse (R_o), se utiliza para discriminar entre transporte por fondo y en suspensión.

En nuestro estudio, la escala de longitudes se determinó de forma que el perfil de playa tuviera cabida dentro del tanque de oleaje, resultando una escala de longitudes $\lambda_l = 8$. A partir de esta escala, mediante las ecuaciones (2) y (3), se calculó el tamaño de grano y densidad del sedimento objetivo ($d_{50t} = 0.379$ mm y $\rho_{st} = 1496$ kg/m³). La densidad del sedimento escogido para los ensayos está restringida a las densidades de los materiales disponibles en el mercado. En este estudio se empleó sedimento sintético de características

RESUMEN EN ESPAÑOL

muy similares a los valores objetivo ($d_{50} = 0.37$ mm y $\rho_s = 1500$ kg/m³). Con este sedimento, las escalas resultantes para los 5 parámetros adimensionales escogidos son:

- Número de Froude: $\lambda_F = 1$
- Número de Shields: $\lambda_\theta = 0.997 \cong 1$
- Número de Reinolds de grano: $\lambda_{Re^*} = 1.034 \cong 1$
- Número adimensional de caída de grano (Dean): $\lambda_\Omega = 1.835$
- Número de Rouse: $\lambda_{Ro} = 1.016 \cong 1$

Con el sedimento sintético elegido, 4 de los 5 parámetros (Froude, Shields, Reynolds de grano y Rouse) fueron similares en el prototipo y el modelo. Sin embargo, el parámetro adimensional de caída de grano fue mayor en el prototipo que en el modelo, lo que significa que la playa en el modelo tendería a ser más reflejante que el prototipo.

Configuración experimental

Los ensayos se llevaron a cabo en el Tanque de Oleaje Direccional (TOD) en las instalaciones de IHCantabria. El TOD es un tanque de 28 m de longitud, 8.6 m de ancho y 1.2 m de altura. El tanque se dividió longitudinalmente en 10 canales (Figura 16), seis de ellos se utilizaron para probar diferentes técnicas de recuperación asistida (NABE) bajo las mismas dinámicas marinas, y los cuatro restantes se utilizaron como pasillos de acceso a los perfiles de ensayo para realizar el reperfilado y arado. Cada canal tuvo un ancho de 0.8 m, minimizando los efectos de contorno en el centro de cada canal, donde se realizaron mediciones geométricas del perfil en cada bajamar con un perfilador láser.



Figura 16 Tanque de oleaje direccional (TOD) durante los ensayos.

El sedimento sintético se colocó con una pendiente uniforme inicial de 1/21, y se simularon dos ciclos de marea de olas ligeramente enérgicas ("olas pre-test", Tabla 1) para obtener un perfil de playa disipativo típico de primavera, al comienzo de la temporada de buen tiempo. Luego, se simuló el clima marino de cada ensayo (A, B o C, ver Tabla 1) hasta que se alcanzó la máxima acreción en el frente de playa. Este proceso se repitió para cada ensayo. Todas las simulaciones incluyeron una variación simultánea del nivel del mar de acuerdo con una marea semidiurna con un rango de marea de 2.4 m para el Test A y 1.6 m para los Test B y C.

Tabla 1 Dinámicas marinas simuladas en escala prototipo y modelo.

Config. de oleaje	Prototipo				Modelo			
	H_{sp} (m)	T_{pp} (s)	$Marea_p$ (m)	Ω_p	H_{sm} (m)	T_{pm} (s)	$Marea_m$ (m)	Ω_m
Pre-test A	1.60	6.50	2.40	7.98	0.20	2.30	0.30	4.28
Pre-test B	1.60	6.50	1.60	7.98	0.20	2.30	0.20	4.28
Pre-test C	1.60	6.50	1.60	7.98	0.20	2.30	0.20	4.28
Test A	0.48	8.50	2.40	1.84	0.06	3.00	0.30	0.99
Test B	0.32	8.50	1.60	1.22	0.04	3.00	0.20	0.66
Test C	0.264	4.72	1.60	1.81	0.033	1.67	0.20	0.97

Estas dinámicas marinas afectaron por igual a los seis canales llenos de sedimento sintético. Cada uno de ellos se utilizó para probar una técnica de NABE diferente. La Tabla 2 resume las características de las técnicas ensayadas en cada canal.

Tabla 2 Características de las técnicas NABE ensayadas en cada canal.

	Acrónimo	Técnica	Zona de préstamo	Zona de vertido
Canal 1	PLOUGH	Arado		Surcos y crestas
Canal 2	NAT	Natural	Sin movimiento de arena – Control	
Canal 3	L2B	Reperfilado	Intermareal bajo	Barra intermareal
Canal 4	L2BF	Reperfilado	Intermareal bajo	Frente de playa
Canal 5	L2D	Reperfilado	Intermareal bajo	Duna o playa seca
Canal 6	U2D	Reperfilado	Intermareal alto	Duna o playa seca

El reperfilado a escala prototipo tuvo una profundidad de 0.25 - 0.3 m (recomendado por Carley et al. (2010)) y un ancho de la zona de préstamo de 11.2 m, representando un volumen de 3 m³/ml de arena movilizada. El arado a escala prototipo tuvo una longitud de ~1.5 m y amplitud de ~0.25 m.

4.2. Resultados

Este apartado muestra los resultados obtenidos en los experimentos de laboratorio. El análisis se basó en la geometría del perfil de la playa medido en cada bajamar durante los ensayos. Este apartado muestra (1) la formación de la berma durante condiciones de oleaje de calma, (2) un análisis del aumento del ancho de la playa seca y las características geométricas de la berma en el estado de máxima acreción alcanzado, y (3) el estudio del volumen de acreción. Estos resultados permiten la comparación entre las técnicas NABE y el análisis de su efectividad en términos de aumento del área de playa seca e incremento de la acreción. Todos los resultados presentados en esta sección se muestran en escala prototipo.

Formación de la berma

La Figura 17 muestra la evolución de la berma para cada ensayo y canal, incluyendo el perfil inicial obtenido después de la simulación de las olas de pre-test, el perfil inicial con las técnicas NABE aplicadas y el perfil de máxima acreción lograda en la berma de playa. También se presentan los niveles de pleamar, setup y runup como referencia.

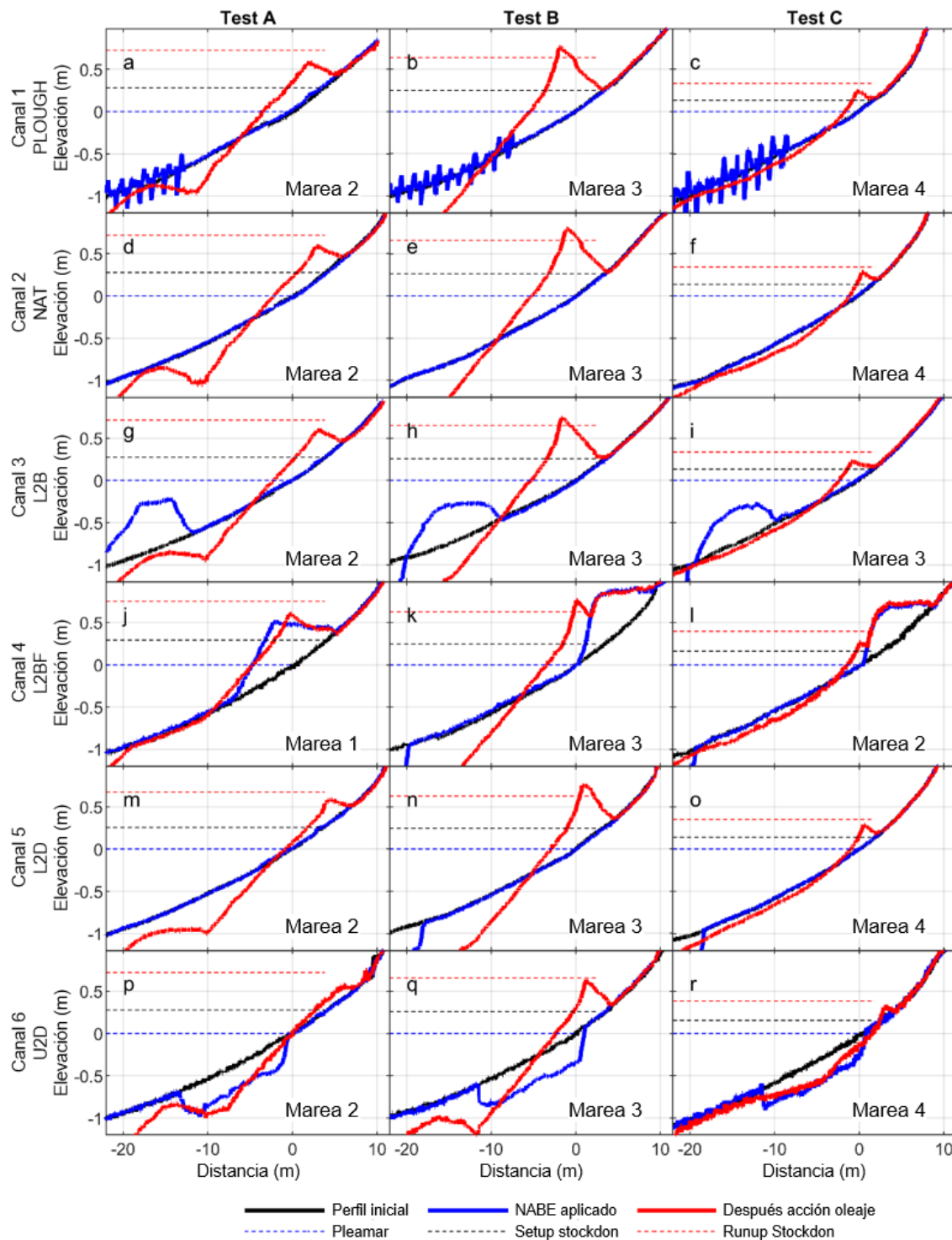


Figura 17 Evolución del perfil de playa hasta alcanzar la máxima acreción en el frente de playa. Las técnicas de recuperación asistida se describen en la Tabla 2 (ver acrónimos).

Cada panel indica el número de ciclos de marea que fueron necesarios para alcanzar la acreción máxima.

RESUMEN EN ESPAÑOL

Se formó una berma en el perfil final de la playa para todos los ensayos y en todos los canales. Esta berma tuvo una forma semejante para todos los canales de cada ensayo (A, B o C). Esto indica que la técnica NABE utilizada no determina la geometría de la berma. Sin embargo, la forma de la berma fue diferente entre los ensayos realizados en el mismo canal. La altura y pendiente de la berma en el frente de playa cambiaron según las dinámicas marinas, como se muestra en la siguiente sección.

Aumento del ancho de playa seca y características de la berma

Se calculó el avance de la línea de costa (aumento del ancho de playa seca) como la diferencia entre las posiciones de la costa (al nivel del setup) al inicio de cada ensayo y en el momento de máxima acreción. Este avance se representa en la Figura 18 junto con la cota máxima de la berma. En la Figura 17 puede verse que esta cota fue similar al nivel del runup, y durante los ensayos se vio que las olas más grandes sobrepasaban la cresta de la berma, depositando arena sobre ella y haciéndola crecer en altura. Como se observa en la Figura 18 la cota de la berma ha resultado ser similar para todos los canales de cada ensayo, y dependiente por tanto de las dinámicas marinas, pero no de la técnica NABE. Resulta notorio que la berma creada artificialmente con la técnica L2BF modifica su cota (marcadores vacíos) hasta alcanzar la misma cota que en el perfil natural.

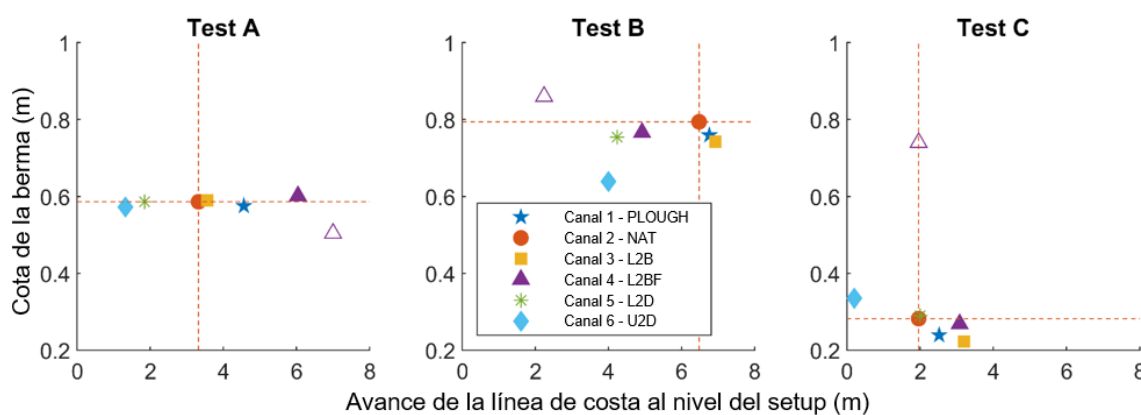


Figura 18 Cota de la berma y avance de la línea de costa alcanzados en el momento de máxima acreción. Las líneas discontinuas se muestran como referencia de las características de la berma formada bajo condiciones naturales. Los marcadores vacíos indican las características de la berma creada artificialmente por el reperfilado L2BF.

El avance de la línea de costa debido al arado (Canal 1) fue de media del 23.41% más que el producido en condiciones naturales. Esto indica que el arado es una técnica innovadora y efectiva para aumentar la acreción. El efecto del reperfilado en el avance de la línea de costa dependió de la ubicación de las áreas de préstamo y vertido de arena. El

Canal 3 (L2B) tuvo un avance de la costa de media de un 25.76% superior al natural. La posición inicial de la línea de costa en el Canal 4 (después del reperfilado mecánico L2BF) en unos casos produjo ancho de playa seca superior al alcanzado de forma natural y en otros inferior. Tras la acción del oleaje el avance de la línea de costa varió entre un 24.07% menos hasta un 81.93% más que el natural. Esto indica que el diseño de la forma de la berma de relleno y su volumen son determinantes para la efectividad de esta técnica. En el Test B el relleno se ubicó en una zona muy alta, prácticamente fuera de la zona afectada por las dinámicas marinas, mientras que el volumen de arena de préstamo fue grande. El déficit de arena producido en el perfil activo hizo que el oleaje no fuera capaz de producir el mismo avance que en el perfil natural. Se encontró un escenario similar para los Canales 5 y 6 (L2D y U2D respectivamente). En ambos Canales, hubo un déficit de sedimento en el perfil de playa activo debido al volumen de arena retirada del área de préstamo y colocada en la duna (fuera del área de acción de las olas durante el verano). L2D logró un avance de la línea de costa final medio de un 25.70% menos que en condiciones naturales. U2D mostró avances un 62.77% inferiores al natural de media.

Se calculó la pendiente en el frente de playa (β_s) al nivel de pleamar, mostrando variabilidad entre ensayos, pero no entre canales, al igual que la cota de la berma. Por tanto, la pendiente (y la cota de la berma, y por tanto la geometría de la berma) únicamente depende de las dinámicas marinas, pero no de la técnica NABE empleada. Las técnicas de recuperación asistida analizadas influyen en el avance de la línea de costa alcanzado, o lo que es lo mismo, la posición de la berma, pero no en su geometría.

Volumen de acreción

El volumen de sedimento acumulado en forma de acreción en la berma de la playa se calculó integrando el área entre el perfil inicial obtenido después de las olas de pre-test y el perfil correspondiente a la máxima acreción lograda. Para los Canales 4 y 6 (L2BF y U2D), debido a la ubicación de las áreas de relleno y préstamo, también se consideró el perfil con la técnica NABE aplicada para el cálculo del volumen. Por lo tanto, se obtuvieron dos cálculos de volumen para los Canales 4 y 6, uno referido al perfil de las olas de pre-test y el otro al perfil después de aplicar las técnicas NABE. La Figura 19 muestra los resultados obtenidos para cada ensayo y canal.

RESUMEN EN ESPAÑOL

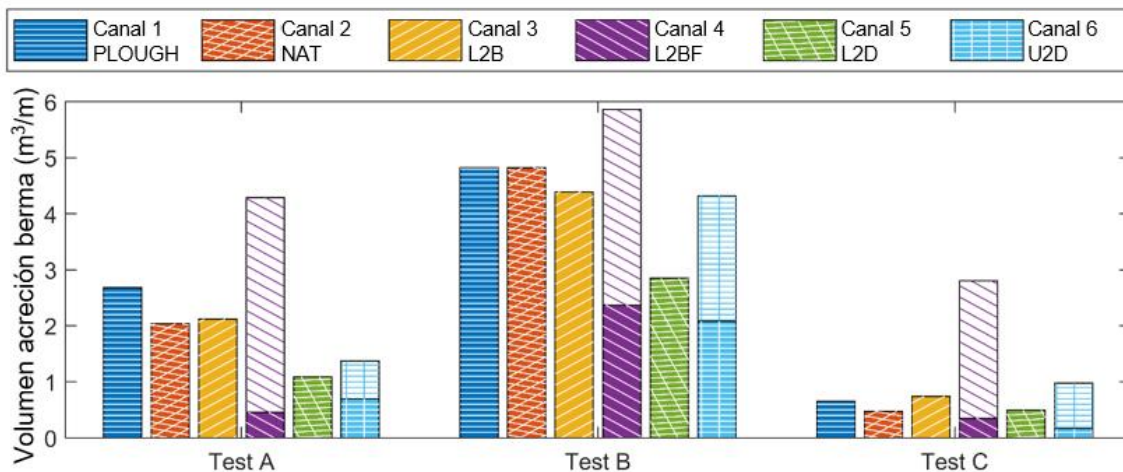


Figura 19 Volumen de acreción en la berma. La barra del Canal 4 muestra los volúmenes de sedimento movilizados manualmente por el reperfilado (relleno blanco con líneas descendentes) y por acción de las olas (relleno morado). La barra del Canal 6 representa todo el volumen movilizado por la acción del oleaje, incluido el volumen de sedimento en la berma (relleno azul) y el volumen de sedimento que llenó parcialmente el área de préstamo (relleno blanco con cruz azul).

El Canal 2 muestra el comportamiento natural de la playa, en el que el volumen acumulado varió dependiendo de las dinámicas marinas simuladas. El mayor volumen se obtuvo para el Test B, que tuvo el parámetro adimensional de caída más bajo (Ω), conduciendo a una playa más reflejante. Estas consideraciones son aplicables a todos los demás canales puesto que habían experimentado las mismas condiciones de oleaje.

Los volúmenes acumulados al aplicar el arado fueron 31.79% y 37.62% mayores que el control para los Tests A y C, respectivamente, e iguales al control para el Test B. Esto demuestra que la técnica del arado puede aumentar la acreción al lograr un mayor volumen de sedimento en la berma y una playa seca más amplia.

El volumen acumulado mediante el reperfilado L2B fue un 4.23% mayor que el control para el Test A, un 8.90% menor para el Test B y un 56.21% mayor para el Test C. Los tres ensayos mostraron más progradación de la línea de costa que el control. El volumen de relleno en la barra intermareal fue de $\sim 3 \text{ m}^3/\text{ml}$, un valor mayor que el volumen acumulado para los Tests A y C, por lo que parte de la arena de la barra fue transportada hacia el mar por el oleaje.

El reperfilado L2BF generó una berma final compuesta tanto por la arena movida artificialmente como por el sedimento naturalmente recuperado por el oleaje. En todos los

ensayos, el volumen final de la berma fue mayor que el del control (110.68%, 21.55% y 491.26% para los Tests A, B y C respectivamente), aunque el volumen de sedimento movilizado por el oleaje fue menor que del control (77.75% en el Test A, 50.89% en el Test B y 26.36% en el Test C). En los Tests A y C el volumen movilizado por la maquinaria ($3 \text{ m}^3/\text{ml}$) fue superior al de la berma natural. Por ello el oleaje únicamente movilizó una pequeña fracción de sedimento, el necesario para que la berma adoptase su geometría de equilibrio de acuerdo a las dinámicas marinas. En el Test B, el volumen de arena movido artificialmente fue menor que el volumen de la berma del perfil de control y las olas pudieron movilizar el 40.41% del volumen total de la berma final del Canal 4. A pesar de eso, la progradación de la línea de costa en el Test B fue menor que en el control. En conjunto, el sedimento reperfilado depositado en el frente de playa no fue erosionado por el oleaje y se produjo acreción natural adicional. Por lo tanto, la técnica de reperfilado L2BF sirvió para incrementar el volumen de arena en la playa seca, que puede actuar como reserva para afrontar las tormentas el invierno.

El reperfilado L2D consiguió una acreción un 46.44% menor que el control para el Test A, un 40.92% menor para el Test B y un 4.22% mayor para el Test C. En esta configuración el volumen de arena que se extrajo del perfil de playa activo fue de $\sim 3 \text{ m}^3/\text{ml}$, que sumado al volumen de acreción excedió el volumen del perfil de control. Por lo tanto, se recuperó un mayor volumen de arena de la parte inferior del perfil de playa y se depositó en el frente de playa y en la zona regenerada artificialmente para hacer frente a la erosión de los temporales del invierno.

El área de préstamo fue el intermareal bajo para las tres últimas configuraciones descritas. Sin embargo, se obtuvo más acreción con el reperfilado L2B, seguido de L2D y finalmente L2BF. Esto indica que la zona de vertido influye en la capacidad de acreción del oleaje.

En el reperfilado U2D, a diferencia del L2D, se extrajo el sedimento del área intermareal alta. En este caso, el sedimento acumulado llenó parcialmente el área de préstamo ubicado junto a la pleamar. El volumen total acumulado fue un 32.68% menor que el control en el Test A, un 10.33% menor en el Test B y un 106.18% mayor en el Test C. Una gran parte de este sedimento se depositó en la zona de préstamo, generando por tanto menores avances de la línea de costa. De hecho, U2D mostró las posiciones de línea de costa más retrocedidas, aunque la cantidad total de sedimento capturado de la parte inferior del perfil de playa fue la mayor de todos los canales (considerando el volumen acumulado por el oleaje y los $3 \text{ m}^3/\text{ml}$ extraídos del área de préstamo). La extracción de arena del área

intermareal superior lleva a una mayor acreción debido a la generación de una geometría del perfil más disipativa.

4.3. Campañas de campo

La técnica de reperfilado L2BF fue aplicada en la parte central de Fuentebravía (ver descripción de la playa en apartado 2.1) el 12 de mayo de 2021. El área reperfilada tuvo una longitud de 250 m a lo largo de la costa, con una zona de préstamo de 0.3 m de profundidad y 15 m de ancho localizada en el intermareal bajo (junto a la bajamar) y una zona de relleno en el frente de playa de 15 m de ancho. La Figura 20 muestra las operaciones de reperfilado realizadas.



Figura 20 Motoraillas realizando el reperfilado de la playa de Fuentebravía.

A ambos lados de la zona reperfilada se disponía de tramos de playa de control. Se realizaron 13 campañas de campo entre mayo y octubre de 2021 recogiendo la evolución de 7 perfiles de playa (3 en la zona reperfilada y 2 de control a cada lado) cuya ubicación se muestra en la Figura 21. Los datos fueron obtenidos mediante un dispositivo RTK-GPS de alta precisión gracias a la colaboración con la Demarcación de Costas Andalucía Atlántico (Ministerio para la Transición Ecológica y el Reto Demográfico).

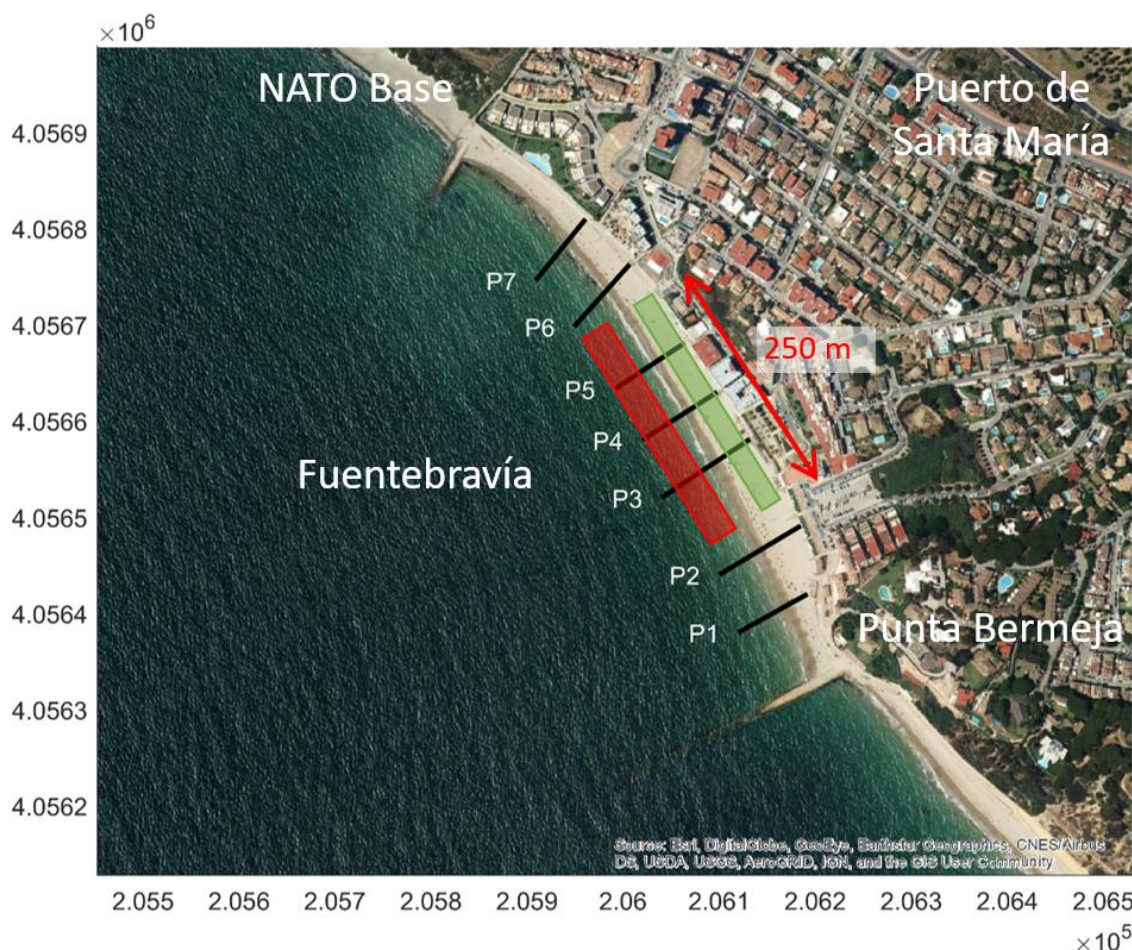


Figura 21 ÁREA REPERFILADA (rojo: área de préstamo, verde: área de vertido) y localización de los perfiles medidos.

En la Figura 22 se compara la evolución del perfil P2 (natural) y P4 (reperfilado). Los gráficos superiores muestran los perfiles medidos justo tras el reperfilado. En los gráficos centrales se incluye el siguiente perfil medido 15 días después, donde se observa que el perfil reperfilado ha avanzado 3.68 m más y acumulado un 24% más de arena, consiguiendo una playa más ancha. Los gráficos inferiores muestran todos los perfiles medidos. Se observa que tras la primera acreción más rápida del perfil reperfilado, posteriormente se ralentiza su recuperación, dejando margen para que el perfil natural alcance los mismos niveles de acreción durante el mes de junio. El comportamiento posterior de ambos perfiles es similar al comportamiento natural descrito en el apartado 2.2. Por ello, el efecto acelerador de la recuperación de la playa del reperfilado parece limitado a unas pocas semanas tras la acción de la maquinaria.

RESUMEN EN ESPAÑOL

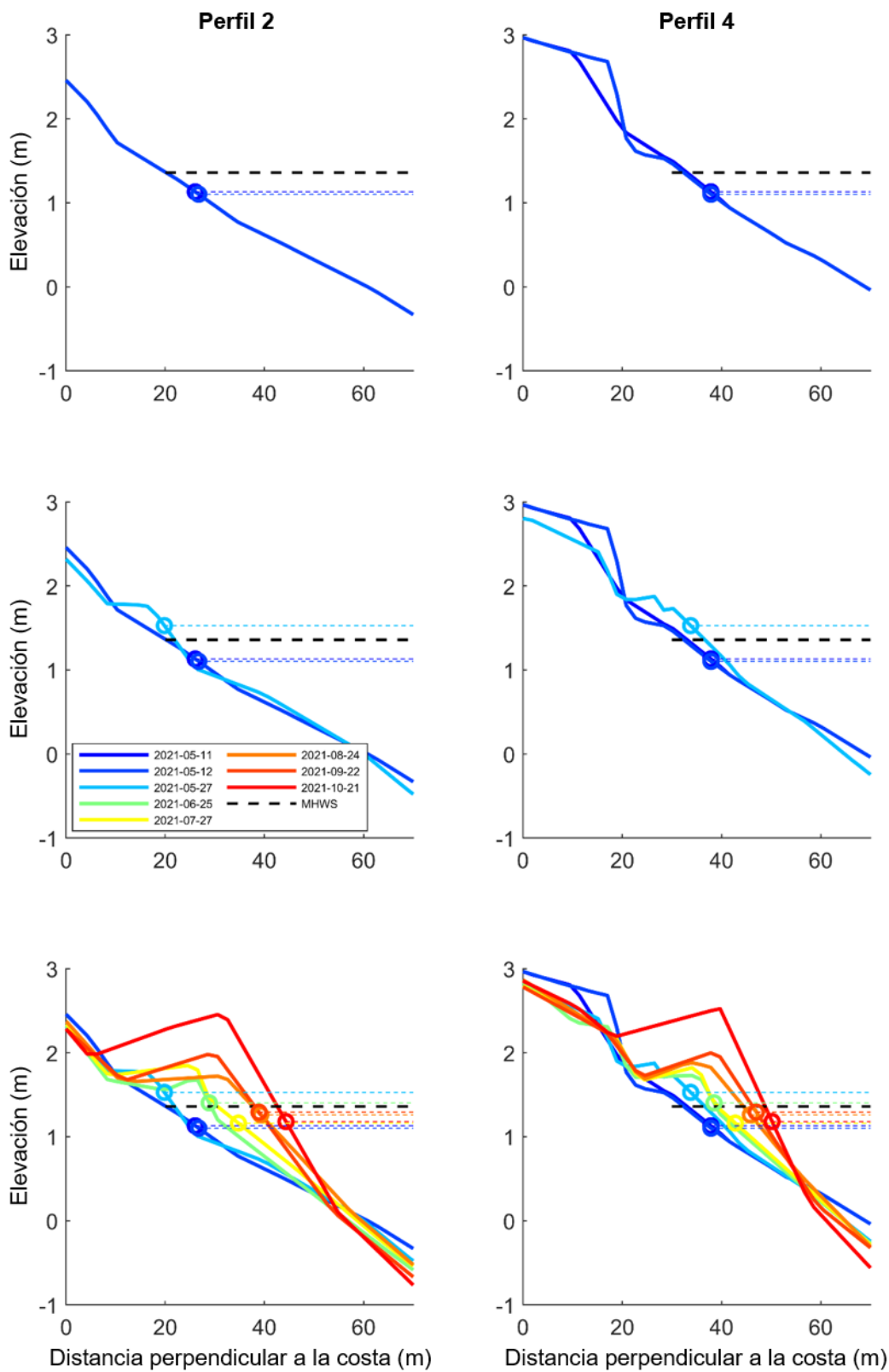


Figura 22 Comparativa de la evolución de los perfiles P2 (natural) y P4 (reperfilado).

4.4. Discusión

Las técnicas NABE se han aplicado en muchas playas, aunque su efecto real sobre la acreción no se había comprobado hasta ahora. El diseño de estas técnicas debe ser acorde al objetivo del proyecto (Carley et al., 2010) y tener en cuenta las dinámicas marinas y eólicas locales, así como aspectos ecológicos. La profundidad máxima recomendada para el área de préstamo a reperfilar es de 0.3 m para playas arenosas (Bruun, 1983) y el volumen debe ser menor que la tasa de recuperación natural de la playa (McNinch y Wells, 1992; Tye, 1983) integrada a lo largo de la temporada de verano. Nuestros experimentos de laboratorio siguieron estas recomendaciones, aunque fue difícil estimar la tasa de recuperación natural de la playa sin monitorizaciones de las temporadas de verano previas (en el prototipo) o pruebas anteriores de las condiciones naturales (en el laboratorio). Además, se encontró que la tasa de recuperación depende de las dinámicas marinas y cambia de una playa a otra. Este resultado indica que es necesario realizar un seguimiento de la evolución de perfiles de playa durante el verano antes de diseñar actuaciones de reperfilado sobre las mismas.

Este estudio muestra que la selección de la técnica NABE más adecuada debe realizarse de acuerdo con el objetivo de cada proyecto de gestión costera específico. Para lograr una playa seca más amplia, las técnicas más adecuadas fueron el arado (PLOUGH) o el reperfilado del área intermareal baja ampliando la berma de la playa (L2BF) o creando una barra intermareal (L2B). Para la regeneración de dunas o la protección contra los temporales del invierno, la mejor solución es reperfilar, ya sea la zona intermareal baja o alta (L2D o H2D), y utilizar la arena para la regeneración de la zona subaérea de la playa. Se ha de tener en cuenta que en el laboratorio solo se probaron condiciones marinas poco energéticas. Esto significa que los resultados obtenidos sólo son válidos para actuaciones NABE realizadas en primavera cuando se espera buen tiempo después (durante las temporadas de primavera y verano).

Smutz et al. (1980) afirmaron que al aplicar el reperfilado, cuanto menos pendiente tenga el perfil próximo a la costa, mayor será la acreción. Esta afirmación se ha confirmado en nuestros ensayos. El reperfilado U2D genera un perfil más tendido que el L2D y se ha medido que produce una mayor acreción.

Se ha observado que en laboratorio la cota de la berma concuerda con la cota de pleamar más el runup. Como en el laboratorio todos los ciclos de marea fueron iguales, esta magnitud se corresponde con el nivel del mar total superado un 1% del tiempo ($TWL_{1\%}$), el cual se relacionó con el nivel de la berma en playas naturales en el apartado 2.2. Esta

RESUMEN EN ESPAÑOL

magnitud da una primera estimación de la cota de la berma que puede ser empleada para el diseño de la berma creada mecánicamente en el reperfilado L2BF.

El uso de la arena reperfilada para la regeneración de dunas permite disponer de más sedimento para hacer frente a la erosión durante el invierno. Cuando se reperfila la playa con el fin de regenerar la duna, se deben considerar algunos aspectos, como el diseño de la duna, la disponibilidad de espacio y la dinámica eólica (“Coastal Dune Management,” 2001). Pellón et al. (2020) proporcionaron herramientas útiles para el diseño de dunas. La ubicación del pie de las dunas primarias y su volumen se pueden determinar en función de las condiciones marinas y eólicas locales. También se recomienda cercar y plantar la zona, ya que la arena vertida puede erosionarse hacia el mar por la acción de grandes temporales de oleaje, o hacia tierra por la acción del viento (Conaway y Wells, 2005).

El impacto ecológico de las técnicas NABE debe ser considerado en detalle, ya que el área intermareal constituye el hábitat y la zona de anidamiento y reproducción de muchas especies (Dare, 2003; Govarets and Lauwers, 2009). Las acciones NABE se consideran perturbaciones a corto plazo (Speybroeck et al., 2006) y se espera que las especies se recuperen rápidamente (Smith et al., 2011). El momento de las acciones debe escogerse para mitigar los posibles efectos negativos (Crain et al., 1995; Erskine and Thompson, 2003).

Los resultados obtenidos en la playa de Fuentebravía concuerdan con los resultados de laboratorio para el canal reperfilado L2BF. En ambos casos se acelera la acreción y se pone de manifiesto la importancia que tiene el diseño de la berma artificial para el máximo aprovechamiento de la arena reperfilada.

5. METODOLOGÍA PARA LA APLICACIÓN DE TÉCNICAS DE RECUPERACIÓN ASISTIDA DE PLAYAS

Los gestores de la costa demandan herramientas y metodologías para implementar Soluciones basadas en la Naturaleza (SbN) de manera efectiva, con el objetivo de mejorar la resiliencia de las playas. Esta tesis analiza las técnicas de recuperación asistida (NABE) que han sido concebidas para acelerar la acreción de arena minimizando las acciones humanas y aprovechando el trabajo realizado por la naturaleza. Estas técnicas abordan la creciente demanda de mayores anchos de playa para turismo, al tiempo que garantizan su sostenibilidad a largo plazo frente a los impactos de las grandes tormentas invernales. Aunque el reperfilado y el arado son herramientas valiosas para los gestores costeros, su aplicación debe ejercerse con cautela y solo en las ubicaciones apropiadas para ello. Es

importante tener en cuenta que estas herramientas por sí solas no pueden resolver problemas de erosión persistente, que a menudo requieren un análisis exhaustivo de las causas subyacentes y las acciones correctivas apropiadas. Para evitar el uso inadecuado de esas técnicas NABE, este apartado describe una metodología para seleccionar y diseñar acciones para lograr los objetivos de manejo costero específicos de cada sitio.

La siguiente metodología, descrita en el apartado 5.1, fue diseñada de acuerdo a la experiencia y conocimientos adquiridos durante el desarrollo de esta tesis. Comprende todas las recomendaciones recogidas en el estado del arte y los nuevos conocimientos descritos en los apartados anteriores. Posteriormente, el apartado 5.2 incluye una discusión de la metodología propuesta. Este capítulo cumple con el objetivo OB7 de esta tesis.

5.1. Metodología

La metodología para la aplicación de las técnicas del arado o reperfilado se esquematiza en la Figura 23 y se divide en tres pasos fundamentales:

- (1) Elección de la técnica NABE más apropiada mediante un árbol de decisión.
- (2) Decisión de que días es apropiado o no aplicar una técnica NABE mediante un sistema operacional.
- (3) Diseño de las acciones NABE. Este paso se divide en 3 opciones de acuerdo con la técnica seleccionada en el paso 1.

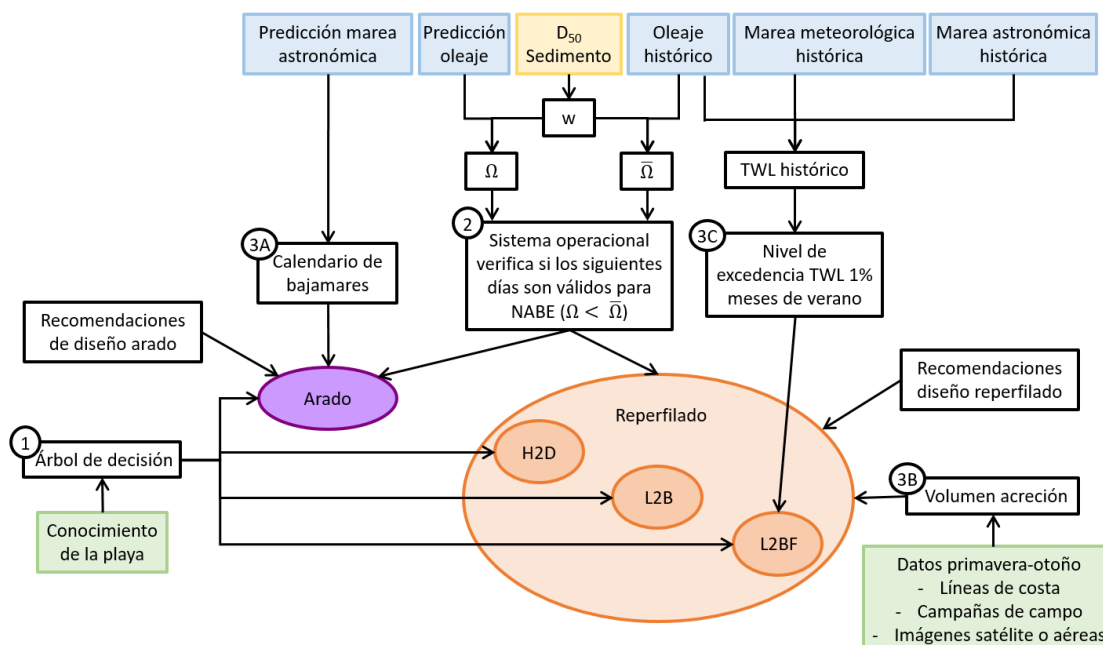


Figura 23 Metodología para la aplicación de técnicas NABE.

RESUMEN EN ESPAÑOL

Paso 1: Árbol de decisión

La elección de la técnica NABE más apropiada para cada sitio de estudio debe hacerse con la ayuda del árbol de decisión de la Figura 24. El diagrama indica el tipo de playas en el que estas técnicas pueden aplicarse y permite su elección a través de unas preguntas sencillas sobre aspectos básicos de la playa de los que el gestor de la costa debe tener conocimiento.

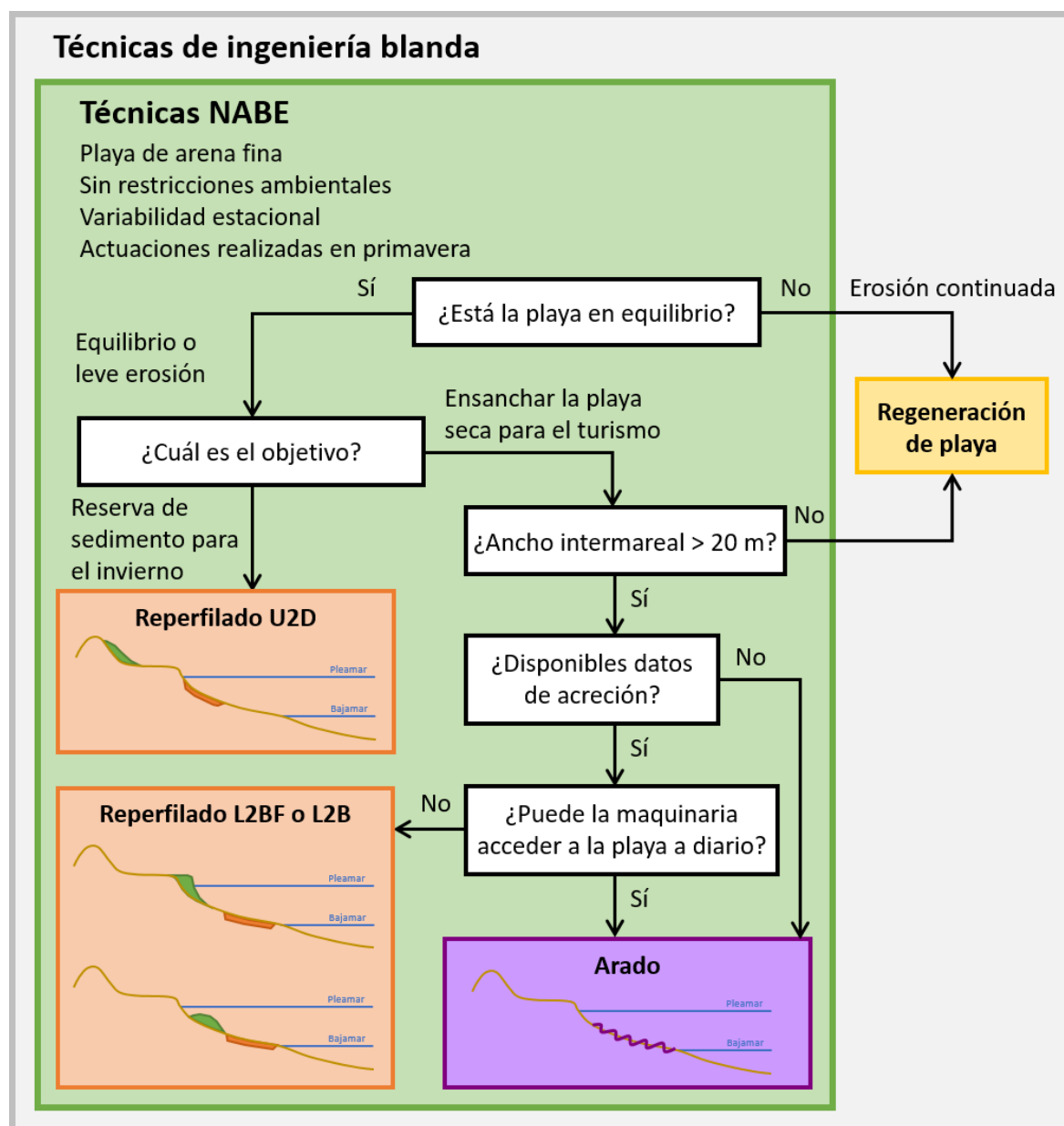


Figura 24 Árbol de decisión para escoger la técnica NABE más apropiada para cada playa.

Paso 2: Cuando aplicar técnicas NABE o no

Estas técnicas deben aplicarse en primavera, cuando se esperan dinámicas marinas de calma tras las acciones mecánicas. Además, se debe minimizar el impacto ecológico de estas técnicas, para lo que es necesario realizar un estudio de las especies que tienen su hábitat en la zona o la utilizan como zona de reproducción. Se deben evitar fechas que coincidan con episodios clave como la reproducción de tortugas o la aparición de especies migratorias. En las fechas que queden disponibles se debe analizar la probabilidad de que se produzca un episodio de tormenta marina de primavera. Esto se realiza mediante un sistema operacional que comprueba si $\Omega < \bar{\Omega}$, donde Ω es el número de Dean predicho durante los próximos días y $\bar{\Omega}$ es su valor medio histórico. Solo si no se prevén tormentas en los próximos 7 días pueden realizarse las operaciones NABE.

Paso 3: Diseño de actuaciones NABE

Cada tipo de actuación NABE requiere unos datos y un diseño específico. En los siguientes apartados se detallan las recomendaciones y cálculos necesarios para cada una.

3A: Diseño del arado

El arado se realiza durante la bajamar, por lo que debe realizarse un calendario de las horas de bajamar diarias durante el verano. En zonas de marea semidiurna se escogerá la bajamar que ocurra durante el día para una mayor seguridad durante los movimientos de la maquinaria. Son preferibles las horas de menor afluencia de público. El arado puede realizarse desde 2 h antes a 2 h después de la bajamar máxima y se seguirán las siguientes recomendaciones:

- La trayectoria del tractor será paralela a la línea de costa en bajamar.
- Preferiblemente las crestas se realizarán en el lado de tierra de los surcos.
- Se harán las filas necesarias para cubrir toda el área intermareal, desde bajamar hasta pleamar, sin arar la playa seca.
- La profundidad máxima de los surcos es de 0.3 m.

3B: Diseño de reperfilado

El volumen máximo de arena a movilizar con el reperfilado debe ser inferior al volumen de arena que recupera la playa naturalmente durante el verano (Carley et al., 2010). Por ello, este volumen debe estimarse a partir de mediciones de acreción en veranos

RESUMEN EN ESPAÑOL

previos. Para ello pueden emplearse datos de campañas de campo, líneas de costa o imágenes de satélite o aéreas, de las que se dispongan datos en primavera y otoño de un mismo año. El volumen resultante puede movilizarse en una única campaña de reperfilado o repartido entre varias campañas separadas al menos 15 días entre ellas. La profundidad máxima de la zona de préstamo debe ser inferior a 0.3 m. El ancho de la zona de préstamo se calculará en función del volumen y la profundidad máxima. En el caso de que la arena se emplee para la regeneración de la duna debe realizarse un diseño de la misma, para lo que puede emplearse la metodología de Pellón et al. (2020).

3C: Diseño de reperfilado L2BF

El caso particular de vertido de la arena reperfilada en el frente de playa para generar un aumento rápido del área de playa seca debe diseñarse con cautela. La elevación de la cresta de la nueva berma de verano generada por la maquinaria debe ajustarse al nivel del mar excedido un 1% del tiempo durante cada mes ($TWL_{1\%}$). Como este valor es cambiante a lo largo del verano, se propone usar un valor medio estimado en función de la serie histórica de nivel del mar total ($\overline{TWL_{1\%}}$), el cual se calcula promediando los valores mensuales de $TWL_{1\%}$ para los meses de verano (entre mayo y octubre) de la serie histórica para el área de estudio.

5.2. Discusión

Los gestores de la costa pueden beneficiarse de esta metodología al aplicar SbN a sus playas. Esta es la primera vez que se considera el punto de vista turístico (ampliación de playa seca) en el desarrollo de pautas para la aplicación de técnicas NABE. Además, también es la primera vez que se propone el arado como herramienta de gestión costera. Otros autores anteriores se centraron en la aplicación del reperfilado para hacer frente a las tormentas invernales. Nuestra metodología presenta un alcance más amplio e integra ambos objetivos.

Las recomendaciones se basan en las sugerencias de autores anteriores (Carley et al., 2010; Crain et al., 1995; Erskine and Thompson, 2003; Gainza et al., 2019) y en nuestra propia experiencia. La mayoría de estas sugerencias fueron concebidas para el reperfilado, aunque consideramos que también son apropiadas para el arado. Ambas técnicas actúan sobre la zona intermareal y afectan a las dinámicas marinas y a los macroinvertebrados de la playa intermareal.

Con el objetivo de trabajar con la naturaleza al arar la playa, se recomienda crear la cresta en el lado hacia tierra del surco. Esto añade una tercera componente al transporte de sedimentos hacia tierra. La primera componente es el aumento del transporte de sedimentos en suspensión cuando las olas rompen sobre las crestas. La disipación del oleaje genera condiciones hidrodinámicas (ola-corriente-nivel) que favorecen la acreción. La segunda componente es el transporte de sedimentos por fondo generado por la migración hacia la costa de las formas aradas. Finalmente, la tercera componente es el movimiento mecánico del volumen de arena desde el surco hasta la cresta, y su efecto acumulativo todos los días hacia el lado de tierra. Las tres componentes ayudan a la acreción y se esquematizan en la Figura 25.

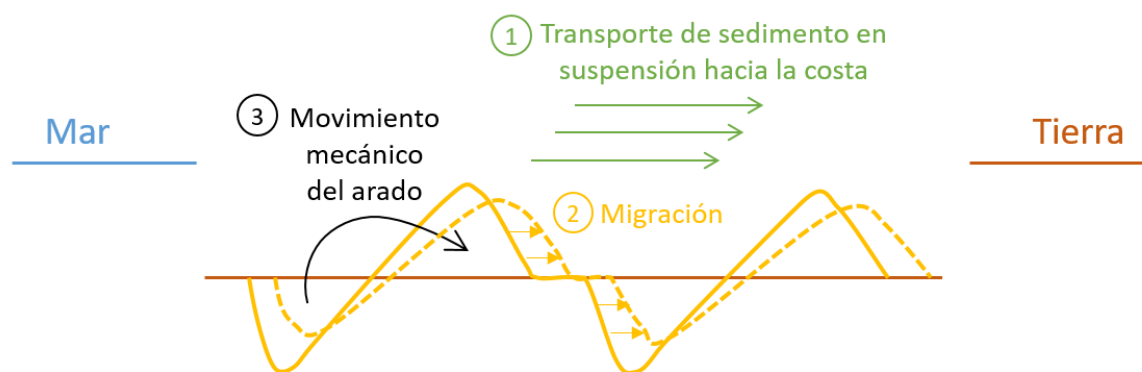


Figura 25 Esquema de las tres componentes que producen un aumento de la acreción al aplicar el arado.

Las dunas primarias son importantes depósitos de arena para luchar contra la erosión y las inundaciones producidas por los grandes oleajes del invierno. El mantenimiento de las dunas en buen estado es clave para el equilibrio a largo plazo de las playas. De acuerdo con el modelo conceptual desarrollado por Pellón et al. (2020), la duna primaria se erosiona y se recupera periódicamente. La erosión se produce por eventos de oleaje extremo y la recuperación se produce lentamente mediante transporte eólico que mueve la arena desde la playa seca hasta la duna. El reperfilado U2D es un ejemplo de herramienta que acelera esta recuperación natural con la ayuda de maquinaria. Las dunas primarias tienen un volumen y una posición de equilibrio y, por lo tanto, la arena debe colocarse de acuerdo con estas restricciones geométricas. Pellón et al. (2020) proporcionan herramientas para el cálculo de esos parámetros de diseño de dunas.

La aplicación de las técnicas NABE debe realizarse cuando sea previsible la acreción en los días siguientes. Aún no están claras las dinámicas marinas y la morfología de la playa que definen el umbral entre la acreción o no. De acuerdo con los hallazgos de esta tesis y la

RESUMEN EN ESPAÑOL

investigación de Phillips et al. (2019), la acreción está asegurada para condiciones de oleaje de calma ($\Omega < \bar{\Omega}$). Este límite se puede redefinir en el futuro si se encuentra un límite de acumulación más preciso. Esto produciría un incremento de los días aptos para la aplicación de las acciones NABE.

La metodología propuesta es modular y puede mejorarse en el futuro gracias a los hallazgos en las siguientes líneas de investigación:

- Nuevas técnicas NABE pueden incluirse en el árbol de decisión.
- Se pueden utilizar nuevos conocimientos sobre los límites de las condiciones marinas que desencadenan la acreción para mejorar los criterios del sistema operativo.
- Las optimizaciones del diseño de la geometría del arado o reperfilado se pueden incorporar en el paso 3 de la metodología.

Se fomenta el seguimiento de las actuaciones NABE en playas prototipo para la mejora de estas técnicas innovadoras y, en consecuencia, de esta metodología.

6. CONCLUSIONES

La acreción es un proceso que produce la recuperación de las playas tras las tormentas. Esta tesis analiza la acreción y la efectividad de las Soluciones basadas en la Naturaleza para acelerar la recuperación. De esta tesis se extraen las siguientes conclusiones.

Conclusiones sobre la acreción natural de playas

En el apartado 2 (chapter 3) se analizó la recuperación natural de playas durante toda la temporada de verano en tres sitios de estudio en ambientes meso/macro-mareales por medio de un total de 24 campañas de campo. Se observó la formación y crecimiento de la berma en los 15 perfiles de playa analizados y se analizó la relación entre los cambios morfológicos y las dinámicas marinas. Se abordaron los objetivos OB1 y OB2 y se extrajeron las siguientes conclusiones:

- Las mediciones realizadas en las playas de Fuentebravía (Cádiz), El Sardinero I y II (Santander), Somo y Loredo (Somo) permitieron observar la formación y crecimiento de la berma, caracterizando la **recuperación total de las playas durante la época estival**.

- El uso de metodologías de toma de datos simples, como un distanciómetro láser, ha demostrado ser preciso y económico.
- En ambientes meso/macro-mareales, las variaciones entre mareas vivas-muertas-vivas condicionan el desarrollo de la berma. La evolución morfológica de un ciclo de marea a otro es compleja. **Durante las mareas vivas, la berma se estabiliza como parte del frente de playa.**
- **El análisis de la recuperación de la playa durante el verano se puede realizar mediante campañas de campo mensuales en la fecha de la marea viva más grande.**
- Durante los **primeros meses** de la temporada de verano, la acreción produce una **progradación de la línea de costa**.
- El **ascenso de la cota de la berma** se produce cuando el nivel del mar total (TWL) se supera al menos un 3% del tiempo durante el mes anterior. En las **costas Atlánticas de España, esto ocurre típicamente en septiembre y octubre**, debido al efecto concomitante de las mareas vivas equinocciales y períodos del oleaje mayores que producen un aumento del runup y el TWL.
- **La cota de la cresta de la berma alcanzada en cada marea viva coincide con** el nivel del mar total superado el 1% del tiempo durante el mes anterior ($TWL_{1\%}$). Por lo tanto, la cota de la cresta de la berma se puede predecir mediante un análisis estadístico de la serie temporal de TWL de temporadas de verano anteriores.
- **La tasa de acreción se relaciona con el parámetro adimensional de caída de grano de equilibrio (Ω_∞)** promediado en el mes anterior a cada observación. Sin embargo, esta relación es débil y se encontraron dos claras excepciones.

Conclusiones sobre la técnica del arado de playas

El arado se analizó por primera vez en condiciones controladas en laboratorio a escala prototípico (1:1) y escala reducida (1:8). El análisis realizado a escala de prototípico comprende dos conjuntos de ensayos que se han detallado en el apartado 3 (chapter 4). El conjunto 1 exploró la efectividad de arar mecánicamente el área intermareal de una playa. El conjunto 2 permitió el análisis de la evolución morfodinámica del arado hasta su desaparición por la acción del oleaje. Además, en el apartado 4 (chapter 5) se mostró el análisis del arado a escala reducida, lo que permitió comparar los resultados con la técnica del reperfilado.

RESUMEN EN ESPAÑOL

Dichos análisis abordan los aspectos relativos al arado de los objetivos OB3, OB4, OB5 y OB6 de la tesis y arrojan las siguientes conclusiones:

- **Arar** el área intermareal en cada bajamar demostró ser una técnica eficaz para **acelerar la acreción y lograr una playa seca más ancha**.
- Los datos recopilados a escala prototipo (1:1) demuestran que **el arado tiene un efecto positivo en el aumento de las tasas de acreción** para todos los niveles de agua que se ensayaron. Tanto los volúmenes de sedimento acumulados como las tasas de transporte de sedimento son mayores en el lado arado que en el lado de control natural de los experimentos.
- El análisis del Conjunto 2 de experimentos mostró que **el arado se suaviza y casi desaparece después de 2-3 h de acción del oleaje**. Por lo tanto, el arado debe repetirse en varias bajamas para lograr un efecto acumulativo.
- El análisis espectral de las formas del lecho, permitió su separación en dos componentes principales: arado y ripples. Su caracterización morfométrica se resume en la Tabla 3.

Tabla 3 Características morfométricas del arado y ripples.

Característica		Arado	Ripples
Longitud de onda		1.62±0.05 m	0.28±0.01 m
Altura	Test A	Altura inicial ~0.3 m se reduce	0.011±0.003 m
	Test B	por debajo de 0.06 m tras 2 h	0.016±0.004 m
Velocidad de migración	Test A	0.18 m/h	0.36±0.15 m/h
	Test B	0.25 m/h	0.33±0.11 m/h
Pendiente de sotamar		Inicial de 34° y 5° tras 3 h	-
Pendiente de barlomar		Inicial de 23° y 5° tras 3 h	-
Otros		Área de la cresta de 0.075 m ²	Los ripples se forman
		reduciéndose exponencialmente a 0.006 m ² tras 2 h	sobre el arado y migran más rápido hacia la costa

- El análisis de los conjuntos 1 y 2 de experimentos mostró que **el arado produce tres efectos para mejorar la acreción**. Los detalles de cada componente se dan a continuación:

1) Mejora del transporte de sedimento en suspensión hacia la costa. El arado aumenta la rugosidad del fondo, lo que genera una disipación adicional del oleaje al romper las olas sobre las crestas. El aumento de sedimentos en suspensión por la mayor rotura del oleaje y las condiciones hidrodinámicas (ola-nivel-corriente) generadas favorecen el transporte de sedimentos hacia tierra.

2) Mejora del transporte de sedimento por fondo hacia tierra gracias a la migración de las formas.

3) Movimiento mecánico hacia tierra, retirando la arena del surco (en el lado de mar) y moviéndola hacia la cresta (en el lado de tierra).

- Los ensayos a escala reducida (1:8) demuestran que el arado es una técnica útil para acelerar la recuperación de la playa, logrando un 23.41% de progradación extra de la línea de costa en promedio y aumentando el volumen de sedimentos disponible en la parte superior del perfil de la playa para luchar contra la erosión invernal hasta en un 37%.

Conclusiones sobre la técnica del reperfilado de playas

El reperfilado se analizó en condiciones controladas de laboratorio a escala reducida (1:8). Los experimentos incluyen cuatro geometrías diferentes de reperfilado (L2B, L2BF, L2D y U2D), con diferentes áreas de préstamo y relleno. La variante L2BF también se probó en la playa de Fuentebravía (Cádiz). Dichos experimentos se detallan en el apartado 4 (chapter 5), abordan los aspectos relativos al reperfilado de los objetivos OB3, OB4, OB5 y OB6 de la tesis y se obtuvieron las siguientes conclusiones:

- **El uso de sedimento sintéticos de densidad reducida permitió la simulación a escala reducida (1:8)** de un perfil completo de playa bajo la acción simultánea de oleaje y mareas.

- **La geometría de la berma** de la playa (cota de la berma y pendiente del frente de playa) fue determinada principalmente por las **dinámicas marinas**. **El arado y el reperfilado** influyeron en la **posición de la línea de costa** y el ancho de la playa.

RESUMEN EN ESPAÑOL

- La creación de una barra intermareal mediante **reperfilado L2B** resultó en playas secas más anchas. El sedimento en la barra intermareal se acrecentó parcialmente a la berma de la playa y se erosionó parcialmente mar adentro.
- La generación de una berma mediante el **reperfilado L2BF** puede producir playas más anchas si se diseñan adecuadamente. La geometría de la berma generada por “maquinaria” influyó mucho en los resultados. La altura de la berma y la pendiente de la zona de swash deben coincidir con la berma formada naturalmente.
- Todas las variantes ensayadas muestran que el **reperfilado** es una técnica útil para potenciar la recuperación de la playa, **aumentando el volumen de sedimento** disponible en la parte alta del perfil para **luchar contra la erosión invernal**. La **regeneración de la duna** con arena extraída del área intermareal **maximizó la reserva de sedimento**.
- **El área de préstamo recomendada para la regeneración de dunas es la parte superior del área intermareal (U2D).** El perfil de la playa se vuelve más disipativo, aumentando el transporte de sedimentos hacia tierra y logrando mayores volúmenes de acreción.
- **El reperfilado ha demostrado su eficacia para acelerar la recuperación de playas** en el laboratorio y en una playa real (Fuentebravía).
- **En la playa de Fuentebravía, el reperfilado aceleró la acreción durante las primeras semanas.** La línea de costa progradó 3.68 m más que en el área de control y la berma acumuló un 24% más de volumen de arena. Por lo tanto, la playa seca era más ancha al comienzo de la temporada turística.

Como conclusión general sobre la eficacia de ambas técnicas NABE (reperfilado y arado), observamos que:

- **La técnica NABE recomendada depende del objetivo.** Para playas donde se busca una playa seca más amplia, las acciones recomendadas son el arado o reperfilado, tomando la arena del intermareal bajo y llenando una barra intermareal o el frente de playa (con un diseño cuidadoso de la geometría de la berma) durante la primavera. Para las playas donde se busca protección contra la erosión y las inundaciones por tormentas invernales, la recomendación es tomar arena del área intermareal durante la primavera (preferiblemente del área intermareal superior) y regenerar la duna o la playa seca.

Conclusiones sobre la metodología para la aplicación de técnicas de recuperación asistida de playas

El apartado 5 (chapter 6) incluye una metodología para la implementación de Soluciones basadas en la Naturaleza (SbN) para acelerar la recuperación de playas, centrándose específicamente en las técnicas de recuperación asistida (NABE). Esta metodología ayuda a los gestores de la costa a seleccionar la técnica NABE más adecuada según el objetivo y las características específicas del sitio. Además, proporciona pautas para el diseño de acciones. Este apartado 5 aborda el objetivo OB7 de la tesis y de él se derivan las siguientes conclusiones:

- Las técnicas NABE, como el arado y el reperfilado, están diseñadas para **acelerar la recuperación de arena aprovechando los procesos naturales, reduciendo la dependencia de las intervenciones humanas**. Además, ambas técnicas se aplican con medios terrestres, lo que las hace económicas y fáciles de aplicar con maquinaria de uso generalizado (para cultivos y obra civil, arado y motoraillas respectivamente).
- Si bien **el reperfilado y el arado** pueden ser herramientas valiosas para la gestión costera, **su aplicación debe ejercerse con precaución y limitarse a los lugares apropiados** (playas arenosas, con variabilidad estacional y sin restricciones ambientales ni problemas de erosión).
- Para garantizar la selección y el diseño adecuados de las acciones NABE, se describe una **metodología que consta de tres pasos principales**: seleccionar la técnica más adecuada mediante un árbol de decisión, aplicar un sistema operacional para determinar si aplicar técnicas NABE o no en un día específico y diseñar acciones NABE adaptadas al sitio específico.
- Se enfatiza la importancia de considerar el impacto ecológico de las técnicas NABE. Es particularmente importante considerar la macrofauna, los períodos de nidación y las especies migratorias. **El momento de las acciones debe planificarse para evitar períodos ecológicos críticos**.
- La **metodología es modulable** para incorporar nuevas técnicas NABE, refinar los criterios operativos basados en **investigaciones futuras** y optimizar geometrías de diseño. Se fomenta el **seguimiento** y evaluación de las acciones NABE para la mejora continua.

7. FUTURAS LÍNEAS DE INVESTIGACIÓN

A pesar de las aportaciones de esta tesis al conocimiento de la recuperación de playas durante la época estival y la eficacia de las técnicas NABE, aún quedan interrogantes sin responder. Las nuevas preguntas de investigación que surgieron durante el desarrollo de esta tesis conducen a las siguientes líneas de investigación sugeridas para ser abordadas en futuros estudios.

Acreción de arena

- Es necesario estudiar la relación entre las dinámicas marinas y el volumen de acreción y determinar el umbral de las condiciones marinas que desencadenan la acreción.
- Estudios adicionales sobre la ocurrencia de formas del lecho y las dinámicas sedimentarias a su alrededor revelarían su importancia para la recuperación de playas.

Técnicas NABE

- Se requieren más pruebas en prototipo (en condiciones naturales en una playa real) para determinar todo el potencial del reperfilado y arado de playas para la ampliación de la playa seca y la aceleración de la acreción.
- Se desconoce el efecto de una tormenta primaveral sobre actuaciones NABE realizadas recientemente.
- Son necesarios más estudios sobre el efecto específico de las acciones de reperfilado y arado sobre todo el ecosistema, desde la zona sumergida hasta la duna, para tener una visión completa del impacto ecológico de estas técnicas.
- Desarrollo de otras técnicas NABE.

Técnica del arado

- Analizar el efecto de los ciclos de mareas vivas-muertas-vivas en el arado.
- Optimizar las características geométricas del arado.

Técnica del reperfilado

- Desarrollar nuevos procedimientos para el cálculo del volumen de arena naturalmente recuperado durante la temporada de verano.
- Investigación adicional sobre el impacto de la geometría de la berma creada mediante reperfilado en la acreción y el ancho de la playa seca.

CHAPTER 1

INTRODUCTION AND SCOPE

1.1. INTRODUCTION AND MOTIVATION

Coastal areas are the most populated regions of the Earth. A high percentage of those inhabited coastal zones are protected by beaches. Marine dynamics hit continuously the shoreline, and beaches act as a flexible defence that modifies their morphology according to these dynamics. Beaches and dunes act as sediment buffers for erosion and constitute a unique ecosystem that is the habitat of countless species. The maintenance of a healthy beach is fundamental for the sustainability of those areas. The dune recovers and builds up due to the sand blown by the wind from the dry beach. Many mammals, birds, plants, macro and micro-invertebrates cannot live in a coastal area if the beach disappears periodically. Additionally, in the last centuries, the beaches constitute a recreational space largely demanded by local people and tourists.

Healthy beaches provide many ecosystem services that can boost the economy of coastal municipalities. They protect coastal areas from erosion and flooding, are space for recreational activities such as sunbathing, swimming, walking, surfing, kitesurf, beach volleyball, and many other sports, are a source of resources such as fish, shellfish, and medicinal algae, and are fundamental for the survival of other species (that do not live in the beach) as beaches constitute the nesting area for turtles, and breeding space for many birds. This is only a small bunch of examples of ecosystem services that healthy beaches can provide, which justifies the need of ensuring the sustainability of these areas.

CHAPTER 1

Beach width changes periodically throughout the year. Beaches normally reach their maximum width in October (Aubrey, 1979), just before the beginning of the winter storms. During winter the beach erodes fast, reducing its width after each marine storm. In spring the beach width is minimum, and sometimes the winter climate is so harsh that the dry beach disappears and the dune erodes as well. The calm weather conditions usual during spring and summer produce the beach recovery. During these months, the sand slowly goes back from submerged areas to the emerged beach in a natural process called accretion. Sometimes, these months are not enough to achieve a full recovery of the beach width. The dune recovers by slow aeolian processes when the wind blows the sand from the dry beach to the foredune toe. As a result, the beach and dune are less prepared for the impact of the next winter storms, which may produce permanent shoreline retreat and frequent flooding of coastal villages or facilities.

Although the seasonal oscillations of the shoreline are widely known and erosion is a deeply studied phenomenon, accretion processes are still poorly understood and the marine dynamics that trigger beach recovery remain under research. Previous studies point out the importance of tides for onshore sandbar migration and welding on the beachfront as a summer berm. For this reason, in the present thesis, we focus on the analysis of accretion on meso/macro-tidal beaches, which is a field that remains scarcely studied.

Historically, coastal erosion and flooding were fought with costly artificial grey infrastructures such as breakwaters, dykes, or seawalls. As the awareness of society raised, green solutions such as beach nourishment widespread their use and Nature-Based-Solutions (NBS) were born. The NBS philosophy seeks sustainable solutions in which human-made actions work hand to hand with nature to achieve the desired effect. When speaking about beach accretion these kinds of actions are called Nature Assisted Beach-Enhancement (NABE) techniques, and aim to accelerate the natural processes of accretion with soft actions of reduced environmental impact. In this thesis, two NABE techniques are analysed: (1) beach scraping, and (2) beach ploughing.

Beach scraping is a widely used technique but few scientific studies have quantified its effectiveness (Carley et al., 2010) nor proposed methodologies for its design. Additionally, here we analyse if beach scraping is suitable for dry beach widening in early spring for touristic purposes, although this technique has only been used to fight against erosion. Besides, beach ploughing is an innovative technique that has only been applied once before (at Laida beach in 2015; Gainza et al., 2019).

The present thesis encompasses field and laboratory experiments (at real and reduced scales) in which accretion is analysed on meso/macro-tidal environments and the effect of beach scraping and beach ploughing are quantified with the goal of proposing efficient, sustainable and innovative techniques able to improve beach conditions for touristic purposes and to fight against winter erosion and flooding.

1.2. RESEARCH QUESTIONS

The following research questions are answered in the present thesis:

- What is the qualitative effect of marine dynamics on beach accretion in a meso/macro-tidal environment?
- Is it possible to enhance natural rates of beach accretion with NABE techniques?
- Does beach scraping enhance natural rates of beach accretion?
- Can beach scraping be used to increase beach width in early summer?
- Is beach ploughing an effective technique to enhance beach accretion in meso/macro-tidal beaches?
- Which NABE technique is the most suitable to enhance accretion on a particular meso/macro-tidal beach?

1.3. OBJECTIVES

The general objective of this thesis is the analysis of the effectiveness of two **Nature-Based Solutions to enhance beach recovery**.

To achieve this goal the following specific objectives are proposed:

- OB1. Improve the knowledge of accretion on meso/macro-tidal beaches, considering the influence of marine dynamics.
- OB2. Perform field surveys on meso/macro-tidal beaches that cover the full recovery during the summer season.
- OB3. Perform laboratory experiments that allow the analysis of NABE techniques under controlled conditions.
- OB4. Analyze if scraping and/or ploughing techniques produce dry beach widening for touristic purposes.

CHAPTER 1

- OB5. Analyze if scraping and/or ploughing techniques increase the volume of sand accreted at the end of the summer, which will be available as a sediment budget to fight against winter erosion and flooding.
- OB6. Evaluate the effectiveness of nature assisted beach enhancement techniques for the acceleration of beach recovery on meso/macro-tidal beaches.
- OB7. Develop a methodology that helps decision-makers to decide which technique is the most appropriate for their beach. It includes guidelines for the design of the selected actions.

Objectives OB1 and OB2 are addressed in chapter 3. Then, chapter 4 focuses on beach ploughing and covers this part of objectives OB3, OB4, OB5 and OB6, while chapter 5 fulfil completely the remaining concerns of these objectives by including the results on beach scraping and a comparison among NABE techniques. Finally, chapter 6 responds to objective OB7, including the aforementioned methodology.

1.4. THESIS OUTLINE

This document is organized as follows:

- **Chapter 1. Introduction and scope**, where the importance of maintaining a healthy beach is introduced and the objectives of the thesis are presented.
- **Chapter 2. Background and literature review**, where the existing studies of the state of the art are detailed.
- **Chapter 3. Natural beach accretion**, where the three field surveys performed are presented, analysing the accretionary behaviour of meso/macro-tidal beaches and relating it with the marine dynamics of each study area.
- **Chapter 4. Beach ploughing**, where the real-scale laboratory experiments on beach ploughing are presented. The effectiveness of beach ploughing to enhance beach accretion is analysed and the evolution and impact of the bedforms (plough artificially created and bedforms that naturally appear) on beach recovery are presented.
- **Chapter 5. Beach scraping**, where the reduced-scale laboratory experiments are presented. It includes physical simulations of four geometries of beach scraping and one geometry of beach ploughing that are analysed comparatively to the natural beach recovery. The results are compared to the field surveys including beach scraping performed at Fuentebravía beach.

- **Chapter 6. Methodology for the application of nature assisted beach enhancement techniques**, where the methodology for the selection and design of the most appropriate NABE technique to each location is presented. This methodology constitutes a valuable tool for decision-makers.
- **Chapter 7. Conclusions and future research**, where the conclusions of the research developed in this thesis are summarized, and the main research lines that were detected through the development of this thesis are presented.
- **References**.

CHAPTER 2

BACKGROUND AND LITERATURE REVIEW

2.1. INTRODUCTION

Beach erosion and coastal flooding are major concerns in coastal areas. Ten per cent of the world's population lives in a nearshore region at less than 10 meters above sea level (McGranahan et al., 2007). Luijendijk et al. (2018) found that 31% of the world's ice-free shorelines are sandy, and 24% of those beaches are eroding at rates exceeding 0.5 m/yr. Coastal erosion and sea level rise effects threaten an important percentage of the world's population. Progressive narrowing of dry beach width and dune deterioration increases the risk of damage to coastal areas.

Beaches provide protection from marine action, have an essential ecological value as transition ecosystems, and enhance tourism due to the multitude of beach-related activities that can be enjoyed. Hardening of the marine climate due to human response to climate change increases beach erosion produced during winter (Toimil et al., 2017) and prevents a full recovery during summer. This leads to steady dry beach narrowing and shoreline retreat which is normally fought by beach nourishment. This thesis analyses the effectiveness of Nature-Based Solutions (NBS) to accelerate beach recovery as an alternative to boost beach health.

The analysis developed in this document requires basic knowledge of the usual nomenclature of relevant beach zones and elements. Figure 2.1 shows and scheme of a

CHAPTER 2

beach profile including the low and high tide levels for reference. This thesis focuses on the study of the sediment exchange produced between the intertidal area and the dry beach due to accretion processes that form the summer berm along the spring and summer seasons.

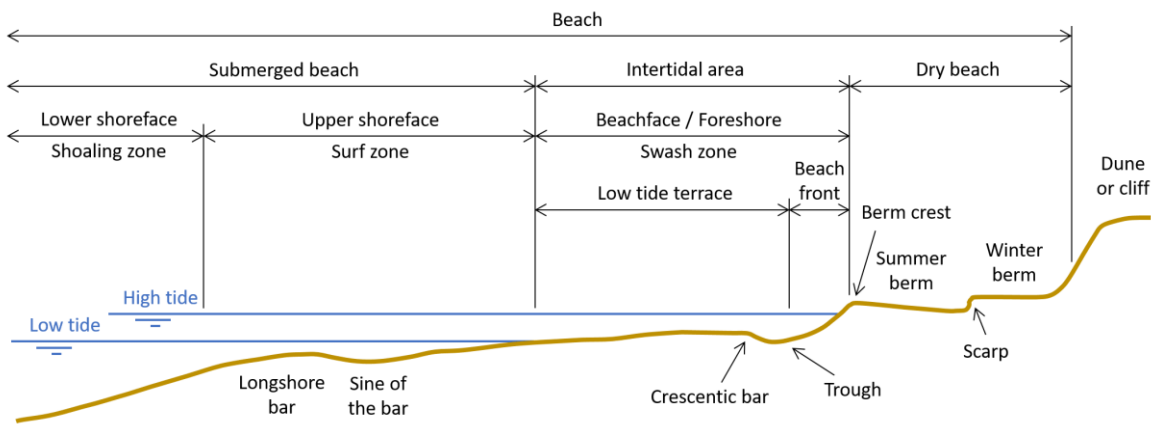


Figure 2.1 Beach profile scheme and nomenclature.

This chapter encompasses the state-of-the-art review of accretion processes, which are still poorly known, in section 2.2. Section 2.3 describes the knowledge of bedforms, that may play an important role in beach recovery. Section 2.4 introduces the concept of Nature-Based Solutions, and section 2.5 focuses on nature assisted beach enhancement techniques, specifically on beach scraping and beach ploughing, which are the techniques studied in this thesis. Then, section 2.6 summarizes previous laboratory experiments related to the ones developed here, and finally, section 2.7 includes the conclusions of the literature review.

2.2. SAND ACCRETION

The effect of marine conditions during winter storms triggers beach erosion. The sand lost from the dry beach is slowly recovered, mainly during calm weather periods throughout the summer (Aagaard et al., 2006; Aubrey, 1979; Gallagher et al., 1998a; Jackson et al., 2016; Yoo et al., 2021), taking several months to achieve a noticeable widening of the upper dry beach area. In locations subject to anomalous energetic winter storms, accretion processes are not enough to re-establish the original shoreline's position before winter, and progressive shoreline retreat may occur both in eroding or equilibrium shorelines (Gordon, 2015; Yoo et al., 2021). Climate change exacerbates this issue, generating a progressive lack of sand over the years and a narrowing of the width of the dry beach (Toimil et al., 2017). Accretion processes are not yet completely understood (Jackson et al., 2016; Phillips et al., 2017) and cannot be accurately modelled.

The process of accretion involves onshore-directed sand movement on the whole active beach profile (from the depth of closure to the dry beach). The formation of sand bars, submerged under the breaking point and its onshore migration has been analysed by many authors (Aagaard et al., 2006; Gallagher et al., 1998a; Jackson et al., 2016). Initially, studies focused on the progressive onshore migration of the bar approaching the dry beach which lead to the formation of the berm and shoreline progradation (by bar welding on the foreshore, Jensen et al., 2009). However, it is known since the sixties (Strahler, 1966) that berm dynamics are complex and tidal cycles may be of great importance in its formation and evolution. Jensen et al. (2009) observed that during the falling tide, the beach profile was close to equilibrium, while during the rising tide, the berm was transformed into an intertidal bar that migrated further onshore by wave action and stabilized when the high tide level was reached. Phillips et al. (2019) analysed tide-by-tide observations on poststorm beach recovery. They observed differentiated episodes of beachface progradation (seaward growth) and berm aggradation (vertical growth), that were previously identified by Dubois (1988), and related those episodes to the absence or presence of swash exceeding the berm crest respectively. Additionally, Phillips et al. (2019) state that berm behaviour is primarily governed by the neap-spring tide variation, and distinguish four behavioural modes of berm recovery (combination of beachface progradation or erosion with berm aggradation or maintenance) depending on the dimensionless fall velocity, the swash exceedance of the berm crest, and the ocean water level (Figure 2.2).

CHAPTER 2

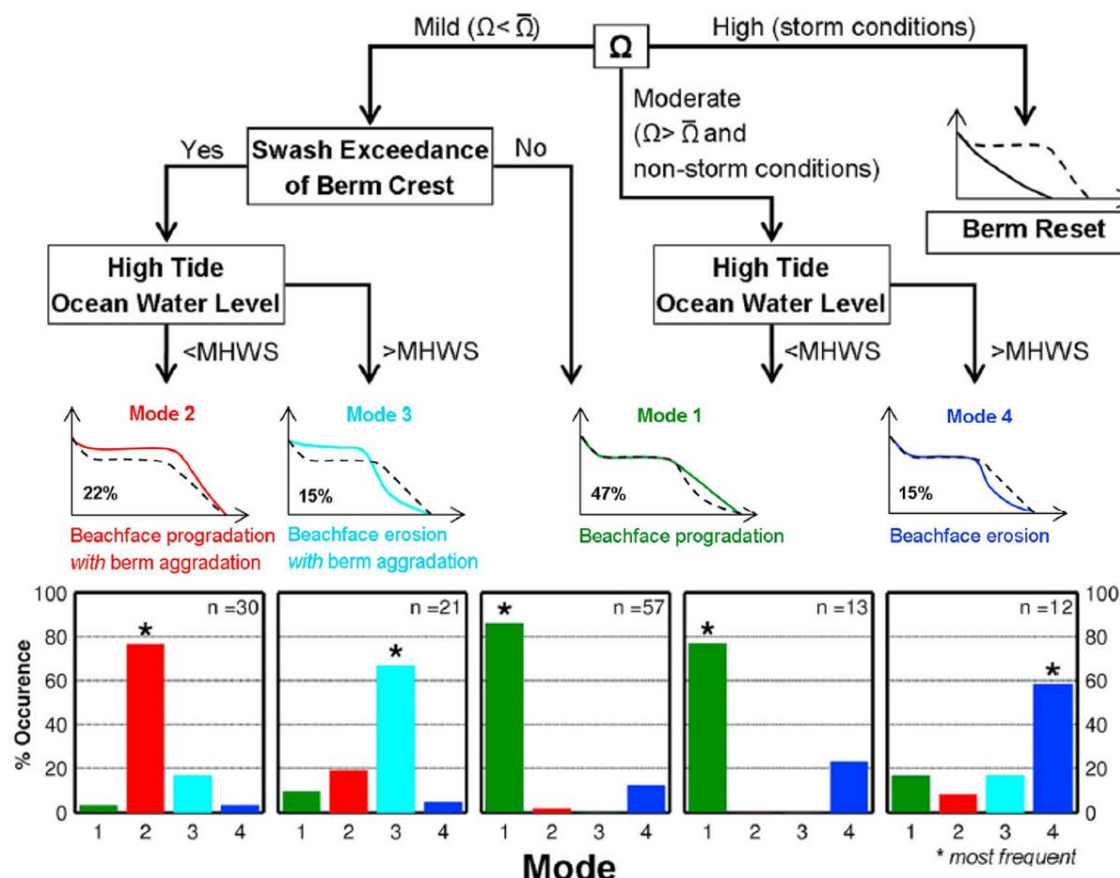


Figure 2.2 Four behavioural modes of berm recovery and decision tree depending on dimensionless fall velocity Ω , swash exceedance of berm crest and ocean water level. Storm conditions refer to significant wave heights above the 5% exceedance level for a minimum duration of one tidal cycle during which $\Omega > 4$. $\bar{\Omega}$ is the average dimensionless fall velocity, and MHWS is the mean high water springs. Adapted from Phillips et al. (2019).

Over a century ago, Hunt & F.G.S. (1904) highlighted the importance of ripple marks as “an important factor and index in the great problem of marine erosion”. Since then, studies were performed that analysed bedform characteristics and dynamics, but few of them addressed their influence on beach accretion processes. Miles & Thorpe (2015) found that bedform contribution to cross-shore sediment transport (accretion) averages 15% of the total transport produced around the breaking point. This refers to the upper shoreface (or breaking zone), but in the lower shoreface (or shoaling zone), the influence of bedforms on accretion could not be verified, although studies have been performed (Guerrero et al., 2021).

In the upper shoreface, the importance of longshore bar formation and evolution for beach profile evolution has been widely recognized (Holman and Sallenger, 1993; Masselink et al., 2006), and recently, Guerrero (2018) proposed that smaller bedforms could

also affect beach recovery. Different bedform sizes can appear in the same location and time moment. The smaller ones appear on top of the larger ones and migrate faster (Guerrero and Guillén, 2020; Venditti et al., 2005). Smaller bedforms appear frequently on top of intertidal bars (see Figure 2.3), and their migration can contribute to speeding up onshore bar migration and welding to create a wider beach. Ripples that appear lying on the backs or stoss sides of larger bedforms migrate and reach the crest of a host bedform and influence the nature of the sediment deposition on the lee side (Guerrero and Guillén, 2020; Reesink and Bridge, 2007). On the upper shoreface, ripples migrate onshore and can be seen as a process helping beach recovery (Guerrero et al., 2021). Improving the knowledge of bedforms can lead to the comprehension of accretion processes and the development of new techniques to enhance beach recovery.



Figure 2.3 Superposition of bedforms at El Puntal beach, Cantabria, Spain. Images were taken in September 2020. Top: Shore parallel intertidal bar (low-amplitude ridge). Bottom: The image was taken from the middle of the bar on the image of the top pointing to the dry beach. Megaripples ($\lambda \sim 1.5$ m) with ripples ($\lambda \sim 0.1$ m) over them.

CHAPTER 2

2.3. BEDFORMS

A beach shoreface is a highly dynamic environment in which several types of bedforms may appear with a wide range of spatial and temporal timescales. Jackson (1975) proposed a general classification of bedforms based on their size and time span of existence, identifying macroforms, mesoforms, and microforms (see Figure 2.4) ranging from large, persistent, and environmental conditions dependent, to small, temporal, and event-related. Some researchers have attempted to summarize and find correspondence between the wide range of nomenclature used for these bedforms that can appear in different fields of knowledge: rivers, sandy beaches, and continental shelves. Ashley (1990) indicated that similar processes form all large bedforms (wavelength > 1 m), and thus the term dunes is proposed to refer to them, although they are often referred to as megaripples, large ripples, or sand waves. Flemming (1988) measured the wavelength (λ) and height (H) of over a thousand bedforms and found the relation among those geometric parameters shown in Figure 2.4. On smaller scales (wavelength < 1 m; microforms), ripples are formed. Figure 2.4 shows a similar relationship between the ripple wavelength and height (derived from Raudkivi, 1997), and Baas (2003) noted that their usual dimensions are $\lambda = 0.2$ m and $H = 0.02$ m, and their shape is symmetric or slightly asymmetric if ripples are wave generated.

In the nearshore region, where tides are important, even more features can appear. The most frequent are intertidal bars on the wavelength scale of macroforms, which can be combined with mesoforms or microforms on top of them (see Figure 2.3). Tides strongly influence the morphodynamics of the bedforms in an intertidal region. The tidal level shifts wave processes up and down the beach profile, determining the duration and type (i.e., swash, surf, or shoaling) of wave dynamics (Masselink et al., 2006). There are several types of intertidal bars depending on their orientation (transversal, oblique, or parallel to the shoreline), persistence (temporal or permanent), and size (from tens to hundreds of metres of wavelength). Masselink et al. (2006) identified three types of shore parallel intertidal bars: slip-face bars, low-amplitude ridges, and sand waves (see their geometric characteristics in Figure 2.4). Pellón et al. (2014) proposed a classification for oblique and transverse intertidal bars into four types: transverse bars and rips, large-scale finger bars, finger bars of intermediate beaches, and small-scale low-energy finger bars (see Figure 2.4). All of these bedforms are lower than the expected height (according to Flemming, 1988) if they were formed in a full-time submerged environment.

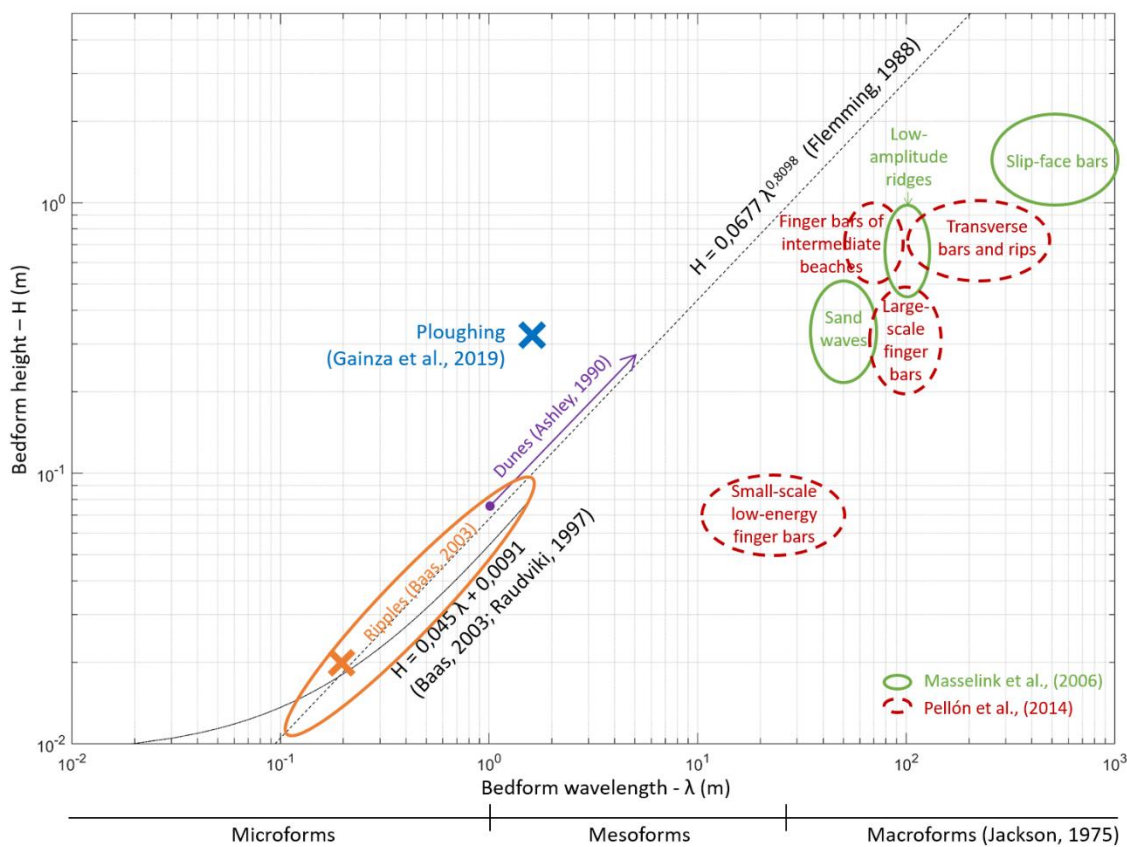


Figure 2.4 Occurrence of bedforms according to their geometric characteristics.

According to Cataño-Lopera and García (2006), the bedform size and shape directly affect the roughness height and the flow resistance through the friction factor. There are three types of sediment transport: (1) bedload generated by skin friction, (2) near-bed suspended sediment, and (3) suspended sediment off the bed (Cataño-Lopera and García, 2006). (1) and (2) are responsible for the migration of bedforms. Additionally, other authors (Allen, 1968; Middleton and Southard, 1984) affirmed that bedform migration can provide a mechanism for bedload sediment transport. In that case, onshore bedform migration could enhance beach accretion. Huntley et al. (1991) proposed an equation that allows the estimation of the sediment transport produced by bedforms (Miles and Thorpe, 2015).

Most of these coastal features migrate according to the hydromorphodynamics in the area. Wave asymmetry is considered the main factor responsible for ripple migration (Traykovski et al., 1999). Intertidal “bars build up and migrate onshore under calm waves and are flattened and may migrate offshore during storms” (Masselink et al., 2006). Intertidal slip-face bar observations analysed by D. W. T. Jackson et al. (2016) indicated prevailing onshore migration, ranging from 0.07 to 1.83 m/day, although 0.38 m/day offshore-directed migration rates were measured after a storm. Smaller bedforms can

CHAPTER 2

appear on top of intertidal bars (see Figure 2.3). Generally, the smaller the bedform is, the faster the migration. Megaripple migration in the surf zone was investigated by Gallagher et al. (1998). Their results indicated that both the mean and wave flows produce their migration, with the main direction oriented to the maximum sediment transport direction. Megaripple migration speeds can range from 0.1 to 1.7 m/h (Gallagher et al., 1998b) depending on waves and currents. Miles et al. (2014) measured ripple and megaripple onshore migration rates up to 1.14 m/h during the beginning or end of a tidal cycle when waves acted on a shallower depth over bedforms. During the higher phases of the tidal cycle, the observed migration speeds were slower. In addition, Clarke & Werner (2004) found that megaripples can be washed out if the swash zone acts over them while the tide falls.

2.4. NATURE-BASED SOLUTION (NBS)

Nourishment actions match a wide diversity of coastal protection attitudes between (1) resistance, (2) little change, and (3) adaptability (Hamm et al., 2002). The design criteria of these actions also vary between improving coastal stability to prevent retreat, increasing coastal protection to prevent flooding, or widening beaches for recreational purposes.

Plentiful shore nourishment experience exists worldwide. The movement of large amounts of sand from reservoirs to coastal areas is a frequent action taken for coastal protection. Due to the increasing difficulty in identifying appropriate reservoirs without ecological value, this type of nourishment is changing to larger but less frequent works. Luijendijk et al. (2017) analysed the profitability of such large nourishments as the Sand Engine in the Netherlands. This new way of thinking triggered the development of working-with-nature lines of action, in which the value of nature is enhanced and used to fight against coastal erosion.

The boom of coastal tourism in the last decades has increased the demand for wider beaches during the spring and summer seasons. Usually, in early spring, beaches are in their narrower state, due to the recent erosion produced by winter storms. It is not until late summer that accretion processes restore beaches to their wider state (Aubrey, 1979).

Coastal decision-makers demand soft engineering tools to deal with coastal erosion threats while providing beach widening for touristic purposes. In this sense, beach nourishment is a widespread measure (Hamm et al., 2002), that may provide a solution for both issues if performed in early spring. The drawback of this kind of solution lies in the

difficulty to find reservoirs with appropriate sand characteristics (size, colour) and where sand dredging does not pose an environmental problem. To tackle these problems, previous studies propose the use of nature assisted beach enhancement (NABE) techniques (Gordon, 2015). These techniques aim to accelerate the accretion processes occurring naturally on the beach in a Building with Nature philosophy.

2.5. NATURE ASSISTED BEACH ENHANCEMENT (NABE)

To ensure coastal protection against flooding and diminish the shoreline retreat, it is necessary to develop techniques that accelerate accretion processes and allow the recovery of all the sand lost during winter storms. These techniques are called nature assisted beach enhancement (NABE) techniques (Carley et al., 2010; Smutz et al., 1980) and can be used to ensure the maintenance of beach width, improve dune health, and obtain wider beaches early in the summer for touristic purposes. Specifically, two NABE techniques are analysed here: (1) beach scraping and (2) beach ploughing.

Beach scraping and beach ploughing techniques aim to accelerate naturally produced sand accretion on the beach profile in order to have wider beaches earlier in the summer. Both techniques deal solely with cross-shore processes, and their main goal is to enhance the recovery of the sand lost to the deeper parts of the beach profile during winter storms (seasonal cross-shore changes). Possible longshore sediment transport unbalances on the application area or long-term erosion issues must be dealt with separately, and are not analysed in this study.

2.5.1. Beach scraping

Bruun (1983) describes beach scraping as the removal of material from the lower part of the aerial beach and subsequent deposition on the upper part of the beach or at the dune's toe. It has a direct effect of reshaping the geometry of the beach profile, which automatically can have a wider dry beach (if the sand is placed on the beachfront), or a recovered dune (if the sand is placed on the dune's toe). This technique is widely used along Australian coasts (Figure 2.5; Carley et al., 2010), where it is known as nature assisted beach enhancement (NABE). This technique has been used since the 20th century, but few scientific studies have analysed its effects (Carley et al., 2010).

CHAPTER 2

Gold Coast 1967



Sydney 2008

Figure 2.5 Examples of beach scraping. Source: Carley et al. (2010).

One advantage of this technique is that the borrowed sand belongs to the same beach system and therefore its characteristics are those of the native sand, so it can be used both for dune nourishment and to generate a wider beach (Dare, 2003). However, such scraping must be done responsibly, following specific rules to avoid adverse effects on the ecosystem or adjacent beaches (Bruun, 1983). For example, the recommended maximum depth of the borrow area is 0.3 m for fine sand beaches, and the volume must not exceed natural accretion rates (McNinch and Wells, 1992; Tye, 1983) integrated over the summer season, to allow the beach to recover.

An additional interesting statement about beach scraping is that it accelerates natural beach accretion (Smutz et al., 1980), capturing more sand from the offshore part of the beach profile that moves naturally to the upper part of the intertidal region or beachfront. This Building with Nature strategy allows the mobilization of a larger volume of sediment with fewer human actions (less cost and less ecosystem disturbance). Carley et al. (2010) and Smutz et al. (1980) state that removing the borrowed sand turns the beach profile flatter or more dissipative, augmenting the disequilibrium between the scraped profile and the equilibrium profile of low energy waves, thus increasing the associated accretion (Figure 2.6). This is the main reason why scraping is also called nature assisted beach enhancement although, to date, no field or laboratory study supports this statement.

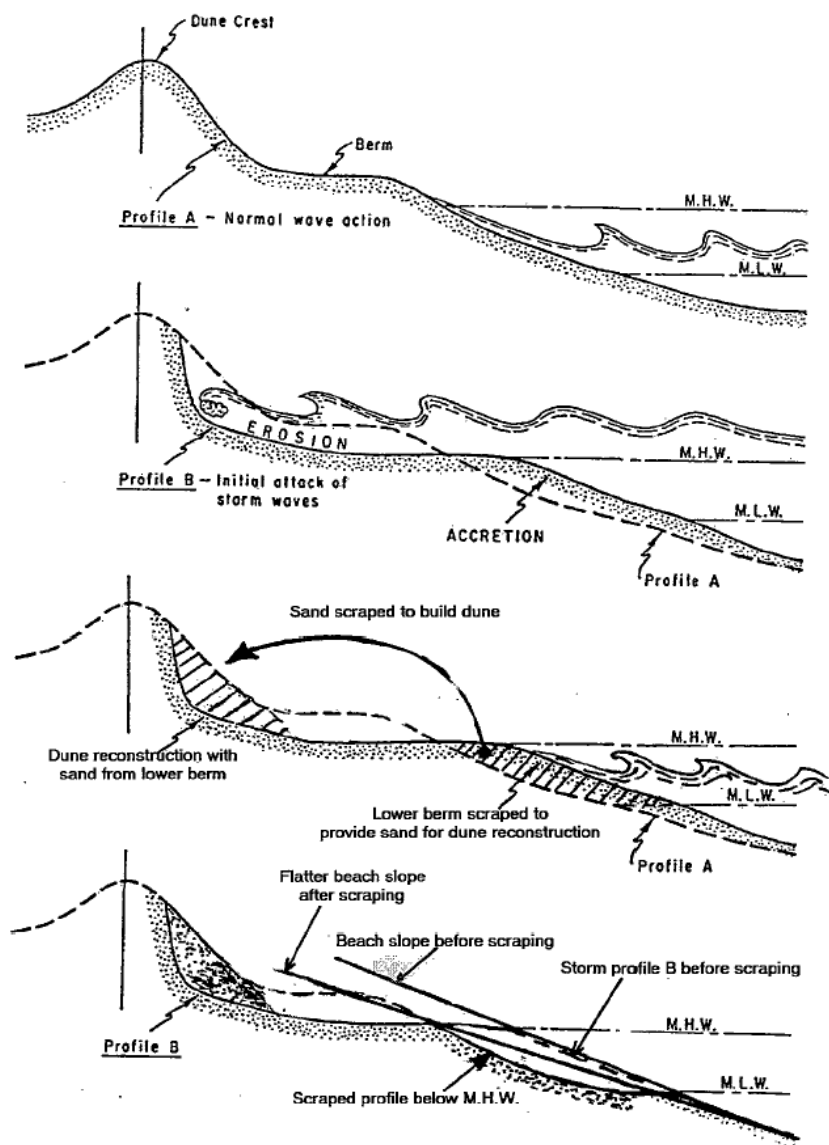


Figure 2.6 Beach scraping concept. Source: Carley et al. (2010).

CHAPTER 2**2.5.2. Beach ploughing**

Beach ploughing is an innovative technique that consists of mechanically ploughing the intertidal area of a beach by terrestrial means during low tide (ridges and furrows are created parallel to the shoreline). Ploughing is expected to modify marine dynamics in the intertidal area and accelerate beach accretion. It is also presented as a nature assisted beach enhancement technique. Monge-Ganuzas et al. (2017) applied ploughing for the first time at Laida beach (northern Spain). In their work, Monge-Ganuzas et al., (2017) conceived ploughing as a soft technique to help accretion build a wider beach earlier in the summer, improving the recreational potential of the beach. The intertidal area of Laida beach was ploughed 22 times, between July and September 2015, generating ridges and furrows with a length of 1.42 m and a height of 0.27 m (Figure 2.7). Gainza et al. (2019) analysed the evolution of the beach and found that ploughing accelerated natural onshore bar migration.



Figure 2.7 Mechanical ploughing being performed at Laida beach during low tide in the summer of 2015.

Beach ploughing does not produce the direct effect of mobilizing sand from the lower intertidal area to the upper beach as scraping does. Its effectiveness relies on the natural mobilization of the sand by the effect of waves over the ridges and furrows. Figure 2.4 shows the geometric characteristics of this innovative nature assisted beach recovery technique. The height is clearly higher than that of naturally formed bedforms for this wavelength; therefore, the induced bed roughness is greater, although progressively

reduced as the ploughing is smoothed out by wave action. The mechanical actions are simpler than the ones required for scraping. Ploughing requires less machinery and can be performed faster, although it should be repeated over several low tides.

2.6. PHYSICAL EXPERIMENTS

Few laboratory experiments have been performed on soft-engineering techniques. Larsen et al. (2023) presented a review of laboratory studies about beach nourishment, but most of them analysed nourishment of the submerged part of the beach profile (bar or through) and therefore their findings do not apply to assessing beach scraping or beach ploughing techniques. Alsina et al. (2012), conducted large-scale experiments and assessed bar migration with two different beachfront morphologies. This morphology can be considered as the reshaping that would be applied in tideless beaches (it only affects the aerial part of the beachfront). The results showed that the bar had a greater tendency to accretion when the beachfront was more dissipative. Sánchez-González et al. (2017) performed large-scale laboratory experiments on beach scraping with the combined effect of waves and tides. They analysed the suitability of two different filling locations for the particular conditions of Orzán and Riazor beach (A Coruña, Galicia). This beach is composed of medium-coarse sediment and presents a beach profile shape that is not commonly observed on other beaches. Therefore, the results cannot be extrapolated to places with different characteristics. Additionally, Sánchez-González et al., (2017) described the experimental layout, but the results and main conclusions extracted from their research have not been published yet.

2.7. CONCLUSIONS

The analysis of the state of the art reveals the following conclusions.

- Accretion processes are poorly understood. Tides and bedforms may play an important role in beach recovery.
- Ploughing is an innovative technique and its real effectiveness needs to be analysed under laboratory-controlled conditions.
- Some authors (Carley et al., 2010; Smutz et al., 1980) affirm that scraping accelerates natural accretion rates but this statement has not been verified by accurate measurements.

CHAPTER 2

- There are not laboratory experimental data available related to scraping nor ploughing techniques.
- Scraping and ploughing may help increase dry beach width in early summer.
- Scraping and ploughing may help increase the sediment budget available on the dry beach and the dune to fight against winter erosion.
- There are no procedures or tools for the selection and design of the most appropriate NBS for beach management according to the specific goal of each location (winter protection or tourism).

CHAPTER 3

NATURAL BEACH ACCRETION

3.1. INTRODUCTION

This chapter analyses the accretion produced on meso/macro-tidal beaches. Despite their relevance for beach recovery, accretion processes are still poorly described in the literature. Accretion rates depend on the previous geometry of the beach profile, the sediment characteristics, the presence of bedforms and the marine dynamics, including wave height, wave period, wave direction, tides and currents. Additionally, accretion is a slow process, making it difficult to measure its characteristics for individual particular marine conditions. Frequently, the measurements can only be made for longer time periods (days), where the accretion is noticeable but a wide range of marine dynamics may have occurred. Numerical models are not able to predict the accreted volume of a particular beach without previous calibration with field data for a particular study site.

The complexity of the combined effect of waves and tides still constitutes a challenge for the knowledge of accretion processes. As stated before, accretion processes are slow, and the morphologic changes associated occur over weeks or months. For this reason, the study of accretion requires a big effort in data collection and is time-consuming (weeks of field surveys or physical simulations). Opposed to erosion, whose effects trigger a direct problem on coastal retreat, accretion is only problematic when it is not able to recover all the sand lost on the beach during eroding episodes. This is not so evident and it is not easy to measure, therefore, the study of accretion has been relegated to a secondary plane. In this

CHAPTER 3

thesis, we acknowledge the importance of understanding accretion in the analysis of coastal stability under present and climate change scenarios.

Quantitative and qualitative description of the behaviour of beaches during calm weather conditions is fundamental for the assessment of the beach resilience and for the design of actions. The NBS proposed in the present thesis were thought to be applied in meso/macro-tidal beaches and therefore, this chapter focuses on those types of beaches, where ploughing and scraping can be applied by terrestrial means during the low tide.

In this chapter, accretion is analysed using field survey data on three study sites. The berm formation along a complete summer season on a meso/macro-tidal, fine sand and gently sloped beach is described here for the first time. The incident marine dynamics are also considered in the analysis. Therefore, the objectives OB1 and OB2 of the thesis are addressed in this chapter 3. Section 3.2 introduces the study site's location, characteristics and summarizes the field survey data collected. Section 3.3 describes the methodologies used for the measurements. Section 3.4 analyses the results, while the discussion and conclusions of these results are shown in sections 3.5 and 3.6, respectively.

3.2. FIELD SURVEY STUDY SITES

This study focuses on meso/macro-tidal beaches exposed to severe marine conditions during winter and mild waves during summer. The differences in incoming wave height between winter and summer lead to sand accretion throughout the summer season. Three study sites were selected on the Atlantic coast of Spain (Figure 3.1): Cádiz (Fuentebravía beach), Santander (El Sardinero I and II beaches), and Somo (Somo and Loredo beaches).

The details and characteristics of each of these sites are detailed in the following. The field surveys on each beach extended from spring to autumn, allowing the measurement of the accretionary evolution during the calm weather period. Each field campaign consisted of the measurement of the geometry of a set of pre-defined beach profiles during low tide. Therefore, the data extends from the dry beach (next to the seafront or the dune foot) to the low tide limit. The set of profiles is shown in the following sections for each beach.

The field surveys' time span and spatial data requirements depend on the processes to be measured. In this study, accretion processes occur during the whole calm weather season (from spring to autumn) and are slow (no need to measure on consecutive days). Additionally, accretion processes might be faster at the beginning (due to a higher

disequilibrium between the actual and equilibrium profiles), and therefore the periodicity of the field surveys was higher at the beginning and lower at the end. As a result, field surveys started in mid-spring, with a weekly or fortnightly periodicity (depending on the study site), and ended in mid-autumn, with a monthly periodicity. The spatial irregularities of accretion are expected to be low. Accretion is a cross-shore process, and therefore, the measurement of individual beach profiles should be enough to analyze it. At least four profiles were selected at each study site, which allows the identification and isolation of other possible effects due to longshore processes. More details on the key factors for the design of field surveys to characterize accretion could be found in Appendix I (in Spanish, Metodología para campañas de campo: caracterización de la acreción en playas), which includes a manual with the periodicity and spatial requirements described above. This manual also takes into consideration the possibility of performing scraping actions on the beach and its survey.



Figure 3.1 Location of the field survey sites.

As indicated in the introduction, marine dynamics are the main responsible for beach accretion. Historical wave and tide characteristics (marine climate) of each study site have been analyzed before the site selection. The existence of a strong difference between winter and summer wave height and the presence of meso/macro-tidal range were verified. Once the field surveys were performed, the marine dynamics that occurred during the surveys' time span were obtained from the IH-Data reanalysis database. Astronomical tide data was extracted from GOT database, storm surge from the GOS database and waves from the

CHAPTER 3

GOW database. The ocean water level (OWL) was obtained by adding the astronomical tide and the storm surge time series. These databases are available at IHCantabria and are described below:

- GOT (Global Ocean Tides): The astronomical tide is generated using the harmonic constants derived from the TPXO7.2 global tides model, developed by Oregon State University. TPXO7.2 is a current version of a global model of ocean tides, which best-fits, in a least-squares sense, the Laplace Tidal Equations and along track averaged data from TOPEX/Poseidon and Jason (on TOPEX/POSEIDON tracks since 2002). The methods used to compute the model are described by Egbert et al. (1994) and further details are provided by Egbert and Erofeeva (2002). The database includes eight primary (M_2 , S_2 , N_2 , K_2 , K_1 , O_1 , P_1 , Q_1), two long period (M_f , M_m), and 3 non-linear (M_4 , MS_4 , MN_4) harmonic constituents, provided in a global grid of 1440×721 points, at $1/4$ degree resolution full global grid. This information is used to reconstruct hourly time series of the tide in any location worldwide using the tool `t_tide` (Pawlowicz et al., 2002).
- GOS (Global Ocean Surges) is a dataset of 43-year (1979-2022) storm surge. GOS encompasses 2 regions: Southern Europe and Latin-America (including Caribbean, Atlantic and Pacific areas). The historical reconstruction of storm surge in the European region (Abascal et al., 2012; Cid et al., 2014) has a spatial resolution of $1/8^\circ$ (~30km), while the American region has $1/4^\circ$ (CEPAL, 2012; Losada et al., 2013). Both regions provide hourly outputs and have reconstructed historical storm surge events. GOS has been performed using the Regional Ocean Model System (ROMS), developed by Rutgers University (Shchepetkin and McWilliams, 2005, 2003). ROMS is a three-dimensional, free-surface, terrain-following ocean model that solves the Reynolds-averaged Navier-Stokes equations using the hydrostatic vertical momentum balance and Boussinesq approximation.
- GOW (Global Ocean Waves) is a historical reconstruction of ocean waves. GOW has been generated from the spectral model WaveWatch III (Tolman, 1991, 1989). Spectral wave models have been developed over the two last decades and have now reached a level of accuracy that enables reproducing significant wave height and peak period with errors below 15%. GOW encompasses several hourly reanalysis projects at different spatial resolutions: a global wave reanalysis as well as several regional wave reanalysis in Europe, America or Arabian region. Adequate configured model and input forcings have been used for each project. More detailed information about particular GOW projects can be found in Reguero et al. (2012) and Reguero et al. (2013).

The time series of marine dynamics extracted from these databases will be presented in the following subsections and the results section of this chapter.

3.2.1. Cádiz

Fuentebravía (Puerto de Santa María, Cádiz) is a pocket beach limited by two groynes, one at the northwest, in the limit between the NATO Naval Base at Rota and the public area (constructed in 1993, Muñoz and Gutiérrez, 1999) and the other at the southeast (constructed in 2014) in front of Punta Bermeja headland (Figure 3.3). The beach length is 630 m and the average width of its dry area is 48 m (Delcamp, 2022). It faces the Atlantic Ocean, and it is partially sheltered by Rota at the west and by Cádiz at the south (see Figure 3.2). Additionally, it is protected by a rocky floor platform (Benavente et al., 2006) at approximately 500 m from the shoreline. Fuentebravia is an urban beach, where both, local people and tourists demand increasing dry beach space.



Figure 3.2 Fuentebravía beach location and surrounding elements that influence the morphodynamics.

CHAPTER 3

Fuentebravía beach underwent continuous recession over the period 1956-2014 (Del Río et al., 2018) despite nourishments were performed in 1992, 1994 and 1996 (Del Río et al., 2013; Muñoz-Pérez et al., 2001), and the groyne at the northwest was built in 1993. Those erosive issues appeared after the construction of Rota harbour, the Naval Base harbour and La Costilla beach groyne at Rota. Those man-made elements blocked the littoral drift (directed southwards) that historically transported sediments from Guadalquivir river mouth to Fuentebravía and Cádiz bay. Additionally, anthropic actions over Guadalquivir and Guadalete rivers reduced their sediment load to this coastal cell. As a consequence of these changes, in 2014 the second groyne was built in front of Punta Bermeja, in order to stabilize the shoreline and generate a pocket beach (Figure 3.3). The beach restoration performed in 2014 included the groyne and a beach nourishment of fine sand with medium grain size of 0.25 mm (Delcamp, 2022). Despite all those actions, Fuentebravía beach still deals with occasional erosion episodes under extreme wave events like the ones that occurred in winter 2015 and 2018 respectively. This evidences that Fuentebravía is a good candidate for coastal management with NABE actions like scraping or ploughing.

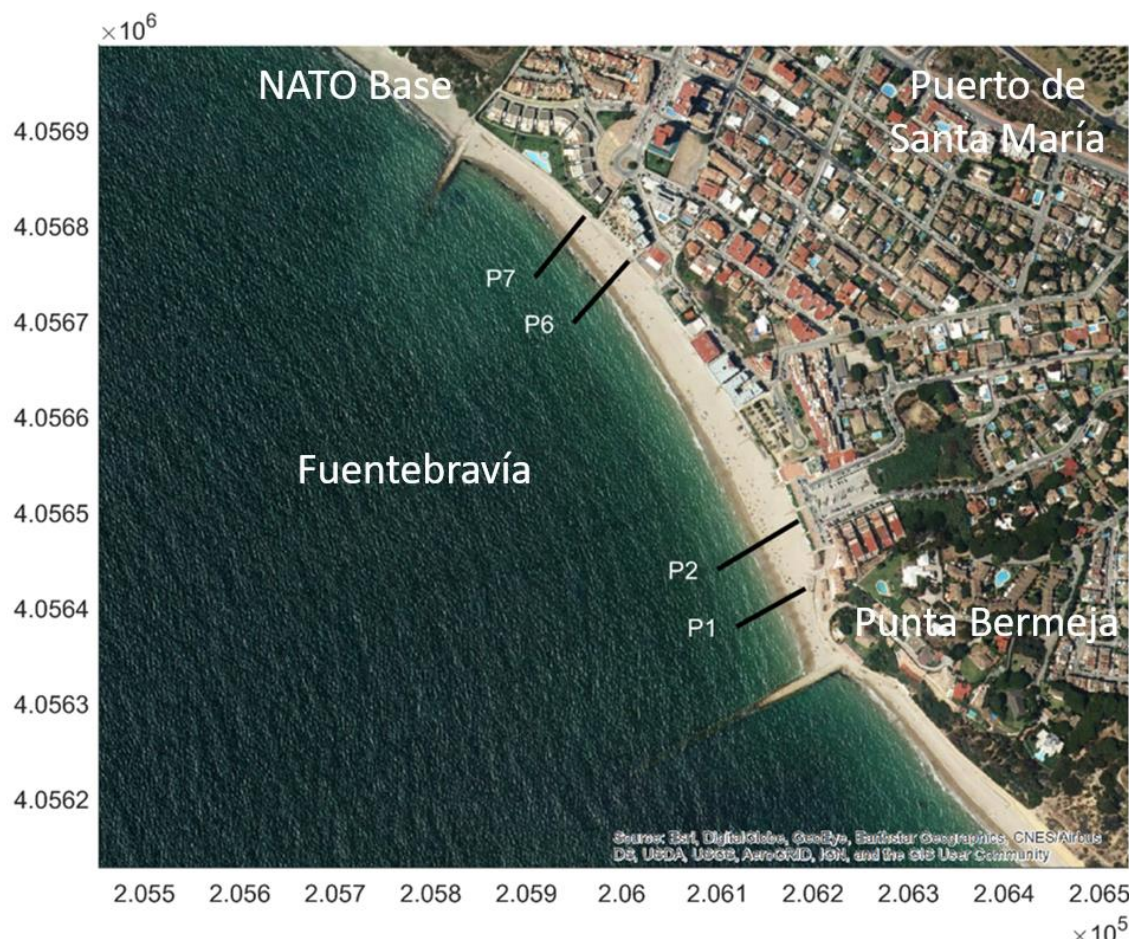


Figure 3.3

Location of measured profiles at Fuentebravía beach.

The incident waves at Fuentebravía in winter typically have significant wave heights between 1 and 2.8 m, a period of around 12 s and come from the west-southwest (with a direction of 260°N). Besides, in summer, the wave height varies between 0.2 and 0.9 m, with a period of around 5 s and come from the west (270°N). Figure 3.4 shows the wave characteristics at Cádiz bay during 2021. The average tidal range is 2 m. More details on marine dynamics are given in the results section.

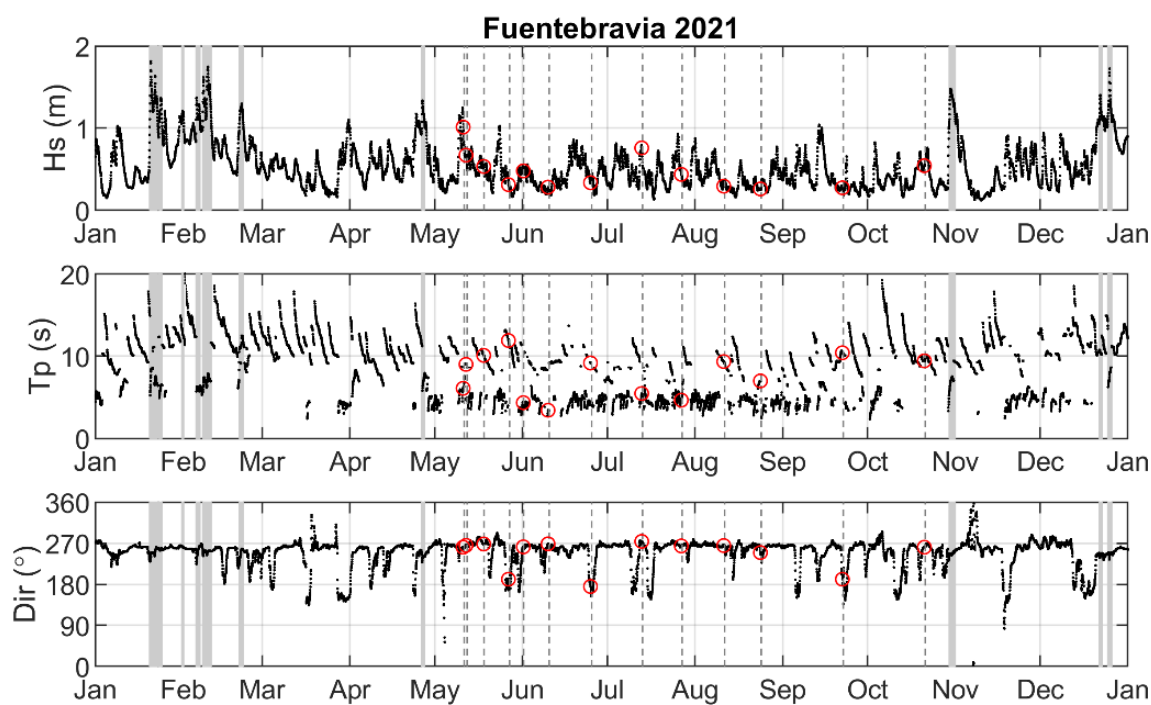


Figure 3.4 Wave characteristics extracted from GOW database at Cádiz bay. Grey-shaded areas indicate storm conditions, where significant wave is above the 5% exceedance level with a minimum duration of one tidal cycle and $\Omega > 4$. Vertical dashed lines are the dates of the field surveys and red circles indicate the wave characteristics at the high tide previous to each survey.

The beach monitoring extended from May to October 2021. During this time period, 13 field surveys were performed on the following dates: 2021-05-11, 2021-05-12, 2021-05-18, 2021-05-27, 2021-06-01, 2021-06-10, 2021-06-25, 2021-07-13, 2021-07-27, 2021-08-11, 2021-08-24, 2021-09-22, 2021-10-21. Each survey consisted of the measurement of the sand elevation along a set of 4 beach profiles (Figure 3.3, exact coordinates shown in Table 3.1), that extended from the dry beach next to the promenade to the low tide limit. Expert surveyors took the measurements with a high-precision RTK-GPS device. This data was obtained thanks to the collaboration with Demarcación de Costas Andalucía Atlántico (Ministerio para la Transición Ecológica y el Reto Demográfico).

CHAPTER 3

Table 3.1 Coordinates that define the beach profiles measured at Fuentebravía beach.
ETRS89-UTM30N coordinate system.

Profile	Origin X	Origin Y	Near low-tide X	Near low-tide Y
P1	206192	4056420	206120	4056380
P2	206185	4056491	206100	4056440
P6	206007	4056763	205949	4056698
P7	205961	4056810	205909	4056746

The aforementioned set of profiles measured the natural behaviour of Fuentebravía beach during the summer season of 2021. Additionally, those surveys were also used to analyse the effect of scraping actions. Scraping was performed on the 12th of May 2021 on the central part of Fuentebravía beach. The measurements taken and the associated results are shown in section 5.4 of chapter 5.

3.2.2. Santander

El Sardinero beach (Santander, Cantabria) is a static equilibrium pocket beach (González and Medina, 2001) limited at the north by the headland of Cabo Menor, and at the south by a rocky floor. The beach is split in two during the high tide, due to the presence of Piquío headland (Figure 3.7). The beach at the south of Piquío is called El Sardinero I (length of 350 m) and the one at the north El Sardinero II (length of 760 m). During the low tide, both beaches are connected. The average width of the beaches is 70 m, and are formed by fine golden sand with an average grain size of 0.2 mm (Álvarez, 2016). The beach is exposed to the Cantabrian Sea (Atlantic Ocean), and it is partially sheltered by the headlands of Cabo Mayor and Cabo Menor at the north (Figure 3.5), and the coast of Cantabria at the west.

El Sardinero is the largest beach in Santander, and it is widely used by local people and tourists. Back in 1849, El Sardinero was popularized as a sea-bathing touristic destination (Walton, 2005), and it has been used for that since then. The beach is in static equilibrium, but the hardening of marine climate due to climate change effects produced sporadic erosion episodes recently. The most relevant one was produced by the storms of February and March 2014 (Gómez, 2020), which produced much damage on the beaches of the north of Spain. El Sardinero eroded due to these storms (Álvarez, 2016), and required nourishment actions to recover. The nourishment performed was nature-based and consisted of dredging 31.000 m³ of sand from the submerged part of the beach profile and placing them on the dry beach (Cores, 2014). The actions were performed in May 2014, with

the same philosophy as the scraping actions analyzed in the present thesis. The main difference is that this nourishment required maritime machinery and the scraping only requires terrestrial means.



Figure 3.5 Santander and Somo study areas' location and surrounding elements that influence the morphodynamics.

The incident waves at El Sardinero in winter typically have significant wave heights of 5 m, a period bigger than 10 s and come from the NNW. Besides, in summer, the wave height varies between 0.2 and 2.2 m, with a period between 5 and 13 s and come from the NW to NE. Figure 3.6 shows the wave characteristics at El Sardinero during 2019. The tides are semi-diurnal with a mean tidal range of 3 m and a spring tidal range of 5 m (Medina et al., 2007). More details on marine dynamics are given in the results, section 3.4.

CHAPTER 3

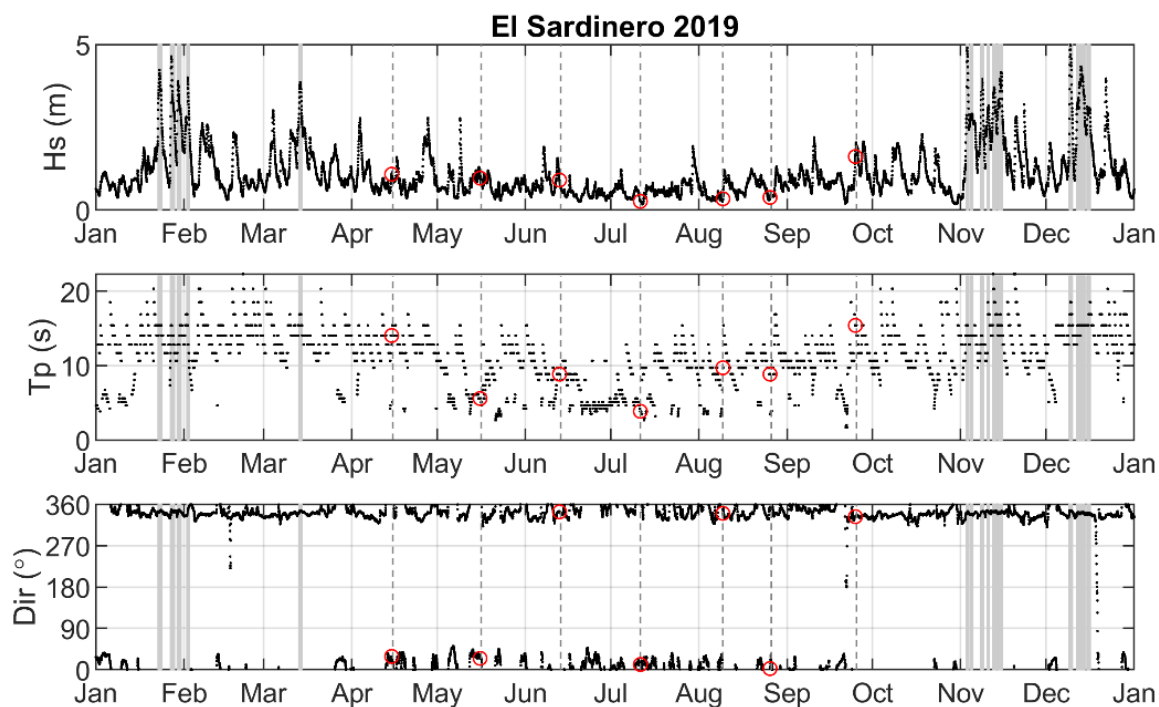


Figure 3.6 Wave characteristics extracted from the GOW database in front of El Sardinero beaches. Grey-shaded areas indicate storm conditions, where significant wave is above the 5% exceedance level with a minimum duration of one tidal cycle and $\Omega > 4$. Vertical dashed lines are the dates of the field surveys and red circles indicate the wave characteristics at the high tide previous to each survey.

The beach monitoring extended from April to September 2019. During this time period, 7 field surveys were performed on the following dates: 2019-04-15, 2019-05-16, 2019-06-13, 2019-07-11, 2019-08-09, 2019-08-26, 2019-09-25. Each survey consisted of the measurement of the sand elevation along a set of 7 beach profiles, three of them in El Sardinero I and four in El Sardinero II (Figure 3.7, exact coordinates shown in Table 3.2), that extended from the dry beach next to the promenade to the low tide limit. The data was measured by two surveyors with a distancemeter device and a target, following the methodology described in section 3.3.2. This methodology was validated with RTK-GPS measurements on a field campaign.

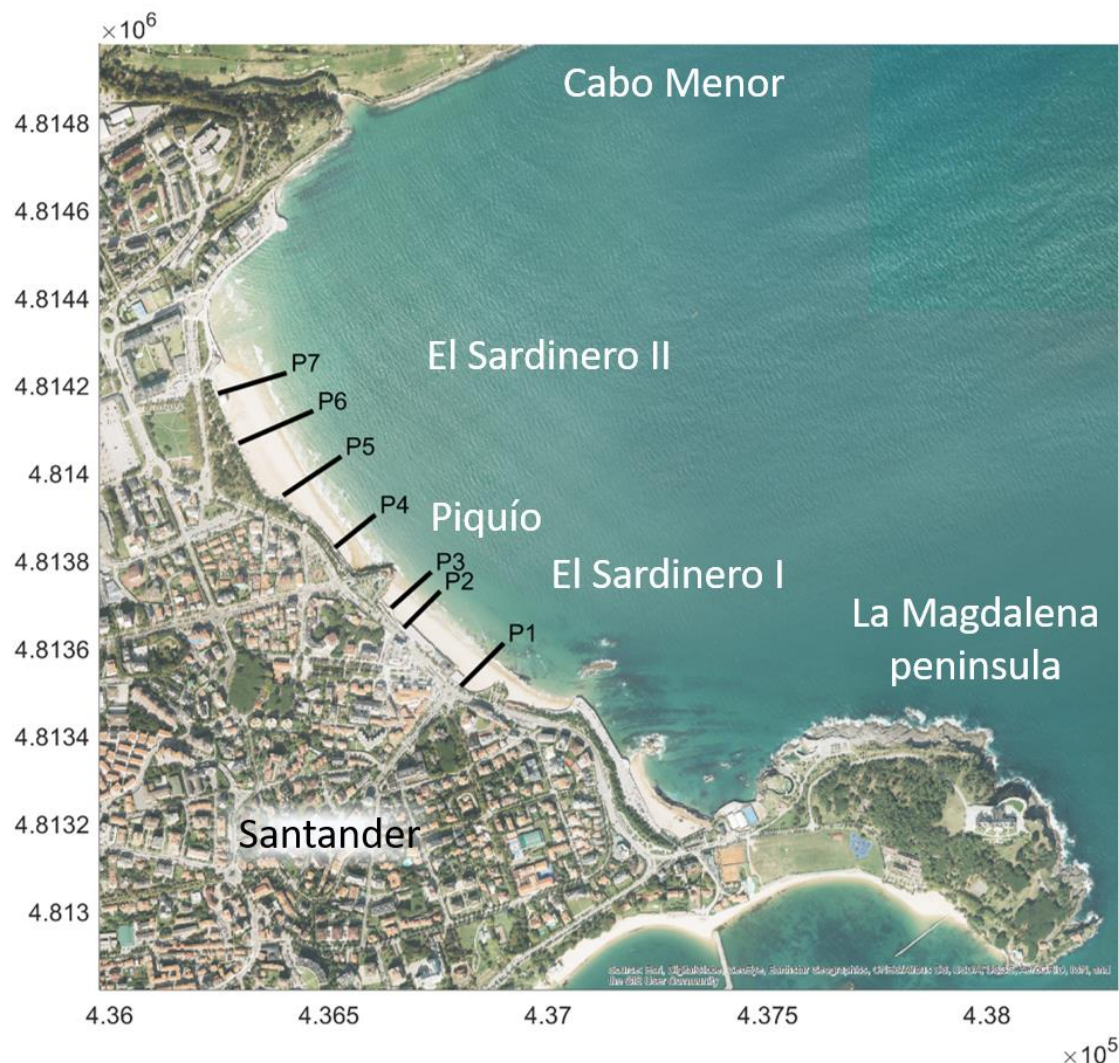


Figure 3.7 Location of measured profiles at El Sardinero I and II beaches.

Table 3.2 Coordinates that define the beach profiles measured at El Sardinero I and II beaches. ETRS89-UTM30N coordinate system.

Beach	Profile	Origin X	Origin Y	Near low-tide X	Near low-tide Y
Sardinero I	P1	436800.067	4813513.88	436898.439	4813612.23
	P2	436670.331	4813646.91	436753.523	4813730.59
	P3	436641.384	4813692.32	436732.984	4813774.57
Sardinero II	P4	436512.891	4813829.96	436605.779	4813905.08
	P5	436395.135	4813949.04	436527.855	4814038.02
	P6	436293.661	4814068.10	436463.958	4814141.93
	P7	436246.681	4814181.32	436402.922	4814228.67

CHAPTER 3

3.2.3. Somo

Loredo, Somo, and El Puntal beaches (Somo, Cantabria) are part of the same coastal system that extends from the surroundings of Santa Marina island to the navigation channel that allows access to Santander harbour in Santander bay. From west to east (Figure 3.5), we find Loreto beach (approximately 1 km long), Somo beach (around 1.3 km long) and El Puntal beach, which is a 2.5 km long spit (Pellón et al., 2014). The average width of the beaches is 50 m, and are formed by fine golden sand with an average grain size of 0.25 mm (Losada et al., 1991). The beaches are exposed to the Cantabrian Sea (Atlantic Ocean), and they are partially sheltered by the La Magdalena peninsula and Mouro island at the northwest, and Santa Marina island at the northeast (Figure 3.5 and Figure 3.8).

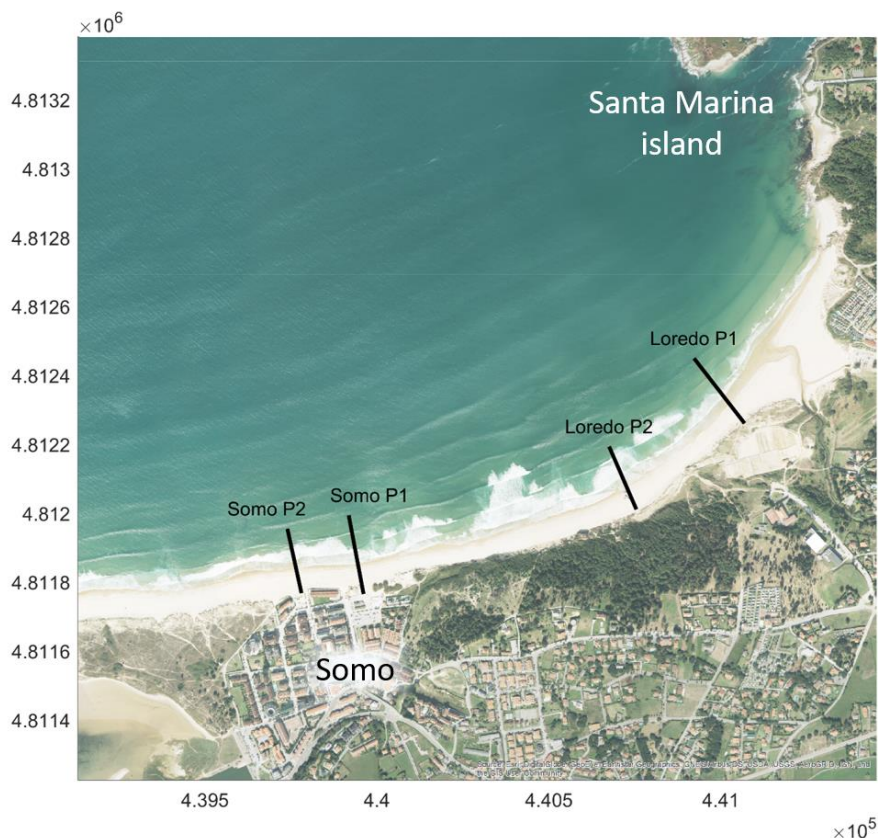


Figure 3.8 Location of measured profiles at Somo and Loreto beaches.

This coastal system is dominated by waves and tidal currents from Santander bay. The dredging operations performed during the 20th century and the land claiming (that reduced a 50% the bay's area) modified the dynamic balance (Losada et al., 1991) between the tidal prism volume, channel dimensions, Las Quebrantas shoal (which disappeared) and the longshore transport along the beaches (from east to west). The dredging of the

channel prevents the spit from growing to the west. The sand dredged was historically used for land reclamation, but since the 1990s this sand is used for the nourishment of Loredo beach (Medina et al., 2007), which suffered erosion due to the lack of sand input as Las Quebrantas shoal disappeared. As a consequence of the extraction of sand from the system, the coast at Loredo and Somo beaches underwent a steady retreat, and the Loredo dune suffered erosion. The application of NABE techniques in this area would be beneficial for the recovery of extra sand volume for the restoration of the dune and dry beach area.

The incident waves at Somo and Loredo in winter typically have significant wave heights of 4.5 m, a period bigger than 10 s and come from the NNW. Besides, in summer, the wave height varies between 0.2 and 2.5 m, with a period between 5 and 13 s and come from the range NW to NNE. Figure 3.9 shows the wave characteristics at Somo and Loredo during 2019. The tides are semi-diurnal with a mean tidal range of 3 m and a spring tidal range of 5 m (Medina et al., 2007). More details on marine dynamics are given in the results section.

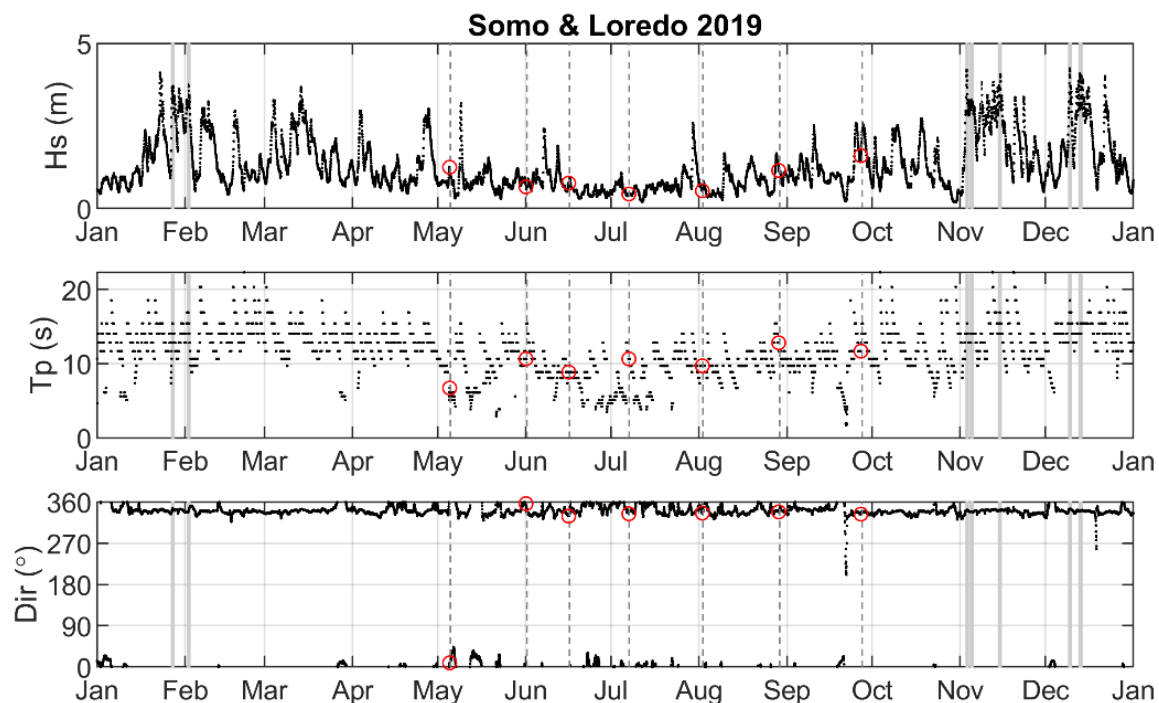


Figure 3.9 Wave characteristics extracted from the GOW database in front of Somo and Loredo beaches. Grey-shaded areas indicate storm conditions, where significant wave is above the 5% exceedance level with a minimum duration of one tidal cycle and $\Omega > 4$. Vertical dashed lines are the dates of the field surveys and red circles indicate the wave characteristics at the high tide previous to each survey.

CHAPTER 3

The beach monitoring extended from May to September 2019. During this time period, 7 field surveys were performed on the following dates: 2019-05-05, 2019-06-01, 2019-06-16, 2019-07-07, 2019-08-02, 2019-08-29, 2019-09-27. Each survey consisted of the measurement of the sand elevation along a set of 4 beach profiles, two of them in Somo and the other two in Loredo (Figure 3.8, exact coordinates shown in Table 3.3), that extended from the dry beach, next to the promenade or on the dune, to the low tide limit. The data was measured by two surveyors with a distancemeter device and a target, following the methodology described in section 3.3.2. This methodology was validated with RTK-GPS measurements on a field campaign.

Table 3.3 Coordinates that define the beach profiles measured at Somo and Loredo beaches.
ETRS89-UTM30N coordinate system.

Profile	Origin X	Origin Y	Near low-tide X	Near low-tide Y
Somo P1	439960.961	4811765.52	439917.757	4811993.85
Somo P2	439780.399	4811768.08	439739.306	4811955.09
Loredo P1	441068.944	4812260.85	440921.967	4812449.56
Loredo P2	440754.383	4812011.01	440675.104	4812193.45

3.3. METHODS

Two measurement methodologies were used for this study. The field surveys at Fuentebavía beach were performed with professional topography devices, using RTK-GPS technology. This type of measurement is highly accurate but expensive, and therefore, the field surveys at El Sardinero, Somo and Loredo beaches were performed with a simpler technique (using a distancemeter) that can be carried out by unexperienced surveyors and result in accurate data with inexpensive tools. The results obtained with this technique were validated with RTK-GPS on a single field survey for each profile.

The details and methodology used for the measurement with each technology are described in the following.

3.3.1. Measurement with RTK-GPS

High-precision measurements were taken with a professional Real-Time Kinematic Global Positioning System (RTK-GPS) device. This technique uses GPS satellite technology and increases its accuracy by employing additional reference bases fixed on land. The device directly measures on ETRS89 coordinate system. Planimetry and altimetry errors are of the order of millimetres. RTK-GPS allows fast and accurate measurements but requires expensive equipment and expert surveyors.

Figure 3.10 shows the RTK-GPS equipment employed during the field survey performed at El Sardinero beach for the validation of distancemeter measurements.



Figure 3.10 Field survey at El Sardinero beach employing RTK-GPS device.

CHAPTER 3**3.3.2. Measurement with distancemeter**

A distancemeter device is based on laser and measures accurately the distance from the device to a target and the inclination, or angle from the horizontal plane to the target. The use of trigonometric relations makes it possible to obtain the topography of a beach profile by concatenation of consecutive measurements. This technique is inexpensive and unexperienced personnel can perform the survey. Ward et al., (2021) is an example of successful surveys performed with a simple technique (similar to the one proposed here) and volunteers.

Before the beginning of the surveys, the profiles to be measured should be defined based on ground references (origin and orientation). The origin should be in the study area and constitute a fixed point on the beach profile to be measured. Examples of valid origin points are railing on the promenade or on a dune elevated path. The orientation of the profile should be approximately perpendicular to the shoreline and can be defined by the alignment of two elements inland. Examples of valid orientation references can be streetlights, the ridge of a roof or mountain summits. Figure 3.11 shows the definition of profile 1 measured at the Somo study site.

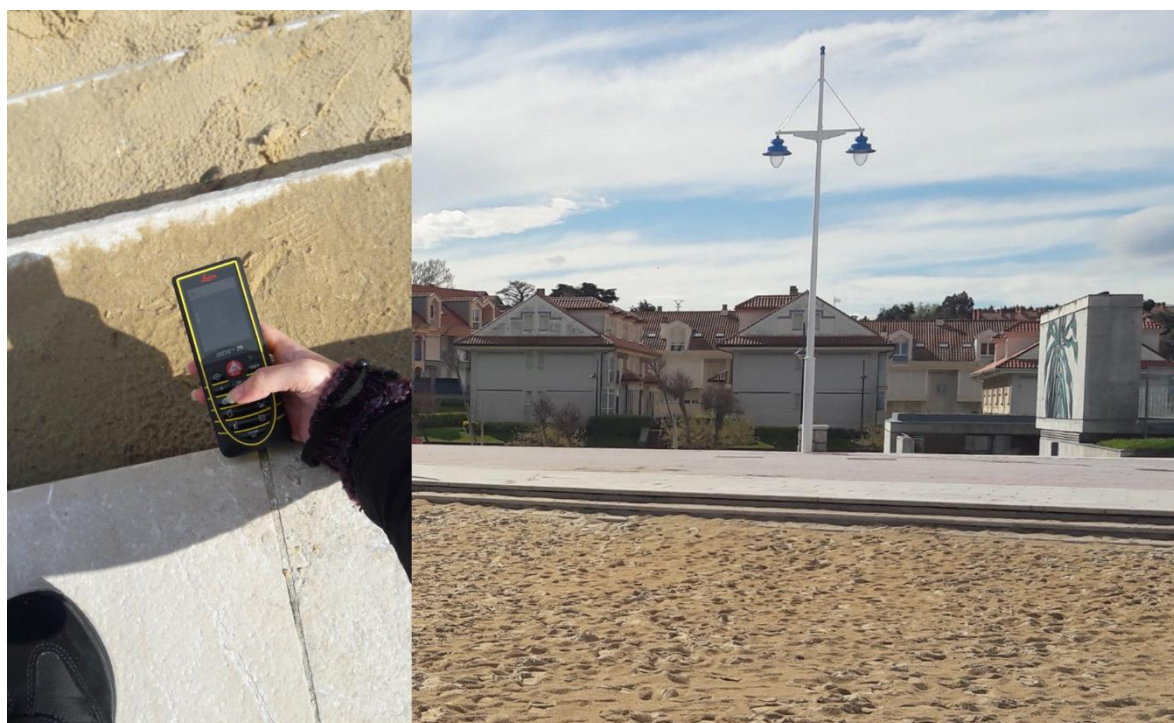


Figure 3.11 Example of profile definition (Somo P1). Left: Origin at the joint between the stone tiles of the upper stair at the entrance to the beach. Right: Orientation definition by the alignment of the streetlight and the ridge of the roof.

The survey of a single beach profile consists of the consecutive measurement of points from the origin to the shoreline (during low tide). Both surveyors are provided with a walking stick of the same length to ensure that the distancemeter device and the target are at the same distance from the ground. One of the surveyors (S1) stands at the origin point with the distancemeter on top of the walking stick. The other (S2) stands at approximately 10 m seawards following the straight line indicated by the orientation reference (with S1 aligned in between the references and S2). S2 holds the target on top of the walking stick while S1 takes the first measurement. The measurements of distance and angle are successively written on a survey notebook (an example can be found in Appendix I). Once the point is measured, S1 occupies the location of S2 and S2 advances approximately 10 m to the sea following the same orientation alignment (Figure 3.12). Successive measurements are taken up to reaching the low tide limit.



Figure 3.12 Measurement procedure for obtaining each profile point. On the left the surveyor S1 with the distancemeter device on the top of the walking stick, and at the right the other surveyor S2 with the target at the top of the walking stick. Both walking sticks were set to the same height.

More details on the measurement procedure of this technique could be found in Appendix I (in Spanish, *Metodología para campañas de campo: caracterización de la acreción en playas*), which includes the survey notebook used for the surveys performed at El Sardinero, Somo and Loredo beaches.

The data collected is then processed by applying trigonometric relations to obtain the distance and elevation of the points along the beach profile. The elevations are referred to the Spanish mean sea level datum (NMMA) based on the RTK-GPS measurement of the elevation of the origin fixed point of each profile. The results have been validated with RTK-

CHAPTER 3

GPS measurement of all the profiles of El Sardinero beach the 2019-09-25 and all the profiles of Somo and Loredo beaches the 2019-09-27. The profiles were measured by both techniques on the indicated dates. The comparison of every single profile showed good agreement (Figure 3.13, the vertical root-mean-square error of distancemeter data was 0.09 m relative to RTK-GPS data), demonstrating that the accuracy of the method described here is enough to characterise beach accretion.

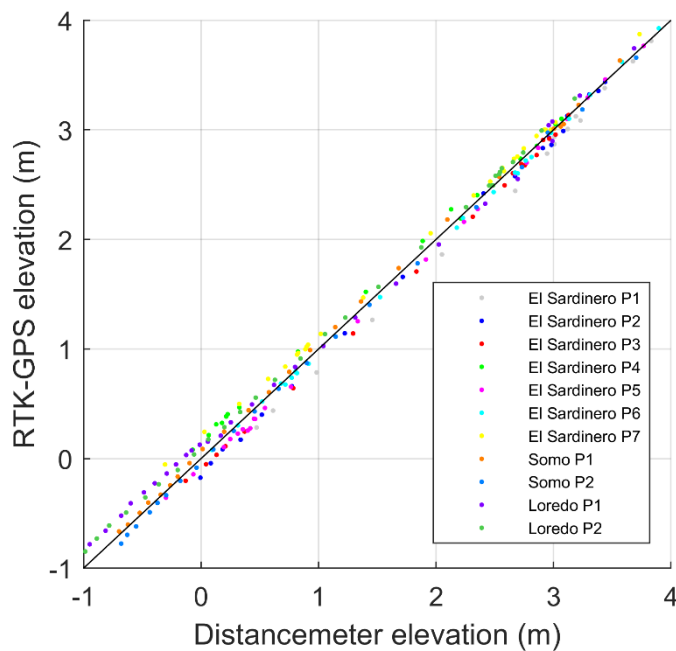


Figure 3.13 Validation of distancemeter measurements with RTK-GPS.

3.4. RESULTS

The data collected during all the surveys were referred to the local mean sea level of each study site and then plotted in Figure 3.14, Figure 3.16, Figure 3.17, and Figure 3.19. Each of these figures shows the beach profile evolution during the whole summer season analysed. Jensen et al. (2009) observed that during the falling tide, the beach profile was close to equilibrium and that the berm migrates onshore during rising tide and stabilizes when the high tide level is reached. Therefore, the geometry of the profiles measured at low tide should be representative of the accretion achieved up to the previous high tide. Accordingly, the plots include the ocean water level (OWL) at the high tide previous to each survey date (dashed line), and the shoreline position (intersection between the OWL at the previous high tide and the measured profile, circle). Both references of the OWL conditions previous to the survey are plotted with the same colour as the profile.

Then, the survey data was processed to obtain the following morphologic parameters:

- Shoreline progradation: It is the shoreline position computed at the level of the mean high water spring (MHWS). The position of the shoreline on the first survey was taken as the reference of the shoreline progradation. This parameter is indicative of the dry beach widening achieved (extra coastal protection and space for tourism).
- Accreted volume: It is the volume of sand accumulated on the berm taking the first survey as a reference. Only areas of accumulation have been considered. The berm extended from the dry beach to the nodal point on the lower profile described by Phillips et al. (2019) when the beachface prograde and the berm aggrade (rises).
- Slope: It is the slope of the beachface at the level of the high tide previous to each survey.
- Berm elevation: The berm crest was manually identified as the highest point around the maximum change of slope between the high tide level and the dry beach. If a profile exhibits two berms, the one closer to the sea was selected, as it is the new berm formed during the previous tidal cycles.

All those morphologic parameters are shown in Figure 3.15, Figure 3.18, and Figure 3.20. Those figures also show the following relevant hydrodynamic parameters:

- Dimensionless fall velocity (Dean, 1973): $\Omega = \frac{H_s}{wT_p}$ computed as a function of the significant wave height (H_s), wave peak period (T_p) and fall velocity of grain particles (w ; Hallermeier, 1981). The mean dimensionless fall velocity $\bar{\Omega}$ of each study site was computed as the average of hourly Ω during the whole year in which surveys took place (plotted with a dashed line).
- Equilibrium dimensionless fall velocity: Ω_∞ proposed by Wright et al. (1985) considering $\Phi = 5$ days and $D = 30$ days as suggested by the authors. This parameter takes into account the morphodynamic states of the beach on previous days and performs a weighted mean considered as beach memory.
- Ocean water level (OWL): Was obtained by adding the astronomical tide and the storm surge time series extracted from GOT and GOS databases, respectively.
- Total water level (TWL): Was obtained as the OWL plus the wave runup (R_2), obtained with Stockdon's et al. (2006) formulation.
- Mean high water spring (MHWS): Was computed for the astronomical tide time series and plotted with a dashed line.

CHAPTER 3

In the following sections, the results for each study site are analysed. After that, the relations between hydrodynamic variables and the morphologic parameters are evaluated.

3.4.1. Cádiz

Figure 3.14 shows the evolution of Fuentebravia beach during the summer season of 2021 by means of the thirteen field surveys performed. The four profiles analysed show similar behaviour, with significant accretion starting in mid-May. The new dry beach is progressively formed from May to September as the beach berm recovers its sand. During this period, shoreline progradation dominates although some changes on the berm level are observed. Finally, during October the berm aggrades, increasing the height of the dry beach and the accreted volume. The last months of surveys, show a progressive steepening of the beachface, generating the nodal point described by Phillips et al. (2019).

The previously explained evolution can be clearly seen in Figure 3.15. Shoreline progradation and accreted volume increase from mid-May to October. The rates are different between profiles, being Profile 1 the one that achieved more accretion and shoreline progradation, and Profile 7 the one that achieved the least. This reveals a clockwise rotation of Fuentebravia beach during the study period. This rotation agrees with the change in the incoming wave direction from 260°N during winter to 270°N during summer. The magnitude of the accretion was enough to prevent the erosion of Profiles 6 and 7 at the northwest end of the beach. Those profiles were able to feed the necessary sand for the rotation without shoreline retreat.

The shoreline progradation was measured at the level of MHWS = 1.36 m, obtained from OWL time series. The shoreline prograde at a rate of ~ 5 m/month for Profiles 1 and 2, and a rate of ~ 2 m/month for Profiles 6 and 7. Shoreline retreat is observed in the second half of July although the accretion volume increases. This is an effect associated with a step in the berm crest elevation and a change in the high tide level due to spring-neap-spring tidal cycles that will be further analyzed in section 3.4.4. Shoreline progradation decelerates in September and October, with a rate of 2.5 m/month for Profiles 1 and 2, and a rate of 0.5 m/month for Profiles 6 and 7.

Besides, the average accretion rate of Profiles 1 and 2 is 6 m³/month from May to September and increases to 15 m³/month in October (2.5 times bigger). In this case, the accretion volume rate increases at the end of the survey period instead of the deceleration observed in shoreline progradation. This effect highlights the importance of the berm level changes due to its impact on the accreted volume. Profiles 6 and 7 accrete at a rate of

7 m³/month from mid-May to mid-June. Then the beach rotation starts and Profiles 6 and 7 struggle to accrete 0.5 m³ in the following three months. Finally, the berm aggradation produced in October produces 7.5 m³ of accretion during the last month. This progressive and quite uniform accretion rate is in agreement with the Ω_∞ values obtained for the summer season at Fuentebravía beach. Ω_∞ oscillates between 1.1 and 4.5 during the study period, while $\bar{\Omega} = 2.58$. During this period, H_s did not exceed 0.9 m and T_p was frequently 5 s, although it reached 12 s during punctual episodes (Figure 3.4). When relatively high waves ($H_s = 0.9$ m) came with those low periods ($T_p = 5$ s) the dimensionless fall velocity Ω increased above $\bar{\Omega}$ although this did not impede beach accretion. Section 3.4.4 includes a detailed analysis of the relation between Ω_∞ and accretion rates.

The beachface slope varies between 0.03 and 0.11 during the first months. This high variability may be caused by the different morphology of the beach profile during the different stages of the spring-neap-spring tidal cycle as will be analyzed in section 3.4.4. The last three surveys were performed during spring tides (similar beach morphologies) and show an increase in beach slope. This is the evidence of the progressive beachface steepening described by Phillips et al. (2019), which indicates the completion of the recovery period. After that, the first storm of the autumn occurred on October 29th. A slope of 0.08 was chosen as representative of the whole study period. This slope was used for the calculation of the runup R_2 with the formula of Stockdon et al. (2006).

The berm crest elevation is represented in the lower panel of Figure 3.15 with the time series of OWL and TWL. MHWS level was represented as a reference. It can be seen that the measurements taken during neap or spring tides below the MHWS level may produce berm crests below MHWS. This process was described by Phillips et al. (2019) as the formation of a new berm during neap tides that progressively aggradates as the tidal range increases. In May and June, two field surveys presented berm crests below MHWS, and therefore, the shoreline progradation generated by the new berm was not measured. This is sometimes reflected as shoreline retreat although the previous shoreline position was recovered with spring tides. Apart from these new berm formation events, the berm crest elevation is quite constant over time and space (all profiles show similar berm levels). Once the berm reaches a level this is maintained with small descents until the berm level is overtopped by TWL, which causes a sudden berm elevation growth. The biggest step in the berm level was produced in October when the berm crest rose 0.35 m. This is associated with an increase in the period of waves, which produces an increase in wave runup and TWL, and a descent in Ω . Additionally, equinoctial spring tides were also produced during the first weeks of October, increasing, even more, the TWL. The relation between the berm crest level and TWL is thoroughly analyzed in Section 3.4.4.

CHAPTER 3

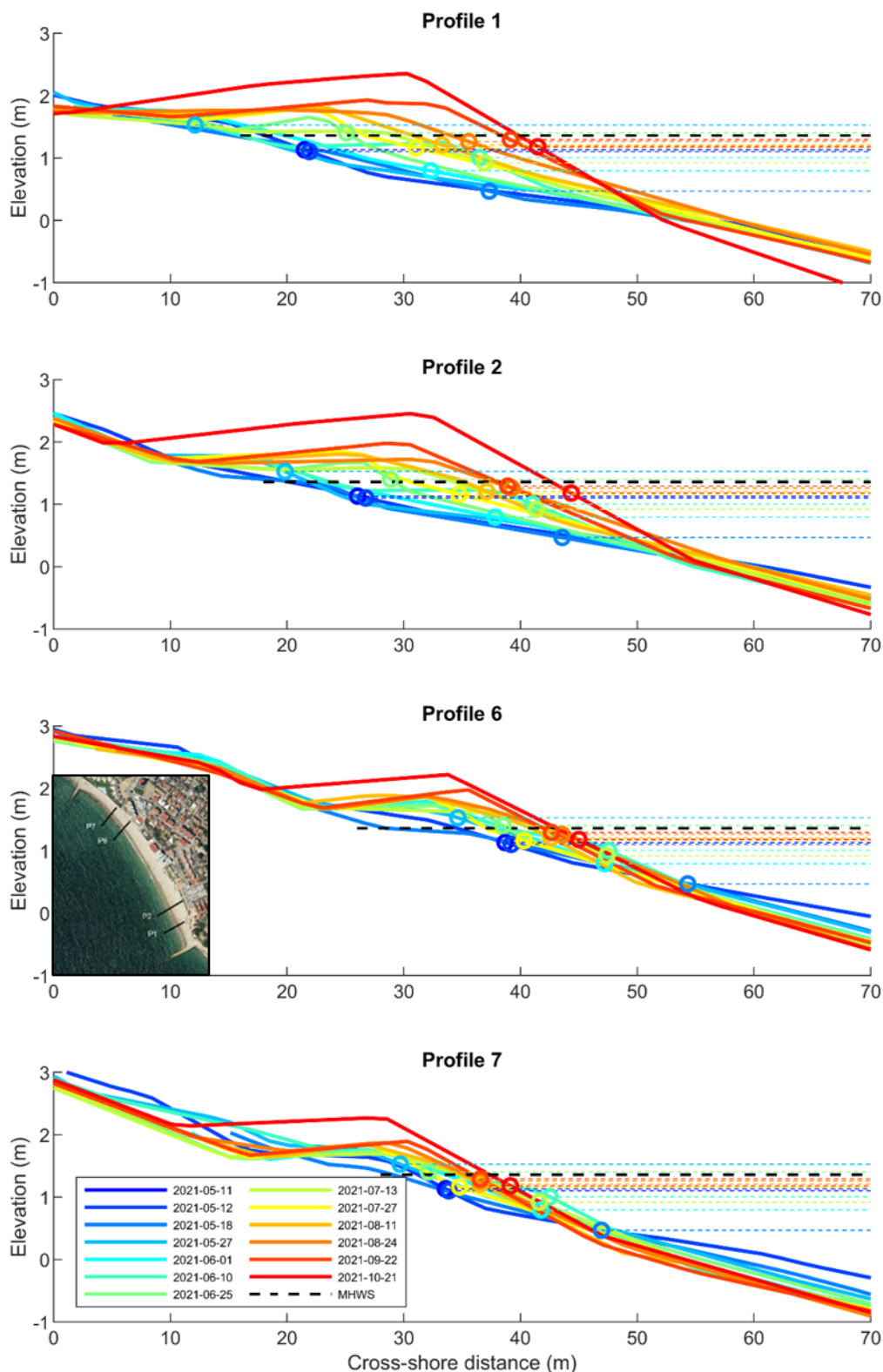


Figure 3.14 Beach profile evolution at Fuentebravíá (dry beach and intertidal zone). Elevation referred to the local mean sea level of Fuentebravíá.

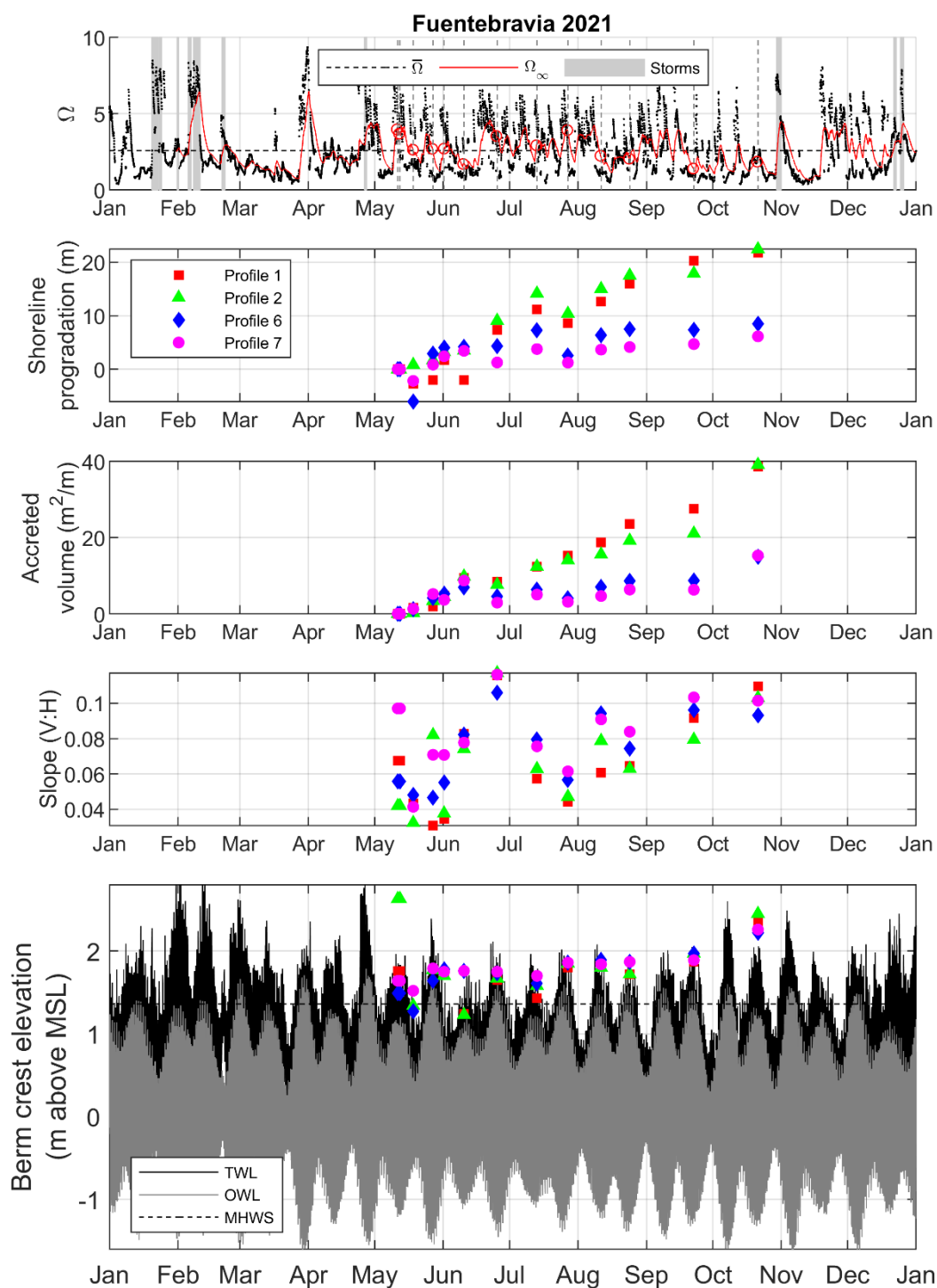


Figure 3.15 Hydrodynamic and morphologic variables measured at Fuentebravía beach. In the upper panel: grey shaded areas refer to storm conditions, where significant wave heights are above the 5% exceedance level for a minimum duration of one tidal cycle; vertical dashed lines are the dates of the field surveys and red circles indicate the Ω_∞ at the high tide previous to each survey.

CHAPTER 3**3.4.2. Santander**

The evolution of El Sardinero beach was analysed by means of the data collected during seven field surveys performed on a monthly basis (around spring tides) from April to September. Figure 3.16 shows the three profiles (1 to 3) measured at El Sardinero I and Figure 3.17 shows the four profiles (4 to 7) measured at El Sardinero II. The beach berm starts its formation in May and the shoreline prograde by and approximately parallel to itself displacement of the beachface. This progradation occurs until the beginning of August when it stops. The berm crest elevation is maintained from May to late August, and it rises in October. Profiles 4 to 7 present a double berm crest in October and an intertidal bar that appears at the beginning of August and progressively migrates onshore. The crest of this bar rises, and in October it forms an intertidal terrace just below the high tide level for Profiles 6 and 7. These profiles are more sheltered from northwest waves by the presence of Cabo Menor headland.

Figure 3.18 evidences the differences between profiles. The rates of shoreline progradation and accretion are similar for all the profiles. Nevertheless, the recovery of the beach starts in mid-April in El Sardinero I, but it delays until mid-May in El Sardinero II. This effect may be caused by the sheltering effect of Cabo Menor headland. Besides, the berm crest elevation is consistently bigger at El Sardinero I and lower at El Sardinero II, in agreement with the greater exposure of El Sardinero I to bigger waves and therefore bigger runup and TWL.

The shoreline progradation was measured at the level of MHWS = 1.82 m, obtained from OWL time series. From April to the beginning of August, the shoreline progradation rate is constant, and reaches 5 m/month at El Sardinero I and 4 m/month at El Sardinero II. Then, in August and September, the progradation rate is reduced below 1 m/month.

The accretion rate is also constant from April to the beginning of August, with rates of 9.5 m³/month and 6 m³/month for El Sardinero I and II, respectively. Then, in August the beach does not accrete, and even slight erosion appears in some profiles. Finally, in September the accretion rate increases again to an average of 11 m³/month in El Sardinero I (1.2 times bigger) and 5 m³/month in El Sardinero II. This progressive and quite uniform accretion rate is partially in agreement with the Ω_∞ values obtained for the summer season at El Sardinero beaches. Ω_∞ oscillates between 2.2 and 7.1 during the study period, while $\bar{\Omega} = 4.44$. During this period, H_s did not exceed 2.2 m (except from a storm that reaches 2.7 m at the end of April) and T_p oscillated between 5 and 13 s (Figure 3.6). The spring storm that occurred at the end of April could be responsible for the delay of the beginning of accretion

in El Sardinero II. Nevertheless, no event could explain the lack of accretion in August. Section 3.4.4 includes a detailed analysis of the relation between Ω_∞ and accretion rates.

The beachface slope oscillates between 0.02 and 0.12. The general trend is toward increasing slopes although there were two episodes (July and October) in which the slope descended. A slope of 0.06 was chosen as representative of the whole study period. This slope was used for the calculation of the runup R_2 with the formula of Stockdon et al. (2006).

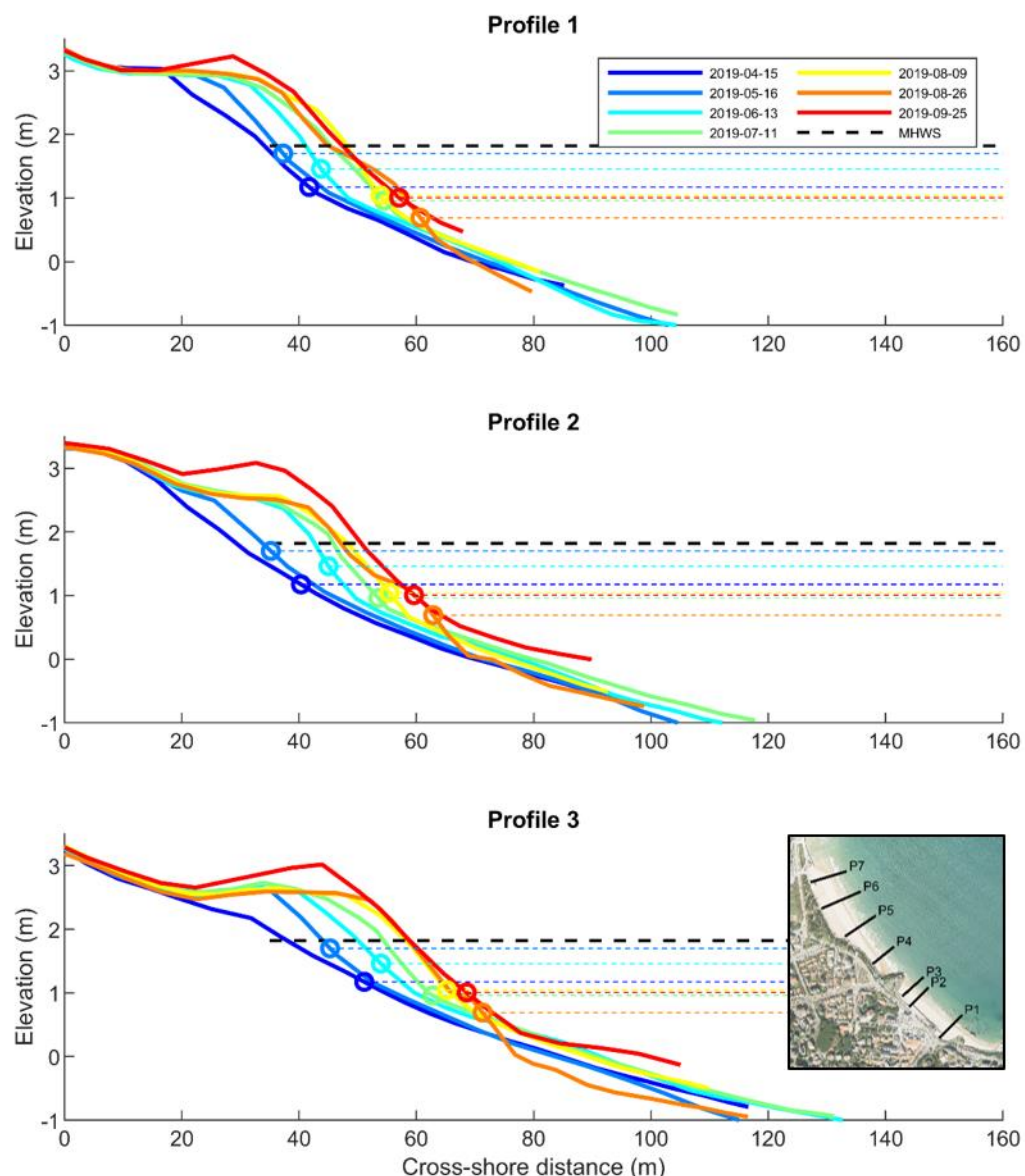


Figure 3.16 Beach profile evolution at El Sardinero I (dry beach and intertidal zone). Elevation referred to the local mean sea level of Santander.

CHAPTER 3

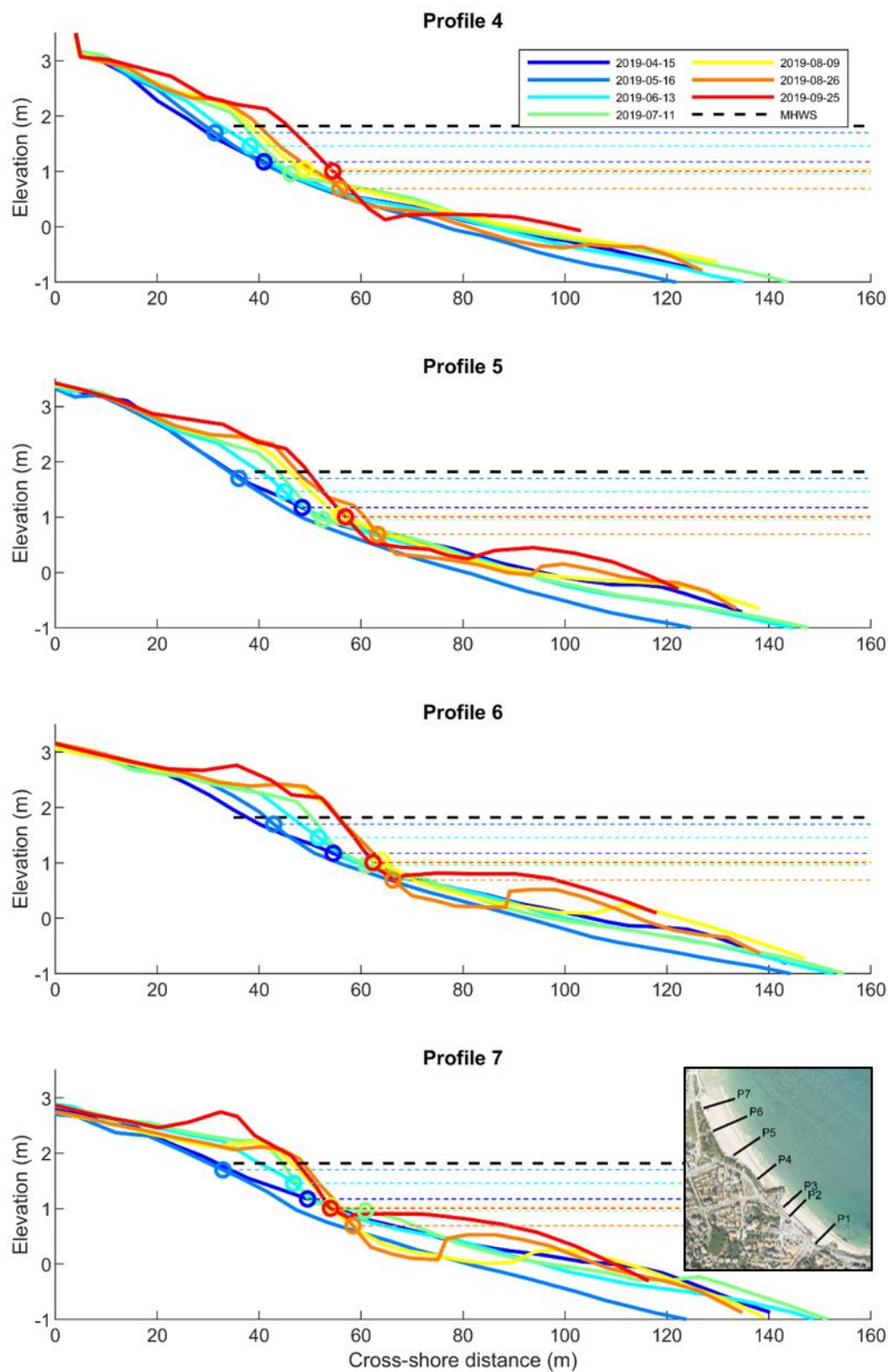


Figure 3.17 Beach profile evolution at El Sardinero II (dry beach and intertidal zone). Elevation referred to the local mean sea level of Santander.

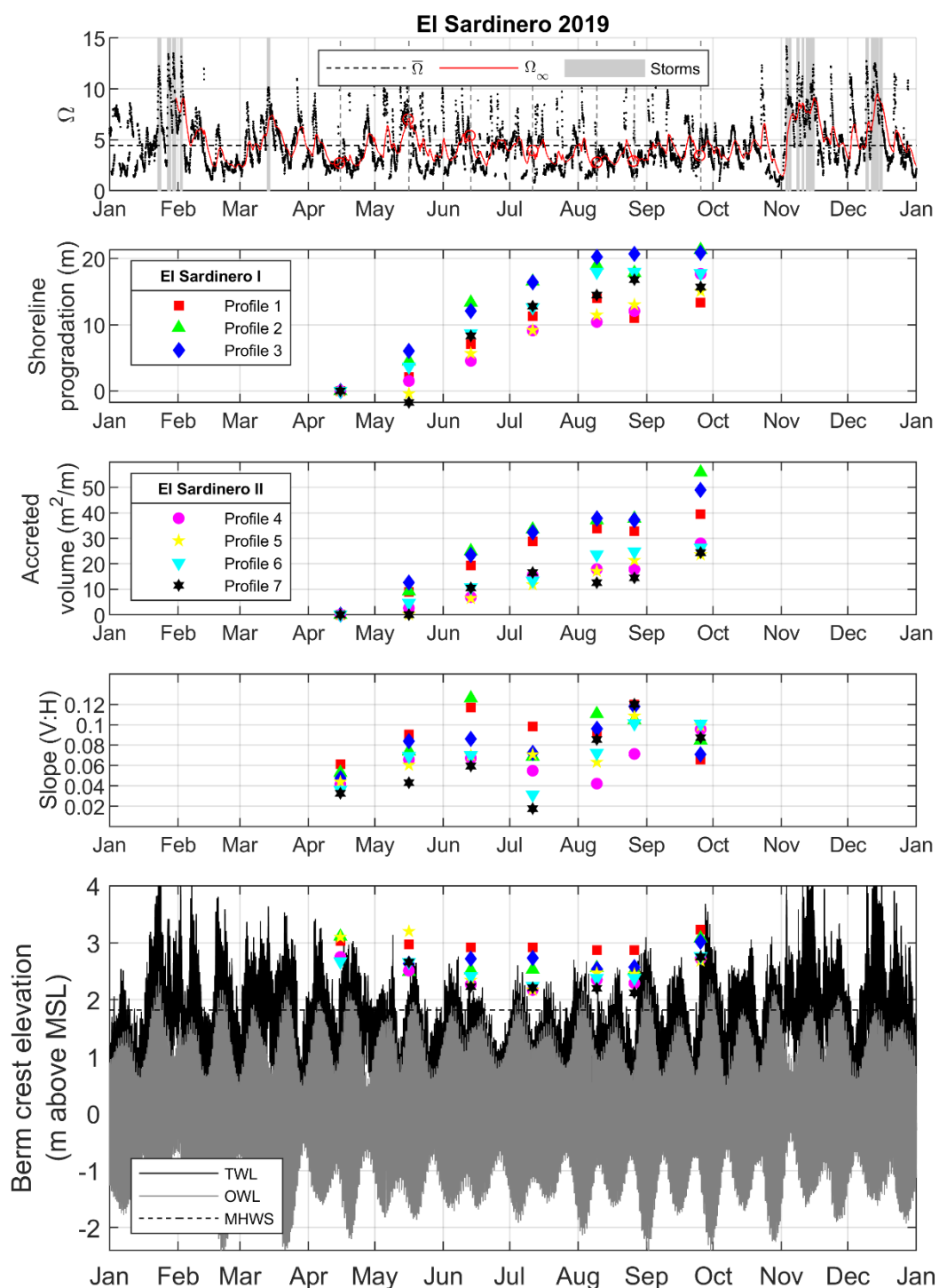


Figure 3.18 Hydrodynamic and morphologic variables measured at El Sardinero beach. In the upper panel: grey shaded areas refer to storm conditions, where significant wave heights are above the 5% exceedance level for a minimum duration of one tidal cycle; vertical dashed lines are the dates of the field surveys and red circles indicate the Ω_∞ at the high tide previous to each survey.

CHAPTER 3

As previously mentioned, the berm crest elevation presents a longshore gradient along the beach, being higher at the SE (Profile 1) and lower at the NW (Profile 7). At the beginning of the study period (April and May), some profiles present a berm formed during winter storms (Profiles 5 and 3). Then, the summer berm starts to develop, and it is clearly visible for all profiles in June. The crest elevation of the berm maintains or slightly decreases in agreement with the natural slope of the dry beach (slightly sloping towards the sea) from June to late August. This is in agreement with the regularity found in the spring high tides (OWL) and the maximum TWL reached during this period. Finally, in September the concomitance of equinoctial spring tides and bigger runup due to an increase in wave period, produce bigger TWL that overtop the previous berm crest and generated berm aggradation (berm crest rises 0.4 m). The relation between the berm crest level and TWL is thoroughly analyzed in Section 3.4.4.

3.4.3. Somo

Somo and Loredo beaches were surveyed from May to September of 2019 by means of seven surveys of four beach profiles (two on each beach). Six of the surveys were performed on spring tides but the survey of June 1st was performed between neap and spring tides. Figure 3.19 shows all the profiles measured, two at each beach. The mean slope of the intertidal area at Somo and Loredo is clearly lower than the slope at the other study sites. This is because Somo and Loredo are exposed to the big waves from the NE and N of the Cantabrian Sea, which reach the beach directly with no diffraction on any headland. The behaviour of the profiles is not as uniform as the previous study sites. This is probably due to the formation of rhythmic patterns which are frequent on Somo and Loredo beaches. Nevertheless, all the profiles show shoreline progradation and berm aggradation (especially in September).

Figure 3.20 reflects that despite the spatial irregularities of the beach profiles, the average shoreline progradation and accretion rates are quite uniform among profiles. The recovery did not start until June, and the new berm crest was not evident in all profiles until July. This suggests that the impact of soft spring storms may have prevented an earlier recovery which did not start until H_s is below 0.8 m and T_p around 5 s.

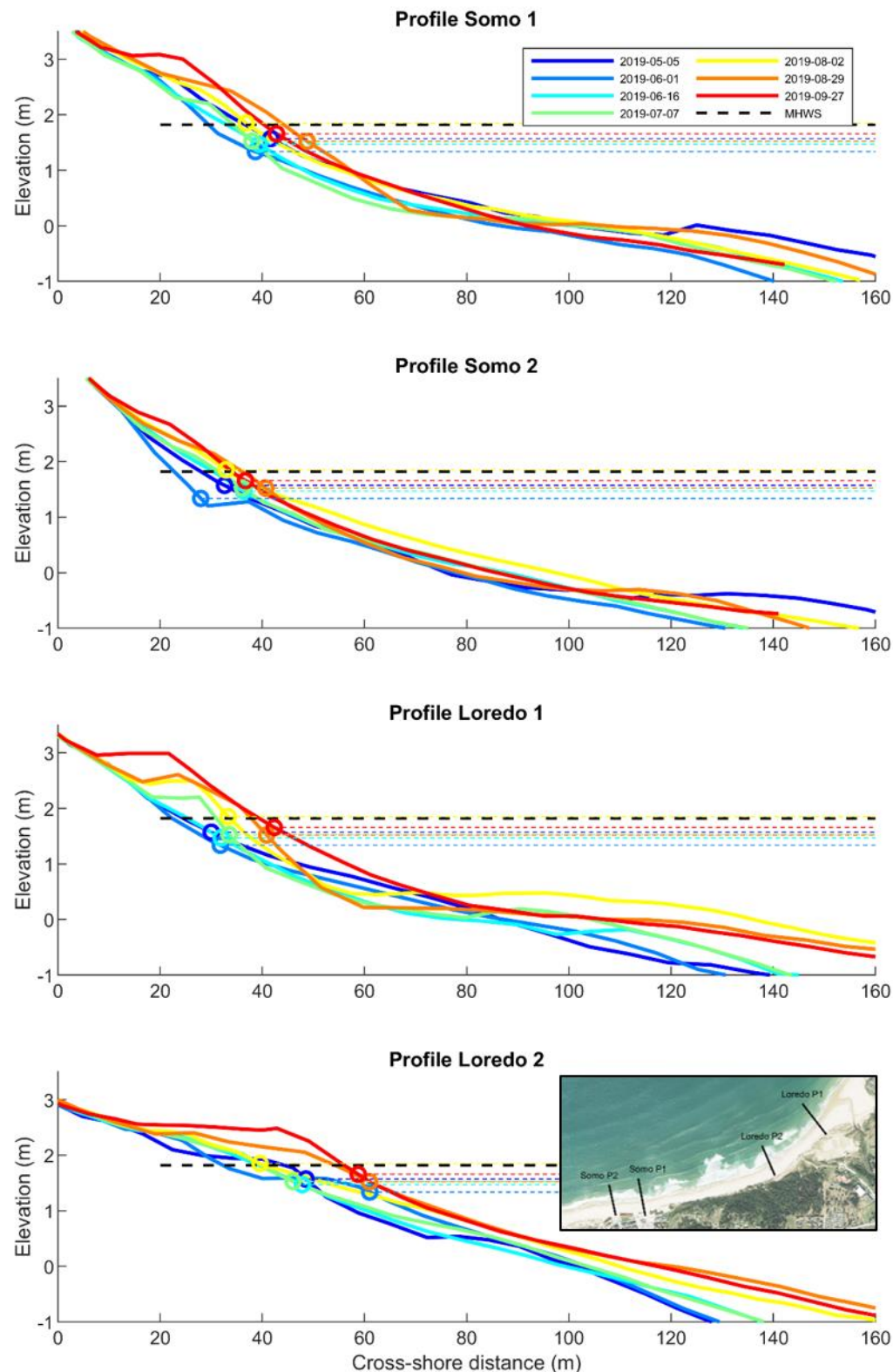


Figure 3.19 Beach profile evolution at Somo and Loredo (dry beach and intertidal zone). Elevation referred to the local mean sea level of Somo.

CHAPTER 3

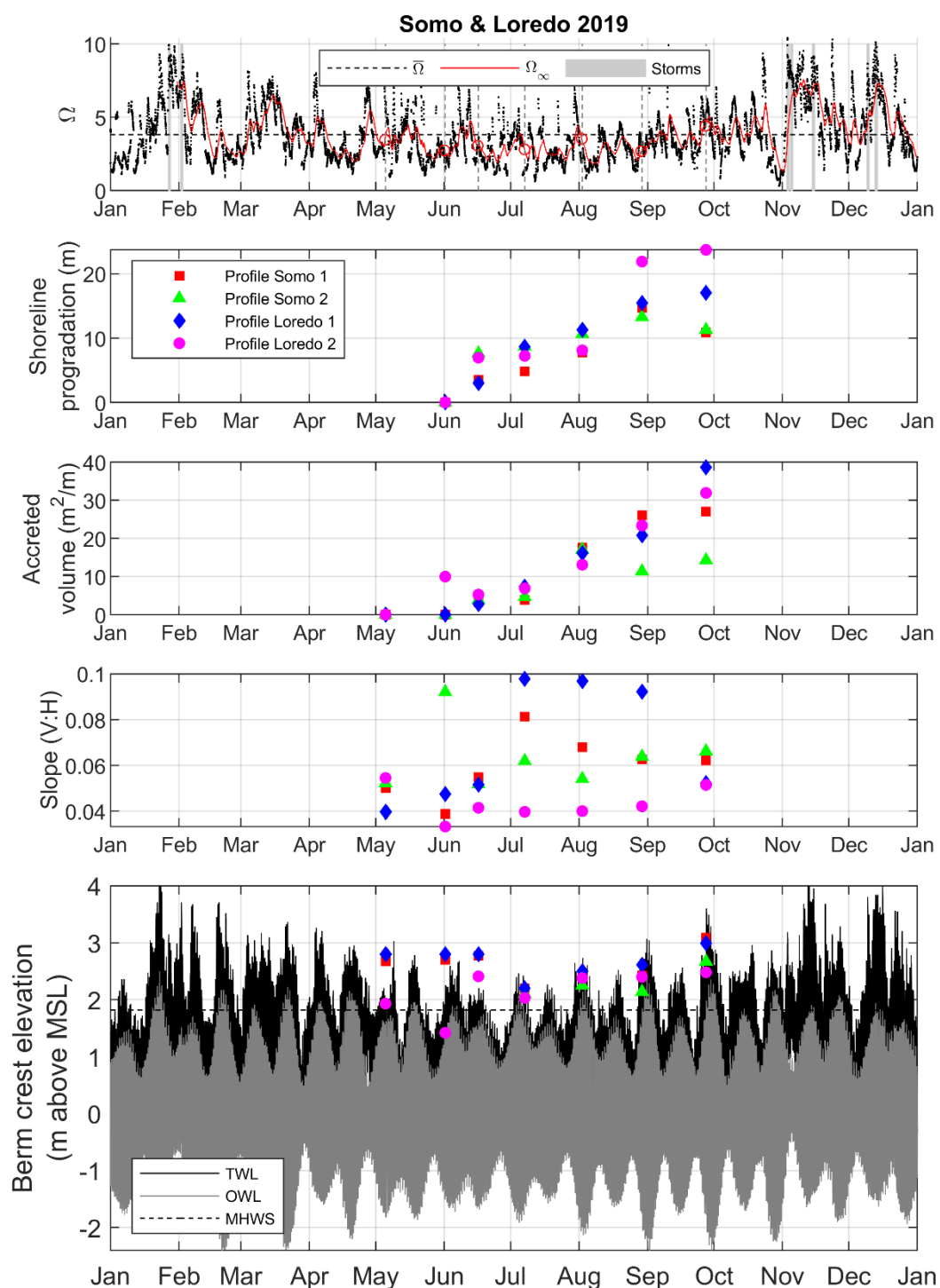


Figure 3.20 Hydrodynamic and morphologic variables measured at Somo and Loredo beaches.

In the upper panel: grey shaded areas refer to storm conditions, where significant wave heights are above the 5% exceedance level for a minimum duration of one tidal cycle; vertical dashed lines are the dates of the field surveys and red circles indicate the Ω_{∞} at the high tide previous to each survey.

The shoreline progradation was measured at the level of MHWS = 1.82 m, obtained from OWL time series. The average rate of shoreline progradation is 5.2 m/month. Besides, the mean rate of accretion is 8 m³/month. There are some profiles whose behaviour differs from the average, especially at the end of the study period (August and September). This progressive and quite uniform accretion rate is in agreement with the Ω_∞ values obtained for the summer season at Somo and Loredo beaches. Ω_∞ oscillates between 1.8 and 5.2 during the study period, while $\bar{\Omega} = 3.81$. During this period, H_s did not exceed 2.5 m (except from a storm that reaches 3.2 m in the first half of May) and T_p oscillated between 5 and 13 s (Figure 3.9). The spring storm that occurred in the first half of May could be responsible for the delay in the beginning of accretion in Somo and Loredo. The recovery does not speed up until mid-June when the wave period is reduced to ~5 s. Section 3.4.4 includes a detailed analysis of the relation between Ω_∞ and accretion rates.

The beachface slope oscillates between 0.03 and 0.1. During May and June, the slope was quite constant and between 0.04 and 0.05. In June, the slope of each profile suddenly changes, and this change is maintained until late August. Finally, in September the slopes of all profiles converge again around 0.06. A slope of 0.04 was chosen as representative of the whole study period. This slope was used for the calculation of the runup R_2 with the formula of Stockdon et al. (2006).

The new summer berm did not exhibit a marked crest until July. Before that, the berm crest elevation considered was the one corresponding to the winter berm. Once the summer berm was formed it continued rising every month, from a height of 2.1 m above MSL in July to 2.8 m in September. The bigger berm aggradation was 0.26 m in September when equinoctial spring tides and a bigger wave period generate and increase of TWL that overtopped the previous berm crest. The relation between the berm crest level and TWL is thoroughly analyzed in Section 3.4.4.

CHAPTER 3

3.4.4. Influence of the hydrodynamic parameters on beach accretion

Spring tides are produced during the alignment of the Earth, the moon and the sun. This occurs twice a month, during new and full moons. Sometimes the tidal range of both monthly spring tides is similar, but there can be high differences in other months. The tides of June and July 2021 at Fuentebravía are examples of this (see Figure 3.15). The new moon occurred on June 10th and July 10th, when the tidal range was about 2.1 m, while the full moon was on June 24th and July 24th, and generated tidal ranges of ~2.9 m. The tidal range during the neap tides in between was ~1.5 m. Field surveys were performed during both types of tides at Fuentebravía beach. Figure 3.21 shows the evolution of Fuentebravía's Profile 1 during June (left panel) and July (right panel). Those observations confirm the importance of tides on meso/macro-tidal environments, and specifically the relevance of the differences in the tidal range between tides, for accretion processes.

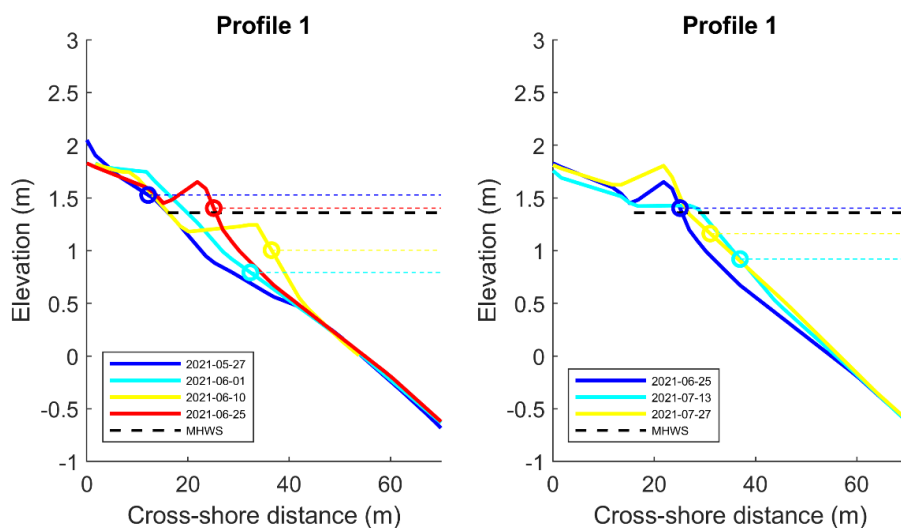


Figure 3.21 Examples of spring-neap-spring tide evolution of the beach profile P1 of Fuentebravía.

The left panel of Figure 3.21 includes a survey during the full moon (large tidal range) spring tide on May 27th, then a survey between spring and neap tide on June 1st, a survey during the new moon (modest tidal range) spring tide on June 10th, and a survey on the full moon spring tide of June 25th. The beachface shows a small progradation produced after the first spring tide, probably when the tidal range was still big because the berm crest maintains the height. After the neap tides and up to the new moon spring tide a new berm appears as described by Phillips et al. (2019) with a berm crest limited to a few centimetres above the high tide level. Note that the berm crest did not reach the MHWS, and therefore

the shoreline progradation produced was not visualized in Figure 3.15. Finally, the last observation shows berm aggradation and shoreline retreat. The berm crest reached again the level of the full moon's spring tides but sand accretion was not enough to maintain the shoreline progradation achieved for the smaller berm generated during the new moon's spring tide.

On the right panel of Figure 3.21, the behaviour is similar. In this case, the first survey corresponds to the full moon's spring tide of June 25th, the second to the new moon's spring tide of July 13th, and the last one to the full moon spring tide of July 27th. During the new moon spring tide, a new berm was formed with a lower berm crest elevation according to the modest tidal range. This berm then aggraded and the berm crest level rose to the full moon spring tide level.

Those observations indicate that berm evolution is highly dynamic during spring-neap-spring tidal cycles. As a consequence, in the following analysis the observations performed once a month, during full moon spring tides, were selected. Those observations show the maximum berm crest level achieved each month and the maximum accreted volume, which will remain stable on the beachface. For the selected monthly surveys, the average berm crest level, shoreline position, and accreted volume among all profiles of each study site are obtained.

The berm crest elevation measured on a monthly basis (around spring tides) shows a high correlation with the TWL exceeded 1% on the previous month ($TWL_{1\%}$; Figure 3.22). The error between both variables is 0.12 m. This means that the berm crest elevation can be predicted with the TWL time series.

Besides, the size and colour of the dots in Figure 3.22 indicate the percentage of time in which the berm crest level was exceeded and the growth or descent of the berm crest produced from the previous to the actual observation, respectively. The graph shows a prevailing red and yellow colour, indicating that most of the months the berm either aggrades or maintains its level. Only three observations correspond to events in which the berm crest level diminishes (blue colour). Furthermore, the reddish the dot the bigger it is, meaning that the previous berm crest level was exceeded a bigger percentage of time during the last month. On the contrary, smaller dots (less than 2% of the time of TWL exceedance) are blue or yellow, meaning that in those cases the berm was not able to aggrade and even could reduce the berm crest level. Altogether, a minimum of 3% of the time of TWL exceeding the berm crest level is needed to observe aggradation on the next spring tide.

CHAPTER 3

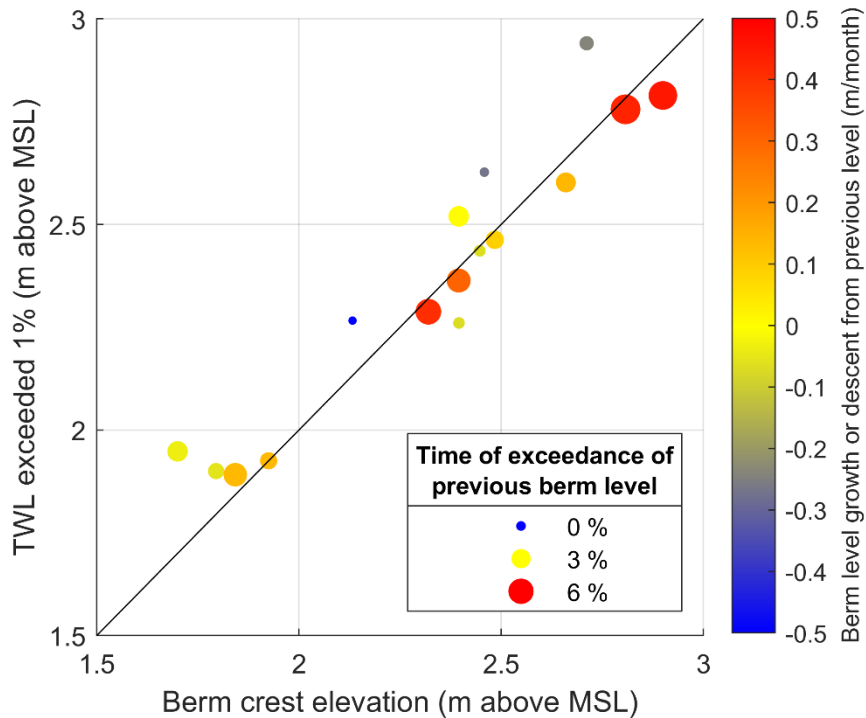


Figure 3.22 Relation between the berm crest elevation and the TWL exceeded 1% of the time in one month (from spring tide to spring tide). Berm level growth (+) or descent (-) is related to the time of exceedance of the previous berm level.

It is widely known that beach accretion is produced when the dimensionless fall velocity (Ω) is small. Wright et al. (1985) found that a weighted average of the previous Ω values (Ω_{∞} , equilibrium dimensionless fall velocity) was the best descriptor for the state of the beach. Figure 3.23 shows the relation between the mean value (on the previous month) of the standardized Ω_{∞} , and the accretion rate measured in this month. The standardized Ω_{∞} was computed as $(\Omega_{\infty}) = (\Omega_{\infty} - \bar{\Omega})/\sigma(\Omega)$, where $\bar{\Omega}$ is the average of the dimensionless fall velocity during all the historical wave time series and $\sigma(\Omega)$ is its standard deviation. By standardizing we ensure that the measurements of all the study sites are comparable. Note that months with an average Ω_{∞} greater than $\bar{\Omega}$ (positive values on Figure 3.23) produce accretion as observed by Phillips et al. (2019) (accretion was produced when $\Omega > \bar{\Omega}$ and non-storm; Figure 2.2). A linear fit on the data shows the expected relation in which decreasing values of Ω_{∞} produce bigger accretion rates. Nevertheless, the dots are scattered and the relation is weak. Furthermore, four observations do not respond to the general trend (the ones labelled with site and date). The dots of El Sardinero occur during August when the accretion rate reduced despite the fact that Ω_{∞} was still low (see section 3.4.2 and Figure 3.18). This may be produced as the beach approaches its equilibrium. Besides, the dots of Somo occur at the beginning, during June. The start of accretion suffered a delay, as

mentioned in section 3.4.3. This may be produced by the high exposure of this site to incoming waves. The sand available for accretion may be further offshore and June would be the necessary time for this sediment to approach the coast.

As mentioned in the previous sections, bigger accretion rates do not necessarily mean larger shoreline progradation. In some cases, all the accretion can be explained by berm aggradation and the shoreline can remain in its position or even retreat. The colour of the dots in Figure 3.23 indicate the movement produced on the shoreline. Most of the time the shoreline progrades (red colours), and hardly ever retreat was observed (lack of blue dots). There is no relation between shoreline movement and $\text{mean}(\text{std}(\Omega_{\infty}))$ values, as the colours of the dots do not follow any rule or trend. Besides, the size of the dots indicates the percentage of time during each month in which $\Omega_{\infty} < \bar{\Omega}$. In this case, the smaller dots (less than 50% of the time) concentrate on the upper part of the figure, corresponding to larger or even positive values of the $\text{mean}(\text{std}(\Omega_{\infty}))$. On the contrary, percentages greater than 50% of the time of $\Omega_{\infty} < \bar{\Omega}$ correspond to lower values of the mean, when accretion frequently speeds up.

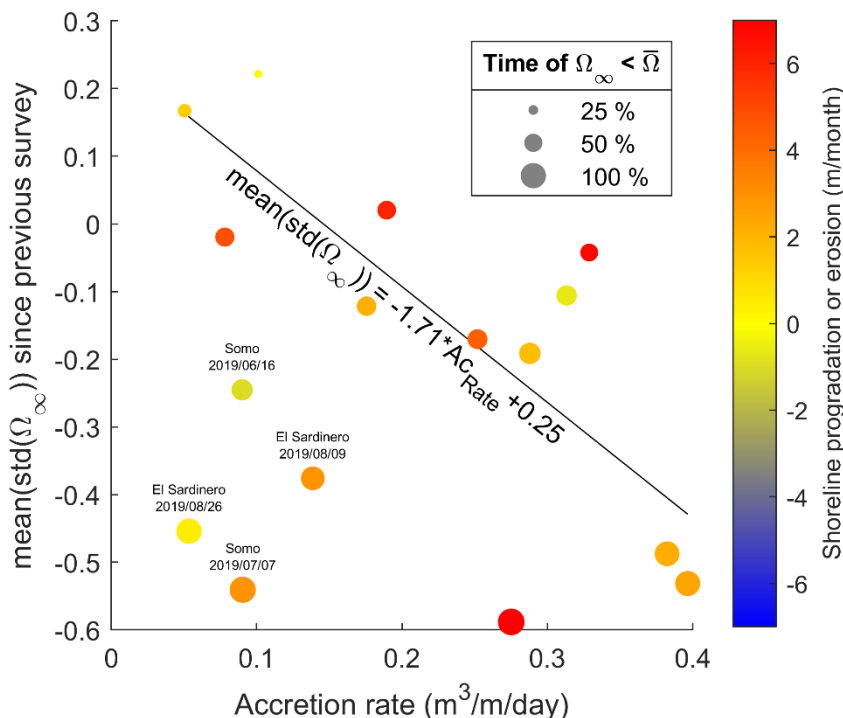


Figure 3.23 Relation of the average value of the standardized equilibrium dimensionless fall velocity parameter ($\text{std}(\Omega_{\infty})$) in one month (from spring to spring tide) and the daily rate of accreted volume. Shoreline progradation (+) achieved and time of $\Omega_{\infty} < \bar{\Omega}$.

CHAPTER 3**3.5. DISCUSSION**

Beach recovery has been analysed here in three meso/macro-tidal beaches throughout the whole summer season. The beaches were surveyed by means of high-precision RTK-GPS (Fuentebavia) and distancemeters (El Sardinero, Somo and Loredo). The distancemeter measurements were validated with RTK-GPS, demonstrating that the vertical root-mean-square error of distancemeter data was 0.09 m. This demonstrates that simple and inexpensive techniques are also valid data sources, with the advantage that non-expensive equipment nor qualified personnel are required. Ward et al., (2021) is another example of successful surveys performed with a simple technique (similar to the one proposed here) and volunteers.

Few studies analyse the evolution of the beach berm and dry beach widening due to accretion processes. Most of the accretion studies focus on the analysis of intertidal or submerged bar formation and onshore migration rates (Aagaard et al., 2006; Gallagher et al., 1998a; Jackson et al., 2016). Strahler (1966) was one of the pioneers in the study of beach berm formation and growth. In his study, first shoreline progradation was observed, and then the berm rose about 0.4 m. This aggradation was interpreted as the effect of larger waves acting at a higher water level and bringing the swash to a higher limit. Thom and Hall (1991) classified beach profiles into six classes and proposed a model for erosion-accretion but information on berm height growing was missing. An analysis of a fine-sand, gently-sloping, micro-tidal beach during a neap-neap tidal cycle (Jensen et al., 2009) showed that the berm was formed by onshore migration of the intertidal bar until it stabilizes as a berm on the foreshore. Then, “on the rising tide and under rising water levels, the berms were transformed to intertidal bars, migrated further onshore and finally stabilized on the uppermost part of the foreshore, increasing the elevation of a pre-existing berm”. This process was also observed at the meso-tidal environment of Fuentebavía beach, where weekly surveys revealed these complex dynamics of the berm between neap and spring tides.

Phillips et al. (2017) analysed post-storm beach recovery on a micro-tidal beach and observed a dominant shoreline progradation at the beginning of the recovery period and then berm height growing at the final phase. They found that accretion rates are three times bigger when berm aggradation occurs. This result matches our findings on meso/macro-tidal beaches, where the accretion rates were up to 2.5 times bigger during the last month when the berm aggraded.

Recently, Phillips et al. (2019) analysed the relation between marine dynamics and accretion morphology on a micro-tidal beach. They proposed four modes of accretion by classifying the observed variation in the morphology of the berm. Those modes were proposed for the analysis of a beach on a tide-by-tide basis. As accretion dominates and the present study was made on a monthly basis, the modes that include shoreline progradation where the prevailing ones here. Shoreline retreat was only observed on inter-spring-spring tide observations, which leads to thinking that those modes proposed by Phillips et al. (2019) will be only present on a reduced number of days but are not dominant on averaged time periods. Phillips et al. (2019) relate those modes with the marine conditions that prevail when they occur. Here, no relation between the modes observed and OWL exceeding MHWS was obtained. Additionally, the threshold between aggradation or not of the berm is not as simple as the presence or absence of TWL exceeding the berm crest. This is probably due to the longer time period between observations considered here (a month instead of a day). Here, berm aggradation occurs when TWL is exceeded 3% of the time during the last month (since the previous spring tide observation).

Neap-spring tidal cycle reproduces the behaviour described by Jensen et al. (2009), Phillips et al. (2019) and Strahler (1966). A new berm is formed during neap tides and then aggrades between neap and spring tides, as the crest of the berm is overtapped. Here we have three meso/macro-tidal environments with strong differences between neap and spring tidal ranges and even higher tidal levels during equinoctial spring tides. The maximum berm crest elevation and accretion are reached during the bigger spring tides of each month, and therefore this moment is considered representative of the evolution of accretion during the whole month. The selection of this day per month for future field surveys at other study sites is recommended. This would allow the survey of the complete recovery of a beach during summer minimizing the effort.

In the study areas, the TWL reached on successive spring tides during the summer were similar and therefore, successive berms accumulated one ahead (seawards) the other, extending dry beach with its natural slope. When the beach is surveyed only at spring tides, the accretion produced by the accumulation of successive berms is seen as the progradation of the beachface, although different shapes of the berm have occurred in between.

At the end of the summer season, the concomitance of equinoctial spring tides and bigger wave periods produce an increase in TWL, which leads to wave overtopping the berm crest and berm aggradation. This process occurs in the three study sites surveyed and seems to be the last stage of beach accretion before the winter. In this stage, the beachface progrades and the berm aggrades following mode 2 described by Phillips et al. (2019). As

CHAPTER 3

observed by previous authors, the beachface steepened, generating a nodal point in the intertidal area. This steepening is described in the literature (Phillips et al., 2019) as an indicator of the completion of the recovery period when the intertidal sandbar welding capacity is exhausted and the sediment feed from the inner nearshore is reduced.

The maximum berm crest elevation (reached during the higher spring tide every month) correlates with the TWL exceeded 1% of the time during the previous month ($TWL_{1\%}$). This means that the berm crest elevation can be predicted with the knowledge of marine dynamics but no need for previous surveys on a beach. Nowadays, time series of waves and tides in a study area are easily accessible. With these data, TWL can be obtained and statistical analysis can predict the berm elevation that will be achieved monthly during the summer season. This is a helpful tool for the design of Nature Assisted Beach Enhancement (NABE) techniques. As an example, the scraping technique proposes the creation of a summer berm with sand borrowed from the intertidal area. The design of the berm geometry requires the prediction of the most appropriate crest level and volume of the berm for each study site.

The use of the dimensionless fall velocity parameter (Ω) for the analysis of the beach state and therefore its accretion or erosion is widely extended. Wright et al. (1985) proposed a new parameter (Ω_∞ , equilibrium dimensionless fall velocity) obtained as a weighted average of the previous Ω values, which takes into account the “memory of the beach”. This parameter explains better than the previous one the state of a beach, but in our study, it could not predict accurately the accretion rate. Furthermore, the same analysis (results not shown) was performed for Ω values, instead of Ω_∞ , and the results were similar. In summer the incident wave height is lower than in winter. This produces a reduction in the values of Ω , leading to accretionary states. However, during summer the wave period also reduces. If the period is reduced on a greater magnitude than the wave height, Ω gets bigger, and therefore the parameter would indicate erosion although the wave energy is lower.

In our study, we found that accretion is produced when Ω_∞ is below $\bar{\Omega}$ (as expected), but it can also be produced in months with an average Ω_∞ greater than $\bar{\Omega}$. This matches the observations of Phillips et al. (2019) (see Figure 2.2), in which accretion was produced when $\Omega < \bar{\Omega}$ but also if $\Omega > \bar{\Omega}$, there are non-storm conditions, and OWL < MHWS (although this last condition is not fulfilled in our observations). Generally speaking, the lower the Ω_∞ (or the Ω) the greater the accretion rate, but there where some exceptions. The observations showed that accretion started 2 months later than expected in one of the beaches, and stopped 2 months before expected in other. These results suggest that both Ω and Ω_∞ could serve as indicators of accretion (accretion is clear when $\Omega < \bar{\Omega}$), although the relationship

obtained (Figure 3.23) is weak. This points out that other parameters may be important for the comprehension of beach accretion. Therefore, further research is required to seed light in this field.

3.6. CONCLUSIONS

Beach recovery during summer was analysed in three meso/macro-tidal study sites by means of a total of 24 field surveys. Berm formation and growing were observed in the 15 beach profiles analysed. The relation between morphologic changes and marine dynamics was analysed and the conclusions are the following:

- The berm development was conditioned by the variations in the tidal range that occur every month (among spring-neap-spring tides). The morphologic evolution during successive tidal cycles is complex. Between spring and neap tides (decreasing high tide level reached), accretion is minimum and berm geometry changes are small. After neap tides, a new berm appears with a low crest level, according to the lower high tide level reached. As the tidal range increases towards spring tides (and high tide level rises), the crest of the new berm is overtapped producing berm aggradation. Finally, at spring tides the berm stabilizes as part of the beachface.
- The analysis of beach recovery during summer can be performed by surveying on a monthly basis on the date of the larger spring tide. In these dates, the berm crest level is maximum and the accreted volume is representative of the sediment stable on the beachface. This avoids the need to interpret the complex and ephemeral variability present in between spring tides and minimises the effort required to characterize the whole recovery of the beach.
- The use of simple surveying methodologies, such as the use of a distancemeter device, has proven to be accurate and inexpensive.
- During the first months of the summer season beach accretion produces shoreline progradation.
- The berm crest elevation reached every spring tide can be explained by the TWL exceeded 1% of the time during the previous month ($TWL_{1\%}$). Therefore, berm crest elevation can be predicted by a statistical analysis of the TWL time series of previous summer seasons.

CHAPTER 3

- Berm aggradation is produced when TWL is exceeded at least 3% of the time on the previous month. On the Atlantic coasts of Spain, this occurs typically in September and October, due to the concomitant effect of equinoctial spring tides and longer wave periods that increase the runup and the TWL.
- Sand accretion rate presents a relation with the average Ω_∞ on the previous month to each observation. Nevertheless, this relation is weak and two clear exceptions were found. According to the equilibrium dimensionless fall velocity, accretion should have started two months before it actually did at Somo and Loredo beaches. In El Sardinero beaches the accretion almost stopped in mid-summer, although Ω_∞ values indicated that accretion should have continued.
- Further research on the processes that lead to beach accretion is needed to fulfil the current gap in the state of the art.

CHAPTER 4

BEACH PLOUGHING[†]

4.1. INTRODUCTION

Monge-Ganuzas et al. (2017) tested a new technique at Laida beach (northern Spain). It consisted of mechanical ploughing of the intertidal region of the beach. In their work, Monge-Ganuzas et al., (2017) conceived ploughing as a soft technique to help accretion build a wider beach earlier in the summer, improving the recreational potential of the beach. Laida beach was ploughed 22 times during the summer of 2015, from July to September. The ridges and furrows generated by the plough had a length of 1.42 m and a height of 0.27 m (see Figure 2.7). An analysis of the bathymetries showed that ploughing accelerated natural onshore bar migration (Gainza et al., 2019), with promising results for beach widening during the summertime.

[†] This chapter is based on Pellón et al. (2023) and Pellón et al. submitted to Coastal Engineering:

Pellón, E., Aniel-Quiroga, I., González, M., Medina, R., Vidal, C., 2023. Working with nature to enhance beach accretion: Laboratory experiments of beach ploughing. *Coast. Eng.* 180. <https://doi.org/10.1016/j.coastaleng.2022.104267>

Pellón, E., Quetzalcóatl, O., Aniel-Quiroga, I., González, M., Medina, R., Vidal, C. Onshore sediment transport enhancement and evolution of bedforms: Laboratory experiments of beach ploughing. Submitted to Coastal Engineering.

CHAPTER 4

In this thesis, the morphological behaviour of artificially created bedforms is analysed. Ridges and furrows are mechanically created by ploughing the intertidal beach parallel to the shoreline (Monge-Ganuzas et al., 2017). Gainza et al. (2019) demonstrated that ploughing accelerates onshore bar migration rate during calm weather. Figure 2.4 shows the geometric characteristics of this innovative nature assisted beach recovery technique. The height is clearly higher than that of naturally formed bedforms for this wavelength; therefore, the induced bed roughness is greater, although progressively reduced as the ploughing is smoothed out by wave action. Here, for the 1st time, the effectiveness of enhancing accretion, attenuation and migration of ploughed bedforms are analysed through laboratory experiments.

In this chapter, laboratory experimental results are thoroughly analysed to confirm the usefulness of ploughing and its applicability from both qualitative and quantitative perspectives. Therefore, the objectives OB3, OB4, OB5 and OB6 are addressed here for ploughing actions. Additionally, chapter 5 includes a comparative analysis of ploughing and scraping techniques, which complement the insights of this section to address the mentioned objectives. Section 4.2 of the present chapter 4 includes a description of the laboratory conditions and measurements. Section 4.3 analyses ploughing effectivity, including the results related to morphology, hydrodynamics, sediment dynamics, and sediment balance. Section 4.4 contains a detailed analysis of ploughing and bedforms evolution, comprehending the methodology, the results, and the discussion of the longer duration laboratory experiments performed, and finally, section 4.5 summarizes the conclusions. The novelty of this work is that for the first time, the ploughing technique is analysed under controlled conditions.

4.2. LABORATORY FACILITIES AND SETUP

The experiments were performed in the Wave-Current-Tsunami Flume (COCoTsu) at IHCantabria facilities in Cantabria, Spain. The flume is 56 m long, 2 m wide and 2.5 m high. The sidewalls of the flume are made of glass. The experiments were performed at a prototype scale (1:1) in this channel, which was split longitudinally into two equal subchannels, each of them 1 m wide. One of these subchannels was used to simulate the morphodynamic evolution of a ploughed intertidal area (see Figure 4.1), and the other was used as a control, with a natural intertidal geometry. Two sets of simulations were performed:

- Set 1: Seven tests with durations of 1 h with different water levels and the same accreting wave characteristics. The results of this set of experiments are described in section 4.3 Ploughing performance.
- Set 2: Two tests with a duration of 4 h with different water levels and the same accreting wave characteristics. The duration of this set of tests was determined after simulating a longer duration test of 7 h of wave simulation. Results (not shown) indicated that bedform characteristics do not change after 4 h, and the ploughed geometry can no longer be analysed (as demonstrated in the following sections). The results of this set of experiments are described in section 4.4 Bedforms evolution.

The initial geometry of each test, the hydrodynamic conditions, and the instrumentation used are described in this section. Figure 4.1 shows an image of the initial geometry of the plough before wave simulation. This geometry was rebuilt for each of the tests performed (for both sets of experiments). The same accreting wave conditions were used for all tests but with different water levels for each one to model different instants of the tidal cycle.

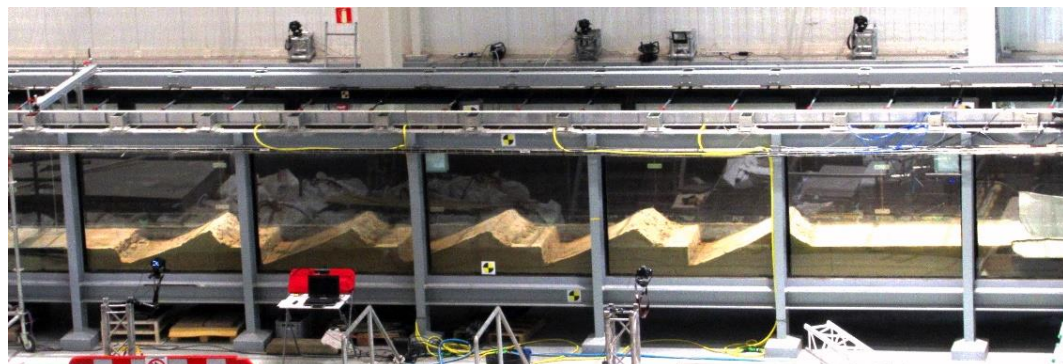


Figure 4.1 Photograph of the plough and sandy area at the experimental facility. The sidewalls of the test section of the COCoTsu channel are made of glass. The image shows the initial ploughed geometry of each test before water inundation.

4.2.1. Morphology

A prototype-scale (1:1) section of an intertidal area was built along the COCoTsu channel. The section contained a hard bottom and a movable sandy bed. Figure 4.2 shows a longitudinal profile of the geometry of the hard bottom constructed in the flume. This hard bottom is formed by a permanent part (in blue colour in Figure 4.2) and an ad-hoc part constructed for these tests (in grey colour). The permanent part is formed by a 4.7 m long concrete ramp with a slope of 1/13.55 that starts 11 m away from the wave generator. A

CHAPTER 4

built-in concrete ramp that was 12 m long with a slope of 1/30 in its first half and 1/60 in its second half covered the permanent bottom. The final 0.3 m of concrete included a rounded transition to avoid sharp edges at the beginning of the sandy area. The top of the concrete ramp reached 0.65 m above the flume bottom at the paddle. The test area was a 10 m long movable sandy bed with a slope of 1/100. The top of the sand reached 0.75 m above the flume bottom at the paddle. The sand was contained by a concrete rounded element whose top edge reached an elevation of 0.75 m. The sandy area was filled with natural sand with a $D_{50} = 0.318$ mm and a density $\rho_s = 2580$ kg/m³. The bed gradient was low ($\tan\beta = 0.01$), which is typical of an intertidal area with high wave energy and beaches with fine-medium sand. A sediment trap box placed shoreward of the sandy area captured the accreted sand. At the end of the channel, wave dissipators prevented wave reflections.

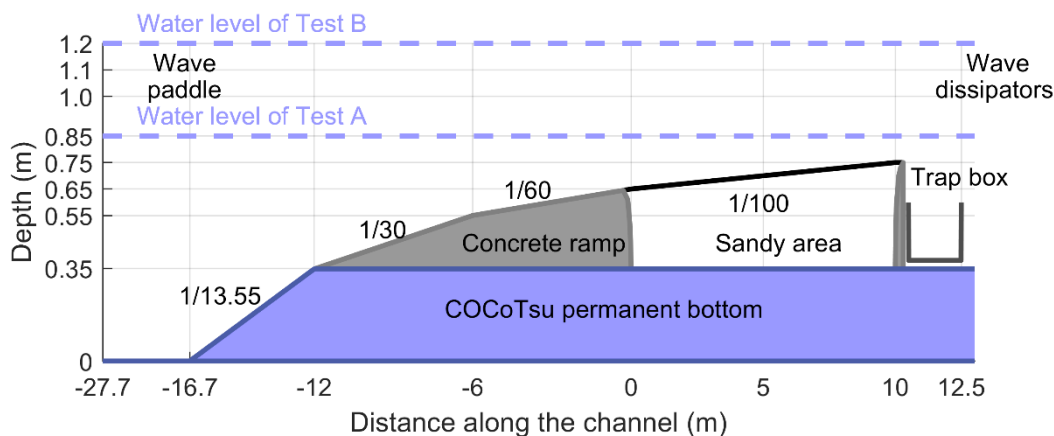


Figure 4.2 Cross-sectional sketch of the longitudinal profile of the COCoTsu showing the experimental setup. The water levels correspond to the two tests of the Set of experiments 2. The vertical scale is 10 times the horizontal scale.

The wave flume was longitudinally split into two 1 m wide equal channels using connected panels acting as a thin wall. The separation extended from the beginning of the concrete ramp to the wave dissipators, so hydrodynamics and morphodynamics were completely independent on both sides. One of the channels was used to simulate natural intertidal conditions for reference. The other channel included the same basic geometry with 5 plough ridges and furrows dug transversally over the sandy region. The ploughing geometry was the same for all tests (see Figure 4.3), with a wavelength of 1.6 m and an amplitude of 0.25 m, corresponding to the ploughing dimensions that a tractor can perform. This initial geometry, natural and ploughed, was rebuilt at the beginning of each test on both sub-channels. On the shoreward side of the sandy area, a 2 m-long trap box was installed on each subchannel. Each trap box covered the full width of the subchannel to ensure that all the accreted sediment was captured.

4.2.2. Instrumentation

The geometry of the surface of the sandy area was measured before and after each test using a high-resolution laser scanner. Water free surface elevation was measured continuously at 50 Hz by 16 capacitive wave gauges (WGs): three of them were placed next to wave generators, 6 were placed over the sandy area of the natural geometry, and 7 were placed over the ploughed side (see exact locations in Figure 4.3). Currents were measured by 4 acoustic Doppler velocimeter (ADV) sensors at the onshore end of the sandy area. The ADV sensors were placed symmetrically, 2 on each side, at 0.1 m and 0.2 m above the initial sandy bottom. Finally, the suspended sediment load was measured by 2 optical backscatter (OBS) point sensors located 0.05 m above the initial sandy bottom, just below the lower ADV on each side.

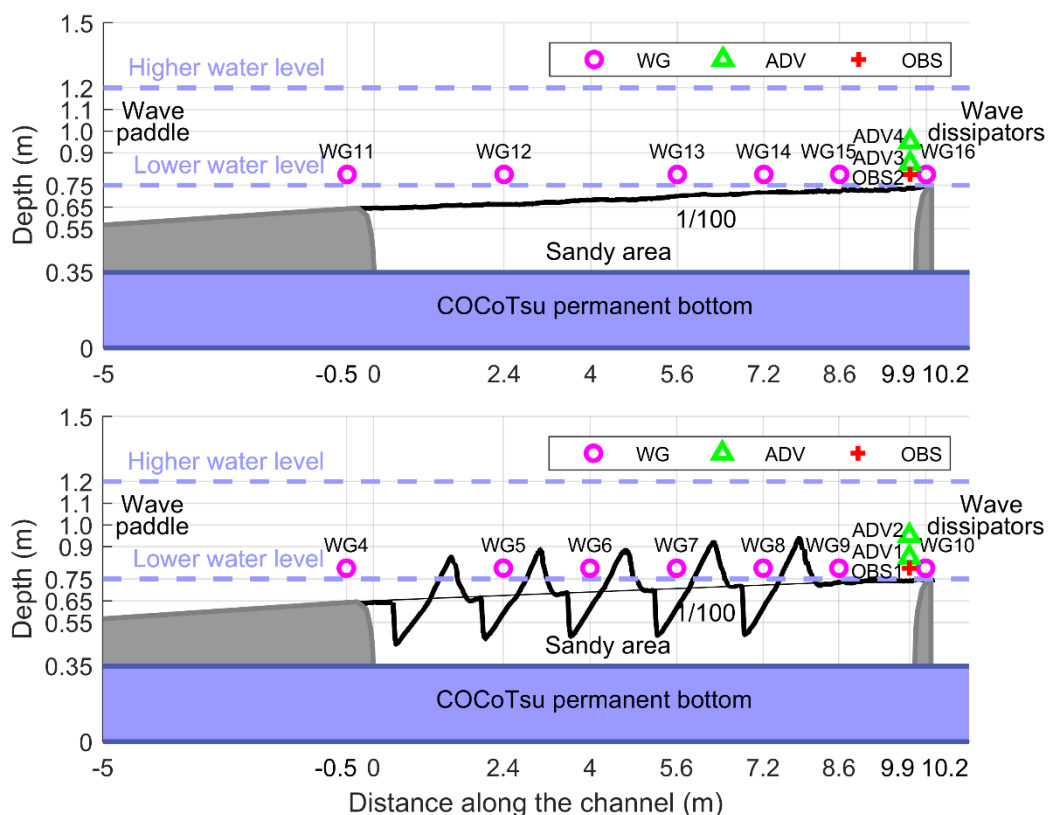


Figure 4.3 The COCoTsu longitudinally split into two channels showing the instrumental layout of each side. Top: Natural geometry side. Bottom: Ploughed geometry side. The vertical scale is 4 times the horizontal scale.

The Set of experiments 2 included extra instrumentation. Two cameras located on the outer part of the ploughed side of the channel and focusing on the glass sidewall of it took synchronized pictures of the evolution of the sandy bottom every 5 min. Targets were

CHAPTER 4

installed on this side of the channel to allow composing of the images of both cameras and rectifying the pictures to real coordinates. The geometry of the surface of the sandy area of both subchannels was measured employing a high-resolution laser scanner four times for each test; at the beginning and after 1 h, 2 h, and 4 h (at the end). The sediment collected on the trap box located at each side of the channel was extracted at the same time instants as the laser scanner measurements (Test A had an additional sediment measurement after 3 h of waves). The collected sediment was vibrated for 3 min to achieve saturated density, the surplus water over the sand surface was eliminated, and then the saturated sediment was weighed.

4.2.3. Hydrodynamics

Wave characteristics were the same for all tests performed (on both sets of experiments). Irregular waves of significant wave height $H_s = 0.3$ m, peak period $T_p = 7$ s, and a standard $\gamma = 3.3$ JONSWAP spectra with active wave absorption to avoid re-reflected waves were generated. The dimensionless fall velocity parameter $\Omega = H_s / (w \cdot T_p) = 1.08$ corresponds to a reflective morphodynamic beach state according to Wright and Short (1984). The methodology of Kraus et al. (1991) was applied to ensure that these waves produced accretion (in this study, $\Omega = 1.08 < 2.4$; thus, accretion is highly probable).

In Set 1, seven tests were performed with different water levels: 0.75 m, 0.8 m, 0.85 m, 0.9 m, 1 m, 1.1 m, and 1.2 m above the bottom of the channel next to the wave generator. Each water level was constant over a test with a duration of 1 h.

In Set 2, two tests were performed with a constant water level of 0.85 m for Test A and 1.20 m for Test B (the reference level is the height of the flat bottom next to the wave generator). The duration of these tests was 4 h, and they were composed of consecutive 1 h wave generation simulations separated by pauses that allowed the measurement of accreted sediment and surface geometry (water was fully drained to allow laser scanner measurements and sand extraction from the trap box and then slowly raised again to the test level). At each pause, the sediment accreted on each subchannel was measured and reloaded over the offshore boundary of the sandy area to reduce erosion on this side.

4.3. PLOUGHING PERFORMANCE

This section shows the analysis carried out to characterize the morphology, hydrodynamics, sediment dynamics, and sediment balance of the study area for the seven tests performed in the set of experiments 1. After this exposition, the results are discussed. Statistical analysis of the results has been accomplished for most of the magnitudes analysed. Individual values for each of the seven tests were grouped as $\mu_i \pm \sigma_i$, where μ_i is the mean value of the results for the magnitude i measured on the seven tests, and σ_i is the standard deviation of those same seven measurements (one for each water level).

4.3.1. Morphology

As indicated above, the 3D geometry of the sandy bottom was measured with a laser scanner before and after wave action. To account for the smoothing effect of slowly submerging bedforms until each test water level was reached, the geometry of the bathymetry was also measured for some tests after raising the water level. Figure 4.4 shows the evolution of a bathymetric longitudinal profile of the natural and ploughed geometries.

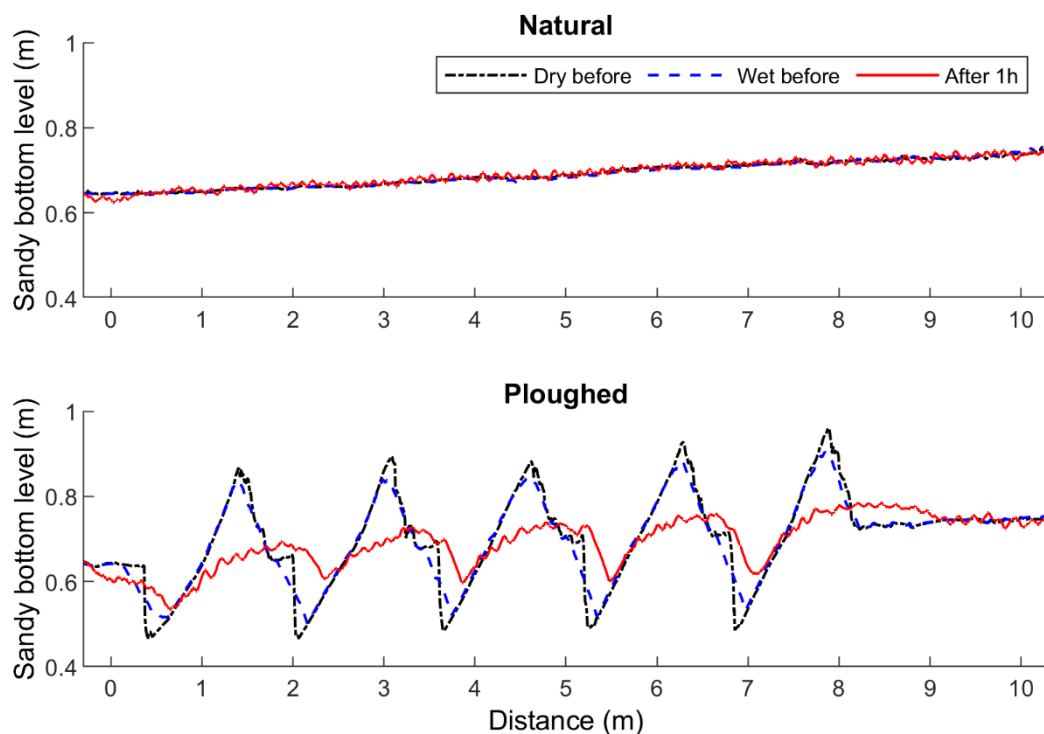


Figure 4.4 Longitudinal profiles extracted from the 3D sandy bottom at three moments in time: (1) dry before: just after manually rebuilding the initial bathymetric geometry, (2) wet before: after slowly raising the water level to the test level, and (3) after 1 h: at the end of the test wave simulation. The test run had a water level of 0.85 m.

CHAPTER 4

Changes (measured as the difference of the sandy surface level on every point of a surface mesh of 0.005 m spacing) between the geometry when it was measured dry (just after placing the sand and ploughing manually) and wet (after the rising water level) before wave generation, average 1.4 mm with a standard deviation of 2.7 mm for the natural side and average 1.9 mm with a standard deviation of 28.8 mm for the ploughed side (positive values of the average values indicate compaction by inundation). Most of the changes on the ploughed side are due to ridge compaction and furrow filling by submerged sand avalanching. Both furrows and ridges reduced their volume (by $6.68\pm2.03\%$ and $11.49\pm1.57\%$, respectively) when submerged, but ridge compaction was larger due to sand compaction and the reduction in artificially created porosity. The volume of the ridges was $8.24\pm3.19\%$ larger than the volume of the furrows just after manual ploughing. Once the bedforms were inundated, this difference reduced to $2.69\pm3.46\%$.

During 1 h of wave simulation, ripples appeared on the natural beach slope and the ploughed profile was smoothed. The sediment eroded from the ridges and was transported shoreward. Part of this sand was deposited in the furrows. Ripples also appeared on flat areas on top of the ridges.

The roughness of the sandy bottom was computed to account for the impact of the bedforms on hydrodynamics and the evolution of the morphology. Two parameters were computed as described by Poate et al. (2018): (1) the roughness parameter (k_σ) and (2) the rugosity parameter (k_R). The roughness parameter was computed as $k_\sigma = 4 \sigma_z$, where σ_z is the standard deviation of the points of the surface from the theoretical initial flat bottom of slope 1/100, measured in m. The rugosity parameter was calculated as $k_R = A_r/A_a - 1$, where A_r is the 3D surface area of the sandy bottom and A_a is the geometric area measured by the laser scanner ($k_R = 0$ for the theoretical initial flat bottom). Both parameters were computed for each laboratory test, and the results were statistically analysed. Figure 4.5 shows that before the wave simulation, the natural geometry is almost equal to the theoretical slope of 1/100 and is smooth ($k_\sigma = 0.029$ m and $k_R = 0.014$). The effect of submerging the sand underwater further reduces the roughness of the natural side. After the simulation of 1 h of waves, ripples appear on the natural side, and therefore, the roughness parameter increases to 0.047 m, and the rugosity parameter increases to 0.06. In contrast, on the ploughed side, the roughness parameter almost reaches 0.4 m, and the rugosity parameter reaches 0.25 at the beginning of each test, just after manual ploughing, and both indices decrease as water and waves act over the ridges and furrows. The inundation of the bedforms reduces both parameters, and the sand movements produced by 1 h of waves progressively flatten the surface. This leads to a final roughness parameter of 0.168 m on the ploughed side, which demonstrates that ridges and furrows are still pronounced. Second, the rugosity parameter

decreases to 0.061, which is close to the final rugosity of the natural side. Figure 4.4 shows evident morphologic differences between the natural and ploughed final bottom geometries, therefore, we can state that the k_R parameter does not show these differences, as it does not take into account the distance between the theoretical flat bottom and real surfaces. Nevertheless, the roughness parameter shows the differences, as k_σ is 3.57 times larger on the ploughed side than on the natural side at the end of the tests.

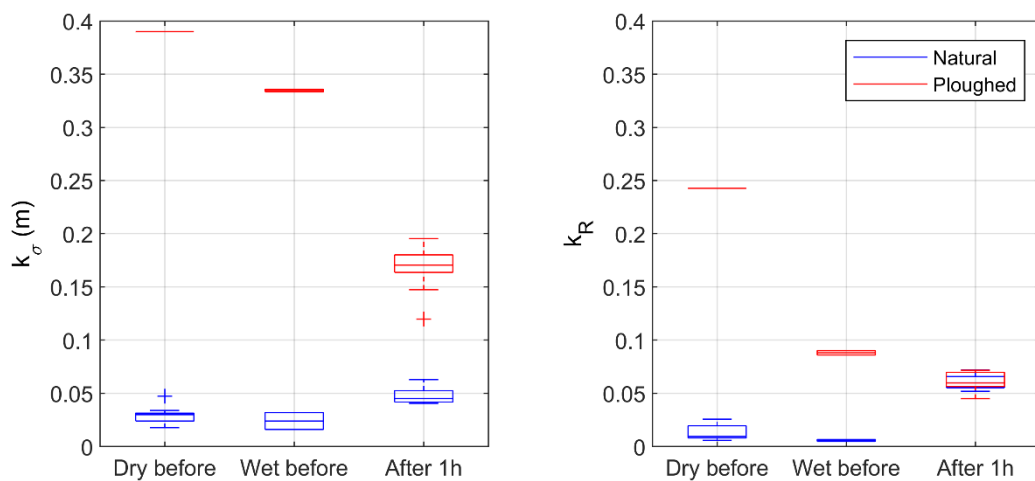


Figure 4.5 Statistical analysis (box plots) of the sandy bottom roughness computed from 3D bathymetry for each laboratory test at three different moments in time: (1) dry before: just after manually rebuilding the initial bathymetric geometry, (2) wet before: after slowly raising the water level to the test level, and (3) after 1 h: at the end of the test wave simulation. Left: Roughness parameter k_σ . Right: Rugosity parameter k_R .

4.3.2. Hydrodynamics

The free surface elevation was continuously recorded by 16 capacitive wave gauges (see Figure 4.3). The significant wave height (H_s) was obtained from hourly records for all tests performed. Two methods were used, spectral analysis and integration, to obtain the zero-order momentum (m_0) followed by $H_s = 4 \cdot \sqrt{m_0}$ and the zero-crossing analysis (results not shown). Both methods show similar results. H_s at generation next to the wave paddle is 0.29 ± 0.01 m. Figure 4.6 shows the evolution of H_s for each test and both sub-channels. The wave height at the beginning of the sandy area is lower for the tests with the lower water level, as more waves break on the concrete ramp. Waves break as they propagate over the sandy bottom. H_s decreases ($H_{s, WG11} - H_{s, WG16}$) 0.059 ± 0.007 m on the natural side and ($H_{s, WG4} - H_{s, WG10}$) 0.071 ± 0.008 m on the ploughed side along the 10 m long sandy area. The low dispersion of these values indicates that wave dissipation over the sand is almost the same for each water level. Additionally, mean values indicate that wave

CHAPTER 4

dissipation on the ploughed side is larger (see the solid markers below the empty markers in onshore points in Figure 4.6), resulting in waves that are $11.08 \pm 7.75\%$ smaller at the end of the ploughed side than at the end of the natural side ($(H_{s, WG16} - H_{s, WG10}) / H_{s, WG16}$). The wave height for most onshore sensors of the test with a water level of 0.75 m could not be calculated because the water level was too low; these sensors were temporarily above the water surface.

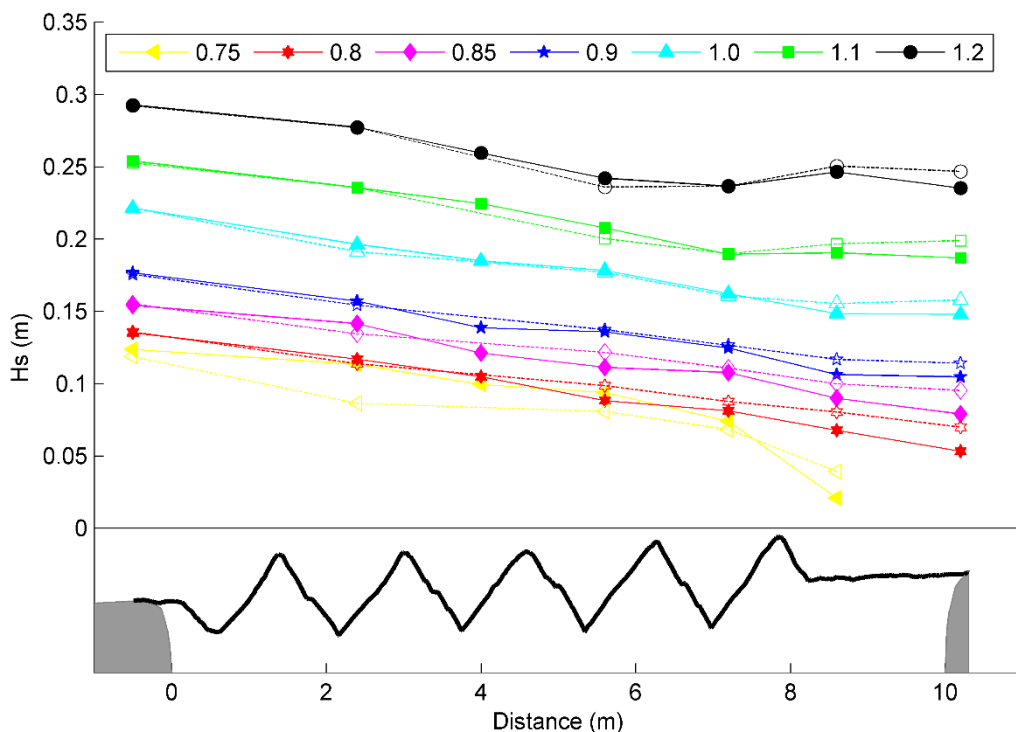


Figure 4.6 Significant wave height evolution along both sub-channels for each test with different water levels (see the legend). Natural beach side values are shown with a dashed line and empty markers. Ploughed side values are shown with a continuous line and solid markers. The diagram on the bottom shows a profile of the ploughed bathymetry for reference to each sensor location.

Wave-energy-flux dissipation per unit water volume cross-shore $D(x)$ was computed from H_s measurements through the Wang and Kraus (2005) formulation:

$$D(x) = \frac{1}{h} \frac{d(EC_g)}{dx} = \frac{1}{h} \frac{d\left(\frac{1}{8} \rho_w g H_{rms}^2 \sqrt{gh}\right)}{dx} \approx \frac{1}{8} \frac{\rho_w g^{3/2}}{h_{mid}} \frac{\Delta(H_{rms}^2 h^{1/2})}{\Delta x} \quad (4.1)$$

where E is the wave energy per unit area, $C_g = \sqrt{gh}$ is the wave group velocity in shallow water, g is the acceleration due to gravity, h is the water depth, $H_{rms} = H_s/\sqrt{2}$ is the

root-mean-squared wave height, ρ_w is the water density and h_{mid} is the water depth at the midpoint between the free surface sensors. Equation (4.1) gives one dissipation value for each pair of consecutive free surface elevation sensors, which is representative of the wave dissipation produced while propagating from one to the other. The results from the application of the above formula show that wave dissipation ranges between 50 and 200 W/m³ along the sandy area, for water levels of 0.75, 0.8, 0.85, and 0.9 m. The results for water levels of 1, 1.1, and 1.2 m present more variability and larger dissipation ratios, reaching 750 W/m³.

Figure 4.7 shows the comparison of wave-energy dissipation rates of the natural and ploughed sides (obtained from a pair of sensors at the natural side and their corresponding ones located at the same cross-shore locations at the ploughed side). Sensors over the seaward half (5 metres) of the sandy bottom indicate a similar dissipation for both sides, but results of sensors over the shoreward half (5 m), after the third ploughed ridge, show bigger dissipation for the ploughed side.

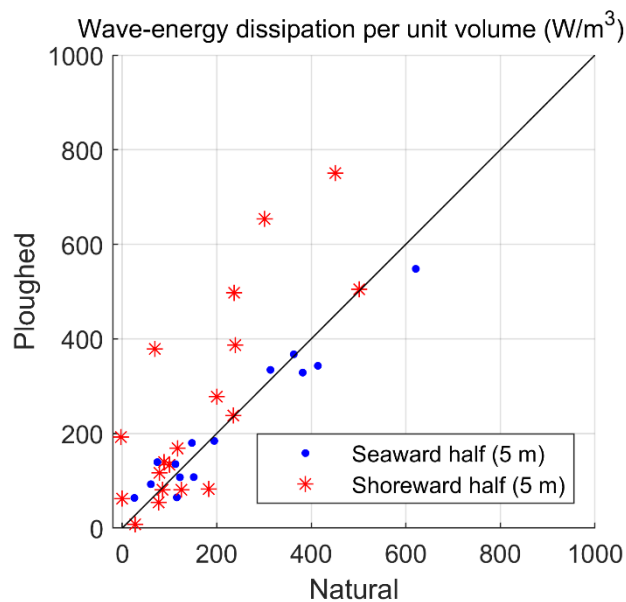


Figure 4.7 Wave-energy dissipation rate comparison for the natural and ploughed sides. The dots on the black line indicate the same dissipation on both sides. The dots in the top-left area indicate that the ploughed side dissipation is larger, and the dots in the bottom-right area indicate that the natural side dissipation is larger.

The water surface elevation power spectrum, $S(f)$, was computed for each sensor and experimental test. Figure 4.8 shows the results for the water level test of 0.85 m as an example. Each panel of Figure 4.8 compares the spectrum on the natural and ploughed sides at the same cross-shore position of the profile with the spectrum generated at the

CHAPTER 4

paddle. The peak period at generation is 7 s (0.143 Hz). From top-left to bottom-right, waves around the peak period break as they propagate over the sandy bottom, reducing the energy of this part of the spectrum. Additionally, on the bottom panels, the energy of the ploughed side sensors is below the corresponding energy of the natural side, indicating that extra energy dissipation is produced for frequencies of more than 0.03 Hz. The results for other water levels (not shown) are similar, except at a water level of 0.75 m, which produces more energy reduction, as the water depth is zero at the top of the sandy area. The sensors over this point emerge most of the time, so this test is not included in further analyses.

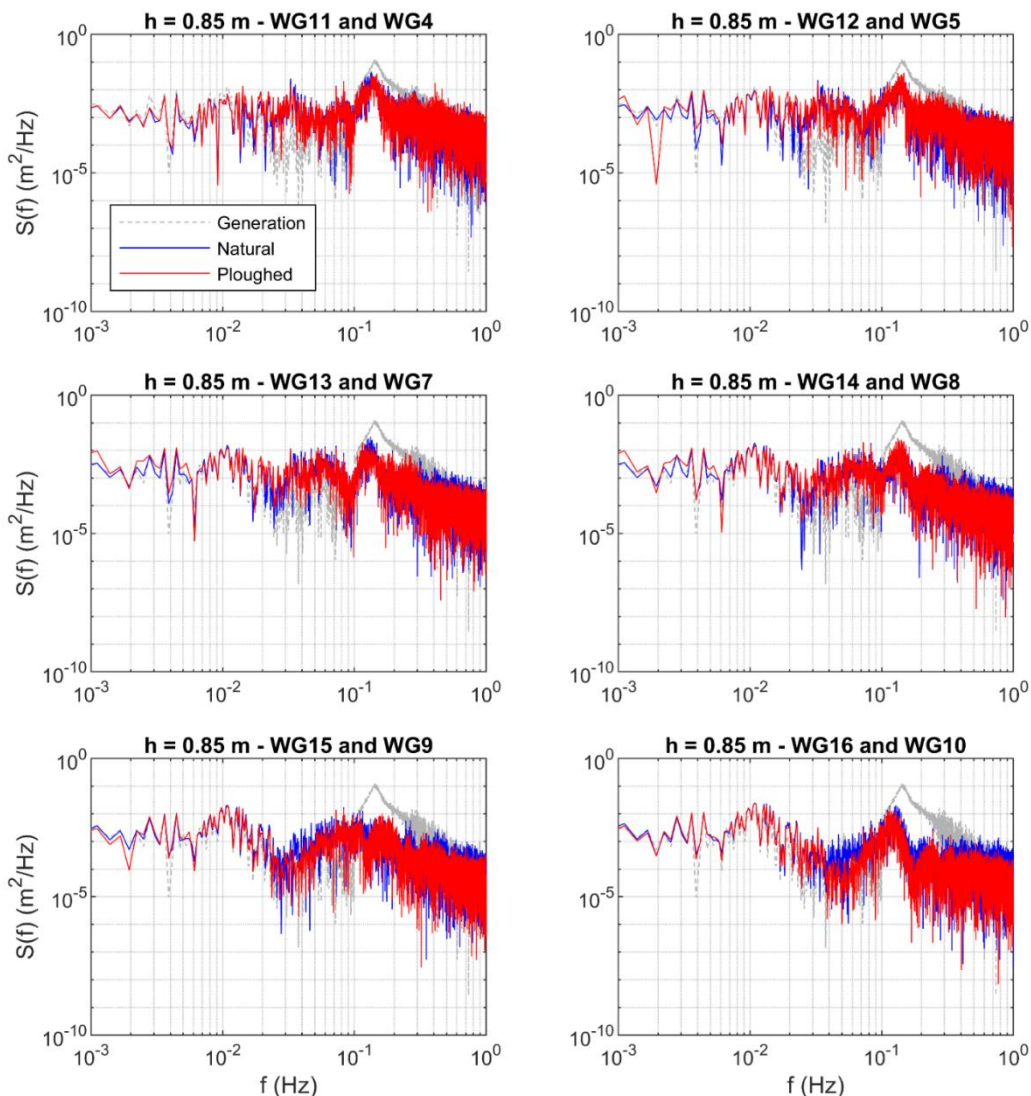


Figure 4.8 Wave energy spectrum at generation (WG1) and each pair of sensors at the same longitudinal position in the channel. The top-left panel corresponds to the offshore end of the sandy area, and the bottom-right panel corresponds to the onshore end (see the position of each sensor in Figure 4.3).

In the following, we focus on the results of sensors WG10 and WG16 (see Figure 4.3) at the onshore end of the sandy area to account for the total energy dissipation and redistribution in the laboratory tests. The total energy for each frequency is computed by integrating small frequency windows of the spectrum according to the following equation:

$$E(f) = \int_{f_1}^{f_2} S(f) df \quad (4.2)$$

The top-left panel of Figure 4.9 shows the energy redistribution produced on the natural side computed with equation (4.3):

$$\text{Wave dissipation on natural side} = \frac{E_{WG16}}{E_{WG1}} \cdot 100 \quad (4.3)$$

where E_{WG1} stands for the integrated energy at WG1 (next to the wave generator) and E_{WG16} stands for the integrated energy at WG16 (natural side).

For the frequencies of windows B and D, wave energy dissipation is dominant for all water levels tested, while energy increases in windows A, C, and E due to nonlinear energy transference to low and high frequencies. The other panels of Figure 4.9 show the total energy integrated for each of windows A to E. Each panel compares the energy at the generation, natural and ploughed sides for each water level tested. The results corroborate that ploughing produces extra energy reduction for frequencies above 0.03 Hz, while the energy remains the same for frequencies below this value (window A). For windows B and D, both sides dissipate energy, but the ploughed side produces extra dissipation at all water levels. Figure 4.10 shows that the relative energy dissipation difference, given by equation (4.4), reaches 45% for frequencies of approximately 0.055 and 0.175 Hz:

$$\text{Extra ploughing energy dissipation} = \frac{E_{WG16} - E_{WG10}}{E_{WG16}} \cdot 100 \quad (4.4)$$

where E_{WG16} and E_{WG10} stand for the integrated energy measured by the wave sensors WG16 (ploughed side) and WG10 (natural side) respectively.

CHAPTER 4

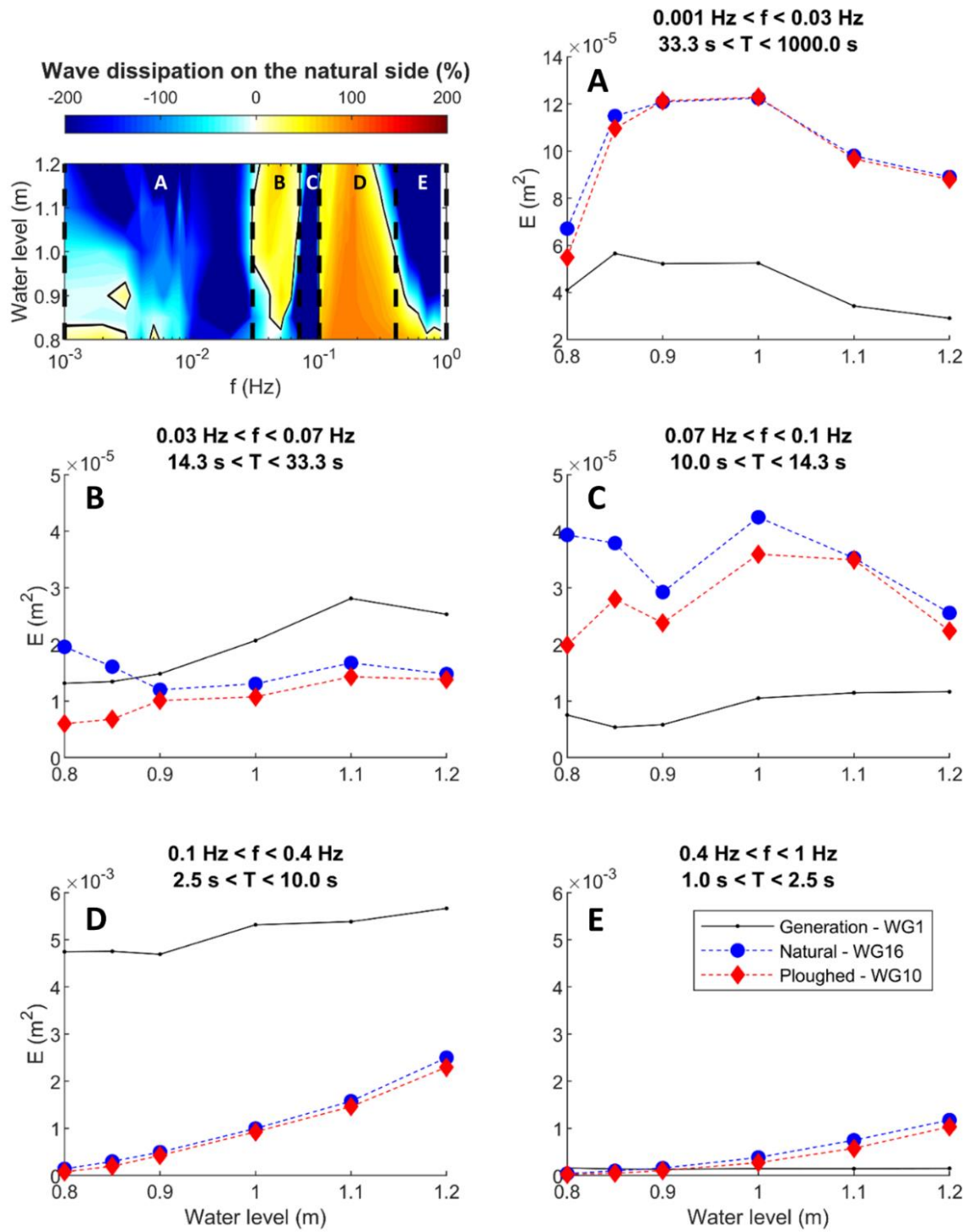


Figure 4.9 The top left panel shows the percentage of wave dissipation (positive dissipation, negative energy increase) for each frequency and water level on the natural side (see equation (4.3)). The other panels correspond to each frequency window identified in the first panel (A, B, C, D, and E). Each panel shows a comparison of the integrated energy (in the indicated windows) for WG1, WG10, and WG16 for each water level tested. Note the different scales of the vertical axes.

Additionally, for windows C and E, both sides show incremental energy, but it is lower for the ploughed side (approximately 10% for section C and 30% for E). The central frequency of window C (0.085 Hz) matches the half frequency of the maximum dissipation peak at 0.175 Hz, showing energy transfer to this sub-harmonic. Figure 4.10 shows that this extra energy dissipation on the ploughed side is larger for the lower water levels tested (0.85 and 0.9 m).

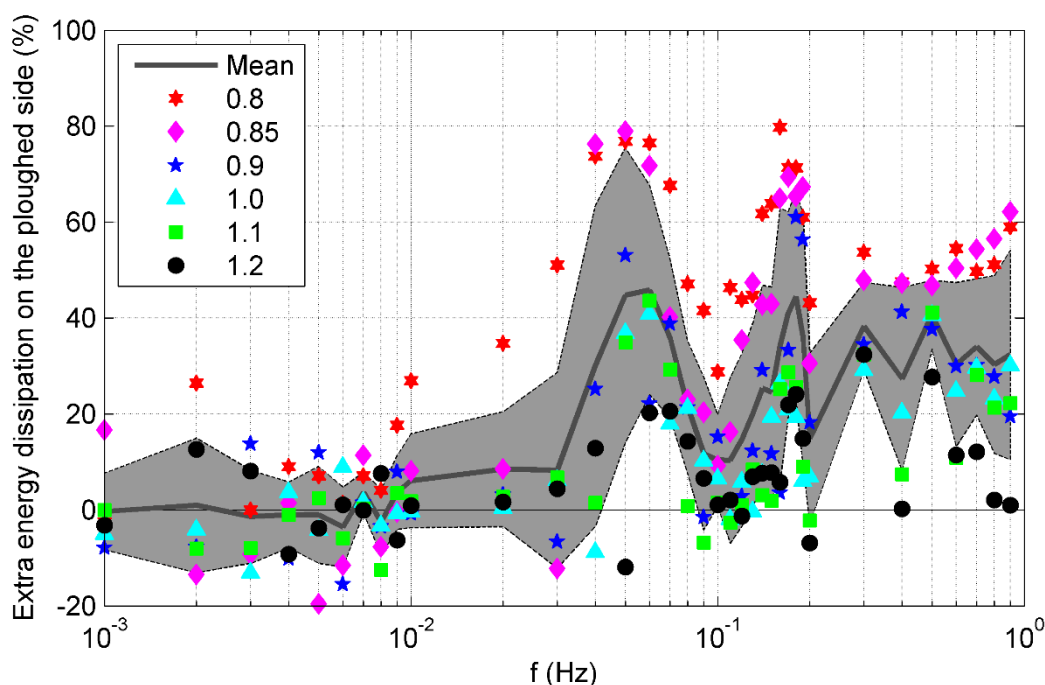


Figure 4.10 Extra energy dissipation on the ploughed side at each frequency of the spectrum (see equation (4.4)). Positive values indicate that the energy on the ploughed side (WG10) is lower than the energy on the natural side (WG16). The shaded grey areas indicate one standard deviation from the mean value.

The data recorded from ADV sensors were low pass filtered with a Butterworth (1930) filter using an order of 6 and a cut frequency of $4 \cdot dt$, where dt is the sampling rate of the ADV sensor (1/50 s). The cross-shore velocity component was extracted from filtered signals and processed to obtain the mean current.

Sensors ADV1 and 3 are located 0.1 m from the sandy bottom and therefore are only fully submerged for tests with water levels higher than 0.85 m. Similarly, sensors ADV2 and 4 are located 0.2 m from the bottom, and measurements could only be taken for water levels higher than 1 m. Figure 4.11 shows the results obtained for each sensor. Mean velocities are higher on the ploughed side than on the natural side (differences of 0.040 ± 0.005 m/s at the lower sensors ADV1 and 3; and 0.045 ± 0.002 m/s at the higher sensors

ADV2 and 4). This indicates that currents on the ploughed side are stronger if directed onshore or weaker if directed offshore. This mean current difference on the ploughed side can help onshore sediment transport. Onshore currents dominate for lower water levels where ADV sensors are at a relatively higher position in the water column (Haines and Sallenger, 1994). In contrast, offshore currents dominate for higher water levels when sensors are located at a relatively low position in the water column; therefore, undertow currents can be affected.

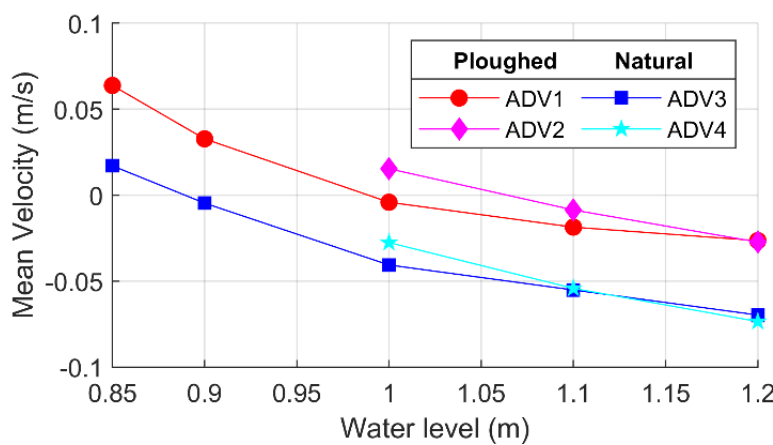


Figure 4.11 Cross-shore current analysis for each water level tested. Sensors ADV1 and 2 are located on the ploughed side, and sensors ADV3 and 4 are located on the natural side (the position of each sensor is shown in Figure 4.3). Positive values of the mean velocity are given onshore.

4.3.3. Sediment dynamics

Net time-averaged cross-shore sediment transport (Q) is obtained from the initial and final bathymetries (Alsina et al., 2012; Baldock et al., 2011, 2007; Baldock and Alsina, 2013) with the Exner equation:

$$Q(x_i) = Q(x_{i-1}) - p \int_{x_{i-1}}^{x_i} \frac{\Delta z}{\Delta t} dx \quad (4.5)$$

where $Q(x_i)$ is the integral volume of sediment transport (m^2/s) at position x_i , Δz is the difference in the bed elevation (m) averaged over the width of the channel between the initial and final measured bathymetries, Δt is the time difference (3,600 s) and p is the solid fraction, which is 0.6. One boundary condition is needed. As all the sediment transport goes shoreward, the condition is $Q(-0.3 \text{ m}) = 0 \text{ m}^2/\text{s}$ on the seaward end of the sandy area over the concrete ramp. Positive values indicate shoreward sediment transport and negative values indicate seaward sand movement.

Figure 4.12 shows the cross-shore sediment transport obtained from initial and final bathymetries (averaged over 1 h of the experiment) for each of the laboratory tests along the sandy area. Note the different scales for the natural and ploughed sides. Accretion dominates on both sides. The mean value of all tests is computed to observe the trend. The natural side shows increasing shoreward sediment transport for the first 4 m (erosion) and then a reduction in sediment transport up to 8 m. This means that accretion is produced between 4 and 8 m, creating a bar that reaches 0.01 m in height. At 8 m, sediment transport is still positive, which means that some of the sediment eroded at the beginning is still passing shoreward. The final 2 m is eroded, producing an increase in sediment transport reaching $Q = 3.44 \times 10^{-6} \text{ m}^2/\text{s}$ at the shoreward end of the sandy area.

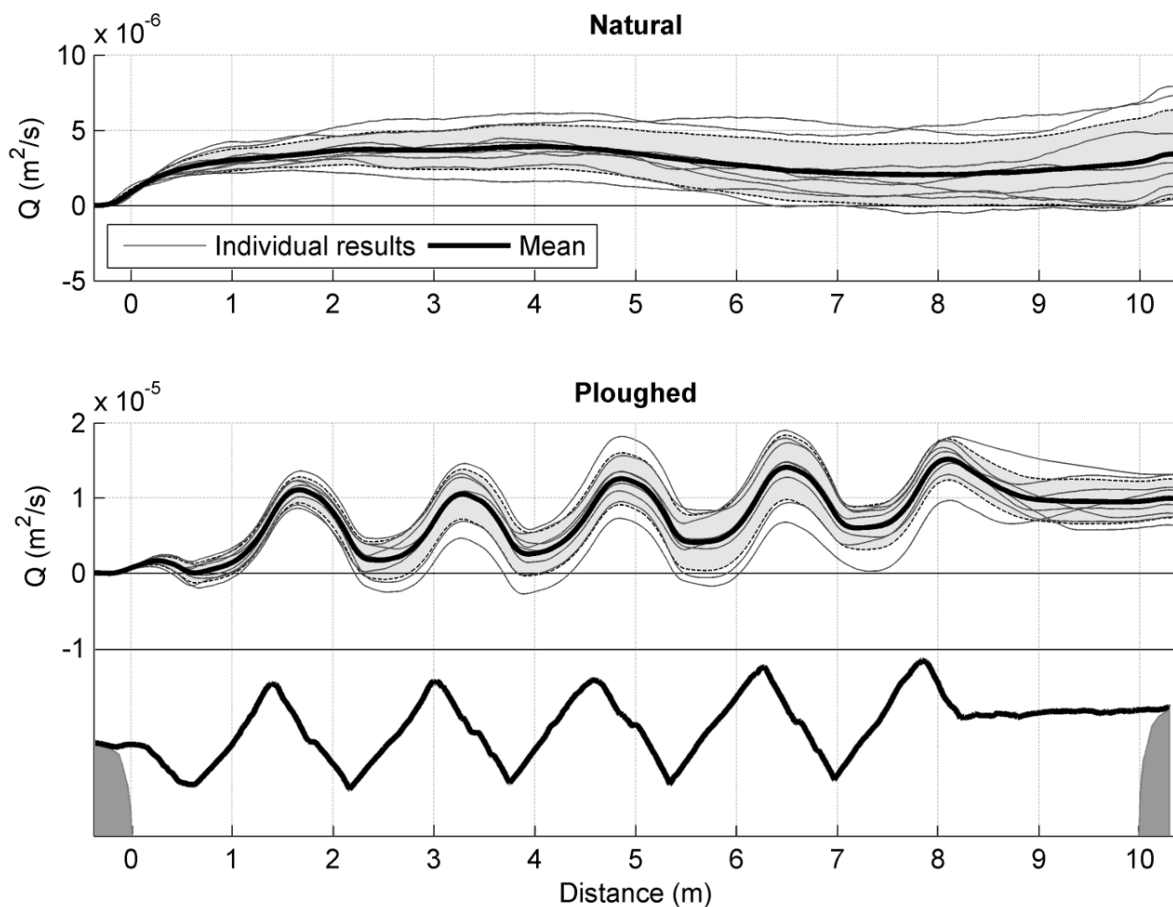


Figure 4.12 Cross-shore sediment transport per unit width (see equation (4.5)). Positive values indicate accretion. The shaded grey areas indicate one standard deviation from the mean value (the thick black line). The light grey lines are the results for each laboratory test with different water levels. The diagram on the bottom shows a profile of the ploughed bathymetry for reference of ridges and furrows location.

CHAPTER 4

The ploughed side shows oscillations in the sediment transport value. Increasing Q values indicate eroded areas, and decreasing Q values match accreting sections. Five accreting sections are located over the ploughed furrows, and the last section is located in the area in which the last ridge is partially dispersed. The ridges are eroded, and part of their sediment passes over the next furrows and increases net onshore sediment transport. At the shoreward end of the sandy area, $Q = 9.96 \cdot 10^{-6} \text{ m}^2/\text{s}$, which is 2.9 times larger than the sediment transport on the natural side.

The suspended sediment concentration (SSC) was measured by two OBS sensors. Each sensor is located at the onshore end of the study area, 0.05 m above the sandy bottom (see Figure 4.3). The time series of the SSC values are statistically analysed and are represented in Figure 4.13. The sensors were not fully submerged during the tests with lower water levels; therefore, data for 0.75 and 0.8 m levels have been discarded. There are higher concentration values associated with breaking waves passing through sensor locations for all tests that have not been represented. These outliers are present on both sub-channels. Those breaking waves produce SSC values between 0.5 and 1.0 g/L for a $3.06 \pm 1.39\%$ of the data, and SSC higher than 1.0 g/L for a $0.89 \pm 0.51\%$ of the data, with a maximum SSC of 3.6 g/L.

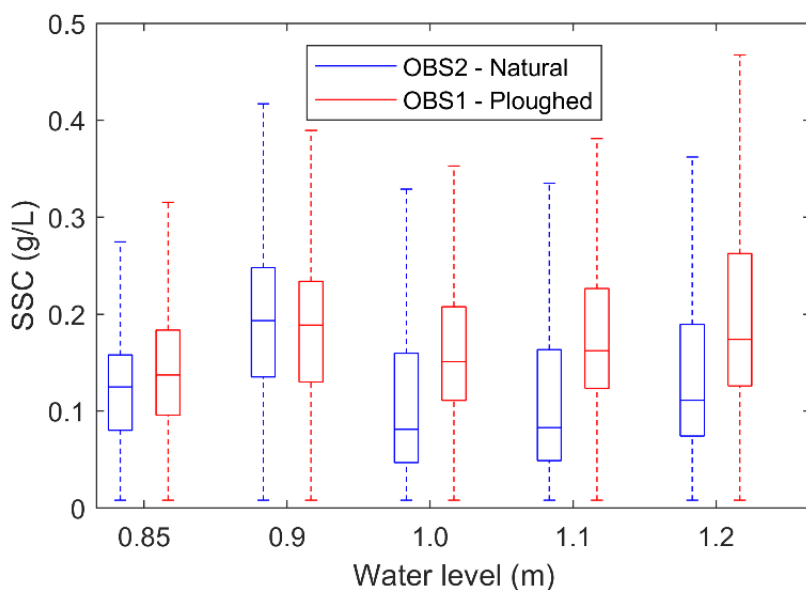


Figure 4.13 Statistical analysis (box plots) of the suspended sediment concentration time series obtained from OBS data for each laboratory test (the position of each sensor is shown in Figure 4.3).

The SSC is larger on the ploughed side in four out of five tests, as shown in Figure 4.13. The median values are 8.98% larger on the ploughed side for the test of the water level of 0.85 m, 46.33% for 1 m, 48.92% for 1.1 m, and 36.09% for 1.2 m. For the test of the water level of 0.9 m, the SSC on the ploughed side is 2.44% lower. These values have been obtained from the OBS measurements, which are taken at a unique point of the water column. Nevertheless, this generalized larger concentration of sediment on the ploughed side was clearly noticeable during the experiments as a larger turbidity of the water in the whole water column from the beginning of each test (visible through the glass sidewall of the channel, see Figure 4.1).

4.3.4. Sediment balance

Laser scanner bathymetries measured before and after wave simulation were used to calculate eroded and accreted volumes of sand. The surface of each sub-channel was discretized on a mesh of square cells with sides of 0.005 m long. The elevation of all points measured by the laser scanner, with X and Y coordinates inside each of the cells of the mesh, were averaged to obtain a representative elevation Z_i of the cell i . The accreted or eroded volume of sand on each cell is computed with equation (4.6) as the difference of elevation before and after each test by the cell size.

$$V_i = (Z_{i,after} - Z_{i,before}) \cdot 0.005^2 \quad (4.6)$$

where V_i is the volume of sand on the cell i , $Z_{i,after}$ is the surface elevation of the cell after the experiment, and $Z_{i,before}$ the surface elevation of the cell before the wave action.

The volumes V_i were integrated over the full mesh of each sub-channel to obtain the erosion volume ($V_{erosion}$, equation (4.7)), and the accretion volume ($V_{accretion}$, equation (4.8)).

$$V_{erosion} = \sum V_i \text{ for } V_i < 0 \quad (4.7)$$

$$V_{accretion} = \sum V_i \text{ for } V_i > 0 \quad (4.8)$$

Figure 4.14 shows these volumes for each of the laboratory tests and the net volume (sum of the eroded and accreted volumes). Mobilized sand volumes are larger on the

CHAPTER 4

ploughed side due to partial ridge erosion and furrow filling. On the natural side, eroded and accreted volumes respond mainly to ripple formation. The results indicate that accretion is produced on both sides, but it is larger on the ploughed one (see larger eroding [negative] values in the scatter plot), which indicates the effectiveness of this innovative technique. There is no clear trend for the different water levels simulated, suggesting that the produced improvement in accretion is similar for all water levels.

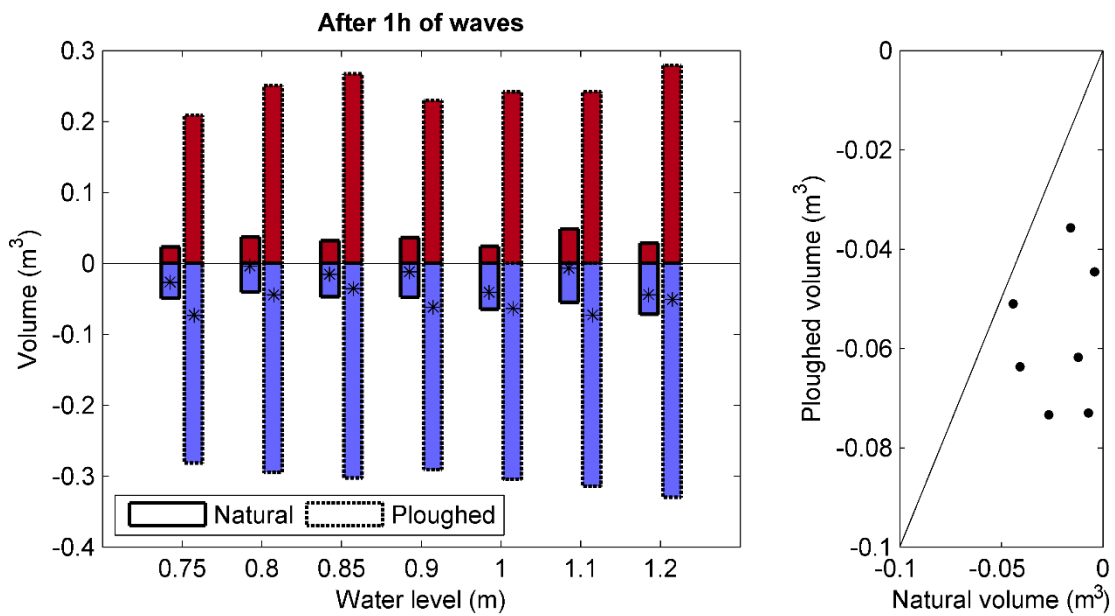


Figure 4.14 Mobilized sediment volumes. Positive values indicate sand accumulation, and negative values indicate sand erosion and onshore mobilization (accretion). Left: Accumulated (red), eroded (blue) and net (*) sediment volumes. Right: Comparison of the net sediment volume accreted (eroded from the sandy area) on both sides (each dot corresponds to a couple of asterisks in the left panel).

4.3.5. Discussion

The laboratory experiments performed in this work show that ploughing the intertidal area of a beach affects the hydrodynamics and sediment transport and accelerates natural beach accretion.

Five ridges and furrows were built at a prototype scale over a movable sandy bottom. These shapes produced a bottom roughness that was more than 3.57 times the final roughness on the natural intertidal geometry used as a control for the experiment. The effects of ploughing include: (1) a reduction in the significant wave height at the onshore end of the study area (H_s on the ploughed side is $11.08 \pm 7.75\%$ smaller than H_s on the natural side), (2) a reduction in the wave energy for all frequencies over 0.03 Hz (reaching 45%

lower energy at 0.175 Hz and 0.055 Hz), (3) an increase of 2.9 times the total onshore sediment transport, and (4) a suspended sediment concentration increase of up to 49%, which together with the tendency towards the coast of the measured currents, may facilitate the increase of onshore suspended transport. Altogether, the results showed that larger volumes of sand were moved onshore in the ploughed geometry than in natural conditions, demonstrating the effectiveness and potential of ploughing techniques to enhance natural beach accretion.

Frictional dissipation may play an important role in ploughing effectiveness. The incident wave height and bed gradient are the same for natural and ploughed geometries, but the bed roughness is clearly larger for the ploughed bottom. Poate et al. (2018) found that the relative importance of frictional dissipation (vs the total wave energy dissipation) increases with a decreasing bed gradient ($\tan\beta < 0.02$), a small wave height ($H_0 < 0.5$ m), and an increasing bed roughness, where friction may account for ~20% of the total wave energy dissipation. In this experiment, the bed gradient is very low ($\tan\beta = 0.01$), and the wave height is low ($H_s = 0.3$ m). The crucial difference between the natural and ploughed sides is the bed roughness. In this case, k_σ averages 0.029 m at the beginning and 0.045 m after the waves on the natural side, and k_σ averages 0.4 m at the beginning and 0.168 m after the waves on the ploughed side. Although bed roughness decreases as waves move the sandy ploughed bottom, the roughness after 1 h of waves is still 3.57 times larger than that on the natural side. This explains the larger wave energy dissipation produced due to ploughing.

Gainza et al. (2019) proposed bed roughness as a possible mechanism causing the acceleration of the accretion effect of ploughing. They also stated that changes in sand porosity, due to the decompaction produced by ploughing sand movements, might lead to sediment transport acceleration by a factor of $1/(1 - p_h)$ according to the mass conservation equation. Given the usual porosity (p_h) values on natural beaches, the effect on final sediment transport is very low. Additionally, in the laboratory tests, the initial sand loosening in the ridges averages 8.24% (the sand volume increases). This sand loosening reduces to 2.69% after rising the water level, and therefore, porosity changes are negligible.

The bottom roughness generated by ploughing produces extra wave energy dissipation for frequencies above 0.03 Hz at the shoreward end of the study area. This energy reduction occurs for all of the water levels that were tested but is larger for the lower ones, where almost all waves break over the sandy area. This extra energy dissipation averages 45% of the energy reduction on the ploughed side for frequencies of approximately 0.055 and 0.175 Hz. The peak frequency of the waves generated is 0.143 Hz, so that 0.175 Hz is close to the mean frequency of the waves simulated. The frequency of

CHAPTER 4

0.055 Hz has low energy and is not present on the wave spectrum at generation. Alsina et al., (2012) found a similar effect of energy reduction for frequencies around 0.065 Hz due to swash zone reshaping. They stated that this frequency component can be attributed to standing long waves being reflected by the beach and a more dissipative beach (in our case due to ploughing) would produce less reflection. The analysis of wave gauge sensors distributed along the study area indicates that an isolated ridge and furrow would not generate this effect. Larger wave energy dissipation rates for the ploughed side are only found for the last 5 m of the sandy area after wave propagation over three ridges and furrows. Further experiments are required to analyse the influence of larger ploughed arrays that could extend over the full width of the intertidal area and therefore produce even more wave energy dissipation.

The smaller wave height measured in the ploughed area leads to a smaller dimensionless fall velocity parameter Ω and a more reflective morphodynamic state of the beach (the beach will evolve towards it). This leads to the thinking that ploughing repeated over several tidal cycles will cause an increase in sand accretion due to creating more reflective wave conditions; this would support the results obtained at Laida beach (Gainza et al., 2019), where the intertidal area was ploughed 22 times and the natural onshore migration of the intertidal bar was accelerated.

The suspended sediment concentration at the shoreward end of the study area is a maximum of 45% larger on the ploughed side than on the natural control side. This larger water turbidity was noticeable with the naked eye through the glass sidewalls of the channel. The larger bottom roughness may be one of the causes, as it generates a longer sandy surface in contact with the water, which allows further sediment resuspension. Additionally, the extra energy dissipation indicates that more breaking is produced on the ploughed side, and therefore, more suspended sediment concentration is expected.

Suspended sediment is moved by water currents. Measurements from ADV sensors located above the OBS showed a higher onshore mean current on the ploughed side. This means that suspended sediment transport is prone to produce more accretion due to ploughing. The water column velocity profile determines the current direction depending on the relative position of the sensor and the water level of each test. Nevertheless, the mean current on the ploughed side is stronger if directed onshore and weaker if directed offshore, indicating that currents are more prone to be directed onshore due to ploughing.

The total sediment transport, including bottom and suspended load, is directed onshore on both sides. Accretion is produced in all tests, as expected from the design of the

experiments. On the ploughed side, mobilized sand volumes are larger, as sand is eroded from the ridges and partially fills the furrows. On the natural side, ripples appear. Despite these bedforms, the sediment that finally passes over the full length of the study area (onshore directed) is larger on the ploughed side. The average sediment transport of all tests at the shoreward end of the ploughed side is 2.9 times larger than that on the natural control side. This agrees with the greater accretion volumes obtained on the ploughed side, which demonstrates the effectiveness of this technique to enhance natural beach accretion.

Ploughing technique is thought to be applied every low tide. Only tides in which predicted incoming wave conditions are expected to produce accretion must be selected. Further research is needed to explore a wider range of wave conditions, in order to define the thresholds in which the potential of ploughing for accelerating natural beach accretion can be exploited.

Soft engineering techniques, such as beach ploughing, deal with cross-shore seasonal sediment movements. Ploughing technique provides a nature-friendly solution for pocket beaches or coasts with longshore sediment transport generating dynamic equilibrium. In these types of coasts, no external sand is required to recover the beach width previous to winter storms (earlier in the summer thanks to ploughing technique). Additionally, coasts with longshore sediment transport producing disequilibrium are also target beaches for ploughing technique, as long-term erosion or accretion issues can be dealt with separately (i.e. with beach nourishments or by-passing) from the seasonal cross-shore processes that can be fought with ploughing technique to have wider beaches at the beginning of the touristic season.

CHAPTER 4**4.4. BEDFORMS EVOLUTION**

This section shows the methodology used to extract data from the side cameras that took images during the set of experiments 2. Then the ploughed morphology is analysed based on these data, and finally, the hydrodynamic effects of ploughing are evaluated from the comparison of the measurements obtained from all the instrumentation placed on the ploughed and control subchannels. After that, the results are discussed. As a remainder, this Set 2 of experiments is composed of two long-duration (4 h) tests of water levels: 0.85 m for Test A and 1.2 m for Test B.

4.4.1. Methodology

This section focuses on the methodology followed to process and extract data from the side cameras pointing at the ploughed subchannel of the experiment. The natural subchannel data were only used for comparison, and therefore, a more simplistic approach was applied by using data from sediment weighting and laser scanners but no continuous images.

Two cameras took images of the ploughed subchannel every 5 minutes. The contour line of the sandy surface next to the glass sidewall was extracted from each image by means of an in-house method. Fisheye correction was applied, and then data rectification based on control points was performed to transform the pixel position to real coordinates along the flume. Figure 4.15 shows the initial snapshots of Test A after its processing. Sandy surface measurements extracted from images were validated with laser scanner data taken after each hour of wave simulation, obtaining differences below 0.01 m. The overlap area between images also showed good agreement and continuity of the extracted bottom profiles.

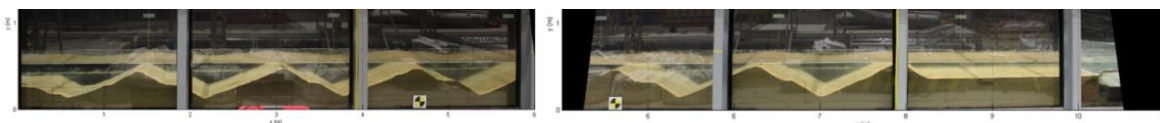


Figure 4.15 Side-channel images after fisheye correction and rectification.

This processing was applied to all the images taken for each laboratory test. Figure 4.16 shows an example of the temporal evolution of the extracted bottom profiles during the whole duration of Test A.

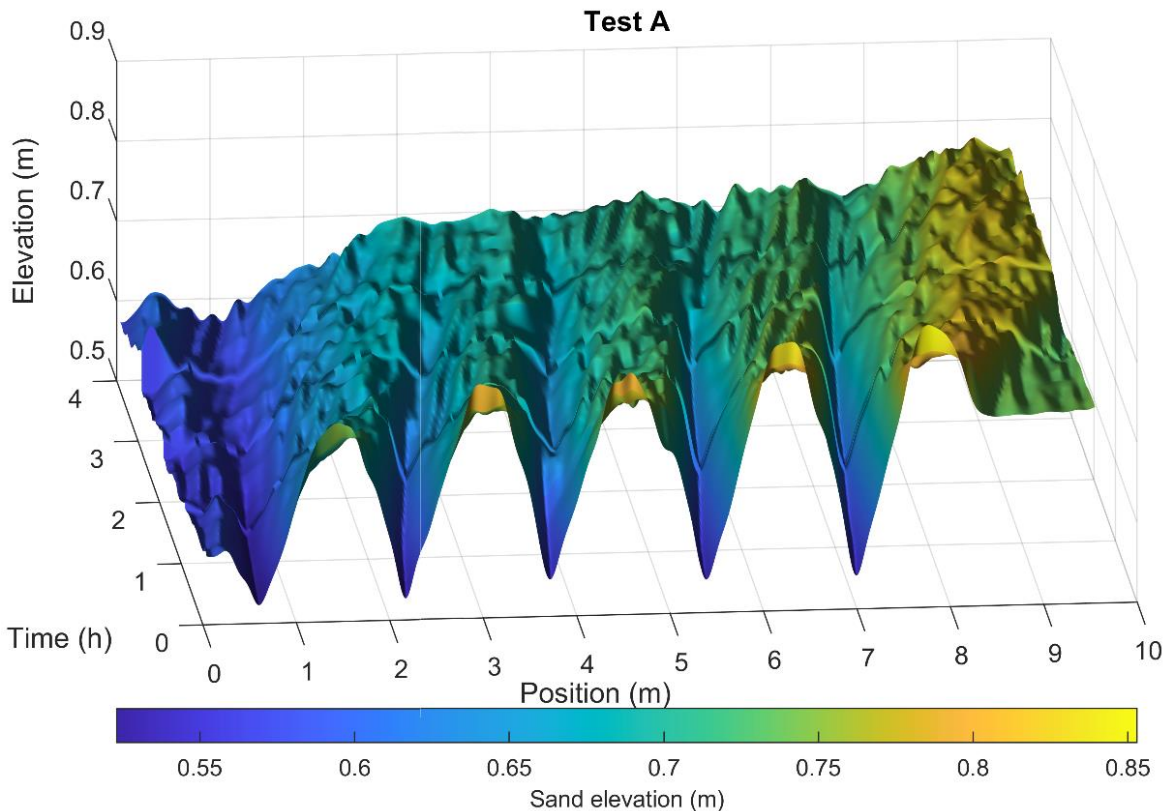


Figure 4.16 3D visualization of the spatial and temporal evolution of the bottom profile during Test A.

The sandy test area was set up with an initial uniform slope of 1/100. This study required data from the ploughed geometry; only the ridges and furrows dug over this uniform slope, which we call the slope-corrected profile (SCP). Therefore, the bottom profile data were transformed by subtracting the uniform slope from the data to obtain the SCP time series (see Figure 4.18).

These SCP data were processed to obtain morphological evolution data. Boundary effects were evident: (1) in the first 2 m (along the channel), where there was a progressively increasing lack of sand and punctual sand refills (over the end of the concrete ramp and initial part of the sandy area); and (2) in the last 1.5 m, where the initial sandy bottom was flat (not ploughed) and sand progressively accumulated over it. For this reason, morphological analysis was performed only for the trench of the profiles from 2 to 8.5 m along the channel. Spectral analysis of these data showed a wide range of wavelength components (see the upper panel of Figure 4.17). Visual inspection allowed the identification of ploughing and the ripples that form over it. To separate both components, a high-pass filter in the frequency domain was applied with a cut-off wavelength of 0.4 m (the same threshold used by Guerrero et al., 2021 to separate ripples). This filter separated

CHAPTER 4

the ripple component (RC) from the rest of the signal (PC, plough component and other bedforms with a wavelength over 0.4 m). Figure 4.17 shows an example of the filtering results.

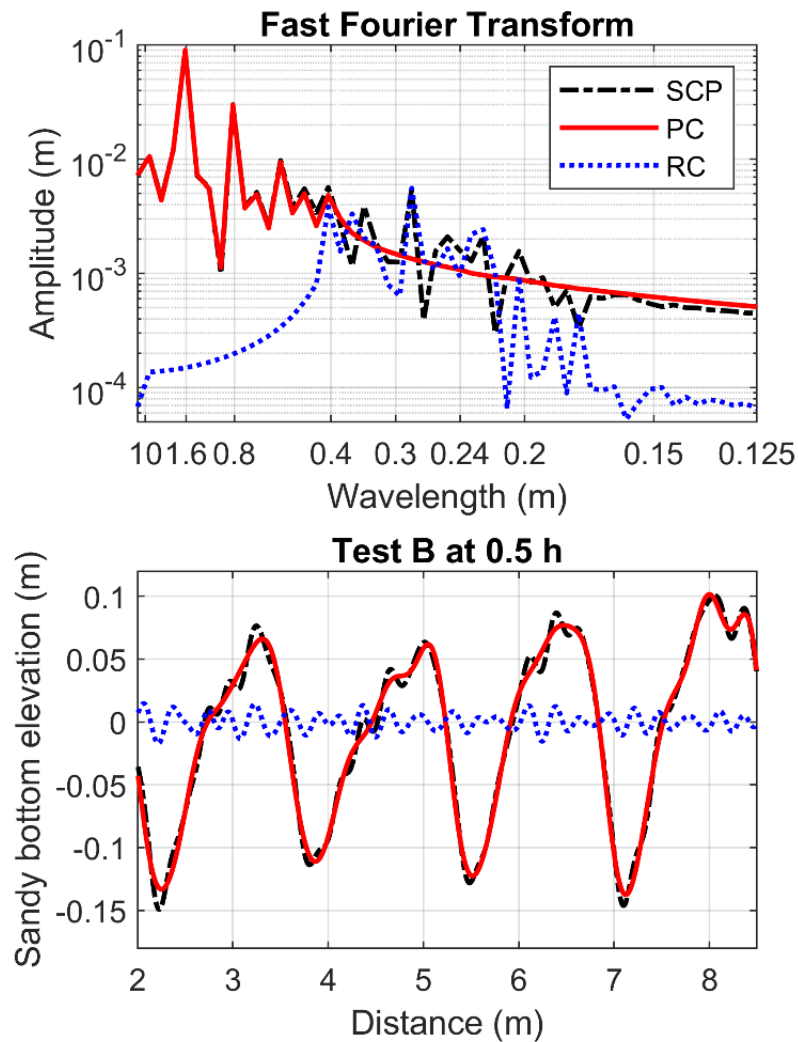


Figure 4.17 Top: Fast Fourier transformation of the SCP signal and wavelength filtering to split the spectra into two components, PC and RC. Bottom: Bathymetry (SCP) separation into two components, PC and RC, by inverse fast Fourier transformation of the spectra of the upper panel.

Each of the bathymetric components (PC and RC) was analysed separately to obtain its height, wavelength, and migration speed. The slip and stoss face slope of the ridges were also analysed for the plough component (PC).

4.4.2. Ploughed subchannel morphology

This section contains the analysis of the morphometric characteristics of the ploughing performed at the laboratory and its temporal evolution. The data used in this section come from the images taken from the outer part of the glass sidewall. Figure 4.18 shows the temporal and spatial evolution of the bed level elevation taking the initial 1/100 uniform slope as a reference (SCP data) for Test A and Test B. In these graphs, ridges are represented with yellow and red colours, and furrows are represented in blue. The white colour represents areas without accumulation or erosion of sand.

The general behaviour of the plough was similar for the two tests. Ridges and furrows progressively migrated onshore and reduced their amplitude. Ripples formed over the ridges during the first hour of wave simulation and migrated faster than ploughed structures. At the end of both tests, ridges and furrows could no longer be identified, corroborating the adequacy of the chosen test duration.

As mentioned before, boundary effects were noticeable at the offshore (from 0 to 2 m) and onshore (from 8.5 to 10 m) ends of the sandy area. For this reason, the spectral decomposition described before was applied to the data from 2 to 8.5 m along the channel to avoid frequency components generated by these boundaries having different behaviours. The two frequency components in which the data were split were analysed separately. The ploughing component with longer wavelength bedforms (PC) was processed in detail to accurately compute their morphodynamic characteristics, which are shown in this section. The ripple component (RC) was also analysed, and morphologic characteristics were found to be constant over time. When no complex time evolution was obtained (for ripples and for ploughing), the results were summarized and shown in the format $\mu_i \pm \sigma_i$, where μ_i is the mean value over the time of the results for the characteristic i , and σ_i is the standard deviation of those same time series results.

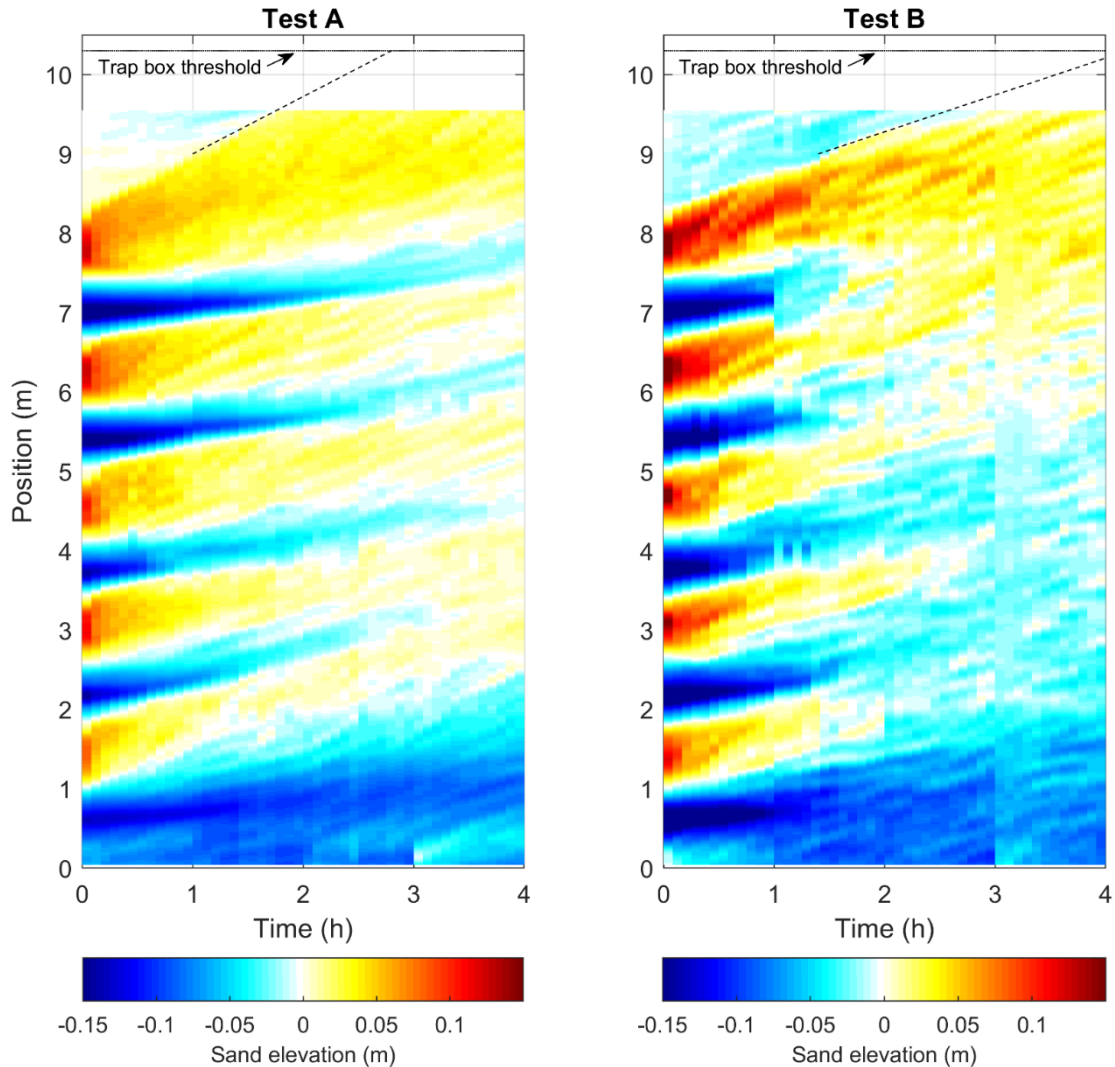
CHAPTER 4

Figure 4.18 SCP data time series for Test A and Test B. From 9.5 to 10.3 m, there are no data as the frame of the glass window (see Figure 4.15) prevents the measurement of the sand surface. The dashed line indicates the estimated location of the onshore boundary of the plough up to the trap box threshold, when the sand begins to fall directly into the trap box.

A. Geometric characterization

The height of the ploughed bedforms ($\eta_{bedform}$) was obtained as a function of its variance employing the Crawford & Hay (2001) equation:

$$\eta_{bedform} = \sqrt{8\sigma^2(z_{bedform})} \quad (4.9)$$

where $z_{bedform}$ is the bed elevation of the PC data and σ is its standard deviation.

Figure 4.19 shows the time evolution of the ploughed height obtained for each laboratory test. The ploughing was initially implemented at a height of approximately 0.3 m (it varied due to the effect of inundation as the water level was raised up to each test level). The ploughing height decreased rapidly at the beginning and then slowed as the test proceeded. After the first hour of waves, the height decreased to 0.12 m, and after 2 h, the height was only 0.06 m. This low height made it difficult to identify the wavelength, as will be shown later.

Similarly, the RC of the signal was analysed following the same methodology. The height of ripples varied from 0.011 ± 0.003 m for Test A to 0.016 ± 0.004 m for Test B.

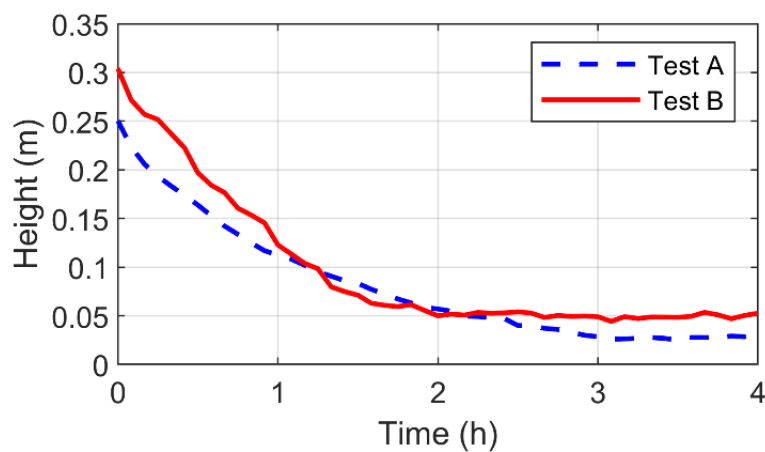


Figure 4.19 Evolution of the ploughing (PC) height for each laboratory test.

The wavelength for each profile data of the PC was calculated as twice the spatial lag corresponding to the strongest negative autocorrelation peak (Miles et al., 2014). The time evolution of the wavelength for each laboratory test performed is shown in Figure 4.20. The mean ploughing wavelength for both laboratory tests was 1.62 ± 0.05 m. The results of Test B showed that the ploughing disappeared after 2 hours, and the algorithm was not able to find further autocorrelations (see the low height identified before). In addition, Test A indicated that ploughing remained with the same wavelength up to the fourth hour, although its height was low, as shown before.

The ripple wavelength was also analysed from RC data with the same methodology. Both test results for wavelength were 0.28 ± 0.01 m.

CHAPTER 4

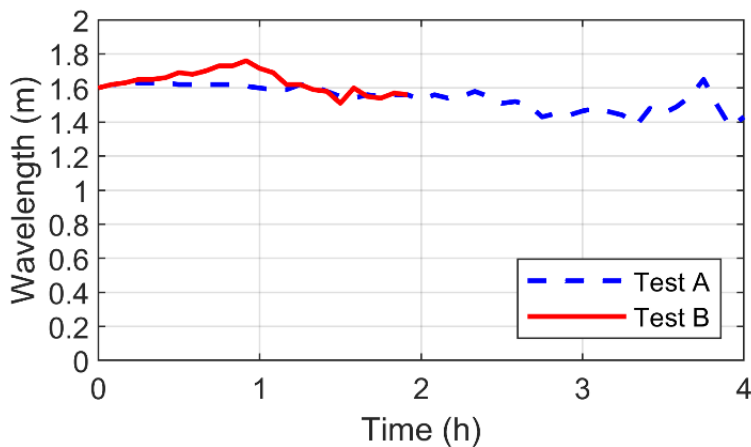


Figure 4.20 Wavelength time evolution of the ploughing (PC) for each laboratory test.

The ploughing formed successive ridges and furrows that constituted sand waves. These sand waves were not symmetric. The slope of the stoss face (seaward) and the slip face (shoreward) of each ridge of the ploughed shape was computed for all the profiles on the PC. These data were cut between 2 and 8.5 m along the channel, and therefore, only furrows number 2 to 5 were present in the PC. Furrow 1 was rejected due to boundary effects. For each furrow, the two mentioned slopes were calculated. On the seaward side of furrow i , the slip face slope of ridge $i-1$ was obtained as the maximum slope (descending while advancing over the profile from offshore to the shore). Similarly, on the shoreward side of furrow i , the stoss face slope of ridge i was obtained as the maximum slope (ascending while advancing over the profile from offshore to the shore). Both angles were measured from a horizontal plane as a reference, as shown in Figure 4.21.

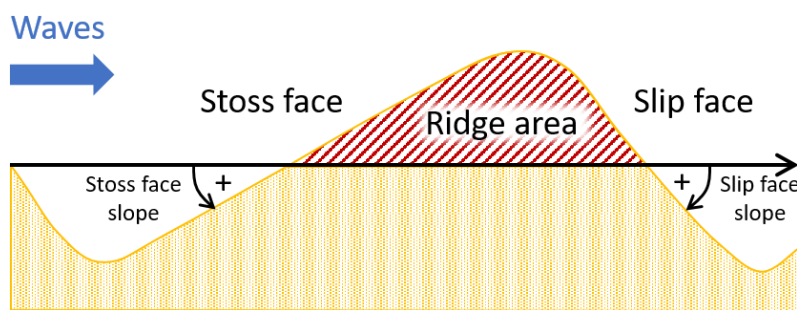


Figure 4.21 Sketch of a cross-shore section of a ploughed bedform. Sign criteria adopted for the characterization of the stoss and slip face slopes and the ridge area.

For each laboratory test and time moment, the computed individual results of the slope of the four furrows were averaged to obtain an averaged time series for each slope and each test. The upper panel in Figure 4.22 shows the time evolution of the slip face slope.

At the beginning of each test, the slip face slope was approximately 34 degrees, which approximates the angle of repose of submerged sand. As the waves eroded the ridges, part of the sediment filled the next furrow. During the first 30 minutes, the slip face slope remained near the maximum limit, and then it progressively decreased to a minimum of approximately 5 degrees in the third hour and following. The lower panel of Figure 4.22 shows the stoss face slope that reveals a similar behaviour. The initial dig slope was 23 degrees, although the punctual maximum slope reached 31 degrees due to punctual sand accumulations under the aerial profile that were later smoothed out by water inundation. The stoss face slope decreased progressively as furrow depth decreased and the seaward side of the next ridge eroded. At the third hour, the slope was reduced to 5 degrees and remained approximately constant until the end of each test. Both slip and stoss face slopes decreased to 5 degrees near the third hour, when ploughing was considered to disappear and only longer wavelength bedforms remained.

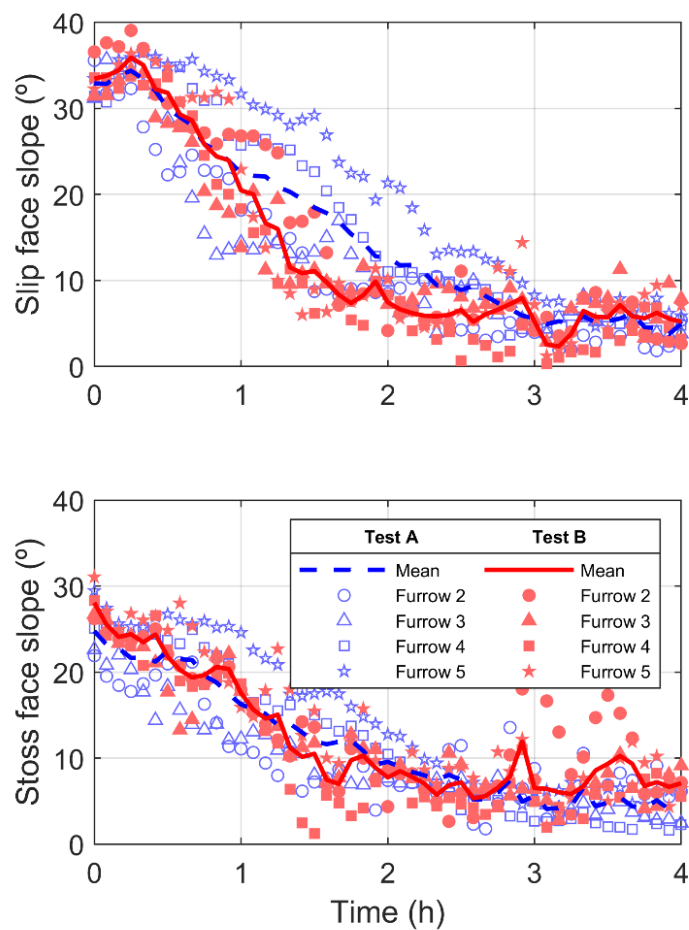


Figure 4.22 Evolution of the slope of the slip and stoss face of the ploughing for each laboratory test.

CHAPTER 4**B. Bedform migration**

The onshore migration rates were calculated from the spatial lag of the maximum cross-correlation peak of consecutive profiles (Masselink et al., 2007). This analysis was performed for both PC and RC time series to compute ploughing and rippling velocities separately. Both bedforms migrated shoreward. PC was analysed for six different spatial lags (from 5 to 30 mins), and all of them showed similar results. Figure 4.23 shows the results for each spatial lag and laboratory test, as well as the average migration velocity. Test A ploughing bedforms migrated at a rate of 0.18 m/h during the first hour and then decelerated to 0.15 m/h during the second hour. After that moment, as the ploughing height decreased, the migration velocity was more difficult to identify, and thus the algorithm showed fluctuations between 0.05 and 0.25 m/h. Test B showed more dispersion, with migration velocities between 0.20 and 0.30 m/h during the first hour and between 0.05 and 0.15 m/h during the second hour. After the second hour, the algorithm was not able to detect autocorrelations. These migration velocities (faster for Test B) indicated that ploughing displacement can accelerate as the water level rises. The ripples migrated onshore with velocities of 0.36 ± 0.15 m/h for Test A and 0.33 ± 0.11 m/h for Test B. Ripples migrated onshore on top of the ploughed sand waves and faster than ploughed bedforms. These results were consistent with visually estimated migration speeds on the whole profile evolution figure (Figure 4.18).

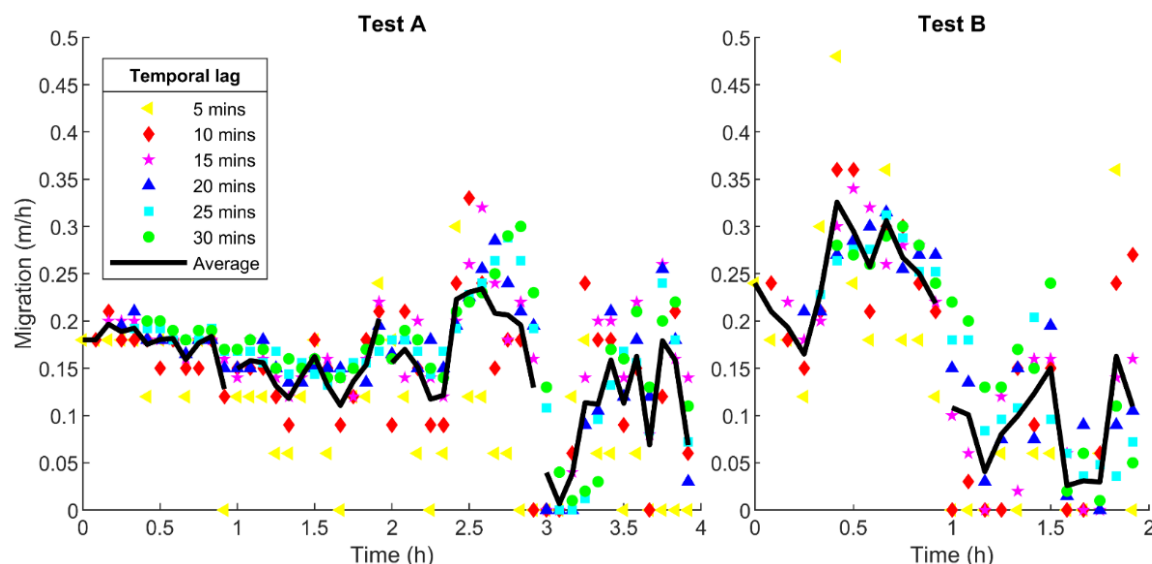


Figure 4.23 Evolution of the onshore migration velocity of the ploughing for each laboratory test.

C. Ridge evolution

The area of each ridge was calculated from the SCP time series. The ridge area was computed as the positive area between the lowest points of two consecutive furrows (see Figure 4.21) for ridges 1 to 4 and each 5 min profile data. Ridge 5 was discarded because it was affected by the boundary conditions. Its behaviour was different from the other ridges, as its onshore side was a flat bottom instead of another furrow (more information on this in the discussion).

The initial theoretical ploughed ridge area was 0.075 m^2 . Slight variations appeared in the initial measured area, including air bubbles, different compaction due to water level, and cross-channel irregularities affecting measurements. Figure 4.24 shows the evolution of the area of ridges 1 to 4 for the two laboratory tests. These ridges behaved similarly, and their evolution can be described by an exponentially decreasing curve. The equation used for fitting is:

$$\text{Ridge area} = 0.075 + A(1 - e^{-Bt}) \quad (4.10)$$

where t is the time in hours, and A and B are the fitting parameters that are shown in Figure 4.24 for both tests.

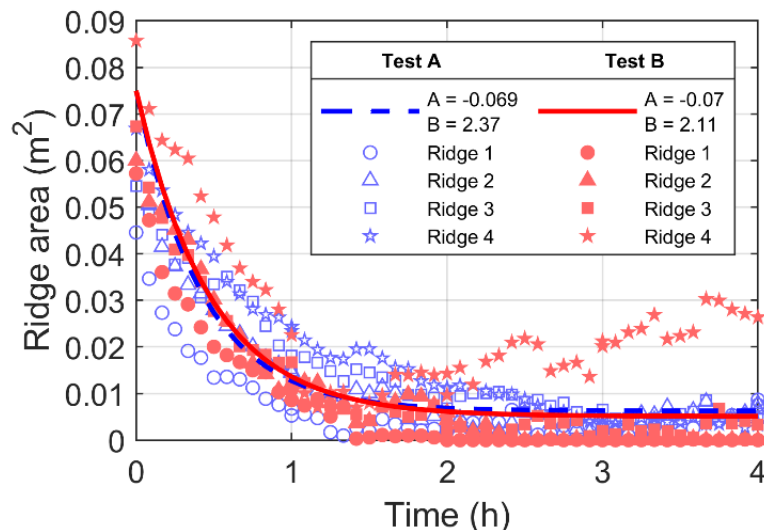


Figure 4.24 Ridge area evolution for both tests and ridges 1 to 4. The lines show the fitting result of an exponential curve of equation (4.10) to the data of each test.

CHAPTER 4

In just 2 h, the area decreased to 0.006 m², corresponding to the residual volume of the ploughing and rippling in the zone. For Test B, the ridge 4 area started increasing again after 2 h of wave simulation. This was due to the formation of a longer wavelength bar with its crest in this zone (this bar also formed in this zone for the natural control side of the experiments).

4.4.3. Hydromorphodynamic effects of ploughing

Ploughing modifies the morphology of the beach profile, which produces a direct effect on bed roughness, wave propagation, and sediment transport. These effects are quantified in this section and compared with those of the simulated natural control geometry.

A. Bottom roughness

The roughness of the sandy bottom was computed from the image data of the ploughed side every 5 min. These results were validated with roughness values obtained from laser scanner bathymetries of the natural and ploughed sides (see Figure 4.25). The roughness k_σ was computed with the standard deviation of the points of the surface (σ_z) from the theoretical initial flat bottom of slope 1/100 as $k_\sigma = 4 \sigma_z$ measured in m (Poate et al., 2018).

The results showed that roughness is progressively smoothed by wave action. At the beginning, k_σ reached 0.4 m. In just 1 h, more than 50% of the artificially generated roughness of the ploughing was lost. The smoothing speed decreased as time passed, so it remained almost constant ($k_\sigma \approx 0.11$ m for Test A and $k_\sigma \approx 0.13$ m for Test B) from the second hour in advance. The results from laser scanner measurements and images showed the same trend. On the natural control side, the roughness increased as ripples appeared, but always lower than the roughness on the ploughed side. In both tests, the natural control side roughness started with $k_\sigma \approx 0.02$ m and increased up to $k_\sigma \approx 0.06$ m after 4 h of wave action. Therefore, even at the end of the 4 h of waves, the remaining ploughing generated extra bottom roughness that could affect wave propagation.

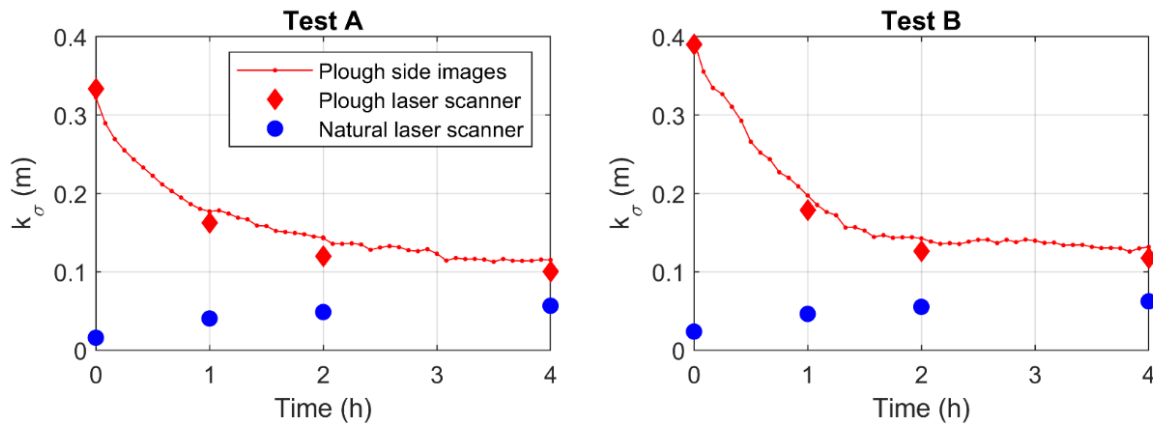


Figure 4.25 Sandy bottom roughness computed from images and laser scanner 3D bathymetry for each laboratory test.

B. Hydrodynamics

The significant wave height (H_s) was obtained from free surface elevation records measured by three wave gauges. Two of them were located at the onshore end of the study area (WG10 and WG16; see Figure 4.3), one on each side of the channel. The third sensor was located next to the generation paddle (WG1). H_s was obtained by spectral analysis and integration to obtain the zero-order momentum (m_0) and then $H_s = 4 \cdot \sqrt{m_0}$. Significant wave height was computed for an hourly time series. Figure 4.26 shows the H_s evolution for each test, allowing for a comparison of the ploughed and control sides. The significant wave height was smaller on the ploughed side for all tests and time moments. The plough reduction of H_s was larger at the beginning of the tests and slowly decreased as each experiment proceeded. This indicated that the extra dissipation produced on the ploughed side was directly produced by the artificially created shape of the bottom and decreased as the bedforms smoothed out. The H_s at the control side was approximately constant during all the test durations, reflecting that the bottom geometry did not change significantly, although ripples appeared.

Test A corresponded to simulations with a water level of 0.85 m at the wave generation paddle, while Test B showed the results for a water level of 1.2 m. The lower water level of Test A produced more wave breaking, and thus H_s at the onshore end of the sandy area was reduced below 0.1 m, while in Test B, only the larger waves broke, and the final H_s remained near 0.25 m (just 0.05 m less than the 0.3 m of generated waves).

CHAPTER 4

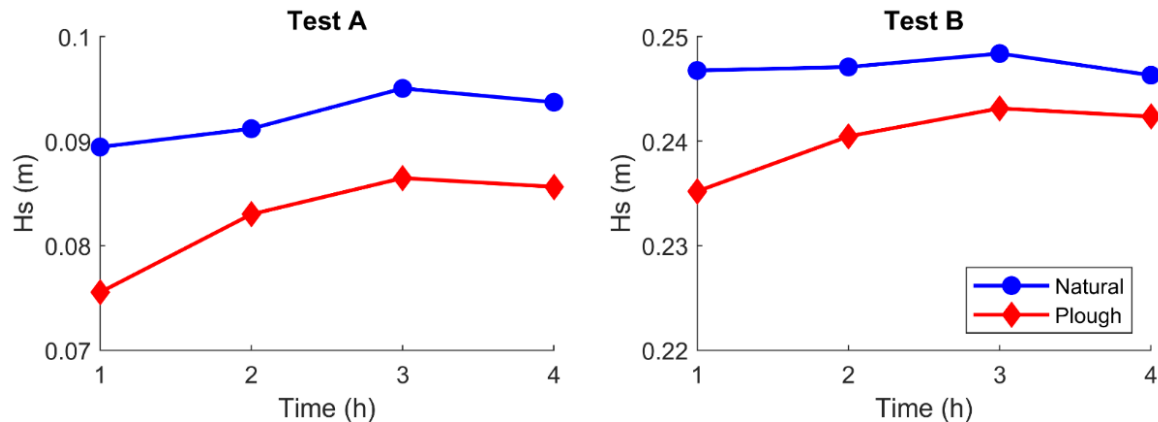


Figure 4.26 Significant wave height at the onshore end of the study area (see sensor location in Figure 4.3). Circle markers refer to WG16 on the natural control side, and diamond markers refer to WG10 on the ploughed side.

The water surface elevation power spectrum, $S(f)$, was computed for the three sensors at each hour of each test. The comparison between the spectra of the three sensors is shown in Figure 4.27. The peak period of the waves at generation was 7 s (0.143 Hz), which can be identified as the strongest energy peak at generation (WG1) in the plots. Waves around this frequency broke in both tests. For Test A, the energy reduction extended to all frequencies larger than 0.1 Hz (period less than 10 s), while for Test B, the energy reduction was lower, and the maximum dissipation was produced for wave frequencies of approximately 0.2 Hz (period of 5 s). The percentage of energy dissipation (or gain due to energy redistribution) for each frequency of the spectrum was computed with the following formula:

$$\text{Wave energy dissipation on natural control side} = \frac{E_{WG16}}{E_{WG1}} \cdot 100 \quad (4.11)$$

$$\text{Wave energy dissipation on ploughed side} = \frac{E_{WG10}}{E_{WG1}} \cdot 100 \quad (4.12)$$

where E_{WG1} is the wave energy measured at WG1, next to the generation paddle; E_{WG16} is the wave energy measured at WG16, at the onshore end of the sandy area on the natural control side; and E_{WG10} is the wave energy measured at WG10, at the onshore end of the sandy area on the ploughed side.

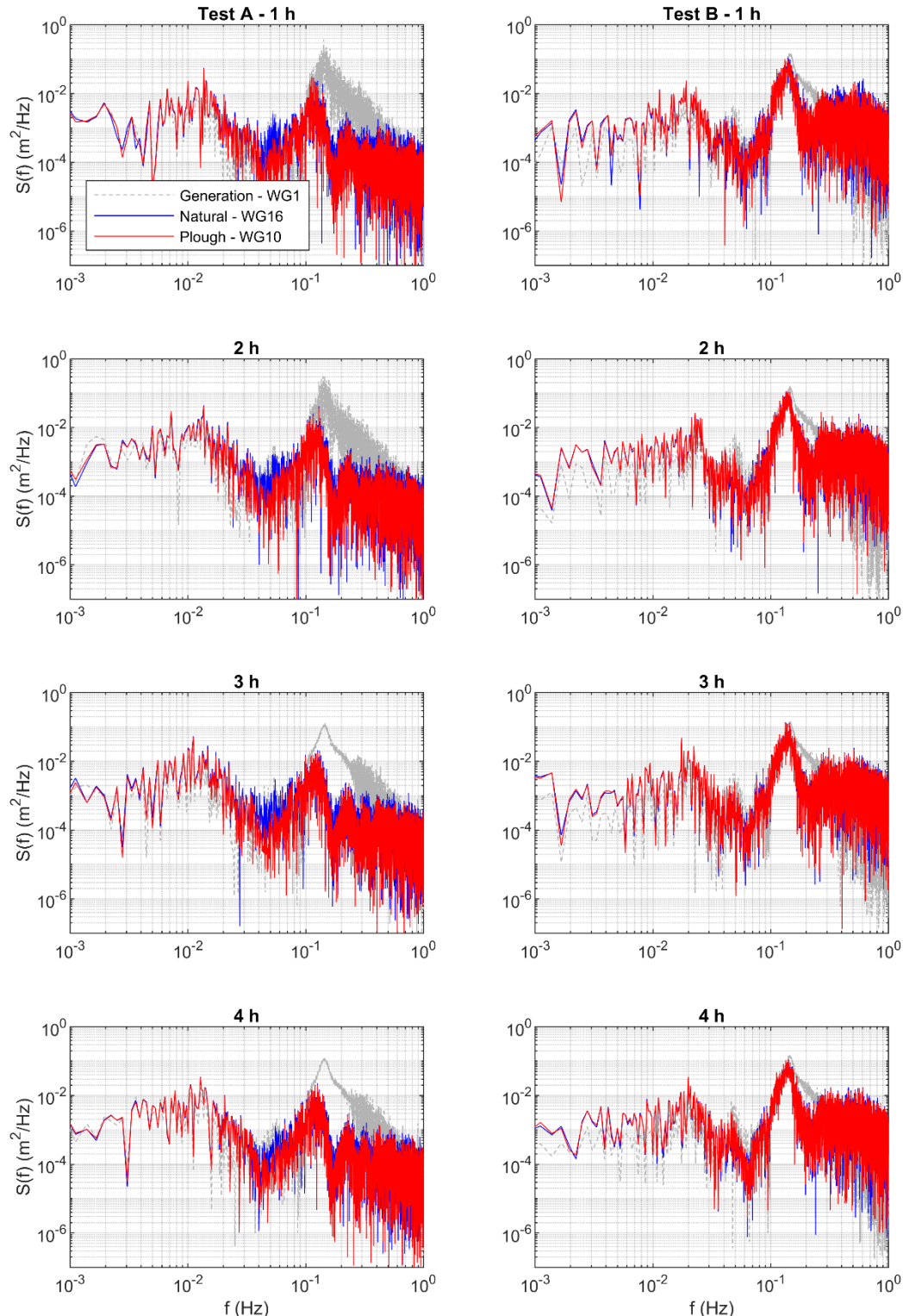


Figure 4.27 Wave energy spectrum at generation (WG1) and the onshore end of the sandy area on the natural control side (WG16) and ploughed side (WG10). The plots on the left show the spectrum for Test A and the plots on the right for Test B. Each plot corresponds to one hour of simulated waves, from the 1st hour in the upper panels to the 4th hour in the lower panels.

CHAPTER 4

Figure 4.28 shows the time evolution of the wave energy dissipation produced for each test with a colour surface on each subchannel. Five regions are identifiable in these spectra and have been marked as frequency windows A to E. In windows B and D (frequencies between 0.03 and 0.07 Hz for window B, and 0.1 and 0.4 Hz for window D), wave energy dissipation was dominant for both tests, while energy increased in windows A and C due to nonlinear energy transference to low and high frequencies. Window E shows energy dissipation in Test A and energy increase in Test B. Most of the energy dissipation was produced in window D, in which the peak period of generated waves was contained. Test A reflected dissipation around 100% of the initial wave energy for all the frequencies of this window D, while the maximum dissipation was only reached for frequencies around 0.02 Hz for Test B. This behaviour was consistent during the 4 h of wave simulations.

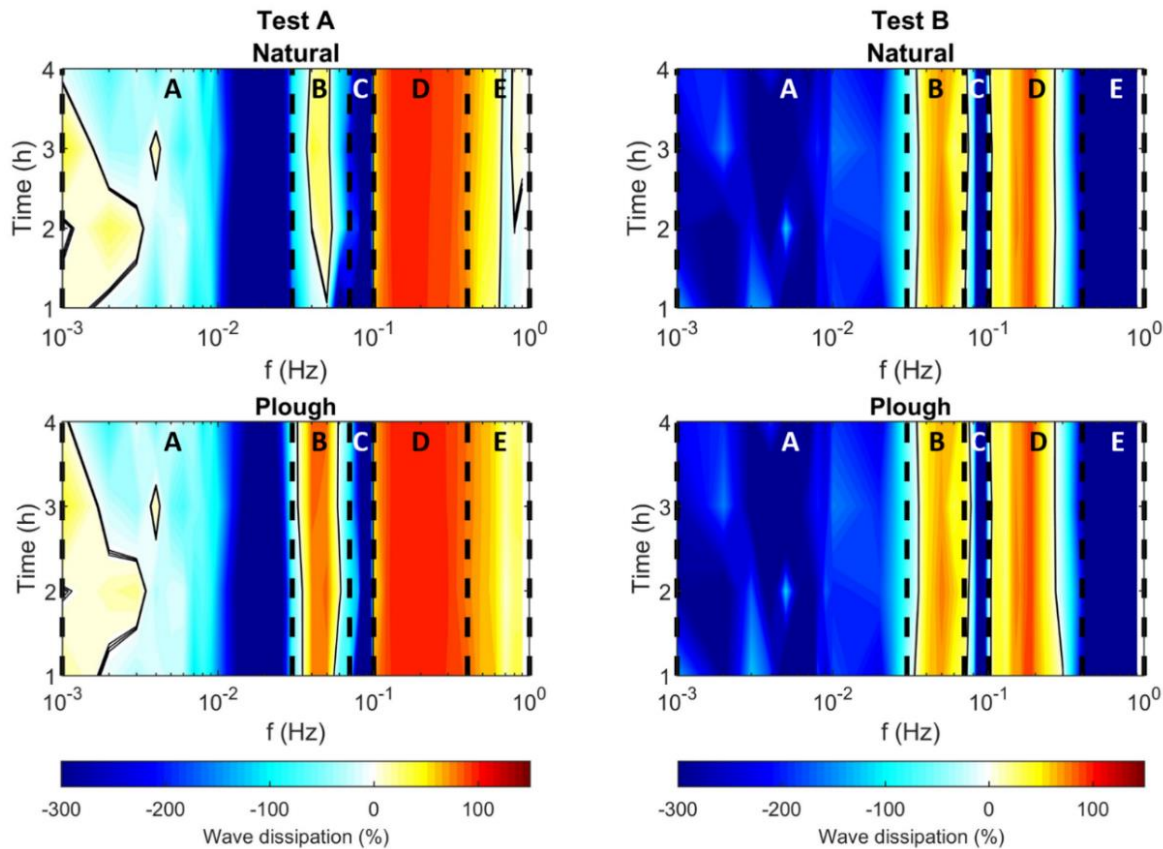


Figure 4.28 Wave energy dissipation for each wave frequency and hour of the experiment.
 Positive values (red and yellow colour) correspond to less energy than the one at generation.
 Negative values (blue colour) correspond to more energy than the one at generation. Panels on the left show the results for Test A and on the right for Test B. Upper panels correspond to the natural control side, and lower panels correspond to the ploughed side.

Figure 4.27 shows a comparison between natural and ploughed side spectra. It is notable in Test A that ploughing produced extra energy dissipation for frequencies around 0.04 Hz. Additionally, Figure 4.28 shows some differences in the amount of wave energy dissipation produced on the natural and ploughed sides. To account for these differences, the relative energy dissipation was computed by equation (4.13):

$$\text{Extra ploughing energy dissipation} = \frac{E_{WG16} - E_{WG10}}{E_{WG16}} \cdot 100 \quad (4.13)$$

where E_{WG16} and E_{WG10} represent the energy measured by wave sensors WG16 (natural control side) and WG10 (ploughed side), respectively.

Figure 4.29 shows the extra energy dissipation on the ploughed side for each frequency of the spectrum. The 4 h of each test were analysed separately, showing similar results for all of them. The mean value and standard deviation of those values are shown in Figure 4.29.

In Test A, the wave energy dissipation on the ploughed side was greater than the wave dissipation produced on the natural control side for all frequencies above 0.01 Hz, except for frequencies around 0.1 Hz, where the dissipation was similar for both sides. The extra dissipation produced by the ploughing was 80% for frequencies between 0.04 and 0.05 Hz. A second peak up to 70% of ploughed extra dissipation was produced for wave frequencies around 0.17 Hz (next to the frequency peak of the waves generated, 0.14 Hz), and then the extra dissipation decreased to 30% for frequencies above 0.2 Hz.

In Test B, the effect of the ploughing was less important. The maximum extra dissipation produced by the ploughing was 20% for frequencies between 0.06 and 0.08 Hz. In Test B, for frequencies around 0.05 Hz, the ploughing dissipated 12% less energy than the natural control side, opposite to Test A, which has its strongest peak of ploughed extra dissipation at this frequency. In Test B, the extra dissipation was below 5% for frequencies between 0.1 and 0.16 Hz, and then the extra dissipation increased to 12% for 0.18 Hz. For frequencies above 0.2 Hz, the extra dissipation of the ploughed side showed values between 5 and 10%.

In both tests, the ploughed side presented extra wave energy dissipation in window D (frequencies between 0.1 and 0.4 Hz), where most of the generated wave energy was concentrated (see Figure 4.27).

CHAPTER 4

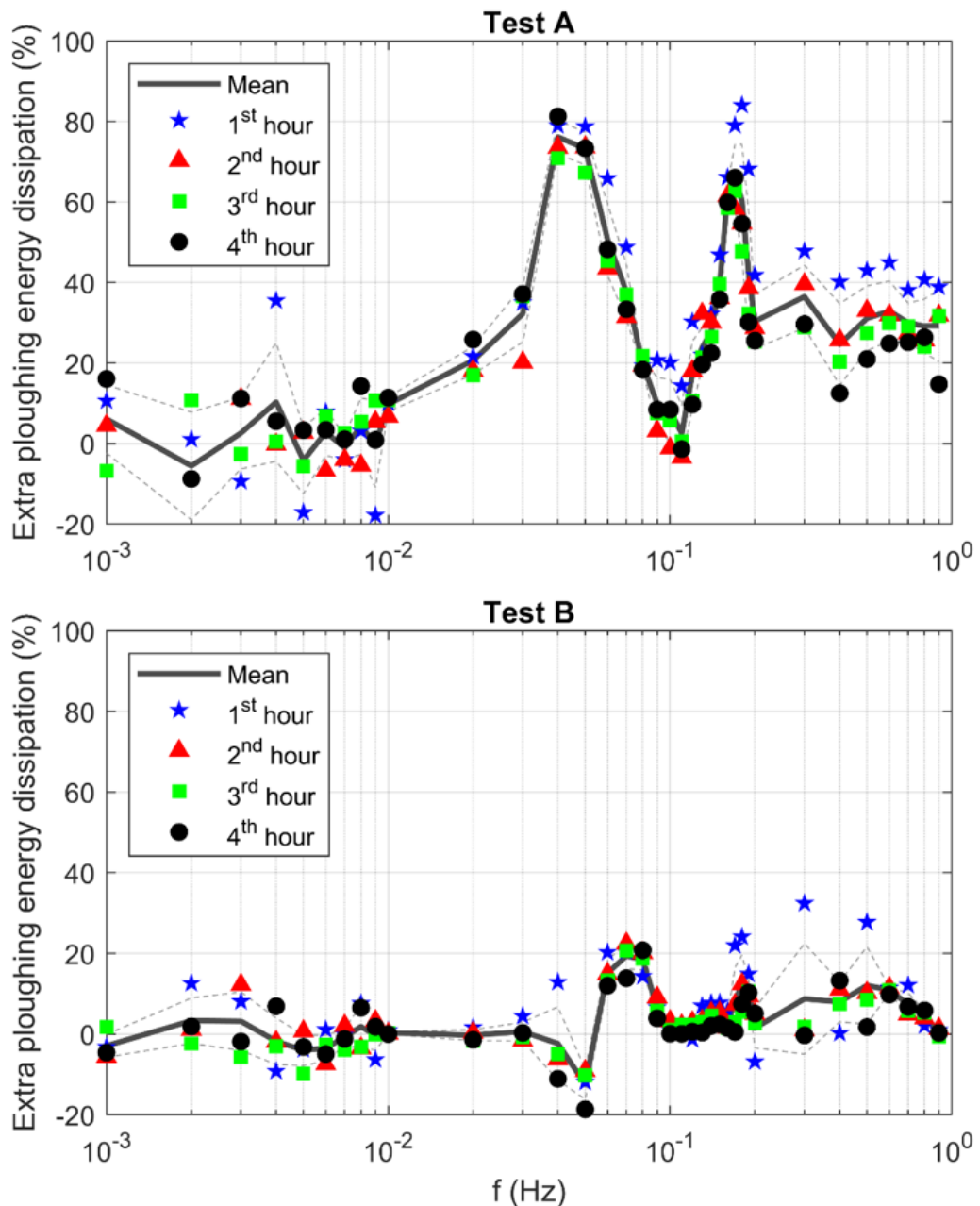


Figure 4.29 Extra energy dissipation produced on the ploughed side compared to the natural side for each test and frequency of the spectrum (see equation (4.13)). Positive values indicate that the energy on the ploughed side (WG10) is lower than the energy on the natural side (WG16). The black thick continuous line indicates the average value for the four hours analysed. Discontinuous grey lines indicate one standard deviation from the mean value.

The velocity of the water on the onshore end of the sandy area was measured by four ADV sensors, two at each subchannel (see location in Figure 4.3). The data recorded from ADV sensors were low-pass filtered with a Butterworth (1930) filter using an order of 6 and a cut frequency of $4 \cdot dt$, where dt is the sampling rate of the ADV sensor (1/50 s). The cross-

shore velocity component was extracted from filtered signals and processed to obtain the mean current of each hour of simulation. Figure 4.30 shows the mean current velocity obtained for each test and sensor.

The water level for Test A was 0.85 m; therefore, only sensors ADV1 and 3 were fully submerged and in a relatively high position of the water column. For this reason, the obtained velocities were onshore directed (Haines and Sallenger, 1994), with a magnitude of approximately 0.04 m/s on the natural control side and 0.07 m/s on the ploughed side. For Test A, the currents on the ploughed side were consistently stronger and onshore directed. The difference between natural and ploughed currents decreased as time passed.

The water level for Test B was 1.2 m, allowing for measurement with two ADV sensors at different heights of the water column. Both sensors were located at a relatively low position of the water column, and thus the velocities measured were offshore directed, corresponding to undertow currents. During the first hour of wave simulation, the magnitude of the undertow was 0.07 m/s on the natural control side and 0.03 m/s on the ploughed side. This led to less sediment potentially moving seaward on the ploughed side. In the second and following hours of simulation, the undertow currents at both sides were similar at approximately 0.05 m/s.

These results indicated that onshore sediment transport on the ploughed side can be enhanced due to currents that are stronger if directed onshore or weaker if directed offshore.

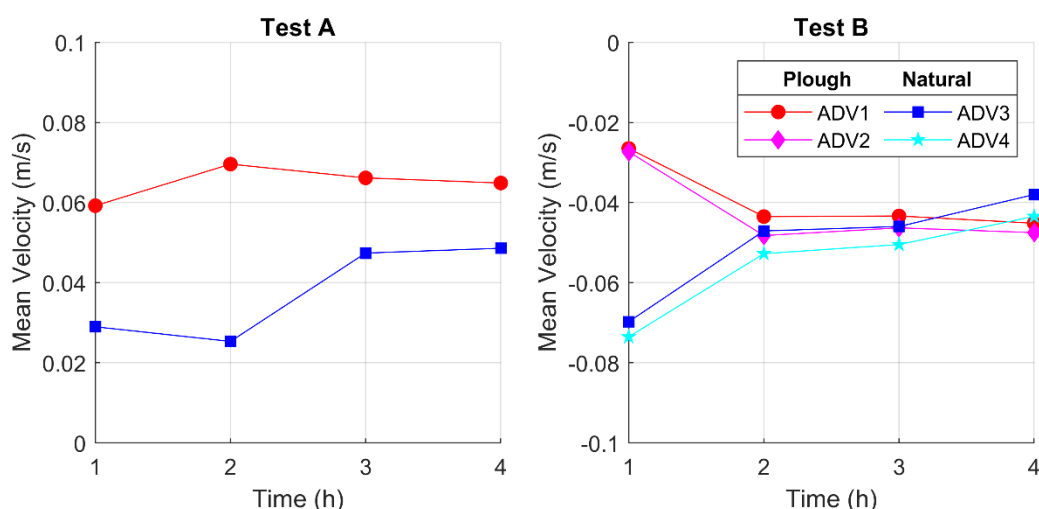


Figure 4.30 Cross-shore currents measured by ADV sensors at the onshore end of the sandy area. Positive values indicate onshore directed currents. See the location of each sensor in Figure 4.3.

CHAPTER 4

C. Sediment transport

The suspended sediment concentration (SSC) was measured by two OBS sensors located at the onshore end of the sandy area (see Figure 4.3), one at each subchannel. The sensors were placed 0.05 m above the sandy bottom. Figure 4.31 shows a statistical analysis of the hourly time series measured for each test. Breaking waves passing over the sensor location produced high sediment concentration values that have not been represented.

Test A showed larger SSC values for the first hour (approximately 0.1 g/l), and then SSC progressively decreased as time passed down to 0.05 g/l at the 4th hour. Both sides presented similar SSC values.

Test B showed an SSC of approximately 0.1 g/l on the natural control side for 4 h of wave simulation. On the ploughed side, the SSC was 0.17 g/l during the first hour and then progressively decreased to 0.09 g/l in the 3rd and 4th hours.

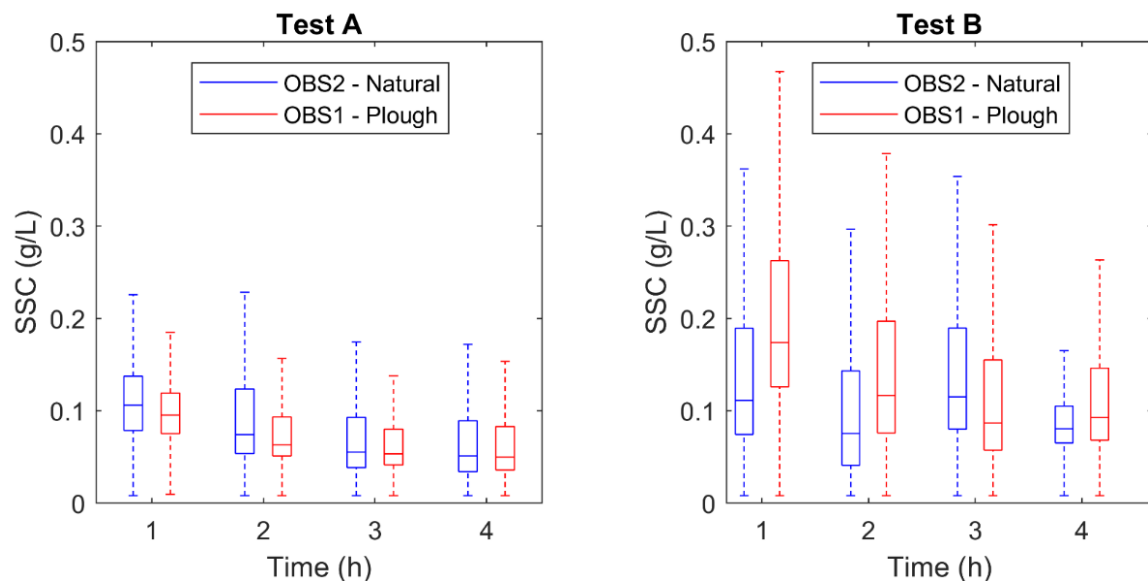


Figure 4.31 Statistical analysis (box plots) of the suspended sediment concentration measured by OBS sensors (see location in Figure 4.3).

The bedform sediment transport (Q_{bedform}) produced by the migration of the ploughing and rippling can be calculated using the Huntley et al. (1991) equation:

$$Q_{bedform} = 0.5(1 - p_h)\rho_s \cdot \eta_{bedform} \cdot M_{r,bedform} \quad (4.14)$$

where p_h is the porosity (0.35 according to Traykovski et al., 1999)), ρ_s is the sediment density (2580 kg/m^3), $\eta_{bedform}$ is the ploughing or rippling height, and $M_{r,bedform}$ is the migration rate of the ploughing or rippling. Both bedforms migrate onshore so that bedform sediment transport is onshore directed.

Figure 4.32 shows the sediment transport produced by the migration of the ploughed bedforms calculated with equation (4.14). At the beginning of the experiments, the height was high, and the migration velocity of the ploughing was fast; consequently, the sediment transport was $Q_{plough} = 38 \text{ kg m}^{-1} \text{ h}^{-1}$ for Test A and $Q_{plough} = 61 \text{ kg m}^{-1} \text{ h}^{-1}$ for Test B. The sediment transport rate progressively reduced as the ploughing height decreased. After the first hour, Q_{plough} was below $14 \text{ kg m}^{-1} \text{ h}^{-1}$ for both tests and below $9 \text{ kg m}^{-1} \text{ h}^{-1}$ after two hours of the experiment.

Equation (4.14) was also applied for ripples that appeared on top of the ploughing. The sediment transport produced due to ripple migration was $Q_{ripples} = 3.32 \text{ kg m}^{-1} \text{ h}^{-1}$ for Test A and $Q_{ripples} = 4.43 \text{ kg m}^{-1} \text{ h}^{-1}$ for Test B. Ripples migrated faster than ploughing and on top of it, so these sediment transport rates ($Q_{ripples}$) aided the migration of ploughing (note that Q_{plough} is larger than $Q_{ripples}$ up to the third hour). At the fourth hour, $Q_{plough} \approx Q_{ripples}$, supporting the hypothesis of Venditti et al. (2005) that the sediment transport rate can be invariant to the scale of the bedforms if the size and migration rates are proportional (smaller bedforms migrate faster).

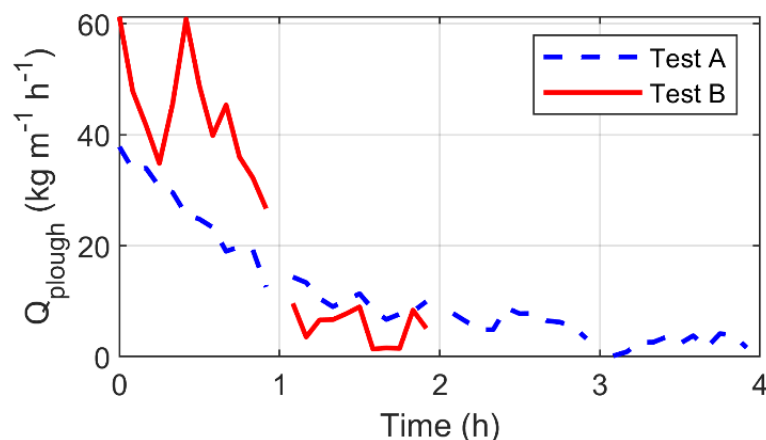


Figure 4.32 Sediment transport produced by the migration of the plough.

CHAPTER 4

D. Sediment accretion

Sediment accretion was measured periodically as the sand was deposited on a trap box located at the onshore end of the study area. Two trap boxes were used: one on the natural control side and the other on the ploughed side. The captured sand was extracted and weighed (following the methodology described in Section 4.2.2) at each pause of the tests. For Test A, measurements were taken after each of the four hours of the experiment. For Test B, the measurements were taken after 1 h, 2 h, and 4 h. The total amount of sand captured from the beginning of each test was calculated, and the trends were adjusted to obtain accretion rates for each case (see Figure 4.33).

Test A showed accretion rates of 12.68 kg/h for the natural control side and 17.79 kg/h for the first 3 h of waves on the ploughed side. After the third hour, the accretion rate increased because the last ridge started to fall directly into the trap box (see Figure 4.18 and Section 4.4.4, discussion).

Test B showed accretion rates of 20.76 kg/h for the natural control side and 22.64 kg/h for the ploughed side during the first hour. In Test B, at the 4th hour, the last ridge was still over the flat end of the study area but did not fall into the trap box (see Figure 4.18). The accretion rate of both sides for Test B decreased with time following an exponential curve. The lower sand weight could be a direct response to the reduced roughness in the second half of the experiment (see Figure 4.25). Nevertheless, the exponential curves fitted to the data indicated that the natural control side could potentially accrete 71 kg of sediment, while the ploughed side could reach 132 kg; at the fourth hour, the natural control side had accreted 53.19 kg of sand, while the ploughed side had accreted 69.90 kg.

Accretion rates were higher on the ploughed side than on the natural control side for both analysed tests. On the ploughed side of Test A, the accretion rate was 40.30% larger than that on the natural control side. For Test B, the accretion rate in the first hour was just 9.06% larger on the ploughed side, but it could potentially produce 86.88% of the extra weight of accreted sand. In fact, at the fourth hour of the simulation, the weight of sand accreted on the ploughed side was 30.85% larger than the sand accreted on the natural control side. This proves the effectiveness of the ploughing technique to enhance natural beach accretion.

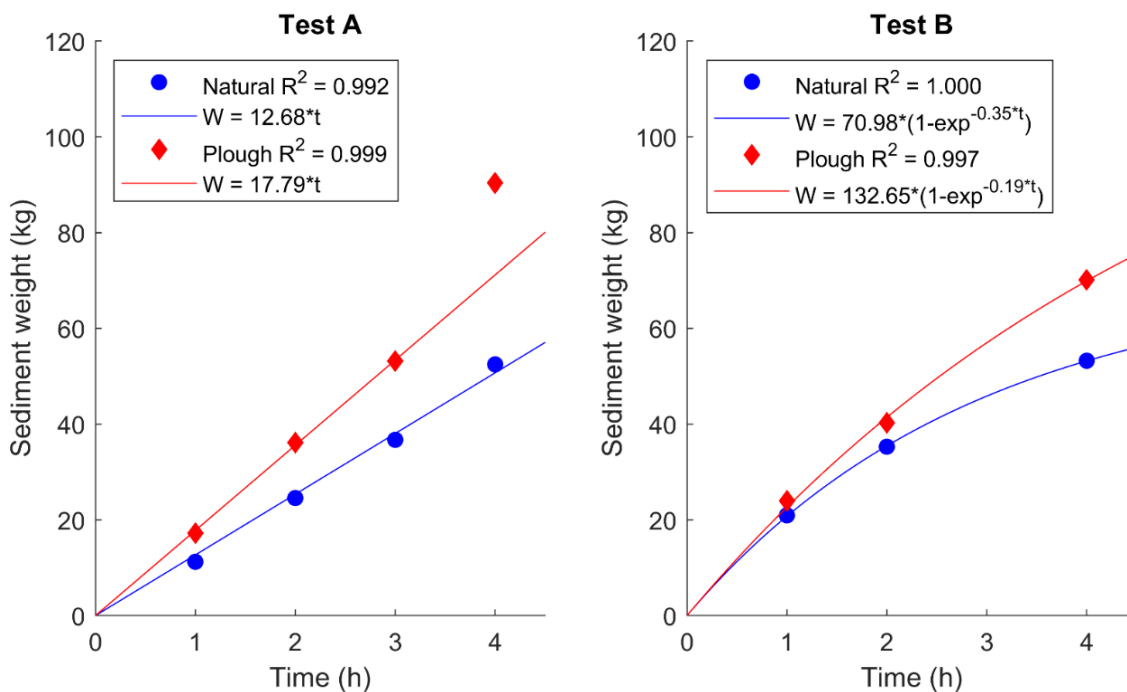


Figure 4.33 Cumulative weight of the sediment accreted since the beginning of each test.

4.4.4. Discussion

The morphodynamic behaviour of artificially created ploughed bedforms was analysed through laboratory experiments. Ploughed bedforms had a wavelength of 1.62 m, an initial height of 0.3 m, and migrated onshore at a rate of approximately 0.2 m/h. The initial shape attenuated as wave action acts over the crests of the ridges, reducing the ploughed height to 0.06 m in the second hour. This reduced height corresponded to the theoretical equilibrium for the ploughed wavelength according to numerous authors (Figure 2.2; Ashley, 1990; Baas, 2003; Flemming, 1988; Raudkivi, 1997), and it was maintained until the end of the experiments at the fourth hour.

Ripples appeared at the top of the ridges of the ploughed bedforms. Their wavelength was 0.28 m (microforms according to Jackson, 1975), with a height of 0.011 m and onshore migration velocity of 0.36 m/h for Test A. In addition, for Test B (higher water level), the height was larger (0.016 m) and the migration velocity was slower (0.33 m), supporting the idea that the larger the bedform is, the slower the migration (Venditti et al., 2005). Additionally, ploughed bedforms were also larger than ripples and migrated slower. This faster migration of the ripples on top of the ploughing allowed their contribution to the migration of the host bedform. Reesink and Bridge (2007) identified this phenomenon,

CHAPTER 4

where smaller bedforms go up the stoss side of the host bedform and avalanche over the lee side, contributing with sediment to the migration of the host bedform.

The sediment transport produced by the onshore migration of the ploughing and rippling was computed using the Huntley et al. (1991) equation. Ripples had a constant sediment transport rate of approximately $4 \text{ kg m}^{-1} \text{ h}^{-1}$ during the whole duration of the experiments, while ploughing exhibited a sediment transport rate one order of magnitude larger at the beginning, decreasing until the fourth hour when the rates for rippling and ploughing were equal. At this fourth hour, the ploughing height decreased to the equilibrium corresponding to its wavelength, and the sediment transport rate seemed to become invariant with the scale of the bedform, as proposed by Venditti et al. (2005).

An analysis of the sediment dispersion of the fifth ridge over the flat bottom shoreward corroborates that all the sediment captured in the trap box comes from the sediment transport produced by other mechanisms but not bedform migration. As shown in Figure 4.18, the onshore end of the sediment of the fifth ridge progressively dispersed over the flat bottom but did not reach the trap box threshold until the third hour for Test A (but excluded from the analysis of Section 4.4.3.D) and after the fourth hour for Test B. Figure 4.34 shows the evolution of ridge 5 during the experiment. The ridge height decreased as the sand was deposited over the flat bottom of the shoreward end of the sandy area. The shoreward end of the ridge did not reach the trap box threshold during the experiment (for Test B and up to the fourth hour for Test A); therefore, the sand mobilized by bedform migration is not accounted for in the accretion analysis.

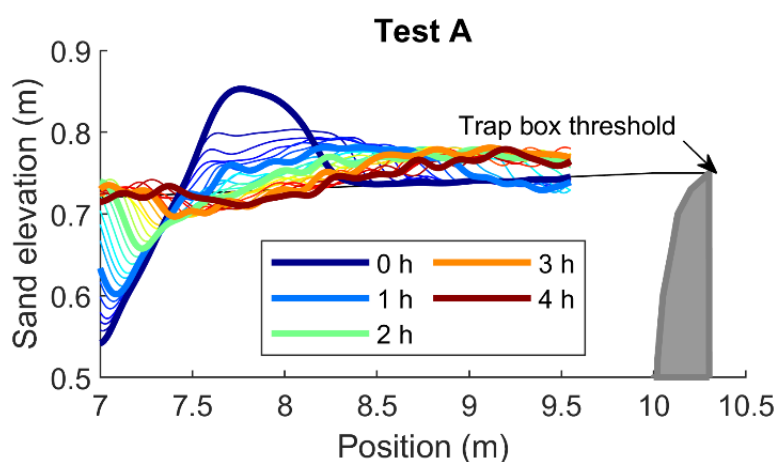


Figure 4.34 Ridge 5 time and spatial evolution for Test A. Bold lines represent each hour. Thin lines every 10 min.

The results demonstrate that ploughing enhances beach accretion by two mechanisms: increasing the hydraulic roughness of the bottom and the migration of the bedforms. Both mechanisms have been previously proposed by other authors and measured in this study for the 1st time. Guerrero et al. (2021) highlighted the importance of onshore ripple migration for beach recovery and supported her idea on the work developed by other authors (Allen, 1968; Middleton and Southard, 1984; Reesink and Bridge, 2007; Venditti et al., 2005). In addition, Gallagher et al. (1998b) focused on the effect of bedforms on the hydrodynamics through the modification of the hydraulic roughness. This effect has been investigated by many authors (Dalrymple et al., 1978; Garcez Faria et al., 1998), and some of them stated that bedforms contribute to bottom boundary layer hydrodynamics and sediment transport (Miles et al., 2014). Together, both natural mechanisms reinforced the idea of Hunt and F.G.S. (1904) that bedforms are an important factor for beach erosion and recovery. Furthermore, in this particular case of artificially generated ploughed bedforms, the movement of the sediment performed by a tractor at every low tide also contributed to sediment accretion, and for this reason, it is recommended to implement ridges on the shoreward side of the furrows.

All the measurements taken during the experiments allowed us to gain insight into the processes that produce accretion enhancement through hydraulic roughness modification. The bottom roughness of the ploughed side at the beginning of the experiments was approximately one order of magnitude larger than the roughness at the natural control side. This extra roughness produced extra wave dissipation, which was translated into measured smaller waves at the onshore end of the study area of the ploughed side. The extra wave dissipation generated larger sediment stirring measured by OBS sensors, and the smaller waves (measured by free surface sensors) generated hydrodynamic conditions more prone to accretion. The combined effect of sediment resuspension, waves, and currents (measured by ADV sensors) translated to 30% more sediment recovered on the trap box of the ploughed side, demonstrating that this technique enhances sediment accretion.

The hydromorphodynamic behaviour was slightly different depending on the water level used for each test. In Test A, the water level was low, and most of the waves broke over the sandy bottom. The suspended sediment concentration was similar for the ploughed and natural sides, but onshore currents were stronger on the ploughed side, mobilizing more sediment shoreward. In Test B, the water level was higher, and waves only broke over the ridges of the ploughed side. This produced a larger suspended sediment concentration on the ploughed side that was transported onshore. As the ridges eroded, the SSC was reduced and finally equalled the natural control side.

CHAPTER 4

The results showed a fast reduction in plough-induced roughness during the first 2 hours of wave simulation. The area of the ridges, which was mainly responsible for the extra wave dissipation due to its extra depth reduction, decreased rapidly and almost disappeared in the first three hours. This indicates that the promising effect of ploughing to enhance beach accretion was reduced to the first 2 or 3 hours of waves while the tide was going up. To increase the effect, the mechanical process of ploughing should be repeated for every tidal cycle. Nevertheless, the analysis performed for the behaviour of ridge 5 (Figure 4.34) suggests that a larger spacing between plough ridges and the next furrows could enlarge its durability and effect. The results showed that when the flat bottom follows a ridge, the sand deposits over it and progressively disperses, with a prograding onshore end of the ridge. The extra roughness and higher level of the bottom in this area last longer. In addition, a close inspection of the first furrow showed that when there is a lack of sediment from another ridge on the seaside, the furrow size enlarges seaward, and its depth also lasts longer. Further studies should be performed to analyse the optimal distance between ploughed ridges and furrows to maximize accretion enhancement. We note that ploughing should be done in a way that its shape lasts long enough to affect wave propagation during the rising as well as the falling tide, trying to avoid the ridged sand filling the next furrow. Additionally, the separation of the ploughed lines allows the enlargement of the beach area so that a single tractor can plough during low tide, making this technique even more cost-effective.

4.5. CONCLUSIONS

The effect of mechanically ploughing the intertidal area of a beach has been tested for the first time under controlled conditions. The analysis of **Set 1 of experiments** yielded the following conclusions:

- The data collected demonstrate that ploughing has a positive effect on increasing natural beach accretion rates for all water levels that were tested. Both accreted sediment volumes and sediment transport rates are larger on the ploughed side than on the natural control side.
- Wave dissipation was larger on the ploughed side, leading to a smaller wave height at the shoreward end of the ploughed area. The wave energy at this point was a maximum of 45% lower on the ploughed side for wave frequencies of 0.175 Hz (the peak frequency of the waves generated is 0.143 Hz) and 0.055 Hz. Bottom friction, due to a final bottom

roughness that was 3.57 times larger, is proposed as the main cause of this extra energy reduction.

- The shoreward half of the study area showed greater wave dissipation rates. Therefore, it is expected that a longer cross-shore extent of ploughing would lead to an enhancement of wave dissipation and accretion effects.
- The ploughed ridges and furrows were partially smoothed after 1 h of waves, but their shapes were still distinctive, and the roughness was larger than that of the natural geometry used as a reference. Further experiments (Set 2) are needed to determine how long this shape lasts.

The Set 2 of experiments allowed the analysis of ploughing morphodynamics until their smoothing by wave action, as well as the characteristics of other bedforms that naturally appeared during the tests. The analysis of **Set 2 of experiments** yielded the following conclusions:

- Spectral analysis of the bedforms, for the longer duration tests of Set 2, allowed their separation into two main components: ploughing and rippling.
 - o The morphometric characterization of ploughing was as follows:
 - 1) 1.62 ± 0.05 m of wavelength constant during the experiment duration.
 - 2) ~0.3 m of initial height, which decreased exponentially and reduced below 0.06 m at 2 h.
 - 3) Slip and stoss face slopes starting from the manually dug geometry (34 and 23 degrees, respectively) and decreasing to 5 degrees at 3 h (later it maintains around this value).
 - 4) Onshore migration speed of 0.18 m/h for Test A and 0.25 m/h for Test B during the first hour and decreasing as time passed.
 - 5) 0.075 m² of ridge initial area, decreasing exponentially to 0.006 m² after 2 h.
 - o The rippled morphometric characteristics were as follows:
 - 1) 0.28 ± 0.01 m of wavelength constant during the experiment duration.
 - 2) 0.011±0.003 m of height for Test A and 0.016±0.004 m for Test B.
 - 3) 0.36±0.15 m/h of onshore migration speed for Test A and 0.33±0.11 m/h for Test B.
 - 4) Ripples formed over the ploughed larger bedforms and migrated faster onshore.

CHAPTER 4

- This characterization indicated that the morphometric ploughing characteristics remained relevant for the first 2-3 h of the experiments, which indicated that ploughing should be repeated at each low tide to maintain its effect.
- Ploughing generated artificial bottom roughness ($k_o \approx 0.4$ m at the beginning of each test), which progressively smoothed due to wave action. The roughness reduction was produced exponentially, at approximately 50% less during the first hour. After the second hour, the roughness decreased to $k_o \approx 0.1$ m and later remained at this value, accounting for ripples over the bottom. On the natural control side, the roughness was always lower than that on the ploughed side, with a maximum of $k_o \approx 0.06$ m at the end of each test.
- The extra bottom roughness produced more wave dissipation at the ploughed side of the experiments. A comparison of the significant wave height measured at the onshore end of the sandy area showed that H_s was always smaller at the ploughed side (for all the tests and during the whole duration).
- ADV measurements showed that onshore sediment transport on the ploughed side can be enhanced due to currents that are stronger if directed onshore or weaker if directed offshore.
- This lower significant wave height and favourable currents produced more accretive conditions on the ploughed side, as demonstrated by higher accretion rates measured on the trap box of this side (up to 40% larger rates depending on the test). The artificially created bottom roughness was the main cause of this accretion enhancement.
- Additionally, the migration of the bedforms was onshore directed and produced sediment transport rates up to $61 \text{ kg m}^{-1} \text{ h}^{-1}$ for ploughing at the beginning, which progressively decreased below $10 \text{ kg m}^{-1} \text{ h}^{-1}$ after the second hour. The ripples also produced onshore sediment transport rates of approximately $4 \text{ kg m}^{-1} \text{ h}^{-1}$. These rates produced additional accretion that was not measured in the trap box and was caused by the migration of bedforms.
- All the results of this study indicate that ploughing plays a role in enhancing sediment accretion. Other bedforms (naturally or artificially formed) might be important as well, and their relevance for beach accretion should be analysed in future studies.
- Ploughing almost disappears after 2–3 h of wave action under constant water level tests.

As a general conclusion of this chapter, ploughing has been proven to enhance natural beach accretion with a nature-based philosophy.

These conclusions on beach ploughing are extended in chapter 5, where ploughing performance is compared with scraping effects on dry beach widening and sediment budget increase (on the dry beach and dune). The effectiveness of ploughing under the combined effect of waves and tides on a full tidal cycle, and its repetition during every low tide, was tested on the reduced-scale laboratory experiments presented in chapter 5.

CHAPTER 5

BEACH SCRAPING[‡]

5.1. INTRODUCTION

Beach scraping (Bruun, 1983) was born as a soft engineering technique to redistribute sand among the beach profile to increase coastal protection. It avoids the troublesome need of finding sand reservoirs that provide sand for beach nourishment in beaches with cross-shore seasonal changes but not longshore sediment losses. Beach scraping consists of removing by mechanical means, a thin layer (~0.3 m) of sand from the lower part of the intertidal profile, and placing the borrowed sand on the upper part of the beach profile (to build a dune or on the beachfront). It has a direct effect of reshaping the geometry of the beach profile, which automatically can have a wider dry beach (if the sand is placed on the beachfront). This technique is widely used along Australian coasts (Carley et al., 2010), where it is known as nature assisted beach enhancement (NABE). This name points out a second interesting effect of this technique: it accelerates natural accretion processes on beaches (Smutz et al., 1980), achieving greater coastal protection with a reduced environmental impact.

Depending on the location of borrow and filling areas, beach scraping presents multiple possibilities. The aim of this chapter is to determine the most appropriate NABE technique to enhance the natural recovery of the beach. To achieve this goal, we present a

[‡] This chapter is based on Pellón, E., Vidal, C., Gomes, P., Aniel-Quiroga, I., González, M. and Medina, R. Laboratory evaluation of the effectiveness of nature assisted beach enhancement techniques. Under review in Coastal Engineering.

CHAPTER 5

comparative analysis of the effect of beach scraping and ploughing (see chapter 4 for further details) based on reduced-scale laboratory experiments. Additionally, beach scraping with borrow area in the low part of the intertidal area and filling on the beachfront was tested on Fuentebravia beach during the summer of 2021. All the information collected during the field surveys is analysed here and compared to the physical modelling results.

The reduced-scale experiments were conducted to consider the simultaneous effect of waves and tides. To the authors' knowledge, this is the first time that beach scraping is assessed under these conditions in the laboratory, allowing the validation of Carley's et al. (2010) and Smutz's et al. (1980) statements that scraping enhances beach accretion. Although this chapter focuses on beach scraping, we also compare beach scraping effectiveness with natural and ploughing behaviour. Therefore, this chapter (in combination with chapter 4) addresses the objectives OB3, OB4, OB5 and OB6 of this thesis. This chapter 5 is structured as follows: The laboratory experiments scaling design and setup are described in section 5.2, and the results are shown in section 5.3. The field surveys performed at Fuentebravia beach (Cádiz) including beach scraping are presented and analysed in section 5.4. The discussion of both, laboratory and field survey results is detailed in section 5.5. Finally, section 5.6 presents the main conclusions.

5.2. LABORATORY EXPERIMENTS DESCRIPTION / METHODS

Reduced-scale laboratory experiments were performed at the Directional Wave Tank (Tanque de Oleaje Direccional, TOD, in Spanish) at IHCantabria's facilities. The beach profile was reproduced with low-density synthetic sediment to reduce scale effects on sediment transport processes. Both techniques, scraping and ploughing were analysed under three different accretive wave conditions including simultaneous tide simulation. In this section, the scaling design and the experimental setup are described.

5.2.1. Scaling design

Movable-bed, reduced-scale laboratory modelling is still a challenge. Reproducing all the dimensionless parameters that determine coastal hydrodynamics and sediment transport at these reduced scales has not been achieved yet. The state-of-the-art covers two approaches: (1) the use of real sediment with the same density as in nature, and (2) the use of low-density synthetic sediment. The use of real sediment makes scale effects inevitable, and some authors do not even indicate a scale or prototype (Baldock and Alsina, 2013; Guannel et al., 2007; Larsen et al., 2023). Sánchez-González et al. (2017) scaled sediment

grain size to reduce scale effects in the breaking zone. Few studies use low-density sediment although it allows the similarity between 4 out of 5 of the desired dimensionless parameters. The use of low-density materials reduces scale effects but should be designed with care and is costly. Different approaches can be followed, such as the one proposed by Grasso et al. (2009) or the methodology described throughout this section 5.2. The advantage of the methodology proposed here is that the calculations can be made with simpler expressions, as shown in the following paragraphs.

The scale of a magnitude M (λ_M) is defined here as the ratio between the value of this magnitude in the prototype, M_p , and the corresponding value in the model, M_m , as shown in equation (5.1):

$$\lambda_M = \frac{M_p}{M_m} \quad (5.1)$$

The Kinematics of free surface flows are mostly controlled by gravity. If in Newton's 2nd law, the inertial forces (F_i) are divided by the gravitative ones (F_g), the non-dimensional expression corresponding to gravity forces is called the Froude number, see equation (5.2).

$$F_n = \frac{F_i}{F_g} = \frac{L}{gT^2} \quad (5.2)$$

where g is the acceleration of gravity, T is a magnitude of time and L is length. In the case of gravity wave flows, the correct scaling of the processes of shoaling, refraction and diffraction implies the use of non-distorted models, so the length scale λ_l should be applied to the three spatial dimensions. The similarity between the Froude number in the flow of the prototype and that of the model (sub-indexes p and m , respectively), $\lambda_F = \frac{F_p}{F_m} = 1$ implies that the time and velocity scales are the square root of the length scale, equation (5.3):

$$\lambda_t = \lambda_V = \sqrt{\lambda_l} \quad (5.3)$$

Bed load sediment transport of non-cohesive sands under waves and currents is mainly controlled by the following dimensional variables:

- d_{50} : Median sediment grain size

CHAPTER 5

- ρ_s : Sediment grain density
- ρ_w : Water density
- ν : Water kinematic viscosity
- u^* : Bottom friction velocity

If u^* , ρ_w and d_{50} are assumed as fundamental variables, the application of the π -Buckingham theorem (1914) produces the non-dimensional expressions indicated in equations (5.4) and (5.5).

$$R_{e*} = \frac{u_* d_{50}}{\nu} \quad (5.4)$$

$$\theta = \frac{\rho_w u_*^2}{(\rho_s - \rho_w) g d_{50}} = \frac{\tau_0}{(\rho_s - \rho_w) g d_{50}} \quad (5.5)$$

where (in (5.5)), τ_0 is bed shear stress. Equation (5.4) is the grain Reynolds number (R_{e*}) and controls the shape of the bottom boundary layer, i.e. the tension of the flow over the sediment grains. Equation (5.5) is the Shields (1936) number (θ) and controls the initiation of motion of the sediment.

If the movable bed experiments are carried out assuming that the Shields number in the prototype and model are equal, then the scale of the Shields number should be equal to 1, equation (5.6):

$$\lambda_\theta = \frac{\theta_p}{\theta_m} = 1 \quad (5.6)$$

Under the wave's oscillatory motion, the peak bed shear stress can be expressed in terms of the orbital velocity amplitude on top of the bottom boundary layer, U_δ using a wave friction factor, f_w , as in equation (5.7):

$$\tau_0 = \frac{1}{2} \rho_w f_w U_\delta^2 \quad (5.7)$$

Soulsby (1997) proposed expression (5.8) for the wave friction factor in terms of the bottom orbital excursion, A_b , and Nikuradse's equivalent sand grain roughness, k_s .

$$f_w = 0.237 \left(\frac{A_b}{k_s} \right)^{-0.52} \quad (5.8)$$

Assuming the conventional value $k_s = 2.5 d_{50}$, (Nielsen, 1992), and for shallow waters $A_b = (U_\delta T_p)/(2\pi)$, equation (5.9) is obtained.

$$f_w = 0.993 \left(\frac{d_{50}}{U_\delta T_p} \right)^{0.52} \quad (5.9)$$

where in (5.9) T_p is the sea state peak period.

Using the wave friction factor of (5.9) and the expression (5.7) of the bed shear stress (5.7), the Shields number takes the form of equation (5.10).

$$\theta = \frac{0.496 U_\delta^2 \left(\frac{d_{50}}{U_\delta T_p} \right)^{0.52}}{\Delta g d_{50}} \quad (5.10)$$

where in (5.10), Δ is the sediment's relative submerged density, $\Delta = \frac{(\rho_s - \rho_w)}{\rho_w}$.

Using expression (5.10) and expression (5.6) to calculate the similarity of the Shields number, and taking into account the Froude scale for time and velocity of equation (5.3) and that $\lambda_g = 1$ (the gravity acceleration is the same in the prototype and the model), the following expression (5.11) for the relationship between the length, sediment relative density and grain size scales is obtained.

$$\lambda_d = \frac{\lambda_l}{\lambda_\Delta^{2.083}} \quad (5.11)$$

If the movable bed experiments are carried out assuming the similarity of the grain Reynolds number, then the scale of the grain Reynolds number should be equal to 1, equation (5.12).

CHAPTER 5

$$\lambda_{Re*} = \frac{R_{e*p}}{R_{e*m}} = 1 \quad (5.12)$$

Using (5.5) we can state that $u_* = (\tau_0/\rho_w)^{1/2}$ and the equations for bottom shear stress (5.7) and bottom friction factor (5.9), applied to equation (5.4) lead to the following equation (5.13) for the grain Reynolds number.

$$R_{e*} = \frac{0.704 U_\delta \left(\frac{d_{50}}{U_\delta T_p} \right)^{0.26} d_{50}}{\nu} \quad (5.13)$$

Using expression (5.13) and equation (5.12) to achieve the similarity of the grain Reynolds number and taking into account the Froude scale for flow velocity and time, the relationship (5.14) between the scales of length, grain size and fluid kinematic viscosity is obtained.

$$\lambda_d = \lambda_v^{0.794} \lambda_l^{-0.19} \quad (5.14)$$

Equations (5.11) and (5.14) establish the relationships between the sediment relative density scale, the grain size scale and the length scale that should be taken into account for bed load transport similarity in physical experiments.

In the surf zone of beaches, suspended load transport is also fundamental to describe sediment transport. For a correct description of this transport, besides the variables involved in the Shields and grain Reynolds numbers, the significant wave height, H_s , and the fall velocity of grain particles, w , are determinant. The fall velocity of grain particles depends on grain size and density, as well as on water viscosity, so the only new variable involved is wave height. The most used non-dimensional equation that takes into account this new variable is the dimensionless fall velocity, Ω , (Dean, 1973; Gourlay, 1968) given in (5.15).

$$\Omega = \frac{H_s}{w T_p} \quad (5.15)$$

The dimensionless fall velocity has also been used to explain different beach states (Masselink and Short, 1993; Wright and Short, 1984). Values of Ω higher than 6 correspond to dissipative beaches and those lower than 2 to reflective beaches. Values between 2 and 6 correspond to intermediate beaches that develop longitudinal and transversal bars.

Using equation (5.15) and taking into account Froude's scale for flow velocities and time, the scale of the dimensionless fall velocity is given by equation (5.16) as a function of the length and the fall velocity of grain particles scales.

$$\lambda_{\Omega} = \frac{\lambda_l^{0.5}}{\lambda_w} \quad (5.16)$$

Another non-dimensional number that is used to discriminate between bed load and suspended load transport is the Rouse number (R_o), which gives a relationship between the fall velocity of grain particles and the friction velocity, equation (5.17).

$$R_o = \frac{w}{\kappa u^*} \quad (5.17)$$

where, in (5.17), κ is the von Karman constant. The load transport modes in terms of the Rouse number are given by (Whipple, 2004):

- $R_o > 2.5 \rightarrow$ Bed load
- $1.2 \leq R_o \leq 2.5 \rightarrow$ 50% suspended load
- $0.8 \leq R_o < 1.2 \rightarrow$ 100% suspended load
- $R_o < 0.8 \rightarrow$ Wash load

Using equations (5.5), (5.7), (5.9), and (5.17) the scale of the Rouse number can be expressed as (5.18):

$$\lambda_{Ro} = \frac{\lambda_w}{\lambda_d^{0.26} \lambda_l^{0.24}} \quad (5.18)$$

The problem with the use of the Ω or R_o numbers to obtain the similarity of suspended transport in small-scale experiments is that the fall velocity of grain particles depends on

CHAPTER 5

the falling flow regime (laminar, transition or turbulent). As the prototype and model grains can fall into different flow regimes this gives 6 different possible scales.

Hallermeier (1981) proposed the parameter A to discriminate between the different regimes:

$$A = \frac{\Delta g d_{50}^3}{v^2} \quad (5.19)$$

The proposed fall velocities for the different fall regimes are:

$$\text{Laminar: } A \leq 39; w = \frac{\Delta g d_{50}^2}{18v} \quad (5.20)$$

$$\text{Transition: } 39 < A < 10^4; w = \frac{(\Delta g)^{0.7} d_{50}^{1.1}}{6v^{0.4}} \quad (5.21)$$

$$\text{Turbulent: } A \geq 10^4; w = \frac{(\Delta g)^{1/12} d_{50}^{0.5}}{0.91} \quad (5.22)$$

In this study, the model's sediment properties (grain size and density) are obtained from Shields and grain Reynolds numbers' similarities and the scales of the Ω and R_o numbers are derived quantities. The dissimilarity in these two parameters between the model and the prototype has implications that will be discussed further in this chapter.

The length scale applied in the experiments conducted in this study, $\lambda_l = 8$ was determined by the capabilities and size of the wave tank where the model was built. Other known parameters and resulting scales are given in Table 5.1.

The characteristics of the prototype and the freshwater used in the model are known. The scale relation (5.14) obtained for the similarity of the grain Reynolds number allows the determination of the targeted sediment grain size. Then, the scale relation (5.11) obtained for the similarity in the Shields number, determines the relative submerged density scale and therefore the target sediment density. The target values obtained from the Froude, Shields and grain Reynolds numbers similarities are summarized in Table 5.1.

Table 5.1 Prototype, target and physical model variables and scales for sediment and water.

(1) Known values; (2) Target values obtained from Froude, Shields and Reynolds numbers similarities; (3) Final model sediment variables and scales used in the physical experiments.

	Variable	Symbol	Value	Units
(1) Known values	Prototype sediment density	ρ_{sp}	2650	kg/m ³
	Prototype sediment grain size	d_{50p}	0.27	mm
	Prototype sediment relative submerged density	Δ_p	1.583	---
	Prototype fall velocity of grain particles	w_p	0.0313	m/s
	Prototype water density (salt water)	ρ_{wp}	1026	kg/m ³
	Prototype water kinematic viscosity (salt water)	ν_p	1.223 10 ⁻⁶	m ² /s
	Model water density (freshwater)	ρ_{wm}	1000	kg/m ³
	Model water kinematic viscosity (freshwater)	ν_m	1.141 10 ⁻⁶	m ² /s
	Water density scale	$\lambda_{\rho w}$	1.026	---
	Water kinematic viscosity scale	λ_v	1.072	---
(2) Target values	Target sediment grain size scale, equation (5.14)	λ_{dt}	0.712	---
	Target sediment density scale	$\lambda_{\rho st}$	1.771	---
	Target sediment relative submerged density scale, equation (5.11)	$\lambda_{\Delta t}$	3.194	---
	Resulting fall velocity of grain particles scale	λ_{wt}	1.512	---
	Target sediment grain size	d_{50t}	0.379	mm
	Target sediment relative submerged density	Δ_t	0.496	---
	Target sediment density	ρ_{st}	1496	kg/m ³
(3) Final model values	Resulting fall velocity of grain particles	w_t	0.0207	m/s
	Model sediment grain size	d_{50m}	0.370	mm
	Model sediment relative submerged density	Δ_m	0.500	---
	Model sediment density	ρ_{sm}	1500	kg/m ³
	Model fall velocity of grain particles	w_m	0.0203	m/s
	Model sediment grain size scale	λ_d	0.730	---
	Model sediment density scale	$\lambda_{\rho s}$	1.767	---
	Model sediment relative submerged density scale	λ_Δ	3.166	---
	Model fall velocity of grain particles scale	λ_w	1.542	---

CHAPTER 5

The density of the sediment used for physical models is restricted by the densities of available materials. In this study, we used a synthetic sediment which was very similar to the targeted one (i.e. density $\rho_s = 1500 \text{ kg/m}^3$ and grain size $d_{50} = 0.37 \text{ mm}$, see Table 5.1). With this sediment, the prototype and model regimes of fall velocity, equation (5.19), are in the transition region and the fall velocity of grain particles can be calculated using equation (5.21), see Table 5.1.

The resulting scales of the five non-dimensional parameters are:

- Froude number (flow variables imposed in the wave tank): $\lambda_F = 1$
- Shields number, equation (5.10): $\lambda_\theta = 0.997 \cong 1$
- Grain Reynolds number, equation (5.13): $\lambda_{Re*} = 1.034 \cong 1$
- Fall velocity parameter scale (Dean), equation(5.15): $\lambda_\Omega = 1.835$
- Rouse number scale, equation (5.17): $\lambda_{Ro} = 1.016 \cong 1$

As shown, with the model sediment chosen for the experiments, all parameters (Froude, Shields, Reynolds grain and Rouse) were similar in the prototype and the model. The dimensionless fall velocity however was higher in the prototype than in the model, meaning that the modelled beach would tend to be more reflective than the prototype.

5.2.2. Experimental setup

The experiments were carried out in the Directional Wave Tank (TOD) at IH Cantabria's facilities. The TOD (see Figure 5.1) is 28 m long, 8.6 m wide, and 1.2 m high. The tank was divided longitudinally into 10 channels, six of them were used to test different nature assisted beach enhancement (NABE) techniques under the same marine dynamics, and the remaining four were used as aisles to access the testing profiles while scraping and ploughing. Each channel was 0.8 m wide, minimizing boundary effects on the central part of the channel, where geometric measurements were taken every low tide with a laser profiler.

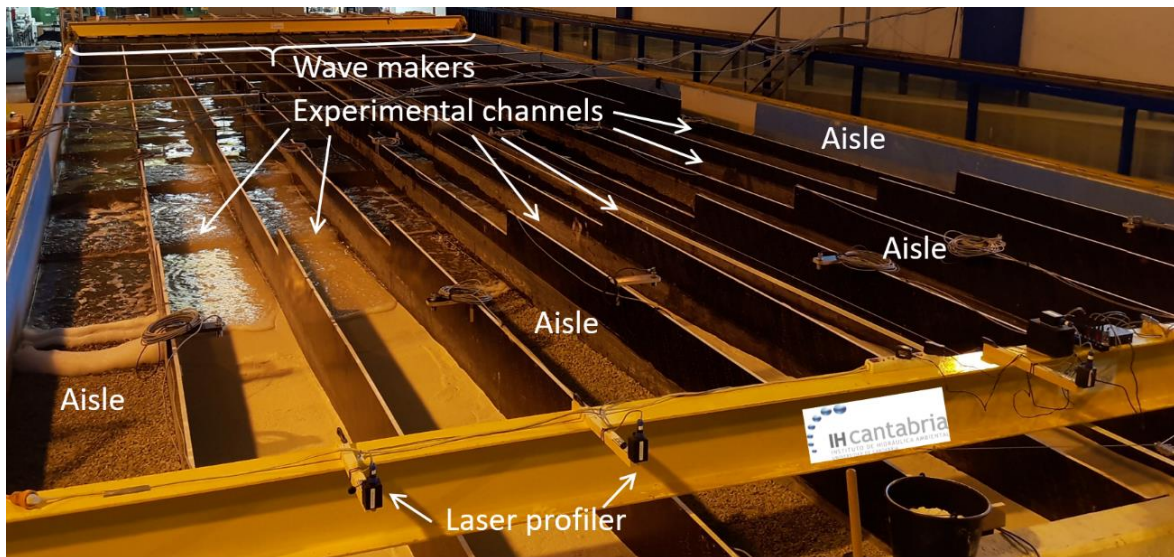


Figure 5.1 Directional Wave Tank (TOD) during the experiments.

Experimental channels were filled with low density ($d_{50} = 0.37$ mm and $\rho_s = 1500$ kg/m³) synthetic sediment to reduce scaling effects (see previous section). The sediment was placed with an initial uniform slope of 1/21, and two tidal cycles of slightly energetic waves (“pre-test waves”, Table 5.2) were simulated to obtain the dissipative beach profile which is typical in spring, at the beginning of the good weather season (Figure 5.2). Then, the marine climate of each Test (A, B, or C, see Table 5.2) was simulated until the maximum accretion on the beachfront was reached. The waves simulated during the Tests were low energetic, typical of spring and summer marine conditions. This process was repeated for each Test, manually restoring the sediment layout with a uniform slope of 1/21 after them, which ensured the same initial conditions for each Test. The “pre-test waves” simulation was used to check the repeatability of the experiments. Four channels lying between the test-channels were used as working aisles (so as not to tread on the experimental channels) and filled with gravel with the same uniform slope to avoid wave reflections.

CHAPTER 5

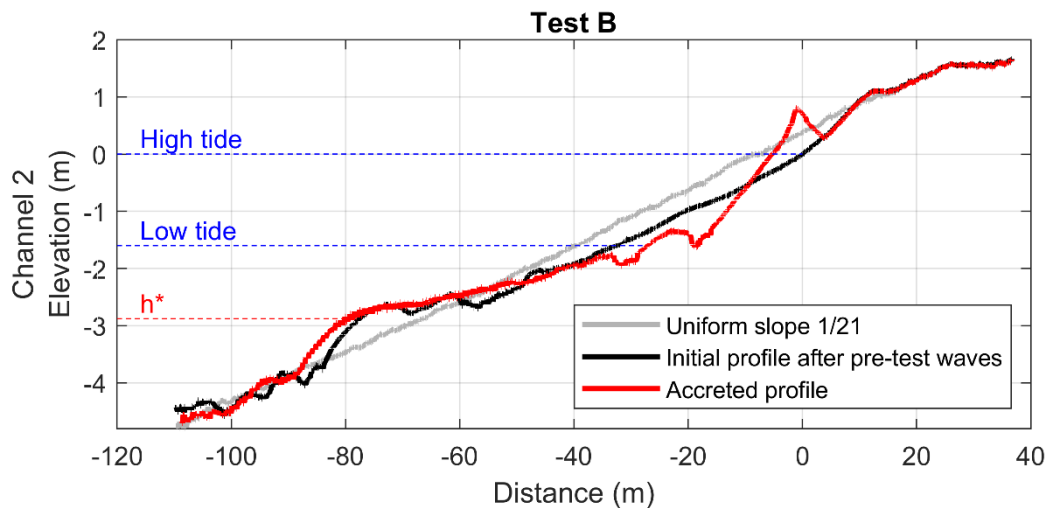


Figure 5.2 Setup, initial profile, and maximum accretion achieved for Test B at prototype scale. h^* is the depth of closure for test waves.

Three Tests were simulated (A, B, and C) with different wave characteristics, all of them ensuring that accretion was produced ($\Omega < 2.4$, indicating highly probable accretion according to Kraus et al., (1991), see Table 5.2). All the simulations included a simultaneous sea level variation according to a semidiurnal tide with 2.4 m of tidal range for Test A and 1.6 m for Test B and C. Pre-test waves were run before each Test, with the same tidal range as that of their corresponding Test, to achieve the initial profile (a dissipative profile generated with waves with $\Omega > 4$). Test C waves were small enough to test the lower limit of accretion that can be produced with natural waves but also had the same Ω parameter as Test A for comparison. Table 5.2 shows the prototype and model wave and tide characteristics of each Test. The wave spectrum used was JONSWAP (Hasselmann et al., 1973).

Table 5.2 Prototype and model marine dynamics simulated.

Wave config.	Prototype				Model			
	H_{sp} (m)	T_{pp} (s)	$Tide_p$ (m)	Ω_p	H_{sm} (m)	T_{pm} (s)	$Tide_m$ (m)	Ω_m
Pre-test A	1.60	6.50	2.40	7.98	0.20	2.30	0.30	4.28
Pre-test B	1.60	6.50	1.60	7.98	0.20	2.30	0.20	4.28
Pre-test C	1.60	6.50	1.60	7.98	0.20	2.30	0.20	4.28
Test A	0.48	8.50	2.40	1.84	0.06	3.00	0.30	0.99
Test B	0.32	8.50	1.60	1.22	0.04	3.00	0.20	0.66
Test C	0.264	4.72	1.60	1.81	0.033	1.67	0.20	0.97

These marine dynamics affect the six channels filled with synthetic sediment equally. Each of them was used to test a different NABE technique. Table 5.3 summarizes the characteristics of the techniques tested on each channel. Channel 2 was used as control, with no NABE applied, and represents the natural evolution of the beach. Ploughing was applied in the intertidal area of Channel 1 every low tide. Scraping was applied in Channels 3 to 6, with different locations of the borrow and filling areas. The borrow area was 0.25 - 0.3 m deep (as recommended by Carley et al., 2010) and had 11.2 m of cross-shore extent at the prototype scale. This means that around 3 m³ of sediment were mobilized per meter of beach.

Table 5.3 Characteristics of the NABE technique conducted in each channel.

	Acronym	Technique	Borrow area	Filling area
Channel 1	PLOUGH	Ploughing		Ridges and furrows
Channel 2	NAT	Natural		No sand movement – Control
Channel 3	L2B	Scraping	Lower intertidal	Intertidal bar
Channel 4	L2BF	Scraping	Lower intertidal	Beachfront
Channel 5	L2D	Scraping	Lower intertidal	Dune or upper dry beach
Channel 6	U2D	Scraping	Upper intertidal	Dune or upper dry beach

Figure 5.3 shows the ploughing and scraping borrow and filling areas for each channel. The borrow area was the low intertidal part of the beach profile for Channels 3, 4, and 5, next to the low tide limit to perform the scraping by terrestrial machinery. In Channel 6 the borrow area was the upper part of the intertidal area, just below the high tide level. All this sediment was placed on an intertidal bar in Channel 3, on the beachfront for Channel 4, and on the dune (taken out of the experimental tank) for Channels 5 and 6. The sand extracted from those channels for dune nourishment was placed back in the next Test to ensure the same amount of sand.

CHAPTER 5

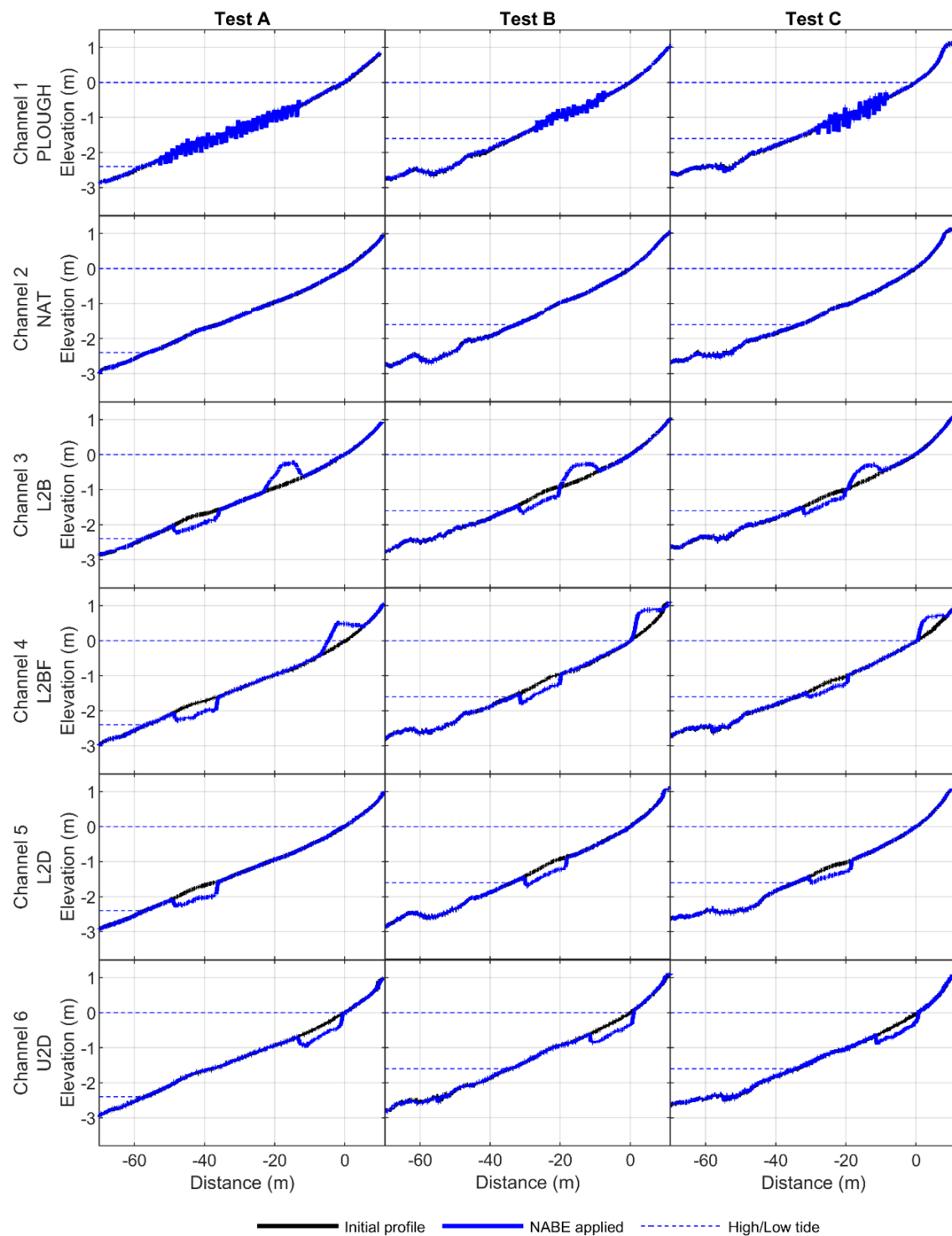


Figure 5.3 NABE techniques applied to each channel and Test. Borrow and filling locations for scraped channels (3 to 6) and ploughing extent (channel 1).

The left panel in Figure 5.4 displays a zoom of the ploughing area shown in the top-left panel of Figure 5.3. Ploughing was designed to be performed by a ploughing tractor at a prototype scale. This machinery can perform ridges and furrows on the sand with a wavelength of ~ 1.5 m and an amplitude of ~ 0.25 m. Therefore, the plough performed in the laboratory (model scale) had a wavelength of 0.18 m and an amplitude of 0.03 m. Ploughing was conducted from the lower part of the intertidal area, next to the low tide level, to the upper part of the intertidal zone. The tidal range was larger for Test A, and therefore the cross-shore extent of the ploughing area was 40 m for Test A and 20 m for Tests B and C (both at prototype scale), corresponding to 28 and 14 ridges and furrows, respectively.



Figure 5.4 Ploughing. Left: Zoom of a profile of the ploughing performed in Channel 1. Centre: Picture of ploughing being conducted at the model at a reduced scale. Right: Example of ploughing at prototype scale at Laida beach (Source: Gainza et al., 2019).

5.3. RESULTS

This section shows the results obtained from the laboratory experiments. The analysis was based on the geometry of the beach profile measured at each low tide during the experiments. This section shows (1) the formation of the beach berm during calm wave conditions, (2) an analysis of the degree of widening of the dry beach and the geometric characteristics of the berm at the maximum accretion state achieved, and (3) the study of the accretion volume. These results allow the comparison among NABE techniques and the analysis of their effectiveness in terms of widening of the dry beach area and accretion enhancing. All the results shown in this section are presented at the prototype scale.

5.3.1. Beach berm formation

Figure 5.5 shows a zoom of the beach profile around the high tide level for each Test and channel. Each panel shows the beach berm's evolution, including the initial profile obtained after the simulation of the pre-test waves, the initial profile after NABE techniques were applied, and the maximum accretion achieved on the beach berm. The high tide, setup, and runup levels are also presented for reference. The setup ($\bar{\eta}$) and runup (R_2) levels were computed with Stockdon's et al. (2006) formulas, as shown in equations (5.23) and (5.24), respectively.

$$\text{setup} = \bar{\eta} = 0.35\beta_s(H_0L_0)^{0.5} \quad (5.23)$$

$$\text{runup} = R_2 = 1.1 \left(0.35\beta_s(H_0L_0)^{0.5} + \frac{(H_0L_0(0.563\beta_s^2 + 0.004))^{0.5}}{2} \right) \quad (5.24)$$

where β_s is swash zone slope, H_0 is deep-water wave height, $L_0 = gT^2/2\pi$ is deep-water wavelength and T is wave period. In this study, the following approximations were considered; $T = T_p$ and $H_0 = H_s$. The swash zone slope (β_s) was computed as the slope of the final beach profile of maximum accretion at high tide level, with a range of $\pm 0.8 H_s$ around high tide level, where the beach slope was quite uniform. Only the slope at high tide was considered, as it determines the wave runup at high tide and consequently the berm's height. The tidal ranges in this experiment were meso/macro-tidal, and therefore the waves only reached the berm during high tide (but not during the falling, rising, and low tides).

A berm was observed in the final beach profile for all Tests and in all channels. There was a resemblance in the shape of the final berm of all channels in each Test (A, B or C). This indicates that the NABE technique used does not determine the geometry of the berm. On the other hand, the shape of the berm was different among Tests carried out in the same channel. The berm's height and slope at the beachfront changed according to marine dynamics, as shown in the following section.

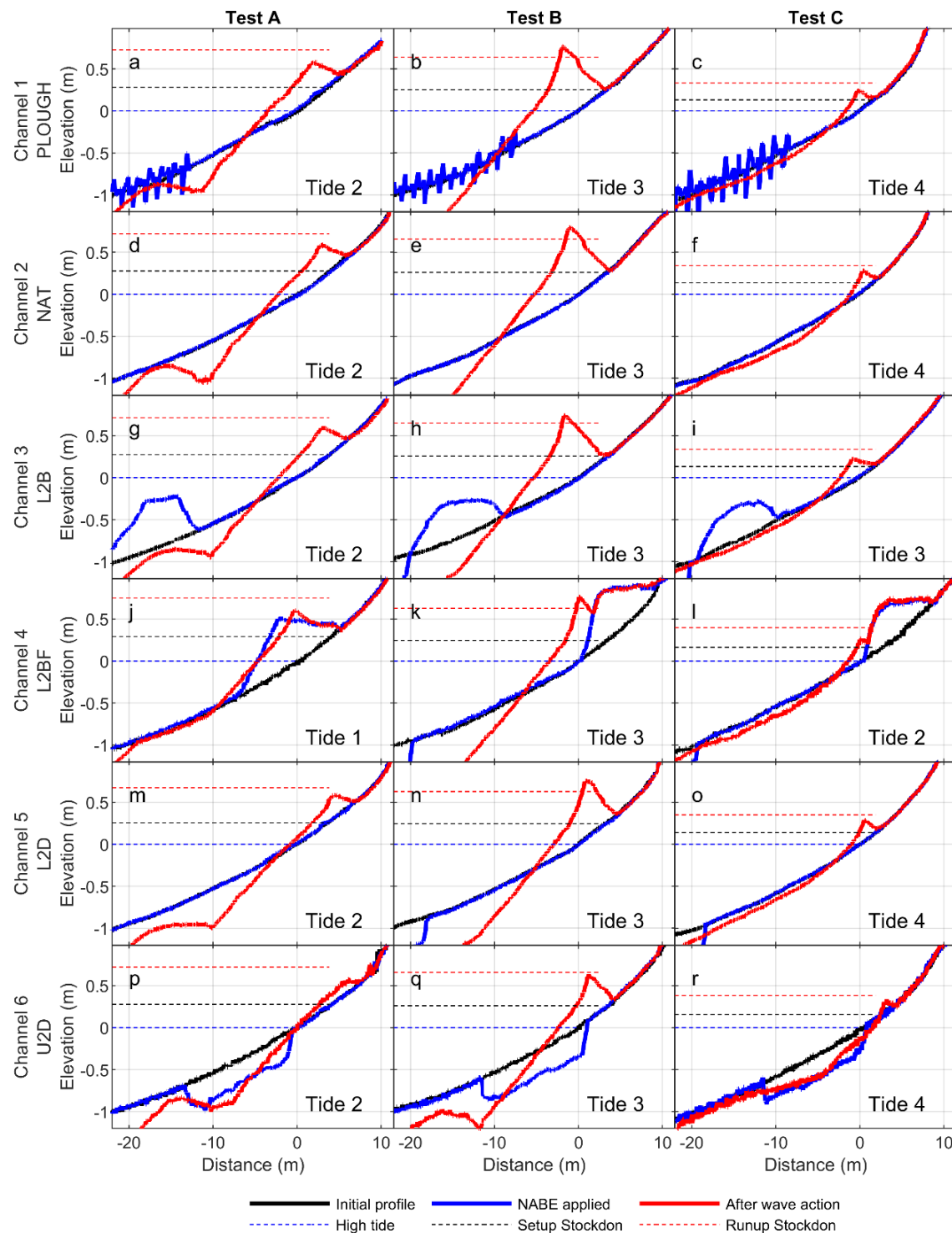


Figure 5.5 Profile evolution up to the maximum accretion achieved at the beachfront. Each graph indicates the number of tidal cycles that were necessary to achieve the maximum accretion.

5.3.2. Dry beach widening and accreted berm characteristics

Shoreline progradation was computed as the difference between the shoreline's position at the beginning of the test, and at the moment of maximum accretion. Shoreline position was taken as the point where the profile elevation is equal to the high tide plus wave setup levels. This measurement indicates the beach width increment due to sand accretion on the berm and it is indicative of the dry beach gain achieved.

Berm height was directly measured on the beach profiles as the highest point of the berm and referred to high tide level. Figure 5.5 shows that the berm height achieved at the maximum accretion state was close to that of the runup level. During the experiments, the highest waves overtopped the maximum height of the berm during high tide. The sediment load carried by the waves during these events was discharged on the top of the berm making it progressively higher (see for instance the sand layer accumulated on top of the berm between -1 and 0.68 m cross-shore in Figure 5.5e; the height step observed at 0.68 m indicates the onshore limit reached by wave overtopping). Figure 5.6 shows a scatter plot of berm height and shoreline progradation for each Test. Dashed lines act as a reference of the characteristics of the berm under natural conditions (Channel 2). The empty marker shows the characteristics of the berm formed artificially by the "machinery" during the L2BF scraping of Channel 4. The berm height achieved by all the NABE experiments was similar to the naturally formed one. The height varied mainly between Tests, which means that the different incoming wave conditions were responsible for this variation but not the NABE techniques used. In Channel 4, when the artificially generated berm's height was not equal to the height of the naturally formed berm, it changed under wave action (Figure 5.5j, Figure 5.5k and Figure 5.5l). In Test A, the artificial berm was lower than the equilibrium one, and therefore wave overtopping was produced during high tide. Those waves progressively moved the sand from the beachfront to the upper part of the berm (Figure 5.5j), generating a retreat of the shoreline and a higher berm. In Tests B and C, the height of the artificially created berm was higher than the natural one, and therefore the upper part of the scraped sand was not necessary for protection during summer conditions. In these cases (Channel 4 – L2BF, Test B and C, Figure 5.5k and Figure 5.5l, respectively) a new and shorter berm was formed seaward of the position of the artificially created one with the new sediment accreted through wave action.

The final shoreline progradation achieved due to beach ploughing (Channel 1) was between 4.32% and 37.35% larger than in natural conditions for all Tests (mean of 23.41%).

These results indicate that ploughing is an innovative and effective technique for beach accretion enhancement. The effect of beach scraping on shoreline progradation depended on the location of the borrow and filling areas. Channel 3 (L2B) showed an enhanced shoreline progradation compared to natural conditions between 6.79% and 63.26% (mean of 25.76%). The initial position of the shoreline in Channel 4 (after L2BF beach scraping) ranged from shorelines located landward to shorelines located seaward of the final shoreline position achieved under natural conditions (from 65.43% less to 110.84% more progradation in comparison to the profile with no NABE applied). Wave action modified the shape of the berm and the final shoreline progradation ranged between 24.07% less and 81.93% more (mean of 38.33%) than natural progradation. In this Channel 4, shoreline progradation did not exceed the natural one only for Test B, where the artificially created shoreline progradation retreated considerably compared to the expected final natural shoreline's position. In this case, the reduced amount of sediment due to removing sand and not using it to artificially induce shoreline progradation prevented the waves to produce the desired accretion. A similar scenario was found for Channels 5 and 6 (L2D and U2D respectively). In both Channels there was a lack of sediment on the active beach profile due to the volume of sand removed from the borrow area and placed on the dune (out of the area of wave action during summer). L2D achieved a final shoreline progradation between 44.58% less and 2.04% more (mean of 25.70% less) than under natural conditions. U2D showed shoreline progradations that were smaller than under natural conditions in all Tests, with values ranging between 38.27% and 89.80% less (mean of 62.77% less).

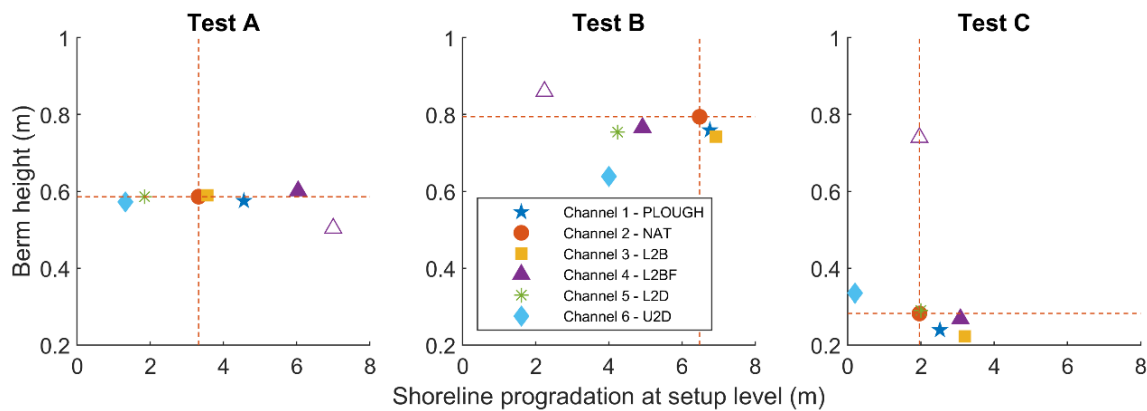


Figure 5.6 Berm height and shoreline progradation achieved at maximum accretion. Dashed lines are plotted as a reference of the natural behaviour of the beach. The empty marker indicates the characteristics of the artificial berm created by scraping Channel 4.

Figure 5.7 shows the swash zone slope (β_s) obtained for each Test and channel as a function of the shoreline progradation previously described. As with berm height, the swash zone slope only varied among Tests but not among Channels. This means that the

CHAPTER 5

swash zone slope was also determined by marine dynamics, while NABE techniques did not affect the final accreted equilibrium geometry. The empty marker shows the swash zone slope of the artificially generated beach berm in Channel 4 during the L2BF scraping operations. As berm height, the swash zone slope also changed toward the equilibrium slope of the accreted berm under wave action.

In Figure 5.7 the black dot next to the vertical axis of each graph indicates the initial swash zone slope and shoreline progradation (0 m because it is the reference) of the pre-test waves profile. The slope was around 0.67 for all Tests, which is typical of an intermediate beach. After the low-energy wave action, the swash zone became steeper, with slopes between 0.10 and 0.15, which is common for reflective beaches.

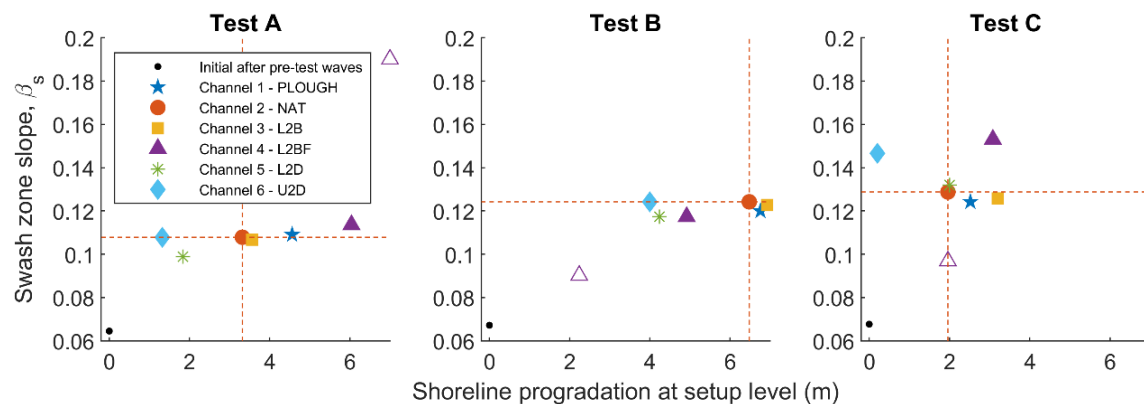


Figure 5.7 Swash zone slope and shoreline progradation achieved at maximum accretion.

Dashed lines are plotted as a reference of the natural behaviour of the beach. Empty markers indicate the characteristics of the berm created artificially by scraping Channel 4.

5.3.3. Accreted volume

The volume of sediment accreted on the beach berm was measured by integrating the area between the initial profile obtained after the pre-test waves and the profile corresponding to the maximum accretion achieved. Only positive accretion areas around the beach berm were considered, which means from -12 m to 10 m cross-shore (i.e. from the dry beach to around 0.7 m below high tide level). For Channels 4 and 6 (L2BF and U2D), due to the location of the filling and borrow areas, the profile in which the NABE technique was applied was also considered for volume calculation. Therefore, two volume calculations were obtained for Channels 4 and 6, one referred to the pre-test waves profile and the other to the profile obtained after NABE techniques were applied. Figure 5.8 shows the results obtained for each Test and channel.

Channel 2 shows the natural behaviour of the beach. In such natural conditions, the accreted volume varied depending on the different marine dynamics simulated. The largest accretion volume was obtained for Test B, which had the lowest dimensionless fall velocity (Ω), indicating more reflective conditions (the lower the dimensionless fall velocity, the higher the beach slope). Test A and C had similar Ω (higher than Test B) and achieved lower accretion volumes, as expected. Although the dimensionless fall velocity was similar for both Tests, in Test C wave height and peak period were lower, as well as sediment transport capabilities, resulting in a smaller accreted volume. These considerations were also valid for all the other channels that had undergone the same simulated wave conditions.

The ploughing technique was tested in Channel 1. The accreted volumes obtained were 31.79% and 37.62% larger than the control for Test A and C respectively, and equal to the control for Test B. This demonstrates that the ploughing technique can enhance beach accretion by achieving a larger accreted volume of sediment and a wider dry beach (as shown before).

Channel 3 tested a scraping technique that moved the sediment from the lower intertidal area to an intertidal bar (L2B). The accreted volume was 4.23% larger than the control for Test A, 8.90% smaller for Test B, and 56.21% larger for Test C. The three Tests showed more shoreline progradation than the control. Test A and B showed similar accreted volumes to Channel 2, while the additional shoreline progradation was 7.23% and 6.79%, respectively. Besides, Test C achieved an additional 63.27% shoreline progradation, which agrees with the extra 56.21% accreted volume. The filling volume on the intertidal bar was around $3 \text{ m}^3/\text{m}$, a value larger than the accreted volume for Tests A and C. This means that for these Tests, part of the sand from the bar was moved offshore by the waves.

The L2BF beach scraping that moved the sediment from the lower intertidal area to an artificially created beach berm was carried out in Channel 4. In this case, the final berm was composed of both the artificially moved sand and the naturally accreted sediment due to wave action (see both components represented by the purple bars in Figure 5.8). In all Tests, the final berm volume was larger than the control one (110.68% for Test A, 21.55% for Test B, and 491.26% for Test C), although the naturally accreted sediment volume was smaller than the control in all tests (77.75% in Test A, 50.89% in Test B, and 26.36% in Test C). It is remarkable that the amount of artificially moved sediment (around $3 \text{ m}^3/\text{m}$) was larger than the naturally accreted sediment volume for Tests A and C in the control profile. This fact can be related to the low portion of sediment that was accreted by waves in those Tests, which was 10.56% of the volume of the final berm for Test A and 12.46% for Test C, respectively. The required sand volume to form the berm was already moved by the

CHAPTER 5

“machinery” and therefore natural accretion only moved the sediment required to reach the final equilibrium geometry according to the swash zone slope and berm height that matched the simulated waves. In Test B, the artificially moved sand volume was lower than the volume of the berm of the control profile. In this case, the waves were able to mobilize 40.41% of the total berm volume of Channel 4. Despite that, shoreline progradation in Test B was smaller than in the control. Altogether, the scraped sediment deposited on the beachfront was not eroded by wave action, and an additional natural accretion occurred. Therefore, the L2BF scraping technique was efficient to increment dry beach sand volume, which may act as backup for winter storms.

Channel 5 (L2D) shows the results of scraping the sediment from the lower intertidal area and taking it out of the summer’s wave action area (sand used for inland operations to nourish the dune or the upper part of the dry beach). In this case, the accreted volume was 46.44% smaller than the control for Test A, and 40.92% smaller for Test B. Both Tests showed smaller shoreline progradations than the control. In Test C, the accreted volume was 4.22% larger than the control, corresponding to an extra 2.04% of shoreline progradation achieved. Note that for all Tests, the volume of sand that was removed from the active beach profile was around $3 \text{ m}^3/\text{m}$ (taken from the borrow area, not showed in Figure 5.8), which, summed to the naturally accreted volume, exceeded the accreted volume in the control. Therefore, a larger volume of sand was recovered from the lower part of the beach profile and deposited on the beachfront and on the artificially nourished area to act as a buffer for winter erosion.

The location of the borrow area was the same (the lower intertidal area) for Channels 3, 4, and 5 (L2B, L2BF and L2D scraping techniques). However, the final volume accreted due to wave action was different, with more accretion occurring in L2B, followed by L2D, and finally L2BF. These differences can be explained by the fact that L2B had more volume of sand available in the active beach profile (the filling area was an intertidal bar). In the other two, the sand was moved completely (L2D) or partially (L2BF) out of the area affected by waves. It is noteworthy that the lowest natural accretion was achieved when filling was performed on the beachfront (L2BF). This may be due to the more reflective beach profile geometry created when filling the berm. Such reflective conditions reduced the disequilibrium between the equilibrium and the actual beach profile and, consequently, reduced sediment transport. The Tests performed for L2BF resulted in wider dry beaches than L2D but a smaller volume of sediment in the upper beach, which reduces the protection capacity during eventual erosive winter storms.

As in Channel 5 (L2D), in Channel 6 (U2D) the sediment was also extracted from the area under the effect of summer waves but was borrowed from the upper intertidal area,

next to the high tide level. In this case, the accreted sediment partially filled the borrow area. Therefore, the berm's accreted volume was composed of the sum of the sediment that filled the borrow area and the sediment accumulated on the initial beach profile (without using NABE). Figure 5.8 shows both components. The accreted volume was 32.68% smaller than the control in Test A, 10.33% smaller in Test B, and 106.18% larger in Test C. A considerable amount of this sediment filled the borrow area: 48.98% of the accreted volume in Test A, 51.86% in Test B, and 83.25% in Test C. As a consequence, the volume that generated a new berm and produced shoreline progradation was lower than the control for all Tests, matching the results of less shoreline progradation presented before. In fact, U2D showed the most retreated shoreline positions at the end of the experiments, although the total amount of sediment captured from the lower part of the beach profile was the largest one of all channels (taking into account the volume accreted by waves and the $3 \text{ m}^3/\text{m}$ extracted from the borrow area). By comparing the results from L2D and U2D, it can be stated that sand extraction from the upper intertidal area leads to more accretion on the beach profile due to the generation of a more dissipative beach profile geometry, as suggested by previous authors.

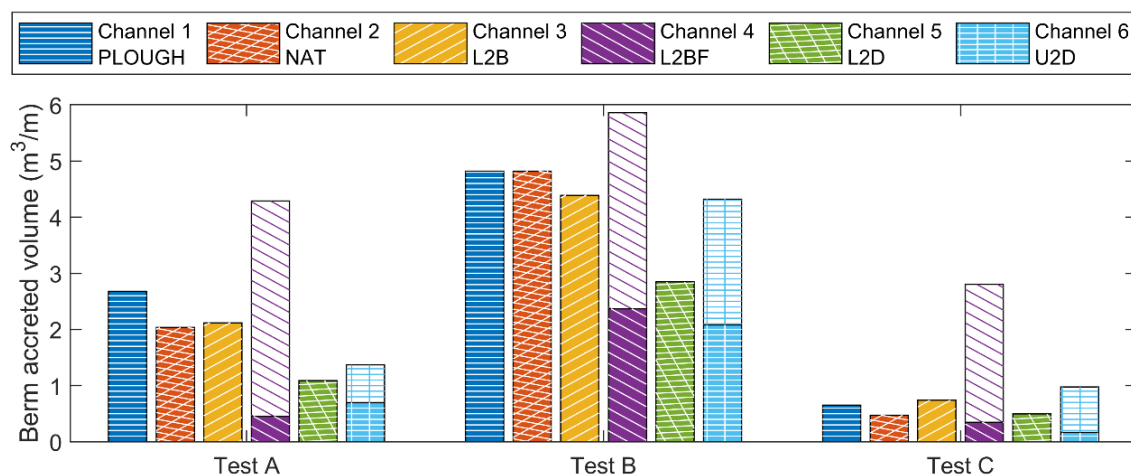


Figure 5.8 Maximum accreted volume on the berm. The bar for Channel 4 shows the volumes of sediment manually mobilized by scraping (white fill with purple descending lines legend on top of purple bars) and by wave action (purple fill) filling the berm. The bar for Channel 6 represents all the volume mobilized by wave action, including the volume of sediment on the berm (blue fill) and the volume of sediment that filled the borrow area partially next to the high tide level (white fill with blue cross-squared legend on top of blue bars).

5.4. FIELD CAMPAIGN

Fuentebravía is a pocket beach located in the bay of Cádiz. Its characteristics and location have been described in section 3.2.1 of chapter 3. Beach scraping was applied to the central part of Fuentebravía beach on May 12th, 2021. The scraped area extended 250 m alongshore, leaving enough space of natural beach at both sides that act as control areas. Figure 5.9 shows the two scrapers used while performing scraping actions. The borrow area was designed with a maximum depth of 0.3 m, following the recommendations of Carley et al. (2010) for responsible scraping. The width of the borrow area was 15 m, next to the low tide limit. Therefore, the volume of sediment mobilized by the machinery was 5 m³/m of beach. This sand was placed on the beachface, extending the winter berm 15 m seaward.



Figure 5.9 Scrapers performing beach scraping at Fuentebravía beach.

Fuentebravía beach was surveyed from May to October 2021, through 13 field surveys (more details and dates in section 3.2.1). Each survey consisted of the measurement of the sand elevation along a set of 7 beach profiles, four of them (P1, P2, P6, and P7) for the analysis of the natural evolution of the beach (Figure 3.3, exact coordinates shown in Table 3.1), and the three profiles left (P3, P4, and P5) for the study of scraping effect (Figure 5.10, exact coordinates shown in Table 5.4). Each profile extended from the dry beach next to the promenade to the low tide limit. Expert surveyors took the measurements with a high-precision RTK-GPS device. This data was obtained thanks to the collaboration with Demarcación de Costas Andalucía Atlántico (Ministerio para la Transición Ecológica y el Reto Demográfico).

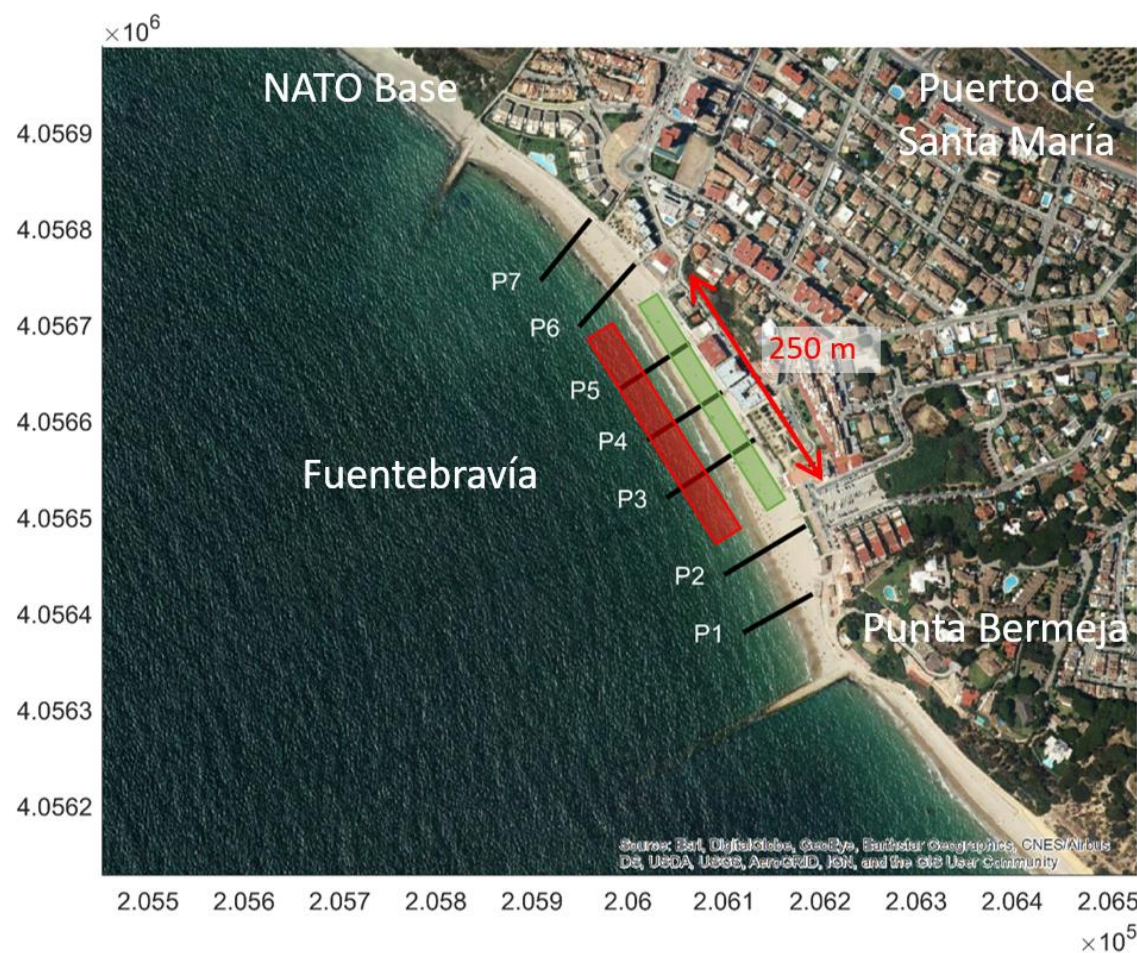


Figure 5.10 Beach scraping extent (red colour: borrow area, green colour: filling area) and location of the surveyed profiles at Fuentebravía beach.

Figure 5.10 shows the location of the borrow and filling areas. Measurements were taken before (May 11th, 2021) and after (May 12th, 2021) scraping operations. The filling area is noticeable in Figure 5.11.

Table 5.4 Coordinates that define the beach profiles measured at Fuentebravía beach.
ETRS89-UTM30N coordinate system.

Profile	Origin X	Origin Y	Near low-tide X	Near low-tide Y
P3	206132	4056581	206040	4056520
P4	206098	4056630	206020	4056580
P5	206064	4056681	205991	4056633

CHAPTER 5

The evolution of the scraped profiles from mid-May to October 2021 is shown in Figure 5.11. The three profiles show similar behaviour. The beach progrades fast at the beginning, during May, just after the scraping operations. Then the progradation is slower, with steady dry beach widening up to September. During these months, the berm crest level was approximately constant, and it matches the level of the berm crest of the natural profiles. Therefore, the berm crest elevation could have been predicted by the $TWL_{1\%}$ (as demonstrated in section 3.4.4, Figure 3.22) Note that the berm created by machinery was located in a higher position, matching the winter berm level but not the lower level of the summer berm. Finally, in October the beach berm aggraded, both in natural and scraped profiles.

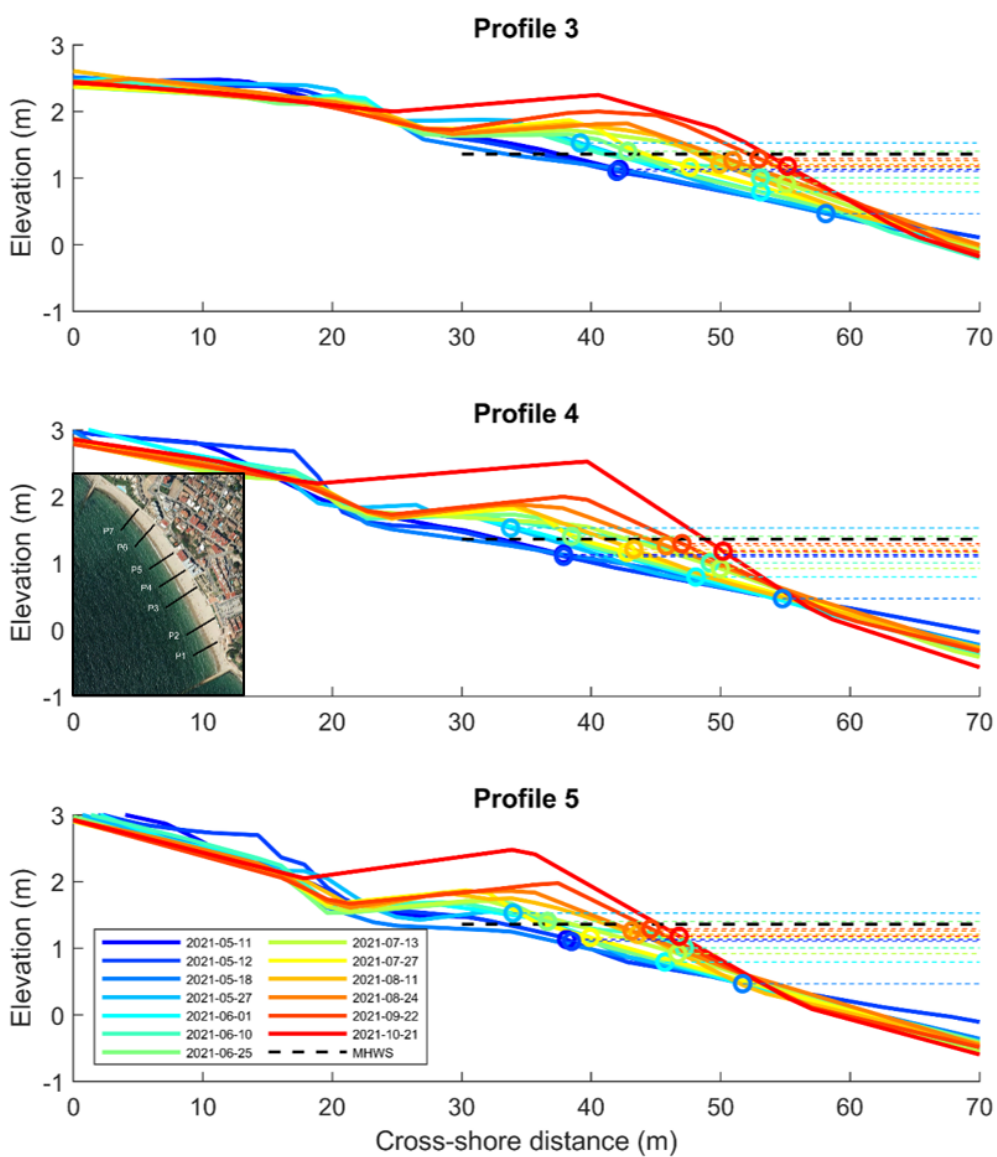


Figure 5.11 Scrapped beach profile evolution at Fuentebravíá.

The comparison between natural and scraped profiles allows the verification of the effectiveness of scraping actions. Figure 5.12 shows the comparison of the evolution of natural (P2) and scraped (P4) profiles. Only the survey dates with spring tides have been selected for simplicity (see section 3.4.4 that justifies this decision).

The graphs on the top show the data from the surveys performed the day before and after the scraping. The graphs in the centre include the measurement made on May 27th, 2021. It is noticeable that the scraped profile accreted more sand volume and its shoreline prograded more, achieving a wider dry beach. The comparison between the average of the scraped profiles and the average of the natural profiles indicates that the shoreline prograded 3.68 m more and accreted 24 % extra sand when scraping is applied (during the first 15 days).

The graphs on the bottom include all the survey period. Note that accretion speeded up in June for the natural profile, while it was slower for the scraped profile. The shoreline progradation average is now only 0.32 m bigger for the scraped profile. The accreted volume is similar for natural and scraped profiles. This means that during June, the natural behaviour of the beach made the shoreline almost reach the same progradation previously achieved by the enhanced accretion of scraping. Therefore, the effect of scraping on enhancing beach recovery seems to be limited to the first weeks after the machinery actions. From July to October, the behaviour of natural and accreted profiles is similar, confirming that the scraping effect had finished.

CHAPTER 5

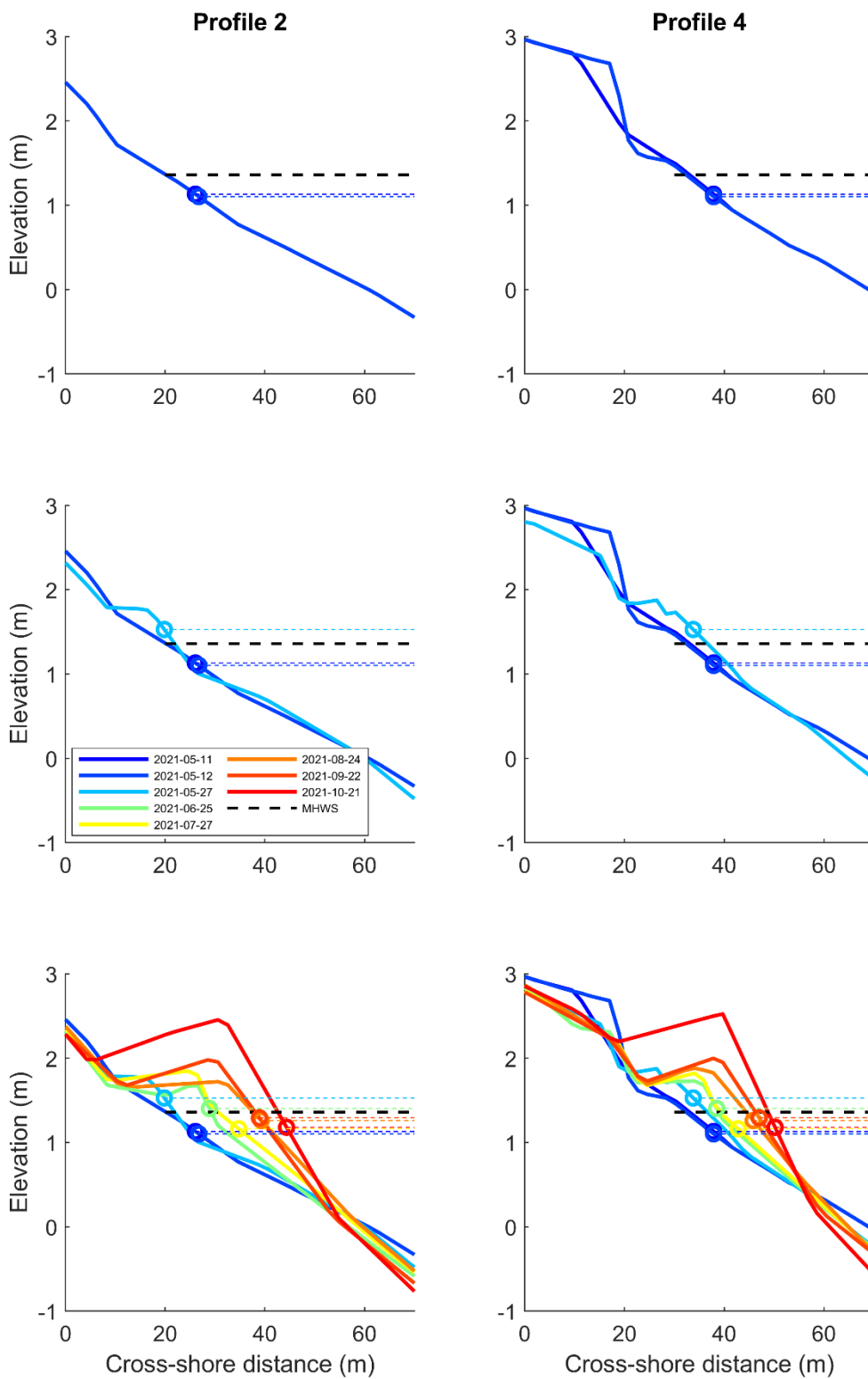


Figure 5.12 Comparative of scraped (Profile 4) and natural (Profile 2) beach profiles evolution.

5.5. DISCUSSION

NABE techniques are widely applied on many beaches, although their actual effect on beach accretion had not been checked until now. The design of NABE techniques should match the aim of the project (Carley et al., 2010), and take into consideration local marine and aeolian dynamics, as well as ecological concerns. The recommended maximum depth of the borrow area to be scraped is 0.3 m for sandy beaches (Bruun, 1983) and the volume should be less than the natural recovery rate of the beach (McNinch and Wells, 1992; Tye, 1983) integrated over the whole summer season. These guidelines were followed during our laboratory experiments although it was difficult to estimate the natural recovery rate of the beach without monitoring previous summer seasons (on the prototype) or formerly testing experiments of the natural conditions (on the laboratory). Additionally, the recovery rate was found to depend on marine dynamics and change from one beach to another. This result indicates that it is necessary to monitor the evolution of beach profiles during summer before designing scraping actions on them.

The innovative NABE ploughing technique has proved to accelerate natural beach accretion in field experiments (Gainza et al., 2019), and in the laboratory at both a real scale (Pellón et al., 2023; chapter 4) and a reduced one (this chapter). The main advantages of the ploughing technique are: its easy design, the fact that it is inexpensive, it minimizes ecological disturbance, takes advantage of natural processes, and achieves wider dry beaches. Furthermore, the ploughing technique may be easily applied on beaches during routine daily cleaning operations. Due to the novelty of this technique, some questions are still to be answered in future studies, such as: *what is the effect of a spring storm acting over the ploughed bedforms?, and, is it possible to optimize the distance between consecutive ridges to enhance accretion even more and reduce the need for machinery?*.

This study shows that the selection of the most appropriate NABE technique should be determined by the aim of each specific coastal management project. To achieve a wider dry beach the most appropriate techniques were either ploughing (PLOUGH) or scraping the low intertidal area filling the beach berm (L2BF) or scraping creating an intertidal bar (L2B). For dune nourishment or protection against winter storm purposes, the best solution is scraping, either the low or upper intertidal area (L2D or H2D), and using the sand for the nourishment of the subaerial area of the beach. Note that only low-energy marine conditions were tested in the laboratory. This means that the results obtained are only valid for NABE actions performed in the spring when fair weather is expected afterwards (during the spring and summer seasons).

CHAPTER 5

Smutz et al. (1980) stated that, when carrying out a beach scraping, the flatter the nearshore profile, the larger the accretion. This statement has been confirmed in our experiment. Such relationship with the nearshore profile can be seen, for example, through a comparison of the L2D and U2D (channels 5 and 6). In U2D, the borrow area was located next to the high tide level which caused a more dissipative beach profile during the high tide, while in L2D, the borrow area was located at the lower intertidal area and took the profile to more dissipative conditions only during mid-tide. During high tide, the water level stays almost stationary for longer periods than during mid-tide periods, when the water level changes rapidly. The longer duration of the wave action under the dissipative profile of U2D during high tide resulted in a stronger accretion effect. On the contrary, the short duration of dissipative conditions during mid-tide in L2D was not enough to obtain the same effectiveness in terms of accretion. Based on that, in places with a large tidal range, it is recommended to borrow the sediment from areas of the intertidal beach at the limit of the high tide level, in a way that more dissipative conditions are obtained during that tidal period.

Our experiments show that wave overtopping can cause an increase in berm height but not necessarily shoreline progradation. In nature, such processes frequently occur at the end of the summer season (September), when the wave period starts to grow and the wave runup increases. The accreted volume of sand generates a higher berm while beach width is preserved. It is important to highlight that a proper prediction of beach berm height is key for the success of NABE actions that intend to produce beach widening by placing the filling material on the beachfront (L2BF). By identifying the berm's height, it is possible to place the sediment just above the height of the future accretion berm and achieve an optimal use of the sediment to provide the maximum progradation of the shoreline. Figure 5.13 shows a scheme of two non-optimal design possibilities. If the sediment is placed above the height of the future berm (where no waves will reach), this sand could be reshaped to the beachfront, widening the dry beach even more (Figure 5.13b and Figure 5.5k and Figure 5.5l). On the other hand, without a proper estimate, the artificially generated berm may be placed below the current height level of the berm. In this case, the wave overtopping the berm will remove the sediment from the beachfront and place it over the berm, reducing progradation (Figure 5.13c and Figure 5.5j).

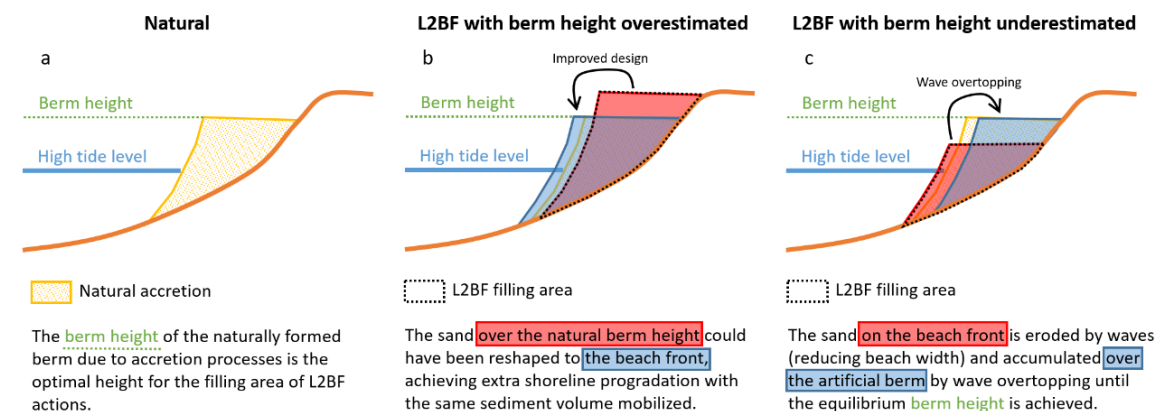


Figure 5.13 Non-optimal design scheme of the L2BF filling area.

Based on the relation between $TWL_{1\%}$ and the berm crest elevation found in chapter 3, in our experiments, we computed the wave runup over high tide level as a proxy to estimate the water level that induces the formation of the berm and related it to berm height. Note that in the laboratory the tidal range was equal for all the tidal cycles simulated, and therefore $TWL_{1\%} \equiv High\ Tide\ Level + R_2$. Following this approach, our results showed that Stockdon's et al. (2006) runup formulation overpredicted berm height in Test A and C but fell below the resulting berm's height in Test B (see reference levels in Figure 5.5). This can be explained by the fact that such formula was based on data from field experiments and some differences are expected when they are applied to scaled laboratory conditions (Gomes da Silva et al., 2020). However, despite the fact that the prediction did not match the resulting berm height perfectly, we consider that such values are accurate enough to be used as a first proxy estimate of berm height for scraping purposes on beaches. Obviously, more accurate formulations for the prediction of runup on reflective beaches are desirable for the design of beach scraping actions (note that this requires good estimates of the swash zone slope too).

Using sand from the borrow area to nourish the dune did not enhance progradation of the shoreline and further beach widening. However, such a technique may still be useful in areas where dune recovery is a priority. When sand is scraped for dune nourishment purposes, some aspects must be considered, such as dune design, space availability, and aeolian dynamics ("Coastal Dune Management," 2001). Pellón et al. (2020) provided useful tools for the design of foredunes (see Appendix II). The dune toe location and foredune volume can be determined as a function of local aeolian and marine conditions. Fencing and planting are also recommended, as the scraped sand may be removed and lost to offshore areas by future extreme wave events, or to inland areas through aeolian sediment transport (Conaway and Wells, 2005).

CHAPTER 5

Another point to consider when applying beach scraping is the ecological impact of such a technique. The upper part of the intertidal area is a habitat for macrofauna, and also a foraging, nesting, and breeding location for avifauna and turtles (Dare, 2003; Govarets and Lauwerts, 2009). The intertidal area is a highly variable and dynamic environment that changes frequently due to wave and tidal action. Thus, the species that live in this environment are expected to be adapted to frequent changes and therefore able to recover quickly from disturbances (Batton, 2007). Additionally, recolonization processes are determined by the duration and intensity of the works. In this sense, the analysed techniques are a 'short-term pulse' disturbance (Speybroeck et al., 2006) and it is believed that species can recover more easily than under the effect of other hard-engineering solutions. Smith et al. (2011) assessed the impact of beach scraping on macroinvertebrates and did not find a detectable effect on biodiversity. Besides, the correct management of the beach can provide new habitats such as a healthy and stable beach and dune. Furthermore, some authors propose timing the actions to avoid turtle nesting periods (Crain et al., 1995) or effects on migratory species (Erskine and Thompson, 2003). Both aspects are site-specific and must be considered during NABE design. Further studies on the specific effect of scraping and ploughing actions over the entire ecosystem, from the submerged area to the dune, are still necessary to have a complete view of the ecological impact of these techniques.

Finally, concerning the physical experiments, it should be mentioned that the morphologic changes caused by the Test waves in the laboratory occurred fast, in a period of only 2 to 4 tidal cycles. This might have been caused by the low-density sediment used, as a scale effect. The reduced dimensionless fall velocity in the model compared to the prototype may accelerate beach accretion as well. Such a quick response of the sediment impeded the development of accretion speed comparisons between the various NABE techniques used in our experiments. This study only analysed beach width and accretion on the beach berm achieved at the maximum accretion state. The obtention of larger accretion volumes could be interpreted as the result of a faster accretion process once wave action begins, with wider beaches being formed earlier in the summer by using these techniques. However, further research must be developed to ensure this desirable effect for touristic purposes.

The field experimentation allowed the confirmation of some of the effects observed at the laboratory. The scraping performed at Fuentebraví reproduced the L2BF variant tested at a reduced scale. The filling area of scraping actions was placed as a continuation of the winter berm. This led to the formation of a new summer berm in front of the mechanically created berm, as observed in Figure 5.5k and Figure 5.5l. The placement of

the filling area above the naturally generated summer berm is a design issue described in Figure 5.13b. This highlights the importance of having a good estimation of the summer berm crest elevation for the design of L2BF scraping actions. As mentioned above, the filling material could have been used to achieve larger dry beach widening since the beginning of the summer season.

As a result of the high position of the filling area, the scraping performed at Fuentebravía was representative of L2D scraping. The sand accretion was enhanced and the shoreline progradated faster during the first month. This matches the results obtained at the laboratory.

The sand volume mobilized by scraping was $5 \text{ m}^3/\text{m}$ of beach. This volume was lower than the $28 \text{ m}^3/\text{m}$ of beach finally accreted (at the end of the summer season) under natural conditions. This followed the recommendations of McNinch and Wells (1992) and Tye (1983), which indicate that the volume scraped should be less than the natural recovery rate of the beach. Nevertheless, the scraped volume could have been bigger, up to $5.6 \text{ m}^3/\text{month}$ measured on the natural profiles as the recovery rate for Fuentebravía beach. The volume scraped was limited by the capacity of the machinery and the duration of the low tide. However, scraping could have been repeated on several days during the summer until the maximum volume of sand ($28 \text{ m}^3/\text{m}$ of beach for Fuentebravía) was mobilized.

The statement of Smutz et al. (1980) that beach scraping enhances sand accretion has been confirmed at Fuentebravía beach, although this effect is limited to the first weeks after scraping actions. It is though that this effect is related to the presence of a hole in the borrow area, as suggested by Smutz et al. (1980). Once this hole is filled by accreted sand, the accretion acceleration effect vanishes.

5.6. CONCLUSIONS

The analysis of the results obtained in the reduced-scale laboratory experiments and the field experiments led to the following conclusions:

- The use of low-density synthetic sediment allowed the reduced scale simulation of a full beach profile under the simultaneous action of waves and tides. Five different Nature Assisted Beach Enhancement (NABE) techniques were tested and their effectiveness was determined by comparison to natural beach behaviour (control).

CHAPTER 5

- Beach berm geometry was mainly determined by marine dynamics. Incoming wave height and peak period conditioned berm height and swash zone slope with no effect from the NABE techniques on these variables. However, beach ploughing and scraping were related to shoreline position and dry beach width. When using these techniques, accretion volume was mainly determined by waves and the geometry of the berm, with variations due to the effect of NABE techniques. Generally speaking, the smaller the dimensionless fall velocity, the larger the accretion. Nevertheless, wave height and period may play a role, as Test A and C had similar dimensionless fall velocity, but for Test C the accretion could have been reduced by the low energy of the simulated waves.
- The recommended NABE technique depends on the objective. For beaches where a wider dry beach is sought, the recommended actions are ploughing or scraping, borrowing the sand from the low intertidal area and filling an intertidal bar or the beachfront (with a careful design of the berm geometry) during spring. For beaches where inland protection from erosion and flooding under winter storms is sought, the recommendation is borrowing sand from the intertidal area during spring (and preferably from the upper intertidal area) and nourishing the dune or the upper dry beach, where the sediment will be available to buffer the erosion caused by winter storms.
- Ploughing the intertidal area at each low tide demonstrated to be an effective technique to enhance beach accretion and achieve a wider dry beach. The combined effect of waves and tides makes ploughing effective and easy to apply.
- The creation of an intertidal bar by scraping the low intertidal area resulted in wider dry beaches. The sediment on the intertidal bar was partially accreted to the beach berm and partially eroded offshore.
- The generation of a berm by the scraping technique may produce wider beaches if adequately designed. The geometry of the berm generated by “machinery” highly influenced the results. The berm height and swash zone slope should match the naturally formed berm due to accretion. These berm’s geometric characteristics are difficult to predict as they depend on marine dynamics and they evolve throughout the summer season. The placement of sediment on the berm reduces the disequilibrium that triggers accretion and therefore the sediment volume that is naturally moved onshore is reduced. Additional research on the impact of berm geometry on accretion and dry beach width is required.
- The recommended borrow area for dune nourishment is the upper part of the intertidal area. The beach profile becomes more dissipative at high tide and this leads to

more disequilibrium between actual and equilibrium geometries, increasing onshore sediment transport and achieving larger accretion volumes.

- Further studies are needed to determine if NABE techniques can result in wider beaches as of the beginning of the touristic summer season or only at the maximum accretion state as was demonstrated in the laboratory.
- Field surveys on Fuentebravia beach during the summer season of 2021 allowed the analysis of the effectiveness of beach scraping in a real environment. The results match the conclusions obtained at the laboratory. Beach scraping enhanced sand accretion during the first weeks after machinery actions. The shoreline prograded 3.68 m more than the control area and the berm accreted 24 % of extra sand volume. Therefore, the dry beach was wider at the beginning of the touristic season. After the first weeks, natural and scraped measurements were similar. Further prototype testing is required to determine the full potential of beach scraping for dry beach widening and accretion enhancement.

CHAPTER 6

METHODOLOGY FOR THE APPLICATION OF NATURE ASSISTED BEACH ENHANCEMENT TECHNIQUES

6.1. INTRODUCTION

Decision makers demand tools and methodologies to implement nature-based solutions (NBS) effectively, aiming to improve the health and resilience of beaches. This thesis analyses nature assisted beach enhancement (NABE) techniques that are designed to enhance sand accretion with reduced human actions and taking advantage of the work done by nature. These techniques address the growing demand for wider dry beaches due to tourism while ensuring their long-term sustainability against the impacts of severe winter storms. Although scraping and ploughing are valuable tools for coastal managers, their application should be exercised with caution, limited to appropriate locations. It is important to note that these tools alone cannot resolve persistent erosion issues, which often require a thorough analysis of their underlying causes and corresponding remedial actions. To prevent improper utilization of those techniques, this chapter outlines a methodology for selecting and designing actions tailored to achieve site-specific coastal management goals.

The following methodology was designed according to the experience and knowledge gained during the development of this thesis. It comprises all the state-of-the-art recommendations and the new insights described in previous chapters.

CHAPTER 6

This chapter includes the general methodology in section 6.2, which is composed of three main steps: (1) selection of the most appropriate technique employing a decision tree, (2) description of the operational system that decides whether to apply a NABE technique on a particular date or not, and (3) the design of NABE actions. Then, the discussion is included in section 6.3, and finally, the conclusions are summarized in section 6.4. Altogether, this chapter meets the objective OB7 of this thesis.

6.2. METHODOLOGY

The methodology for the application of ploughing or scraping techniques is divided into three main steps:

- (1) Selection of the most appropriate NABE technique employing a decision tree.
- (2) Decision of whether to apply a NABE technique or not on a specific day given by an operational system.
- (3) Design of NABE actions. This step is divided into three options (3A, 3B, and 3C), that would be applied depending on the technique selected in step 1.

These steps are shown in Figure 6.1 and detailed in section 6.2.1, section 6.2.2, and section 6.2.3, respectively.

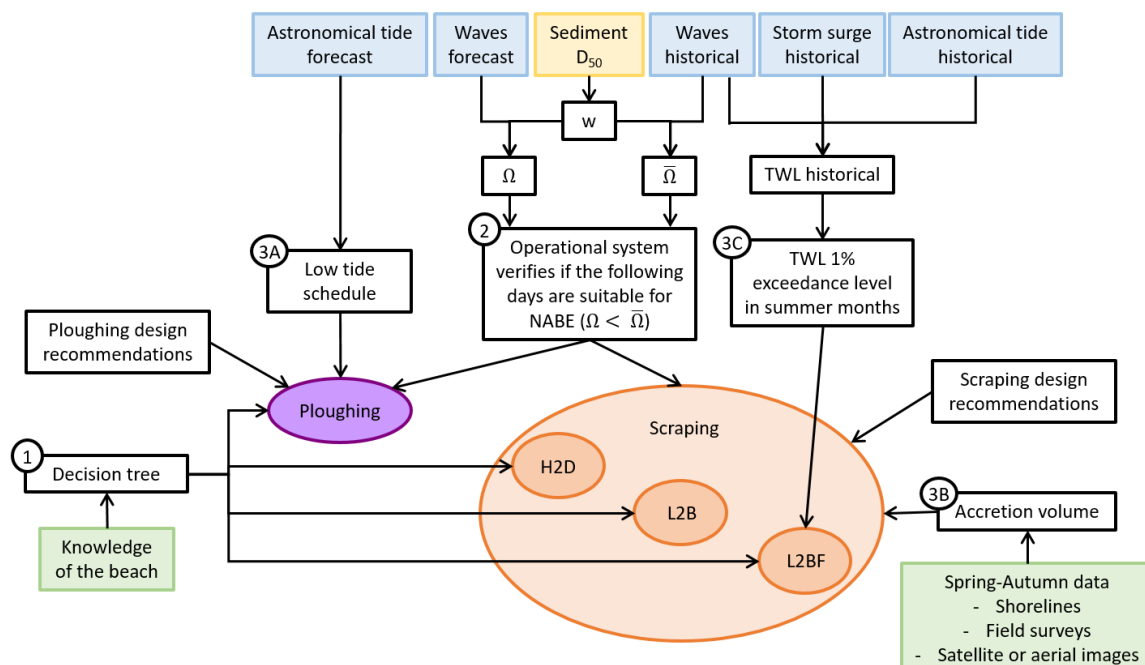


Figure 6.1 Methodology for the application of NABE techniques.

Each of the steps requires basic data on the specific location in which the NABE technique wants to be applied. These data comprehend: knowledge of the beach, sediment characteristics, wave and tides historical time series and forecast for the following days, and historical data of the spring-autumn beach variation. More details on these data can be found in the following sections. The knowledge required to manage these data and achieve the goal is given in the following description of the methodology.

6.2.1. Decision tree

The selection of the most appropriate NABE technique should be made with the support of the decision tree of Figure 6.2. This decision tree also indicates if NABE techniques are adequate for the study area or not. This methodology is only applicable to fine sand beaches (as the ones analysed in this thesis) without environmental restrictions in the area. Additionally, a basic requirement for the applicability of this methodology is the presence of seasonal variability on the beach (therefore the beach presents natural accretion that can be enhanced by NABE techniques).

Decision makers should have basic knowledge of the beach under study to be able to answer the questions included in the nodes of the decision tree. This basic knowledge is the following:

- If the beach is formed by fine sand.
- If there is seasonal variability.
- Whether the beach is in equilibrium or not. In case of noticeable and persistent erosion, NABE techniques are not the solution.
- The main objective pursued by the actions: Dry beach widening for touristic purposes or increase the sediment budget for winter storms.
- The approximated width of the intertidal area. This thesis analysed fine sand beaches on meso/macro-tidal environments, and therefore the intertidal area was wide enough to perform scraping or ploughing. If the intertidal area is too narrow, there will not be enough space for the NABE techniques of this thesis.
- Availability of data that allows the quantification of accretion or dry beach widening during previous summer seasons. These data should be available at least in spring and autumn of the same year and can be shoreline position data, field survey data, and/or satellite or aerial images that allow shoreline identification.
- Availability of easy access for machinery to the beach.

CHAPTER 6

All this basic knowledge should be used to answer the questions of the decision tree to determine the most appropriate NABE technique for the beach under analysis. Once the technique has been selected, the decision-maker should continue in step 2 of the methodology.

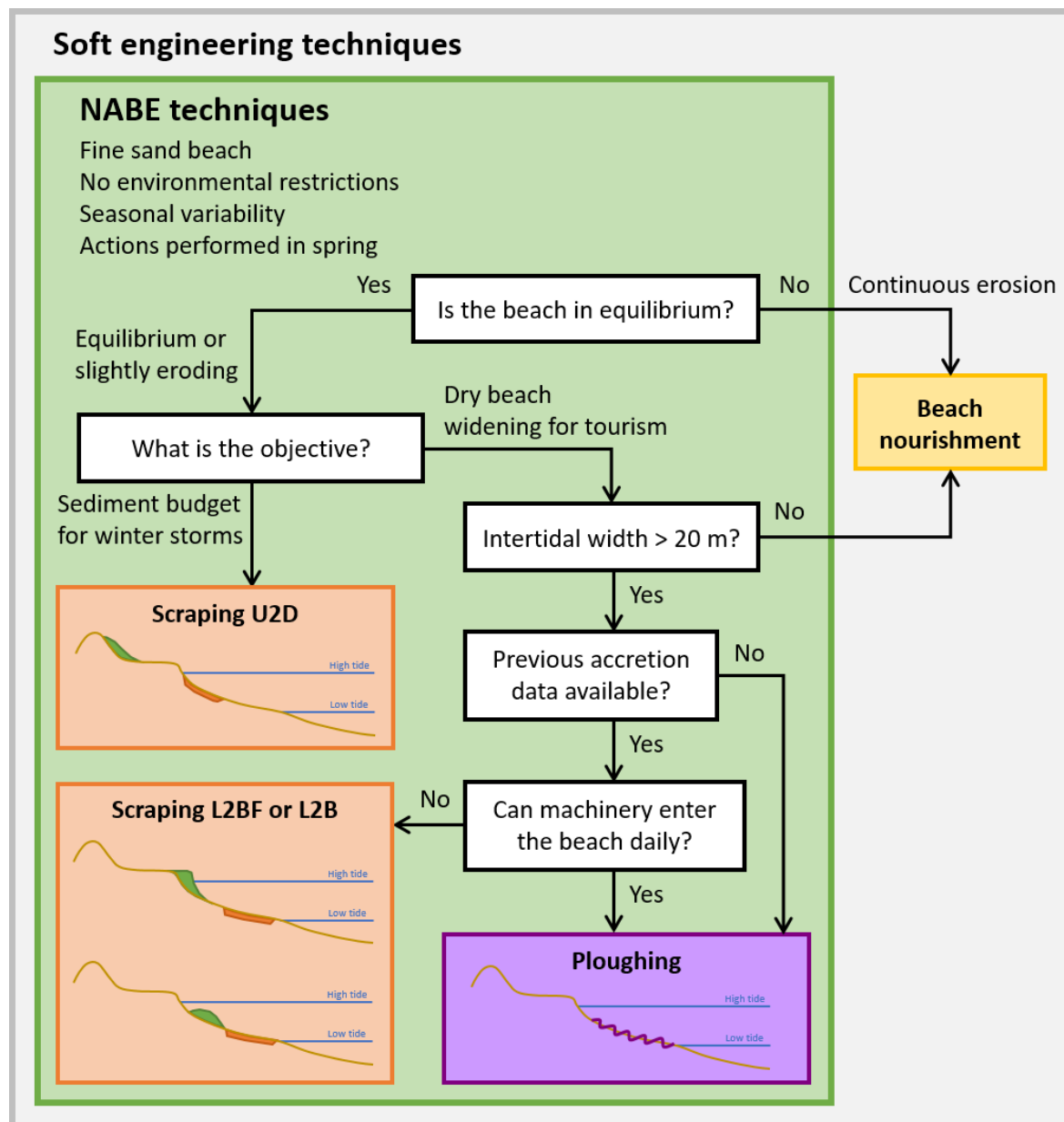


Figure 6.2 Decision tree to choose the best NABE option for a beach.

6.2.2. When to perform a NABE technique or not

NABE techniques should be applied in spring when calm marine conditions are expected. Nevertheless, sometimes an unexpected spring storm can hit the coast under study and we should prevent its impact on scraped or ploughed beaches. For this reason, the setup of an operational system that determines if fair weather conditions are foreseeable is required. The characteristics of this operational system are detailed in the following.

Besides, another point to consider when applying beach scraping or ploughing is the ecological impact of such a technique. The upper part of the intertidal area is a habitat for macrofauna, and also a foraging, nesting, and breeding location for avifauna and turtles (Dare, 2003; Govarets and Lauwers, 2009). The intertidal area is a highly variable and dynamic environment that changes frequently due to wave and tidal action. Thus, the species that live in this environment are expected to be adapted to frequent changes and therefore able to recover quickly from disturbances (Batton, 2007). Additionally, recolonization processes are determined by the duration and intensity of the works. In this sense, NABE techniques are a ‘short-term pulse’ disturbance (Speybroeck et al., 2006) and it is believed that species can recover more easily than under the effect of other hard-engineering solutions. Smith et al. (2011) assessed the impact of beach scraping on macroinvertebrates and did not find a detectable effect on biodiversity. Furthermore, the correct management of the beach can provide new habitats such as a healthy and stable beach and dune. Nevertheless, some authors propose timing the actions to avoid turtle nesting periods (Crain et al., 1995) or effects on migratory species (Erskine and Thompson, 2003). Both aspects are site-specific and must be considered during NABE design.

Once the periods with ecological relevance have been identified and avoided, the rest of the dates of spring should be analysed with the operational system to determine if they are appropriate for the application of NABE or not. The operational system uses the marine dynamics and the sediment characteristics as input, and checks if $\Omega < \bar{\Omega}$, where Ω is the Dean number in the following days (forecast) and $\bar{\Omega}$ is the average value of the Dean number for the historical wave data. If the condition is met, accretion is expected on the following days, and no spring storm is foreseeable, therefore NABE actions can be applied. This operational system should be consulted the day before the machinery actions. Note that ploughing should be performed every day if the operational system recommends it, and scraping can be performed several times during the spring, up to mobilizing the maximum recommended volume (naturally accreted volume), as detailed in step 3 of the methodology.

CHAPTER 6

The parameter $\bar{\Omega}$ can be precomputed at the beginning of the summer season as the average of hourly dimensionless fall velocity or Dean number Ω (Dean, 1973; equation (6.1)):

$$\Omega = \frac{H_s}{wT_p} \quad (6.1)$$

where H_s is the significant wave height, T_p is the wave peak period, and w is the fall velocity of grain particles (Hallermeier, 1981) which depends on the sediment characteristics (median sediment grain size; d_{50}).

Ω should be computed for the historical hourly time series of waves in front of the beach under study. Historical time series of waves are available from reanalysis databases. Then, the average of the complete time series gives the parameter $\bar{\Omega}$ for this beach.

Then, forecast wave characteristics are needed for the computation of Ω in the following days. If $\Omega < \bar{\Omega}$ in the following 7 days, NABE actions can be performed.

6.2.3. Design of NABE actions

Each NABE action requires particular data for its design. In this section, the design recommendations given by previous authors (Carley et al., 2010) and learned through the development of this thesis are detailed. Additionally, details on how to compute the required data for the design of scraping and ploughing are also given here.

Section A includes the guidelines that describe how to perform ploughing (step 3A of the methodology), section B summarizes the guidelines for the implementation of scraping (step 3B), and section C details the procedure required for the design of the filling area of L2BF (from lower intertidal to beachfront) scraping variant (step 3C). The section for the design of actions should be chosen according to the NABE technique selected in step 1 of the methodology.

A. Design of ploughing

Ploughing is performed during the low tide hours. Astronomical tides can be forecasted easily, and the schedule of the daily low tides is freely available on the internet for any location (at least for the Spanish coasts). In the case of semidiurnal tides, the one

that occurs during the daylight should be chosen to ensure the safety of the operations. Additionally, the hours with less affluence of people on the beach are preferable. These criteria allow the generation of a schedule of the hours of daily minimal tidal level during spring. The ploughing actions can be performed from two hours before to two hours after the minimum tidal level occurrence. The requirements of machinery can be computed based on machinery performance, the availability of four hours working window, and the extent of the beach.

Besides, it is important to adhere to the following recommendations when implementing ploughing:

- The trajectory of the tractor should be parallel to the low tide shoreline. This means that ridges and furrows are created parallel to the shoreline as well.
- It is preferable to generate the ridge on the landward side of the furrow.
- There should be enough rows of ploughing to cover the maximum width of the intertidal area, from the low tide shoreline to the high tide shoreline marks. Do not plough the dry beach area.
- The maximum depth of the furrows should be 0.3 m.

B. Design of scraping

One of the recommendations of Carley et al. (2010) for scraping is the limitation of the maximum mobilized volume that should be less than the naturally accreted volume during the summer season (the one produced with no NABE actions applied). The volume of accretion depends on the beach under study and the incoming marine dynamics. The calculation of this volume requires data on the evolution of the beach in previous summer seasons (from spring to autumn). The valid data for this purpose (options are given in order of preference to improve the precision of the result) and how to estimate the natural accreted volume is detailed in the following:

- Topographic field surveys of the dry beach and intertidal area (up to the low tide limit) performed in spring and autumn of the same year. The surveys can cover the full topography of the beach or only beach profiles. The difference between the sand elevation in spring and autumn allows the computation of the accreted volume.
- Shoreline position data of spring and autumn of the same year. Note that the tidal level may influence the shoreline position. Therefore, the shoreline position should be corrected to the high tide level (SP_{HT}). The natural accretion volume per meter of length of the beach can be estimated with equation (6.2)

CHAPTER 6

under the hypothesis that the nodal point of accretion (Phillips et al., 2019) is formed around the mid-tide level (Figure 6.3):

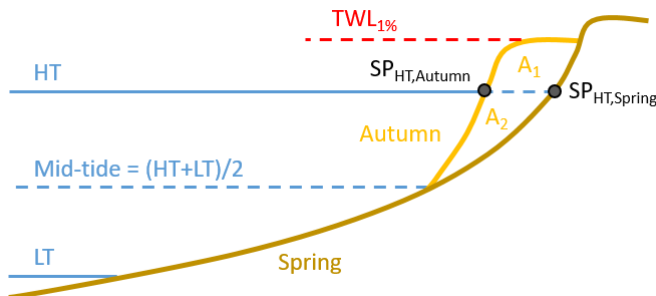


Figure 6.3 Natural accretion volume estimation scheme.

$$\begin{aligned}
 \text{Natural Accretion Volume} &= A_1 + A_2 \\
 &= (SP_{HT,Autumn} - SP_{HT,Spring}) * (TWL_{1\%} - HT) \\
 &\quad + \frac{1}{2} * (SP_{HT,Autumn} - SP_{HT,Spring}) * \frac{HT + LT}{2} \\
 &= (SP_{HT,Autumn} - SP_{HT,Spring}) * \left((TWL_{1\%} - HT) + \frac{HT + LT}{4} \right)
 \end{aligned} \tag{6.2}$$

where SP_{HT} is the shoreline position at high tide (in spring and autumn), $TWL_{1\%}$ is the summer average of the total water level exceeded 1% monthly (see section 6.2.3.C for details on how to compute it), HT is the high tide level, and LT is the low tide level.

- Satellite or aerial images that allow shoreline identification in spring and autumn of the same year. Once the shoreline position is identified, equation (6.2) can be applied.

Ideally, as the accretion volume depends on the marine dynamics (that can be different among summer seasons), the natural accretion volume should be estimated for as many years as possible and the final maximum volume for scraping computed as the average of all years.

Besides, it is important to adhere to the following recommendations when implementing scraping:

- The maximum depth of the borrow area should be 0.3 m.

- Scraping can be performed on various days during spring. The sum of all the scraped volumes should not exceed the maximum scraping volume described above. A minimum lag of time of 15 days between scraping operations is recommended.

The width of the borrow area can be calculated as the maximum volume for scraping (or the chosen volume if scraping is performed on various days) divided by the recommended borrow area depth (0.3 m). The performance of the scrapers would determine the machinery required to perform the scraping during a working window of four hours around the low tide (see section 6.2.3.A).

Note that the placement of the borrow area depends on the variant of the scraping technique. L2B and L2BF take the sand from the low intertidal area, and therefore, the borrow area should approach the low tide limit as much as possible. On the contrary, U2D take the sand from the upper intertidal area, and therefore, the borrow area should start from the high tide limit towards the sea.

The tools provided by Pellón et al. (2020), and summarized in Appendix II, are recommended for the design of the filling area when the scraped sand is used for dune nourishment (U2D). Foredunes constitute a sediment budget for winter erosion. The foredune has a volume and position of equilibrium according to the aeolian and marine dynamics of the study area. Therefore, the scraped sand should be placed according to these geometric parameters to build an equilibrium foredune that will last longer. As stated by Pellón et al. (2020), the foredune toe should be located at the level of the total water level of 10 years of return period. This means that the foredune would only be eroded once every 10 years, and consequently, vegetation would have enough time to develop. The equilibrium foredune volume can be estimated according to the marine dynamics or the aeolian dynamics. The difference between the equilibrium foredune volume and the actual volume of the dune may help to determine the sand requirements of scraping. Note that the scraped volume must not exceed the natural accretion volume and therefore more than one year of scraping may be necessary for the complete recovery of the foredune (or additional external sand sources). The conceptual model of foredune morphology described in Pellón et al. (2020) and Appendix II may help to understand the behaviour of foredunes. Tools for the calculation of the foredune toe position and the foredune volume are provided in Pellón et al. (2020) and Appendix II.

CHAPTER 6

C. Design of L2BF scraping option

The faster dry beach widening is achieved by the L2BF (Lower intertidal to Beachfront) variant of scraping. In this case, the borrow area is located in the low intertidal area and the sand is placed on the beachfront, extending the dry beach towards the sea. The design of the filling area is fundamental for the success of the actions. The naturally formed summer berm presents a crest elevation that matches the $TWL_{1\%}$ level. Placing the sand in a higher position will lead to less dry beach gain, and placing it in a lower position can cause the retreat of the machinery-created high tide shoreline by wave overtopping the berm crest.

Therefore, the artificially created berm of L2BF technique should try to mimic this natural berm crest level. Note that $TWL_{1\%}$ (and the berm crest level) is a dynamic variable that evolves monthly. According to the observations of this thesis, it has an approximately constant value from May to August and rises in September and October. As a consequence, we propose $\overline{TWL}_{1\%}$ as a first proxy for the berm crest level. The procedure to calculate this value is described in the following and can be computed as the mean of monthly $TWL_{1\%}$ values during the summer season.

The $\overline{TWL}_{1\%}$ is the average of the $TWL_{1\%}$ values during the summer months (from May to October) excluding the months that had storms if any. Storm conditions refer to significant wave heights above the 5% exceedance level for a minimum duration of one tidal cycle during which $\Omega > 4$ (Phillips et al., 2019). Figure 6.4 shows a scheme that illustrates the procedure to compute $\overline{TWL}_{1\%}$. This procedure is structured in the following steps:

- (1) The TWL historic time series can be obtained as the sum of the historical series of the astronomic tide, storm surge, and the wave runup (R_2), obtained with Stockdon's et al. (2006) formulation (equation (5.24)) from historical wave data time series. All these data must be obtained in the proximity of the beach under study (around 20 m depth).
- (2) Then the time series of TWL should be split into monthly periods, with cutting points in the highest monthly spring tide, and the spring and summer months without storms (significant wave height above the 5% exceedance level with a minimum duration of one tidal cycle and $\Omega > 4$) selected.
- (3) The total water level exceeded 1% of the time ($TWL_{1\%}$) should be computed for the selected summer months of the historic TWL time series. The cumulative distribution function (CDF) is computed for each of the monthly TWL series.

Then, the 1% exceedance level is extracted as the 0.99 probability level, which gives the $TWL_{1\%}$ for each month.

- (4) Finally, the average of those monthly $TWL_{1\%}$ values gives the $\overline{TWL}_{1\%}$. This value should be computed with the monthly values of at least one year, but several years can be considered if there is data available.

According to the findings of this thesis, we propose this level as an approach for the summer berm crest elevation, and therefore the filling material of L2BF scraping technique should be placed on the berm up to this height.

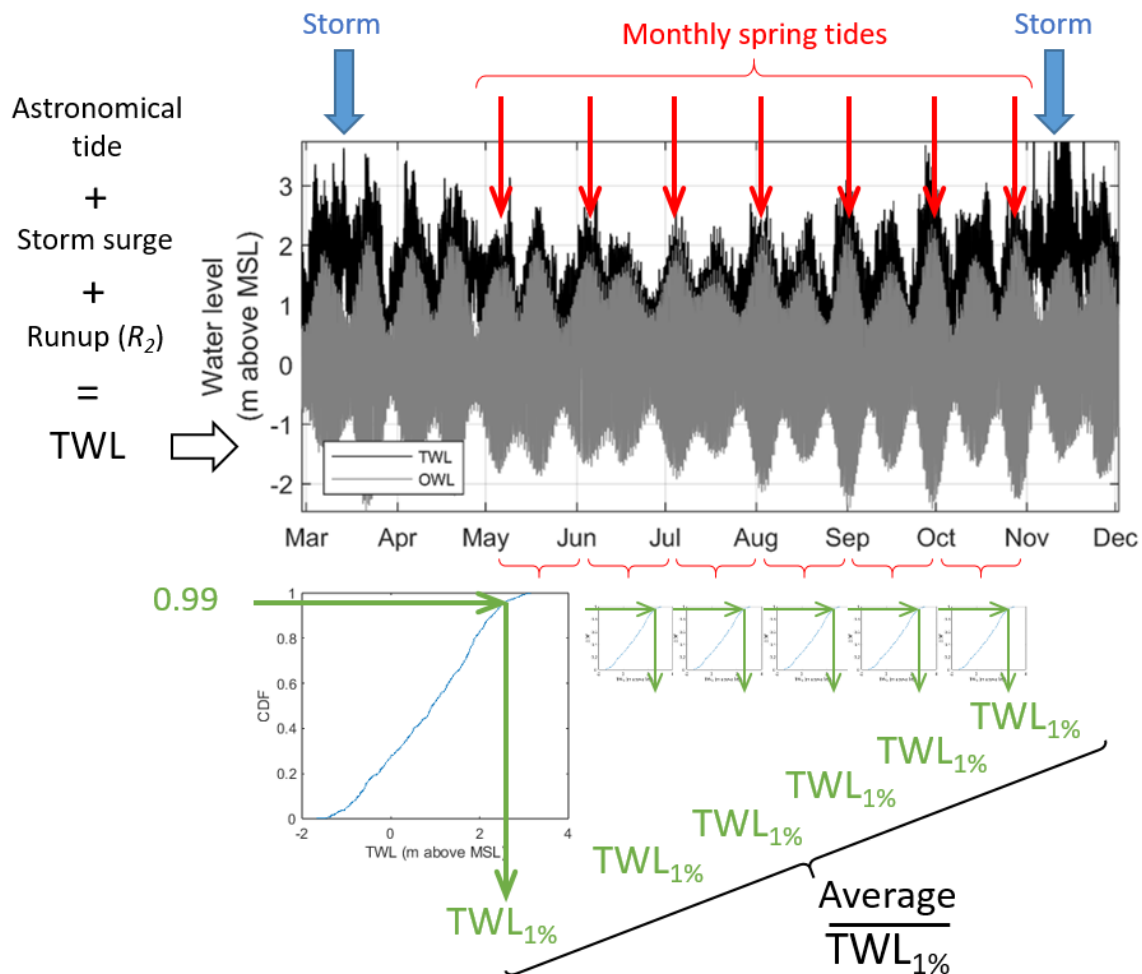


Figure 6.4 Scheme of the procedure to compute $TWL_{1\%}$.

CHAPTER 6**6.3. DISCUSSION**

Decision-makers may benefit from this methodology when applying NBS to their beaches. This methodology not only takes into account beach sustainability but also considers goals such as beach widening for touristic purposes (economic profitability) as the main reason for the application of NABE techniques. This is the first time that the touristic point of view (through dry beach widening) is considered in the development of guidelines for the application of NABE techniques. Additionally, it is also the first time that ploughing is proposed as a coastal management tool. Previous authors focused on the application of scraping to improve beach health to face winter storms. This was achieved by means of a sediment budget increase by filling the beachfront or nourishing the dune with scraped sand. Our methodology presents a wider scope and integrates both objectives, describing the necessary calculations for the design of the actions for the implementation of the most appropriate NABE technique according to the coastal management goal.

The techniques differ on the frequency of the actions (daily for ploughing but not for scarping), the data requirements for its design (no data for ploughing and accretion volume –among others- for scraping), and the machinery required (ploughing tool or scrapers). The cost and the ecological impact of both techniques are minimal compared to other soft engineering tools such as beach nourishment.

The recommendations are based on the suggestions of previous authors (Carley et al., 2010; Crain et al., 1995; Erskine and Thompson, 2003; Gainza et al., 2019) and our own experience. Most of these suggestions were thought for scraping, although we consider that are also appropriate for ploughing. Both techniques act over the intertidal area and affect the same marine dynamics (mainly wave breaking) and the macroinvertebrates of the intertidal beach.

With the objective of working with nature when ploughing the beach, it is recommended to create the ridge on the landward side of the furrow. This adds a third component to the onshore sediment transport. The first component is the enhancement of the suspended sediment transport by wave breaking over the ridges. The wave dissipation generates hydrodynamic conditions (wave-current-level) that favour onshore sediment transport. The second component is the bottom sediment transport generated by the onshore migration of the ploughed bedforms. Finally, the third component is the mechanical movement of the volume of sand from the furrow to the ridge, and its cumulative effect of ploughing every day towards the landward side. The three components aid accretion and are schematized in Figure 6.5.

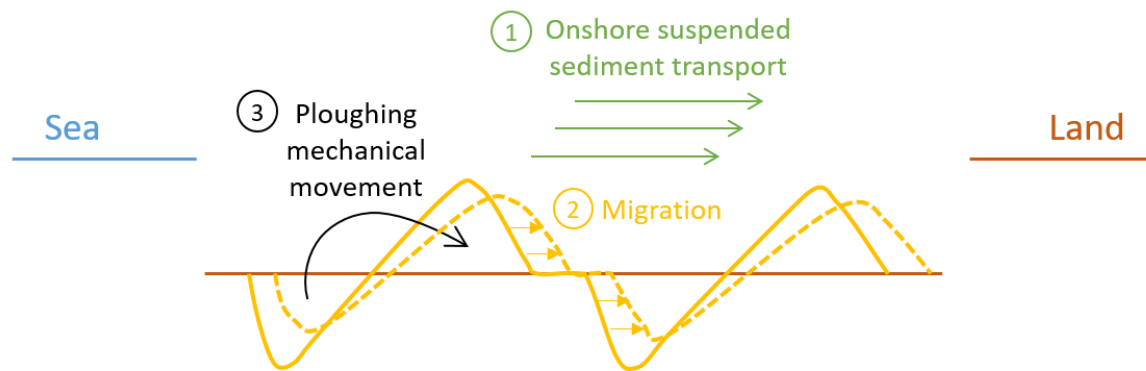


Figure 6.5 Scheme of the three components that enhance onshore sediment transport when ploughing is applied.

Foredunes are important sand reservoirs to fight against winter erosion and flooding. The maintenance of healthy dunes is key for the long-term equilibrium of beaches. According to the conceptual model developed by Pellón et al. (2020) and summarized in Appendix II, the foredune periodically erodes and recovers. The erosion is produced by extreme wave events (10 years of return period) and removes part of the sand from the foredune toe. Then, this sand is recovered slowly by aeolian sediment transport that moves the sand from the dry beach to the foredune. This recovery process can be accelerated by foredune nourishment. The scraping variant U2D is an example of a tool that accelerates this natural recovery with the aid of machinery. The foredune has an equilibrium volume and position and therefore, the sand borrowed by scraping should be placed according to these geometrical constraints. Pellón et al. (2020) provide tools for the calculation of those foredune design parameters (also shown in Appendix II).

The application of NABE techniques should be done when accretion is foreseeable in the following days. The characteristics of marine dynamics and morphology of the beach that define the threshold between accretion or not are still unclear. According to the findings of this thesis, and the decision tree (Figure 2.2) proposed by Phillips et al. (2019), accretion is ensured for mild wave conditions ($\Omega < \bar{\Omega}$). Although bigger values of the dimensionless fall velocity parameter can also produce accretion, we decided to propose the aforementioned more conservative limit for the operational system described in section 6.2.2. This limit can be redefined in the future if a more precise limit of accretion is found. This would produce an increment of the days that are suitable for the application of NABE actions.

CHAPTER 6

Future lines of research may improve the methodology in the future. In this sense, the methodology has been designed flexible and easily adaptable to new findings. Some of the foreseeable improvements are:

- New NABE techniques can be easily included in the decision tree.
- New insights into the limits of marine conditions that trigger accretion can be used to improve the criteria of the operational system.
- Optimizations of the design of ploughing or scraping geometry can be incorporated in step 3 of the methodology.

Monitoring of NABE actions on prototype beaches is encouraged for the improvement of those innovative techniques and consequently this methodology.

6.4. CONCLUSIONS

The methodology proposed here discusses the implementation of nature-based solutions (NBS) for beach enhancement, specifically focusing on nature assisted beach enhancement (NABE) techniques. The following conclusions can be drawn from this chapter 6:

- NABE techniques, such as ploughing and scraping, are designed to enhance sand accretion by taking advantage of natural processes, reducing the reliance on human interventions. Additionally, both techniques are applied with terrestrial means, making them inexpensive and easy to apply with widely used machinery (for crops and civil works, plough and scrappers respectively).
- While scraping and ploughing can be valuable tools for coastal management, their application should be exercised with caution and limited to appropriate locations. These techniques alone cannot solve persistent erosion problems, which require a thorough analysis of underlying causes and remedial actions. The NABE techniques proposed here are suitable for their application during spring on sandy beaches that present seasonal variability and do not have environmental restrictions.
- To ensure the proper selection and design of NABE actions, a methodology is outlined, consisting of three main steps: selecting the most appropriate technique using a decision tree, determining whether to apply NABE techniques based on an operational system, and designing NABE actions tailored to the specific site's coastal management

goals. The data required for decision-making and the design of actions is easily accessible, and the calculations are simple.

- The decision tree assists in selecting the suitable NABE technique by considering factors such as beach equilibrium, management goals, intertidal area width, and availability of data on accretion.
- The operational system helps to determine whether to apply NABE techniques based on marine dynamics, particularly by comparing the Dean number (Ω) forecasted for the following days with the average historical Dean number ($\bar{\Omega}$). Only when favourable conditions for accretion occur ($\Omega < \bar{\Omega}$) NABE actions should be applied.
- The importance of considering the ecological impact of NABE techniques is emphasized. It is particularly important to consider macrofauna, nesting periods and migratory species. Timing of actions should be planned to avoid critical ecological periods.
- The design of NABE actions varies depending on the chosen technique. Ploughing is performed every day during low tide hours, while scraping has specific recommendations regarding the maximum mobilized volume, borrow area depth and filling area design. When the filling area is an artificially created berm, the berm crest height should match the summer-average of monthly total water level exceeded 1% of the time. Besides, when the scraped sand is used for foredune nourishment, a site-specific design should be performed.
- The presented methodology aims to support decision-makers in implementing NABE techniques effectively while considering beach sustainability and touristic objectives. It provides guidelines for the technique selection, operational system setup, and action design, based on previous research and practical experience gained throughout the development of this thesis.
- The methodology is adaptable to incorporate new NABE techniques, refine operational criteria based on future research, and optimize design geometries. The monitoring and evaluation of NABE actions is encouraged for continuous improvement.

CHAPTER 7

CONCLUSIONS AND FUTURE RESEARCH

7.1. CONCLUSIONS

Beach accretion is an important process that produces beach recovery after storms. This thesis analyses accretion and the effectiveness of Nature-Based-Solution to enhance beach recovery. The following conclusions have been derived from this thesis.

Conclusions on natural beach accretion

Chapter 3 analysed the natural beach recovery during the full summer season in three meso/macro-tidal study sites by means of a total of 24 field surveys. Berm formation and growth were observed in the 15 beach profiles analysed. The relation between morphologic changes and marine dynamics was analysed and the following objectives were addressed:

- OB1. Improve the knowledge of accretion on meso/macro-tidal beaches, considering the influence of marine dynamics.
- OB2. Perform field surveys on meso/macro-tidal beaches that cover the full recovery during the summer season.

The conclusions derived from the analysis of chapter 3 are the following:

- The beaches of Fuentebravía (Cádiz), El Sardinero I and II (Santander), Somo, and Loredo (Somo) were surveyed from April to October. These measurements allowed the

CHAPTER 7

observation of the berm formation and growing, characterizing the **full recovery of the beaches during the summer season.**

- The use of simple surveying methodologies, such as the use of a distancemeter device, has proven to be accurate and inexpensive.
- In meso/macro-tidal environments, tidal range variations among a **spring-neap-spring tidal cycle** condition berm development. The **morphologic evolution** during successive tidal cycles **is complex**. Between spring and neap tides (decreasing high tide level reached), accretion is minimum and berm geometry changes are small. After neap tides, a new berm appears with a low crest level, according to the lower high tide level reached. As the tidal range increases towards spring tides (and high tide level rises), the crest of the new berm is overtapped producing berm aggradation. Finally, **at spring tides the berm stabilizes as part of the beachface.**
- The **analysis of beach recovery during summer can be performed by surveying on a monthly basis on the date of the larger spring tide**. In these dates, the berm crest level is maximum and the accreted volume is representative of the sediment stable on the beachface. This avoids the need to interpret the complex and ephemeral variability present in between spring tides and minimises the effort required to characterize the whole recovery of the beach.
- During the **first months** of the summer season beach accretion produces **shoreline progradation**.
- **Berm aggradation** is produced when the total water level (TWL) is exceeded at least 3% of the time in the previous month. **On the Atlantic coasts of Spain, this occurs typically in September and October**, due to the concomitant effect of equinoctial spring tides and longer wave periods that increase the runup and the TWL.
- The **berm crest elevation reached every spring tide can be explained by** the total water level exceeded 1% of the time during the previous month (**$TWL_{1\%}$**). Therefore, berm crest elevation can be predicted by a statistical analysis of the TWL time series of previous summer seasons.
- **Sand accretion rate** presents a **relation with the average equilibrium dimensionless fall velocity (Ω_∞) on the previous month** to each observation. Nevertheless, this relation **is weak** and two clear exceptions were found.

Conclusions on beach ploughing

Beach ploughing was analysed for the first time under laboratory-controlled conditions at prototype scale (1:1) and reduced scale (1:8). The analysis performed at prototype scale comprehends two sets of experiments that have been detailed in chapter 4. Set 1 explored the effect of mechanically ploughing the intertidal area of a beach. Set 2 of experiments allowed the analysis of ploughing morphodynamics until their smoothing by wave action, as well as the characteristics of other bedforms that naturally appeared during the tests. Besides, the analysis of ploughing at a reduced scale was shown in chapter 5, allowing the comparison of the results with scraping technique. Those analyses address the aspects relative to beach ploughing of the following objectives of the thesis:

- OB3. Perform laboratory experiments that allow the analysis of NABE techniques under controlled conditions.
- OB4. Analyze if scraping and/or ploughing techniques produce dry beach widening for touristic purposes.
- OB5. Analyze if scraping and/or ploughing techniques increase the volume of sand accreted at the end of the summer, which will be available as a sediment budget to fight against winter erosion and flooding.
- OB6. Evaluate the effectiveness of nature assisted beach enhancement techniques for the acceleration of beach recovery on meso/macro-tidal beaches.

The analysis of ploughing yielded the following conclusions:

- **Ploughing** the intertidal area at each low tide demonstrated to be an effective technique to **enhance beach accretion and achieve a wider dry beach**. The combined effect of waves and tides makes ploughing effective and easy to apply.
- The data collected at a prototype scale (1:1) demonstrate that **ploughing has a positive effect on increasing natural beach accretion rates** for all water levels that were tested. Both accreted sediment volumes and sediment transport rates are larger on the ploughed side than on the natural control side of the experiments.
- The analysis of the Set 2 of experiments showed that ploughing smooths and almost **disappears after 2–3 h of wave action** under constant water level tests. Therefore, **ploughing should be repeated on several low tides** to achieve a cumulative effect.

CHAPTER 7

- Spectral analysis of the bedforms, for the longer duration tests of Set 2, allowed their separation into two main components: ploughing and rippling. Their morphometric characterization is summarized in Table 7.1.

Table 7.1 Morphometric characteristics of ploughing and rippling.

Characteristic		Ploughing	Ripples
Wavelength		1.62±0.05 m	0.28±0.01 m
Height	Test A	~0.3 m of initial height and	0.011±0.003 m
	Test B	below 0.06 m at 2 h	0.016±0.004 m
Onshore migration speed	Test A	0.18 m/h	0.36±0.15 m/h
	Test B	0.25 m/h	0.33±0.11 m/h
Slip face slope		Initial 34° to 5° at 3 h	-
		Initial 23° to 5° at 3 h	-
Other		0.075 m ² of ridge initial area, decreasing exponentially to 0.006 m ² after 2 h	Ripples formed over the ploughed larger bedforms and migrated faster onshore

- The analysis of Set 1 and 2 of experiments showed that **ploughing produces three effects for accretion enhancement**. Details on each component are given in the following:

1) Enhancement of the suspended onshore sediment transport. Ploughing increases bottom roughness, which generates extra wave dissipation by wave breaking over the ridges. The suspended sediment increase due to enhanced wave breaking and the hydrodynamic conditions (wave-current-level) generated, favour onshore sediment transport. The following measurements evidence this mechanism.

- **Ploughing generated artificial bottom roughness** ($k_o \approx 0.4$ m at the beginning of each test), which progressively smoothed due to wave action. The roughness reduced ~50% during the first hour, and decreased to $k_o \approx 0.1$ m at the second hour and later, accounting for ripples over the bottom. On the natural control side, the roughness was always lower than that on the ploughed side, with a maximum of $k_o \approx 0.06$ m at the end of each test.
- **The extra bottom roughness produced more wave dissipation** at the ploughed side of the experiments. A comparison of the significant wave height measured at the onshore end of the sandy area showed that H_s was always smaller at the ploughed side (for all the tests and during the whole duration). The wave energy at the shoreward end of the ploughed area was a maximum of 45%

lower on the ploughed side for wave frequencies of 0.175 Hz (the peak frequency of the waves generated is 0.143 Hz) and 0.055 Hz. Bottom friction, due to a final bottom roughness that was 3.57 times larger (after 1 h of wave action), is proposed as the main cause of this extra energy reduction

- The shoreward half of the study area showed greater wave dissipation rates. Therefore, it is expected that a longer cross-shore extent of ploughing would lead to an enhancement of wave dissipation and accretion effects.
- ADV measurements showed that onshore sediment transport on the ploughed side can be enhanced due to **currents that are stronger if directed onshore or weaker if directed offshore**.
- SSC measured by OBS sensors showed larger concentrations of suspended sediments in 80% of the tests performed.
- This lower significant wave height and favourable currents produced more accretive conditions on the **ploughed side**, as demonstrated by **higher accretion rates** measured on the trap box of this side (up to 40% larger rates depending on the test). The artificially created bottom roughness was the main cause of this accretion enhancement.

2) Enhancement of the onshore bottom sediment transport.

- The **migration of the bedforms was onshore directed and produced sediment transport** rates up to $61 \text{ kg m}^{-1} \text{ h}^{-1}$ for ploughing at the beginning, which progressively decreased below $10 \text{ kg m}^{-1} \text{ h}^{-1}$ after the second hour. The ripples also produced onshore sediment transport rates of approximately $4 \text{ kg m}^{-1} \text{ h}^{-1}$. These rates produced additional accretion that was not measured in the trap box and was caused by the migration of bedforms.

3) Landwards mechanical movement.

- The mechanical movement should be performed by moving the sand from the furrow (on the seaward side) to the ridge (on the landward side). The cumulative effect of **mechanically ploughing every day towards the landward side aids accretion**.
- The experiments at a reduced scale (1:8) demonstrate that **ploughing** is a useful technique to enhance beach recovery, achieving an average of **extra shoreline progradation, and increasing the volume of sediment** (up to 37% of extra volume) available on the upper part of the beach profile **to fight against winter erosion**.

CHAPTER 7

Conclusions on beach scraping

Beach scraping was analysed under laboratory-controlled conditions at a reduced scale (1:8). The experiments include four different geometries of scraping, with different borrow and filling areas:

- L2B: Sand borrowed from the lower intertidal area and placed in an intertidal bar.
- L2BF: Sand borrowed from the lower intertidal area and placed on the beachfront.
- L2D: Sand borrowed from the lower intertidal area and placed in the dune or upper dry beach.
- U2D: Sand borrowed from the upper intertidal area and placed in the dune or upper dry beach.

Additionally, the variant L2BF was also tested at Fuentebravía beach (Cádiz).

Those experiments are detailed in chapter 5 and address the aspects relative to beach scraping of the objectives OB3, OB4, OB5, and OB6 of the thesis.

The analysis of scraping yielded the following conclusions:

- The use of **low-density synthetic sediment allowed the reduced scale (1:8) simulation** of a full beach profile under the simultaneous action of waves and tides. **Five** different Nature Assisted Beach Enhancement (**NABE**) **techniques** (four scraping geometries and ploughing) were tested and their effectivity was determined by comparison to natural beach behaviour (control).
- **Beach berm geometry was mainly determined by marine dynamics.** Incoming wave height and peak period conditioned berm height and swash zone slope with no effect from the NABE techniques on these variables. However, **beach ploughing and scraping were related to shoreline position and dry beach width.** When using these techniques, accretion volume was mainly determined by waves and the geometry of the berm, with variations due to the effect of NABE techniques. Generally speaking, the smaller the dimensionless fall velocity, the larger the accretion. Nevertheless, wave height and period may play a role.
- **The creation of an intertidal bar by scraping the low intertidal area (L2B) resulted in wider dry beaches.** The sediment on the intertidal bar was partially accreted to the beach berm and partially eroded offshore.

- **The generation of a berm by the scraping technique (L2BF) may produce wider beaches if adequately designed.** The geometry of the berm generated by “machinery” highly influenced the results. The berm height and swash zone slope should match the naturally formed berm due to accretion. These berm’s geometric characteristics are difficult to predict as they depend on marine dynamics and they evolve throughout the summer season. The placement of sediment on the berm reduces the disequilibrium that triggers accretion and therefore the **sediment volume that is naturally moved onshore is reduced**.
- All the variants tested show that **scraping** is a useful technique to enhance beach recovery, **increasing the volume of sediment available on the upper part of the beach profile to fight against winter erosion. The nourishment of the dune with sand extracted from the intertidal area maximized the sediment budget**.
- **The recommended borrow area for dune nourishment is the upper part of the intertidal area (U2D).** The beach profile becomes more dissipative at high tide and this leads to more disequilibrium between actual and equilibrium geometries, increasing onshore sediment transport and achieving larger accretion volumes.
- **Beach scraping has proven its effectiveness in enhancing beach recovery** in the laboratory. Additionally, beach scraping was also effective at a real beach (Fuentebavía).
- **Field surveys on Fuentebavía beach** during the summer season of 2021 allowed the analysis of the effectiveness of beach scraping in a real environment. The results match the conclusions obtained at the laboratory. **Beach scraping enhanced sand accretion during the first weeks after machinery actions.** The shoreline prograded 3.68 m more than the control area and the berm accreted 24 % of extra sand volume. Therefore, the dry beach was wider at the beginning of the touristic season. After the first weeks, natural and scraped measurements were similar.

As a general conclusion on the effectiveness of both NABE techniques (scraping and ploughing), we observed that:

- **The recommended NABE technique depends on the objective.** For beaches where a wider dry beach is sought, the recommended actions are ploughing or scraping, borrowing the sand from the low intertidal area and filling an intertidal bar or the beachfront (with a careful design of the berm geometry) during spring. For beaches where inland protection from erosion and flooding under winter storms is sought, the recommendation is borrowing sand from the intertidal area during spring (and preferably

CHAPTER 7

from the upper intertidal area) and nourishing the dune or the upper dry beach, where the sediment will be available to buffer the erosion caused by winter storms.

Conclusions on the methodology for the application of nature assisted beach enhancement techniques

Chapter 6 includes a methodology for the implementation of nature-based solutions (NBS) for beach enhancement, specifically focusing on nature assisted beach enhancement (NABE) techniques. This methodology helps decision-makers to select the most appropriate NABE technique depending on the goal and site-specific characteristics. Additionally, it provides guidelines for the design of actions. This chapter 6 address the following objective of the thesis:

- OB7. Develop a methodology that helps decision-makers to decide which technique is the most appropriate for their beach. It includes guidelines for the design of the selected actions.

The following conclusions are derived from the development of this methodology:

- **NABE techniques**, such as ploughing and scraping, are designed to **enhance sand accretion by taking advantage of natural processes, reducing the reliance on human interventions**. Additionally, both techniques are applied with terrestrial means, making them inexpensive and easy to apply with widely used machinery (for crops and civil works, plough and scrappers respectively).
- While **scraping and ploughing** can be valuable tools for coastal management, their **application should be exercised with caution and limited to appropriate locations**. These techniques alone cannot solve persistent erosion issues, which require a thorough analysis of underlying causes and remedial actions. The NABE techniques proposed here **are suitable for their application during spring on sandy beaches that present seasonal variability and do not have environmental restrictions**.
- To ensure the proper selection and design of NABE actions, a **methodology** is outlined, **consisting of three main steps**: selecting the most appropriate technique using a decision tree, determining whether to apply NABE techniques based on an operational system, and designing NABE actions tailored to the specific site's coastal management goals. The data required for decision-making and the design of actions is easily accessible, and the calculations are simple.

- The **decision tree assists in selecting the suitable NABE technique** by considering factors such as beach equilibrium, management goals, intertidal area width, and availability of data on accretion.
- The **operational system helps to determine whether to apply NABE techniques based on marine dynamics**, particularly by comparing the Dean number (Ω) forecasted for the following days with the average historical Dean number ($\bar{\Omega}$). Only when favourable conditions for accretion occur ($\Omega < \bar{\Omega}$) NABE actions should be applied.
- The importance of considering the ecological impact of NABE techniques is emphasized. It is particularly important to consider macrofauna, nesting periods and migratory species. **Timing of actions should be planned to avoid critical ecological periods.**
- **The design of NABE actions varies depending on the chosen technique.** Ploughing is performed every day during low tide hours while scraping has specific recommendations regarding the maximum mobilized volume, borrow area depth and filling area design. When the filling area is an artificially created berm, the berm crest height should match the summer-average of monthly total water level exceeded 1% of the time. Besides, when the scraped sand is used for foredune nourishment, a site-specific design should be performed.
- The presented methodology aims to support decision-makers in implementing NABE techniques effectively while considering beach sustainability and touristic objectives. It provides guidelines for the technique selection, operational system setup, and action design, based on previous research and practical experience gained throughout the development of this thesis.
- **The methodology is adaptable** to incorporate new NABE techniques, refine operational criteria based on **future research**, and optimize design geometries. The **monitoring** and evaluation of NABE actions are encouraged for continuous improvement.

CHAPTER 7

7.2. FUTURE RESEARCH

Despite the contributions of this thesis to the knowledge of beach recovery during the summer season and the effectiveness of NABE techniques, there are still questions that remain unanswered. The new research questions that arose during the development of this thesis lead to the following suggested research lines to be addressed in future studies.

Sand accretion

- **The relationship between marine dynamics and the volume of sand accretion needs to be studied and the threshold of marine conditions that trigger accretion determined.**

Further research on the processes that lead to beach recovery is needed to fulfil the current gap in the state of the art. It is clear that waves and tides play a fundamental role in sand accretion, but this morphodynamic process has not been solved yet. The sand accreted on the beachface stabilizes on the berm during the monthly-maximum spring tides. The height of the crest of this berm can be explained by the TWL exceeded 1% during the previous month (since the previous monthly-maximum spring tides). Generally speaking, the smaller the wave height the bigger the accretion volume. Nevertheless, the relation between the volume of sand accreted and the Dean parameter (Ω) is weak.

Two approaches are proposed for the study of accretion in real environments:

- Daily observations. Phillips et al. (2019) started this research line and proposed four modes of recovery (combinations of berm progradation and aggradation) based on their observations. They take into account the complex morphodynamic evolution of the berm shape during spring-neap-spring tidal cycles. This approach is useful for the analysis of the processes that trigger sand accretion.
- Monthly observations. This thesis started this research line, based on the knowledge that the accreted sand that stabilizes on the berm becomes stable on the monthly-maximum spring tides. Monthly observations allow the monitoring of the full recovery period during summer with minimal effort. This approach is useful for the analysis of the recovery achieved before winter storms from a holistic perspective.

Laboratory experiments for the analysis of accretion should include simultaneous simulations of waves and tides with variable tidal range, simulating spring-neap-spring tidal range variations.

The prediction of the accretion sand volume based on marine dynamics is still a challenge. Phillips et al. (2019) tried to relate the accretion mode with $\bar{\Omega}$ but they discovered that accretion is also possible if $\Omega < \bar{\Omega}$. This also occurred in the study sites of this thesis. Additionally, we found that the relation between the volume of sand accreted and the average of Ω_∞ during the previous month is weak.

- **Further studies on shoreface bedforms occurrence and sediment dynamics around them would reveal their importance for beach recovery.**

The results of this thesis indicate that bedforms (naturally or artificially formed) might play a role in enhancing sediment accretion. Bedforms produce two effects: (1) an increased bed roughness and (2) sediment transport due to their migration. The increased bed roughness leads to bigger wave dissipation and suspended onshore sediment transport. The migration of the shoreface bedforms increases sediment transport and contributes to accretion if the migration is onshore-directed. Detailed analysis of naturally formed bedforms should include:

- Analysis of the marine conditions that trigger their formation, stability and evolution.
- Analysis of the effects that bedforms induce on marine and sediment dynamics.
- Analysis under accretive and erosive conditions.
- Analysis of the bedform wavelength that is stable in each environment.
- Analysis of the bedform migration and induced sediment movement.

Then, the analysis of artificial bedforms should determine if wavelengths or amplitudes bigger/smaller than the ones of naturally formed bedforms allow an enhancement of beach recovery.

CHAPTER 7*NABE techniques*

- Further prototype testing (under natural conditions on a real beach) is required to determine the full potential of beach scraping and ploughing for dry beach widening and accretion enhancement.

This thesis has proven the effectiveness of ploughing and scraping NABE techniques to enhance beach accretion under highly accretive laboratory conditions. Additionally, scraping also proved its effectiveness in a natural environment (in the framework of this thesis) and ploughing did so in previous studies (Gainza et al., 2019). The methodology proposed in this thesis may help the design of the most appropriate techniques to test on each environment.

- The effect of a spring storm acting over the recently performed NABE actions remains unknown.

This effect should be analysed, determining the threshold of marine dynamics that produce accretion. The development of reliable operational systems able to predict marine dynamics joint with an accurate determination of the threshold of sand accretion are required to avoid possible issues (erosion, removal of the sand moved by machinery, etc).

- Further studies on the specific effect of scraping and ploughing actions over the entire ecosystem, from the submerged area to the dune, are still necessary to have a complete view of the ecological impact of these techniques.

Previous studies affirm that the species of the intertidal area are able to survive despite scraping actions. The species that live in this environment are expected to be adapted to frequent changes and therefore able to recover quickly from disturbances (Batton, 2007). Additionally, recolonization processes are determined by the duration and intensity of the works. In this sense, the scraping techniques are a ‘short-term pulse’ disturbance (Speybroeck et al., 2006) and it is believed that species can recover more easily than under the effect of other hard-engineering solutions. Smith et al. (2011) assessed the impact of beach scraping on macroinvertebrates and did not find a detectable effect on biodiversity. The eventuality and reduced extent affected by the machinery actions, allows the species to recover. This statement was also considered applicable for ploughing actions, as the extent affected by the furrows is smaller than the borrow area of scraping, and the filling area for ploughing are the ridges which are closer to the original position of the sand. Additionally, these techniques have positive effects as they generate a healthier and more

sustainable beach, which constitute a better environment for species and may favour biodiversity. Nevertheless, the effect of scraping and ploughing should be analysed from a holistic point of view.

– **Development of other NABE techniques.**

Other NABE techniques can be analysed and incorporated into the methodology proposed in this thesis. The methodology is flexible and easily adaptable. Even new nature-based solutions (NBS) can be proposed for enhancing beach accretion by taking advantage of the natural processes. The combination of scraping and ploughing techniques may produce concomitant effects that remain unexplored.

Ploughing

– **Analyse the effect of spring-neap-spring tidal cycles on beach ploughing.**

Ploughing has been analysed under the simultaneous effect of accretive waves and tides (of constant tidal range). The effect of spring-neap-spring tidal cycles has proven to be important for beach accretion and therefore it should be analysed when ploughing should be applied.

– **Optimize ploughing geometric characteristics.**

Besides, the proposed ploughing geometry matches the higher density possible of ridges and furrows made with the dimensions of a standard ploughing tool in crops. Parameters like the ploughing extent over the intertidal area, the cross-shore spacing between ploughing lines, and their dimensions may play a role in the optimization of accretion enhancement. Note that the results of this thesis suggest that: (1) the wider the intertidal extent the bigger the wave dissipation produced, and (2) increasing the cross-shore spacing may produce the same accretion with less machinery effort. Additionally, this thesis followed the recommendation of Carley et al. (2010) of a maximum depth of the NABE of 0.3 m for beaches of fine sand. Although this recommendation was made for scraping, it was considered applicable to ensure the survival of intertidal macrofauna, the comfort of beach users, and because it matches the geometry of standard ploughing tools. The effect of changing the aforementioned parameters should be determined to optimize the ploughing technique.

CHAPTER 7*Scraping*

- Develop new procedures for the calculation of the naturally accreted sand volume during the summer season.

The recommendations of Carley et al. (2010) indicate that the maximum sand volume mobilised by scraping should be less than the volume of sand recovered by nature during the summer season. The lack of data from previous summer seasons makes it difficult to calculate the volume of sand accreted naturally. New procedures for the calculation of this volume should be developed. Additionally, the effects of exceeding this volume limit have not been tested, and therefore further research on that is encouraged.

- Additional research on the impact of scraping berm geometry on accretion and dry beach width.

Undoubtedly, the NABE action that produces faster dry beach widening is scraping by placing the sand on the beachface, generating a new summer berm immediately. However, the results of this thesis indicate that the effectiveness of this scraping variant is highly sensitive to the design of the filling area. The scraping volume, berm crest level, and shoreface slope determine the dry beach achieved and the extra volume of sand accreted. In some cases, this technique reduces the amount of sand accreted by natural means (although the total volume mobilized, considering the scraping volume moved by the machinery, was bigger). Therefore, further research on the implications of the berm geometry on accretion and dry beach width is required.

7.3. FINANCIAL SUPPORT

The author would like to acknowledge the following contributions to the development of this thesis:

The laboratory experiments and field surveys presented in this thesis were developed in the framework of Beach-ART project, which was funded by the Spanish Ministry of Economy, Industry, and Competitiveness under grant BIA2017-89491-R.

Demarcación de Costas Andalucía Atlántico (Ministerio para la Transición Ecológica y el Reto Demográfico) provided all the field measurements of Fuentebravía beach (Cádiz) under the collaboration initiated for Beach-ART project.

The access to IHCantabria's physical modelling facilities (ICTS, Infraestructuras Científicas y Técnicas Singulares) was granted by MARHIS (Maritime Aggregated Research Hydraulic Infrastructures) program.

Two grants from the Government of Cantabria through the Fénix Programme provided the required financial support for the development of the laboratory experiments at COCoTsu and TOD, respectively.

Thank you for the technical assistance of all the laboratory personnel during the experiments.

Volunteer work during the field surveys of El Sardinero and Somo beaches is also acknowledged.

The Contract Program of the Government of Cantabria – Universidad de Cantabria through the project Hybrid shoreline evolution model for long-term scales integrating longshore and cross-shore processes, provided the financial support required during the last months of the thesis.

REFERENCES

- Aagaard, T., Hughes, M., Møller-Sørensen, R., Andersen, S., 2006. Hydrodynamics and sediment fluxes across an onshore migrating intertidal bar. *J. Coast. Res.* 22, 247–259. <https://doi.org/10.2112/04-0214.1>
- Abascal, A., Castanedo, S., Cid, A., Medina, R., 2012. A high resolution storm surge hindcast in Southern Europe: a useful database for coastal applications, in: 33rd International Conference on Coastal Engineering.
- Allen, J.R.L., 1968. Current Ripples. Their relation to patterns of water and sediment motion., North Holland Publishing Company, Amsterdam. Cambridge University Press. <https://doi.org/10.1017/S001675680005946X>
- Alsina, J.M., Cáceres, I., Brocchini, M., Baldock, T.E., 2012. An experimental study on sediment transport and bed evolution under different swash zone morphological conditions. *Coast. Eng.* 68, 31–43. <https://doi.org/10.1016/j.coastaleng.2012.04.008>
- Álvarez, M., 2016. Extreme morphodynamic analysis of the Sardinero and Puntal-Somo-Loredo beaches with XBeach. Universidad de Cantabria, Santander.
- Ashley, G.M., 1990. Classification of large-scale subaqueous bedforms: a new look at an old problem. *J. Sediment. Petrol.* 60, 160–172. <https://doi.org/10.2110/jsr.60.160>
- Aubrey, D.G., 1979. Seasonal patterns of onshore/offshore sediment movement. *J. Geophys. Res.* 84, 6347–6354.
- Baas, J.H., 2003. Ripple, Ripple Mark, Ripple Structure, in: Middleton, G.V. (Ed.), Encyclopedia of Sediments and Sedimentary Rocks. Kluwer Academic Publishers.
- Baldock, T.E., Alsina, J., 2013. Impact of beach scraping on near shore sediment transport and bar migration. *Coasts Ports 2013* 35–40.

REFERENCES

- Baldock, T.E., Alsina, J.A., Caceres, I., Vicinanza, D., Contestabile, P., Power, H., Sanchez-Arcilla, A., 2011. Large-scale experiments on beach profile evolution and surf and swash zone sediment transport induced by long waves, wave groups and random waves. *Coast. Eng.* 58, 214–227. <https://doi.org/10.1016/j.coastaleng.2010.10.006>
- Baldock, T.E., Manoovoravong, P., Pham, K.S., 2007. Beachface morphology and surf beat sediment transport in laboratory scale surf and swash zones. *J. Coast. Res.* 2007, 631–635.
- Batton, R., 2007. Tidal fish habitats, erosion control and beach replenishment. *Queensl. Dep. Prim. Ind. Fish.*
- Benavente, J., Anfuso, G., Río, L. Del, Gracia, F.J., Reyes, J.L., 2006. Evolutive Trends of Nourished Beaches in SW. Source *J. Coast. Res.* II, 765–769.
- Bruun, P., 1983. BEACH SCRAPING. *Coast. Eng.* 7, 167–173.
- Butterworth, S., 1930. On the Theory of Filter Amplifiers. *Exp. Wirel. Wirel. Eng.* 7, 536–541.
- Carley, J.T., Shand, T.D., Coghlan, I.R., Blacka, M.J., Cox, J., Littman, A., Fitzgibbon, B., Mclean, G., Watson, P., 2010. Beach scraping as a coastal management option. 19th NSW Coast. Conf. 1–20.
- Cataño-Lopera, Y.A., García, M.H., 2006. Geometry and migration characteristics of bedforms under waves and currents. Part 2: Ripples superimposed on sandwaves. *Coast. Eng.* 53, 781–792. <https://doi.org/10.1016/j.coastaleng.2006.03.008>
- CEPAL, 2012. Efectos del cambio climático en la costa de América Latina y el Caribe: dinámicas, tendencias y variabilidad climática. CEPAL.
- Cid, A., Castanedo, S., Abascal, A.J., Menéndez, M., Medina, R., 2014. A high resolution hindcast of the meteorological sea level component for Southern Europe: the GOS dataset. *Clim. Dyn.* 43, 2167–2184. <https://doi.org/10.1007/s00382-013-2041-0>
- Clarke, L.B., Werner, B.T., 2004. Tidally modulated occurrence of megaripples in a saturated surf zone. *J. Geophys. Res. C Ocean.* 109, 1–15. <https://doi.org/10.1029/2003jc001934>
- Coastal Dune Management, 2001. . NSW Dep. L. Water Conserv.
- Conaway, C.A., Wells, J.T., 2005. Aeolian dynamics along scraped shorelines, Bogue Banks, North Carolina. *J. Coast. Res.* 21, 242–254. <https://doi.org/10.2112/01-089.1>

- Cores, M., 2014. El Sardinero se prepara para recuperar su arena [WWW Document]. El D. Montañés. URL <https://www.eldiariomontanes.es/20140507/local/santander/reposicion-playa-segunda-sardinero-201405071916.html?> (accessed 4.20.23).
- Crain, D.A., Bolten, A.B., Bjorndal, K.A., 1995. Effects of Beach Nourishment on Sea Turtles: Review and Research Initiatives. *Restor. Ecol.* 3, 95–104. <https://doi.org/10.1111/J.1526-100X.1995.TB00082.X>
- Crawford, A.M., Hay, A.E., 2001. Linear transition ripple migration and wave orbital velocity skewness : Observations. *J. Geophys. Res.* 106, 14113–14128.
- Dalrymple, R.W., Knight, R.J., Lambiase, J.J., 1978. Bedforms and their hydraulic stability relationships in a tidal environment, Bay of Fundy, Canada. *Nature* 275, 100–104. <https://doi.org/10.1038/275100a0>
- Dare, J.L., 2003. Alternative Shore Protection Strategies: Innovative Options and Management Issues. Proj. Rep. Submitt. to Mar. Resour. Manag. Progr. Coll. Ocean. Atmospheric Sci. Oregon State University Partial fulfilment Requir. degree Master Sci. 91.
- de Almeida, L.R., González, M., Medina, R., 2019. Morphometric characterization of foredunes along the coast of northern Spain. *Geomorphology* 338, 68–78. <https://doi.org/10.1016/j.geomorph.2019.04.019>
- Dean, R.G., 1973. Heuristic Models of Sand Transport in the Surf Zone. *Proc. Conf. Eng. Dyn. Surf Zo.* 208–214.
- Del Río, L., Benavente, J., Gracia, F.J., Anfuso, G., Aranda, M., Montes, J.B., Puig, M., Talavera, L., Plomaritis, T.A., 2018. Beaches of Cadiz. Spanish Coast. *Syst. Dyn. Process. Sediments Manag.* 311–334. https://doi.org/10.1007/978-3-319-93169-2_14/FIGURES/7
- Del Río, L., Gracia, F.J., Benavente, J., 2013. Shoreline change patterns in sandy coasts. A case study in SW Spain. *Geomorphology* 196, 252–266. <https://doi.org/10.1016/J.GEOMORPH.2012.07.027>
- Delcamp, E., 2022. Diagnóstico de la evolución de la Playa de Fuentebravia en Cádiz tras su regeneración. Universidad de Cantabria, Santander.
- Dubois, R.N., 1988. Seasonal changes in beach topography and beach volume in Delaware.

REFERENCES

- Mar. Geol. 81, 79–96. [https://doi.org/10.1016/0025-3227\(88\)90019-9](https://doi.org/10.1016/0025-3227(88)90019-9)
- Egbert, G.D., Bennett, A.F., Foreman, M.G.G., 1994. TOPEX/POSEIDON tides estimated using a global inverse model. *J. Geophys. Res. Ocean.* 99, 24821–24852. <https://doi.org/10.1029/94JC01894>
- Egbert, G.D., Erofeeva, S.Y., 2002. Efficient Inverse Modeling of Barotropic Ocean Tides. *J. Atmos. Ocean. Technol.* 19, 183–204. [https://doi.org/10.1175/1520-0426\(2002\)019](https://doi.org/10.1175/1520-0426(2002)019)
- Erskine, A., Thompson, M., 2003. New Brighton Vegetation Management Plan. Environmental Train. Employ. Inc. EnviTE NSW.
- Flemming, B.W., 1988. Zur klassifikation subaquatischer, strömungstransversaler Transportkörper. *Bochumer Geol. und Geotech. Arb.* 29, 93–97.
- Gainza, J., Garnier, R., Nuñez, P., Jaramillo, C., González, E.M., Medina, R., Liria, P., Epelde, I., Uriarte, A., Monge-Ganuzas, M., 2019. Accelerating Beach Recovery by Plowing the Intertidal Bar: A Field Experiment along the Northern Spanish Coast. *J. Coast. Res.* 35, 973. <https://doi.org/10.2112/jcoastres-d-18-00033.1>
- Gallagher, E.L., Elgar, S., Guza, R.T., 1998a. Observations of sand bar evolution on a natural beach. *J. Geophys. Res. Ocean.* 103, 3203–3215.
- Gallagher, E.L., Elgar, S., Thornton, E.B., 1998b. Megaripple migration in a natural surf zone. *Nature* 394, 165–168. <https://doi.org/10.1038/246170a0>
- Garcez Faria, A.F., Thornton, E.B., Stanton, T.P., Soares, C. V, Lippmann, T.C., 1998. Vertical profiles of longshore currents and related bed shear stress and bottom roughness. *J. Geophys. Res.* 103, 3217–3232.
- Gomes da Silva, P., Coco, G., Garnier, R., Klein, A.H.F., 2020. On the prediction of runup, setup and swash on beaches. *Earth-Science Rev.* <https://doi.org/10.1016/j.earscirev.2020.103148>
- Gómez, A., 2020. Análisis de los temporales marítimos e impactos costeros en la Costa Cantábrica. Universidad de Cantabria, Santander.
- González, M., Medina, R., 2001. On the application of static equilibrium bay formulations to natural and man-made beaches. *Coast. Eng.* 43, 209–225. [https://doi.org/10.1016/S0378-3839\(01\)00014-X](https://doi.org/10.1016/S0378-3839(01)00014-X)

- Gordon, A.D., 2015. When did you last NABE a beach – beach scraping demystified for fun and profit. Proc. 24st NSW Coast. Conf. Forster, NSW, Novemb. 2015. 1–10.
- Gourlay, M.R., 1968. Beach and dune erosion tests. Deltares (WL).
- Govarets, A., Lauwerts, B., 2009. Assessment of the impact of coastal defence structures. OSPAR Comm. Belgium 29.
- Grasso, F., Michallet, H., Barthélemy, E., Certain, R., 2009. Physical modeling of intermediate cross-shore beach morphology: Transients and equilibrium states. *J. Geophys. Res. Ocean.* 114, 1–15. <https://doi.org/10.1029/2009JC005308>
- Guannel, G., Özkan-Haller, H.T., Haller, M.C., Kirby, J.T., 2007. Influence of velocity moments on sand bar movement during CROSSTEX, in: Coastal Sediments '07. ASCE, pp. 28–41.
- Guerrero, Q., 2018. Bedforms And Associated Sediment Dynamics On The Inner Shelves At Different Spatio-Temporal Scales 1–162.
- Guerrero, Q., Guillén, J., 2020. Dynamics of ripples superimposed on a sand ridge on a tideless shoreface. *Estuar. Coast. Shelf Sci.* 242. <https://doi.org/10.1016/j.ecss.2020.106826>
- Guerrero, Q., Williams, M.E., Guillén, J., Lichtman, I.D., Thorne, P.D., Amoudry, L.O., 2021. Small-scale bedforms and associated sediment transport in a macro-tidal lower shoreface. *Cont. Shelf Res.* 225. <https://doi.org/10.1016/j.csr.2021.104483>
- Haines, J.W., Sallenger, A.H., 1994. Vertical structure of mean cross-shore currents across a barred surf zone. *J. Geophys. Res.* 99, 4,223-14,242.
- Hallermeier, R.J., 1981. Terminal settling velocity of commonly occurring sand grains. *Sedimentology* 28, 859–865. <https://doi.org/10.1111/j.1365-3091.1981.tb01948.x>
- Hamm, L., Capobianco, M., Dette, H.H., Lechuga, A., Spanhoff, R., Stive, M.J.F., 2002. A summary of European experience with shore nourishment. *Coast. Eng.* 47, 237–264. [https://doi.org/10.1016/S0378-3839\(02\)00127-8](https://doi.org/10.1016/S0378-3839(02)00127-8)
- Hasselmann, K., Barnett, T.P., Bouws, E., Carlson, H., Cartwright, D.E., Enke, K., Ewing, J.A., Gienapp, H., Hasselmann, D.E., Kruseman, P., Meerburg, A., Müller, P., Olbers, D.J., Richter, K., Sell, W., Walden, H., 1973. Measurements of wind-wave growth and swell decay during the Joint North Sea Wave Project (JONSWAP), Deutches

REFERENCES

- Hydrographisches Institut.
- Holman, R.A., Sallenger, A.H.J., 1993. Sand bar generation: A discussion of the Duck experiment series. *J. Coast. Res. SI*, 76–92.
- Hunt, A.R., F.G.S., M.A., 1904. VI.—The Descriptive Nomenclature of Ripple-Mark. *Geol. Mag.* 1, 410–418. <https://doi.org/10.1017/S0016756800123775>
- Huntley, D.A., Amos, C.L., Williams, J.J., Humphery, J.D., 1991. Estimating bedload transport on continental shelves by observations of ripple migration - an assessment.
- Jackson, D.W.T., Cooper, J.A.G., O'Connor, M., Guisado-Pintado, E., Loureiro, C., Anfuso, G., 2016. Field measurements of intertidal bar evolution on a high-energy beach system. *Earth Surf. Process. Landforms* 41, 1107–1114. <https://doi.org/10.1002/esp.3920>
- Jackson, R.G., 1975. Hierarchical attributes and a unifying model of bed forms composed of cohesionless material and produced by shearing flow. *Bull. Geol. Soc. Am.* 86, 1523–1533. [https://doi.org/10.1130/0016-7606\(1975\)86<1523:HAAAUM>2.0.CO;2](https://doi.org/10.1130/0016-7606(1975)86<1523:HAAAUM>2.0.CO;2)
- Jensen, S.G., Aagaard, T., Baldock, T.E., Kroon, A., Hughes, M., 2009. Berm formation and dynamics on a gently sloping beach; the effect of water level and swash overtopping. *Earth Surf. Process. Landforms* 34, 1533–1546. <https://doi.org/10.1002/ESP.1845>
- Kraus, N.C., Larson, M., Kriebel, D.L., 1991. Evaluation of Beach Erosion and Accretion Predictors. *Am. Soc. Civ. Eng.* 572–587.
- Larsen, B.E., van der A, D.A., Carstensen, R., Carstensen, S., Fuhrman, D.R., 2023. Experimental investigation on the effects of shoreface nourishment placement and timing on long-term cross-shore profile development. *Coast. Eng.* 180, 104258. <https://doi.org/10.1016/j.coastaleng.2022.104258>
- Losada, I.J., Reguero, B.G., Méndez, F.J., Castanedo, S., Abascal, A.J., Minguez, R., 2013. Long-term changes in sea-level components in Latin America and the Caribbean. *Glob. Planet. Change* 104, 34–50. <https://doi.org/10.1016/J.GLOPLACHA.2013.02.006>
- Losada, M.A., Medina, R., Vidal, C., Roldán, A., 1991. Historical Evolution and Morphological Analysis of “El Puntal” Spit, Santander (Spain). *J. Coast. Res.* 7, 711–722.
- Luijendijk, A., Hagenaars, G., Ranasinghe, R., Baart, F., Donchyts, G., Aarninkhof, S., 2018. The State of the World’s Beaches. *Sci. Rep.* 1–11. <https://doi.org/10.1038/s41598-018-0001>

24630-6

- Luijendijk, A.P., Ranasinghe, R., de Schipper, M.A., Huisman, B.A., Swinkels, C.M., Walstra, D.J.R., Stive, M.J.F., 2017. The initial morphological response of the Sand Engine: A process-based modelling study. *Coast. Eng.* 119, 1–14. <https://doi.org/10.1016/j.coastaleng.2016.09.005>
- Masselink, G., Austin, M.J., O'Hare, T.J., Russell, P.E., 2007. Geometry and dynamics of wave ripples in the nearshore zone of a coarse sandy beach. *J. Geophys. Res.* 112, C10022. <https://doi.org/10.1029/2006JC003839>
- Masselink, G., Kroon, A., Davidson-Arnott, R.G.D., 2006. Morphodynamics of intertidal bars in wave-dominated coastal settings - A review. *Geomorphology* 73, 33–49. <https://doi.org/10.1016/j.geomorph.2005.06.007>
- Masselink, G., Short, A.D., 1993. The effect of tide range on beach morphodynamics and morphology: a conceptual beach model. *J. Coast. Res.* 9, 785–800.
- McGranahan, G., Balk, D., Anderson, B., 2007. The rising tide: assessing the risks of climate change and human settlements in low elevation coastal zones. *Environ. Urban.* 19, 17–37. <https://doi.org/10.1177/0956247807076960>
- McNinch, J.E., Wells, J.T., 1992. The Effectiveness of Beach Scraping as a Method of Erosion Control. *Shore and Beach* 60, 13–20.
- Medina, R., Marino-Tapia, I., Osorio, A., Davidson, M., Martin, F.L., 2007. Management of dynamic navigational channels using video techniques. *Coast. Eng.* 54, 523–537. <https://doi.org/10.1016/j.coastaleng.2007.01.008>
- Middleton, G. V., Southard, J.B., 1984. Mechanics of Sediment Movement, Society of Economic Paleontologists and Mineralogists. SEPM (Society for Sedimentary Geology). <https://doi.org/10.2110/scn.84.03>
- Miles, J., Thorpe, A., 2015. Bedform contributions to cross-shore sediment transport on a dissipative beach. *Coast. Eng.* 98, 65–77. <https://doi.org/10.1016/j.coastaleng.2015.01.007>
- Miles, J., Thorpe, A., Russell, P., Masselink, G., 2014. Observations of bedforms on a dissipative macrotidal beach. *Ocean Dyn.* 64, 225–239. <https://doi.org/10.1007/s10236-013-0677-2>

REFERENCES

- Monge-Ganuzas, M., Gainza, J., Liria, P., Epelde, I., Uriarte, A., Garnier, R., González, M., Nuñez, P., Jaramillo, C., Medina, R., 2017. Morphodynamic evolution of Laida beach (Oka estuary, Urdaibai Biosphere Reserve, southeastern Bay of Biscay) in response to supratidal beach nourishment actions. *J. Sea Res.* 130, 85–95. <https://doi.org/10.1016/j.seares.2017.06.003>
- Munoz-Perez, J.J., Lopez, B., Roman-Blanco, S., Gutierrez-Mas, M., Moreno, L., Cuena, G.J., 2001. Cost of beach maintenance in the Gulf of Cadiz SW Spain. *Coast. Eng.* 42, 143–153.
- Muñoz, J.J., Gutiérrez, J.M., 1999. Tipología y eficacia de los espigones de escollera construidos para la mejora de la estabilidad de las playas del litoral Atlántico de la provincia de Cádiz. *Boletín Geológico y Min.* 110, 53–66.
- Nielsen, P., 1992. Coastal Bottom Boundary Layers and Sediment Transport, Advanced Series on Ocean Engineering. WORLD SCIENTIFIC. <https://doi.org/10.1142/1269>
- Pawlowicz, R., Beardsley, B., Lentz, S., 2002. Classical tidal harmonic analysis including error estimates in MATLAB using T_TIDE. *Comput. Geosci.* 28, 929–937. [https://doi.org/10.1016/S0098-3004\(02\)00013-4](https://doi.org/10.1016/S0098-3004(02)00013-4)
- Pellón, E., Aniel-Quiroga, I., González, M., Medina, R., Vidal, C., 2023. Working with nature to enhance beach accretion: Laboratory experiments of beach ploughing. *Coast. Eng.* 180. <https://doi.org/10.1016/j.coastaleng.2022.104267>
- Pellón, E., de Almeida, L.R., González, M., Medina, R., 2020. Relationship between foredune profile morphology and aeolian and marine dynamics: A conceptual model. *Geomorphology* 351, 106984. <https://doi.org/10.1016/j.geomorph.2019.106984>
- Pellón, E., Garnier, R., Medina, R., 2014. Intertidal finger bars at El Puntal, Bay of Santander, Spain: Observation and forcing analysis. *Earth Surf. Dyn.* 2, 349–361. <https://doi.org/10.5194/esurf-2-349-2014>
- Phillips, M., Sydney, U., Harley, M.D., 2017. High-frequency observations of beach recovery using a continuous scanning, in: Coasts & Ports 2017 Conference.
- Phillips, M.S., Blenkinsopp, C.E., Splinter, K.D., Harley, M.D., Turner, I.L., 2019. Modes of Berm and Beachface Recovery Following Storm Reset: Observations Using a Continuously Scanning Lidar. *J. Geophys. Res. Earth Surf.* 124, 720–736. <https://doi.org/10.1029/2018JF004895>

- Poate, T., Masselink, G., Austin, M.J., Dickson, M., McCall, R., 2018. The Role of Bed Roughness in Wave Transformation Across Sloping Rock Shore Platforms. *J. Geophys. Res. Earth Surf.* 123, 97–123. <https://doi.org/10.1002/2017JF004277>
- Quetzalcóatl, O., González, M., Cánovas, V., Medina, R., Espejo, A., Klein, A., Tessler, M.G., Almeida, L.R., Jaramillo, C., Garnier, R., Kakeh, N., González-Ondina, J., 2019. SMC ε , a coastal modeling system for assessing beach processes and coastal interventions: Application to the Brazilian coast. *Environ. Model. Softw.* 116, 131–152. <https://doi.org/10.1016/j.envsoft.2019.03.001>
- Raudkivi, A.J., 1997. Ripples on stream bed. *J. Hydraul. Eng.* 123, 58–64.
- Reesink, A.J.H., Bridge, J.S., 2007. Influence of superimposed bedforms and flow unsteadiness on formation of cross strata in dunes and unit bars. *Sediment. Geol.* 202, 281–296. <https://doi.org/10.1016/j.sedgeo.2007.02.005>
- Reguero, B.G., Méndez, F.J., Losada, I.J., 2013. Variability of multivariate wave climate in Latin America and the Caribbean. *Glob. Planet. Change* 100, 70–84. <https://doi.org/10.1016/J.GLOPLACHA.2012.09.005>
- Reguero, B.G., Menéndez, M., Méndez, F.J., Minguez, R., Losada, I.J., 2012. A Global Ocean Wave (GOW) calibrated reanalysis from 1948 onwards. *Coast. Eng.* 65, 38–55. <https://doi.org/10.1016/J.COASTALENG.2012.03.003>
- Sánchez-González, J.F., Martín-Hidalgo, M., de la Peña Olivas, J.M., 2017. Ensayo en Modelo Físico a Gran Escala de las Operaciones de Reperfilado de Playas para la Protección del Territorio frente a Temporales de Oleaje, in: XIV Jornadas Españolas de Costas y Puertos.
- Shchepetkin, A.F., McWilliams, J.C., 2005. The regional oceanic modeling system (ROMS): a split-explicit, free-surface, topography-following-coordinate oceanic model. *Ocean Model.* 9, 347–404. <https://doi.org/10.1016/J.OCEMOD.2004.08.002>
- Shchepetkin, A.F., McWilliams, J.C., 2003. A method for computing horizontal pressure-gradient force in an oceanic model with a nonaligned vertical coordinate. *J. Geophys. Res. Ocean.* 108, 3090. <https://doi.org/10.1029/2001JC001047>
- Shields, A., 1936. Application of similarity principles and turbulence research to bed-load movement. *Soil Conserv. Serv.* 47.
- Smith, S.D.A., Harrison, M.A., Rowland, J., Fitzgibbon, B.E., 2011. Assessing the Impacts of

REFERENCES

- Beach Scraping on the Macroinvertebrates of New Brighton Beach, Northern NSW. Aust. Coast. Soc. Ltd.; 20th New South Wales Coast. Conf. (Tweed Heads, NSW) 1–13.
- Smutz, M., Griffith, J.W., Yu-Hwa, W., 1980. Nature Assisted Beach Enhancement or Sisyphus Vs Zeus. *Shore and Beach* 32–36.
- Soulsby, R., 1997. Dynamics of Marine Sands, Dynamics of Marine Sands. Thomas Telford Ltd. <https://doi.org/10.1680/DOMS.25844>
- Speybroeck, J., Bonte, D., Courtens, W., Gheskire, T., Grootaert, P., Maelfait, J.P., Mathys, M., Provoost, S., Sabbe, K., Stienen, E.W.M., Van Lancker, V., Vincx, M., Degraer, S., 2006. Beach nourishment: An ecologically sound coastal defence alternative? A review. *Aquat. Conserv. Mar. Freshw. Ecosyst.* 16, 419–435. <https://doi.org/10.1002/aqc.733>
- Stockdon, H.F., Holman, R.A., Howd, P.A., Sallenger, A.H., 2006. Empirical parameterization of setup, swash, and runup. *Coast. Eng.* 53, 573–588. <https://doi.org/10.1016/j.coastaleng.2005.12.005>
- Strahler, A.N., 1966. Tidal Cycle of Changes in an Equilibrium Beach, Sandy Hook, New Jersey. *J. Geol.* 74, 247–268.
- Thom, B.G., Hall, W., 1991. Behaviour of beach profiles during accretion and erosion dominated periods. *Earth Surf. Process. Landforms* 16, 113–127.
- Toimil, A., Losada, I.J., Camus, P., Díaz-Simal, P., 2017. Managing coastal erosion under climate change at the regional scale. *Coast. Eng.* 128, 106–122. <https://doi.org/10.1016/j.coastaleng.2017.08.004>
- Tolman, H.L., 1991. A third-generation model for wind waves on slowly varying, unsteady and inhomogeneous depths and currents. *J. Phys. Oceanogr.* 21, 782–797. [https://doi.org/https://doi.org/10.1175/1520-0485\(1991\)021<0782:ATGMFW>2.0.CO;2](https://doi.org/https://doi.org/10.1175/1520-0485(1991)021<0782:ATGMFW>2.0.CO;2)
- Tolman, H.L., 1989. The numerical model WAVEWATCH: a third generation model for hindcasting of wind waves on tides in shelf seas, NO. 89-2. ed, Communications on Hydraulic and Geotechnical Engineering. Delft Univ. of Techn.
- Traykovski, P., Hay, A.E., Irish, J.D., Lynch, J.F., 1999. Geometry, migration, and evolution of wave orbital ripples at LEO-15. *J. Geophys. Res. Ocean.* 104, 1505–1524. <https://doi.org/10.1029/1998jc900026>
- Tye, R.S., 1983. Impact of Hurricane David and Mechanical Dune Restoration on Folly

Beach, South Carolina. Shore and Beach 51, 3–9.

Venditti, J.G., Church, M., Bennett, S.J., 2005. Morphodynamics of small-scale superimposed sand waves over migrating dune bed forms. *Water Resour. Res.* 41, 1–14. <https://doi.org/10.1029/2004WR003461>

Walton, J.K., 2005. Histories of Tourism.

Wang, P., Kraus, N.C., 2005. Beach Profile Equilibrium and Patterns of Wave Decay and Energy Dissipation across the Surf Zone Elucidated in a Large-Scale Laboratory Experiment. *J. Coast. Res.* 21, 522–534. <https://doi.org/10.2112/03-003.1>

Ward, L.G., Morrison, R.C., Eberhardt, A.L., Costello, W.J., McAvoy, Z.S., Mandeville, C.P., 2021. Erosion and Accretion Trends of New Hampshire Beaches from December 2016 to March 2020: Results of the Volunteer Beach Profile Monitoring Program. *Cent. Coast. Ocean Mapp.* <https://doi.org/https://dx.doi.org/10.34051/p/2021.34>

Whipple, K., 2004. Surface Processes and Landscape Evolution [WWW Document]. MIT OpenCourseWare 12.163. URL <https://ocw.mit.edu/courses/12-163-surface-processes-and-landscape-evolution-fall-2004/pages/lecture-notes/> (accessed 3.9.23).

Wright, L.D., Short, A.D., 1984. Morphodynamic variability of surf zones and beaches: A synthesis. *Mar. Geol.* 56, 93–118. [https://doi.org/10.1016/0025-3227\(84\)90008-2](https://doi.org/10.1016/0025-3227(84)90008-2)

Wright, L.D., Short, A.D., Green, M.O., 1985. Short-term changes in the morphodynamic states of beaches and surf zones: An empirical predictive model. *Mar. Geol.* 62, 339–364. [https://doi.org/10.1016/0025-3227\(85\)90123-9](https://doi.org/10.1016/0025-3227(85)90123-9)

Yoo, H.J., Kim, H., Lee, J.L., Park, J.Y., 2021. Asymmetry between Accretional Advance and Erosional Retreat of Shoreline Position in On-offshore Direction. *J. Coast. Res.* 114, 6–10. <https://doi.org/10.2112/JCR-SI114-002.1>

APPENDICES

APPENDICES

APPENDIX I

METHODOLOGY FOR FIELD SURVEYS ON BEACH ACCRETION

AI.1. INTRODUCCIÓN

This appendix includes the methodology for the design of field surveys to monitor beach accretion and NABE actions performance. This methodology has been summarized in chapter 3 in English, and its original version (in Spanish) is included here.

The methodology includes a survey notebook, which covers all the information that should be captured during the surveys. It also describes the periodicity and spatial requirements of the surveys.

**METODOLOGÍA PARA CAMPAÑAS DE CAMPO
CARACTERIZACIÓN DE LA ACRECIÓN EN PLAYAS**



1. INTRODUCCIÓN

En este documento se resume la distribución temporal y espacial de las campañas de campo requeridas para realizar un seguimiento de los procesos de acreción¹ en playas. Se presta especial atención a playas en las que se llevan a cabo campañas de reperfilado para acelerar estos procesos de recuperación del sedimento en la zona emergida.

Además se proponen las metodologías más adecuadas para realizar dicho seguimiento, exponiendo las diferentes opciones disponibles.

El presente documento se ha estructurado en los siguientes apartados:

- Objetivos. Se exponen los objetivos que se pretenden alcanzar con los datos recogidos durante las campañas de campo.
- Metodologías. Se describen las diferentes metodologías que permiten tomar los datos necesarios para realizar el seguimiento de la playa.
- Cronograma. Se indica la periodicidad mínima que deben tener las campañas y las metodologías más adecuadas en cada una de ellas.
- Distribución espacial. Se describe al área que deben cubrir las medidas.

2. OBJETIVOS

Se quiere cuantificar el volumen de arena que recupera la playa de forma natural durante la época estival para analizar los procesos de acreción.

Se quiere cuantificar el efecto del reperfilado de la playa tras los temporales del invierno. En primavera la arena se recoge por medios mecánicos de la zona intermareal (espesor aproximado de arena retirada 0.3m) y se deposita junto a la duna o en el frente de playa aumentando el ancho de playa seca. La velocidad de los procesos naturales de acreción se ve modificada tras las actividades de reperfilado. Quiere cuantificarse en qué medida el reperfilado acelera la recuperación natural de arena de la playa.

¹ Proceso mediante el cual las playas recuperan arena y aumentan su ancho. Opuesto a erosión.



3. METODOLOGÍAS

Todas las mediciones requeridas para el seguimiento de playas en acreción en entornos meso y macro-mareales, pueden realizarse por medios terrestres. Las campañas deben llevarse a cabo durante la bajamar, para que la zona intermareal de la playa quede correctamente representada.

Se proponen dos tipos de mediciones:

- Mediciones 3D de la totalidad de la playa. Pueden realizarse mediante GPS o LIDAR.
- Mediciones 2D de diversos perfiles distribuidos en la zona de estudio. Pueden realizarse mediante medidor de distancias láser o dispositivo de vasos comunicantes.

3.1. Mediciones 3D

Las mediciones 3D han de llevarse a cabo por personal experto, y permiten la caracterización precisa de cualquier punto de la playa. Si la superficie a caracterizar abarca únicamente la playa seca e intermareal, las medidas pueden realizarse por medios terrestres durante la bajamar. Sin embargo, si las mediciones precisan extenderse bajo el nivel de bajamar, sería necesario combinar medios terrestres y marinos para completar la totalidad de la topobatimetría. Este tipo de mediciones suelen ser costosas, por lo que deben reducirse a situaciones en las que resultan imprescindibles.

3.2 Mediciones 2D

Las mediciones 2D consisten en la caracterización del nivel de la arena a lo largo de diversos perfiles de playa (perpendiculares a la línea de costa). Para ello es imprescindible una correcta definición e instalación (en caso necesario) de elementos de referencia que permitan geolocalizar con precisión, tanto en planta como en elevación, cada uno de los perfiles. Estos elementos de referencia deberán permanecer inamovibles durante todo el periodo de campañas, para asegurar la consistencia entre las medidas tomadas en diferentes campañas. Se suelen tomar como referencia de perfiles, puntos característicos del paseo marítimo, pasarelas en la zona dunar, edificaciones,... Además, para verificar que las medidas se han realizado correctamente, el último punto medido de cada perfil suele estar en agua, anotando la hora y nivel del mar en ese punto para cada uno de los perfiles.

Para realizar estas medidas 2D se plantean 2 metodologías, el uso de un medidor de distancias láser (véase figura 1) o el dispositivo de vasos comunicantes mostrado en la figura 2 (Andrade et al. 2006).





Figura 1. Izquierda: Medidor de distancias laser. Derecha: Trabajo de campo durante la medición de un perfil de playa empleando el medidor de distancias laser.

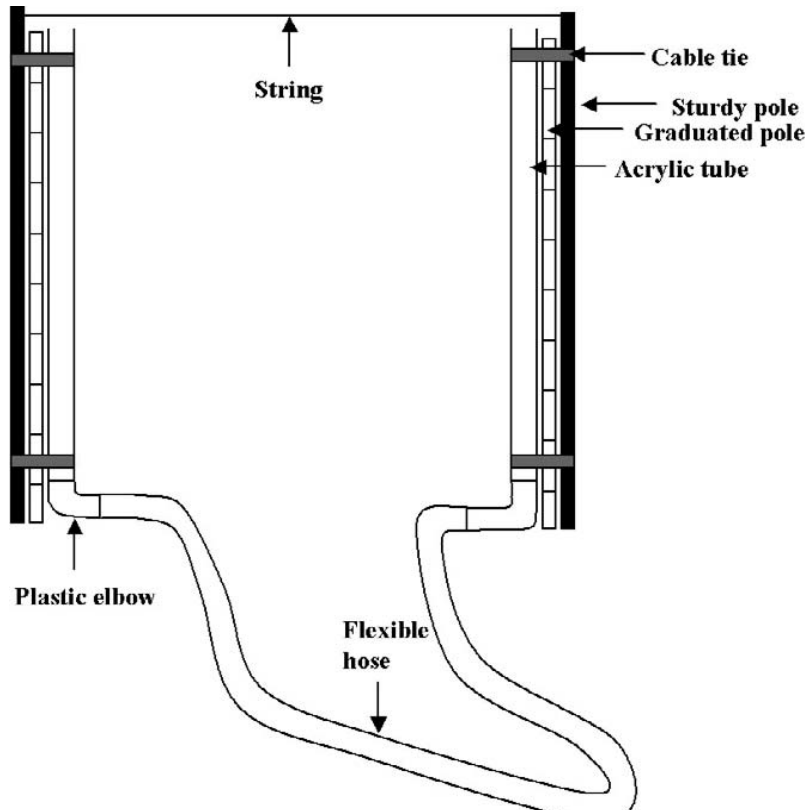


Figura 2. Diagrama del equipamiento empleado para la medición de perfiles mediante la técnica de vasos comunicantes (Andrade et al. 2006).

En ambas técnicas se requiere un estadillo de campo (ver anexo I) que se completa con los siguientes datos:

- Fecha y hora.
- Componentes del equipo de trabajo.
- Localización del perfil a medir y su identificador.
- Cota del suelo del punto inicial respecto a la referencia inicial.
- Distancia y diferencia de nivel entre ambos operarios en los sucesivos puntos de muestreo del perfil. Los operarios han de desplazarse siguiendo la alineación marcada por 2 referencias fijas que indican la dirección del perfil.
 - Medidor de distancias laser. Uno de los operarios sujetá el medidor y el otro una diana, ambos a la misma distancia del suelo. Esta altura debe mantenerse constante durante toda la campaña. Se apunta el medidor a la diana y se apunta en el estadillo la distancia y ángulo registrados. Los operarios avanzan punto a punto ocupando la posición final de una medición como inicio de la siguiente.
 - Vasos comunicantes. Cada operario sujetá uno de los vasos provistos de una regla graduada. Se estira la cuerda que sujetá ambos vasos, obteniendo una distancia fija entre puntos de medida que ha de ser anotada en el estadillo. Esta distancia puede reducirse doblando la cuerda por la mitad. Se anota en el estadillo la diferencia entre los niveles del agua en ambas reglas graduadas. Los operarios avanzan punto a punto ocupando la posición final de una medición como inicio de la siguiente.
- El último punto se toma en agua, anotando la cota del nivel del mar (media de varias olas) en ese momento respecto al nivel del suelo en ese punto.
- Hora de finalización de la medición del perfil.

Este tipo de mediciones resulta sencillo de aprender y puede realizarse por personal colaborador, lo cual permite que las mediciones se realicen frecuentemente. Colaboradores adecuados para esta tarea pueden ser estudiantes de colegios, voluntarios de asociaciones medioambientales o personal de vigilancia de las playas.



4. CRONOGRAMA

Para la correcta caracterización de los procesos de acreción de sedimento en playas, tras una operación de reperfilado, se requieren mediciones periódicas que permitan posteriormente analizar la evolución del volumen de arena en el perfil y planta de playa.

En la figura 3 se muestra una línea de tiempo referida a la fecha de realización de la campaña de reperfilado, la cual se toma como inicio del periodo de campañas. En la figura se indica el tipo recomendado de campaña, 3D o perfiles 2D. Puede verse que cuando se indica campaña 3D también se ha marcado la opción de los perfiles. Esto indica que lo ideal es realizar una campaña 3D en estas fechas, pero si resultase muy costoso, podría sustituirse por una campaña 2D.

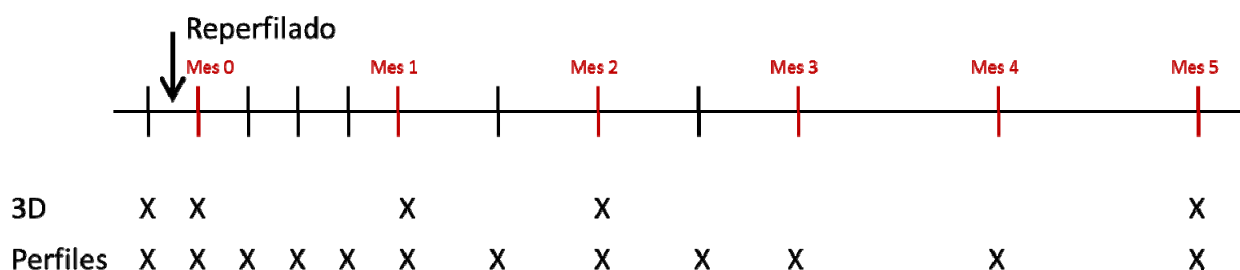


Figura 3. Cronograma de las campañas de campo requeridas para un correcto análisis de la acreción en playas.

Las campañas mínimas requeridas serían una sucesión de mediciones de perfiles 2D en las siguientes fechas:

- Una campaña inmediatamente antes de llevar a cabo el reperfilado (durante la semana anterior).
- Una campaña inmediatamente después del reperfilado (preferiblemente al día siguiente al reperfilado).
- Cuatro campañas, una por semana, durante el primer mes (mes 1).
- Cuatro campañas, una cada 15 días, durante los dos meses siguientes (meses 2 y 3).
- Dos campañas más durante los dos meses posteriores (meses 4 y 5).

Sería recomendable que al menos la campaña previa al reperfilado y la de los 5 meses (última) se realizasen en 3D.



5. DISTRIBUCIÓN ESPACIAL

La extensión en planta de las campañas ha de fijarse para cada playa de estudio, en función de sus características geométricas, la extensión del área reperfilada y la existencia o posibilidad de instalar elementos fijos que sirvan como referencia para la medición de perfiles.

La extensión transversal (perpendicular a la línea de costa) de las campañas es clara, abarcarán desde el paseo marítimo o duna hasta la línea de bajamar, incluyendo algún punto en agua.

Longitudinalmente, las campañas han de caracterizar tanto la zona reperfilada como una zona que permanezca sin alteraciones, en su estado natural, y que este lo suficientemente alejada del área reperfilada.

5.1. Mediciones 3D

La extensión de las campañas realizadas mediante medición tridimensional de la topografía de la playa abarcarán la playa seca e intermareal. Idealmente, estas campañas deben recoger datos de la totalidad del área reperfilada y de parte del área no afectada, sin embargo, si las dimensiones de la playa son excesivas, este tipo de campañas puede reducirse a un área dentro de la zona reperfilada y otra en la zona natural cuya extensión se definiría analizando las características de la playa.

5.2. Mediciones 2D

En el caso de medición de perfiles de playa, su longitud es clara, abarcando desde la duna o paseo marítimo hasta la línea de bajamar, incluyendo un punto en agua en el que se mide el nivel del mar.

La separación entre perfiles puede variar, dependiendo de la existencia de elementos fijos que sirvan como referencia para el origen y orientación de los mismos. En cualquier caso, se considera que el número mínimo de perfiles es de 4 en la zona reperfilada y 2 en la zona natural (suficientemente alejados del área reperfilada). Dependiendo de las características de la playa, se recomienda medir dos perfiles naturales a cada lado del área reperfilada, tal y como se muestra en la figura 4.

6. BIBLIOGRAFÍA

Andrade, F. and Ferreira, M.A., 2006. A simple method of measuring beach profiles. Journal of coastal research.



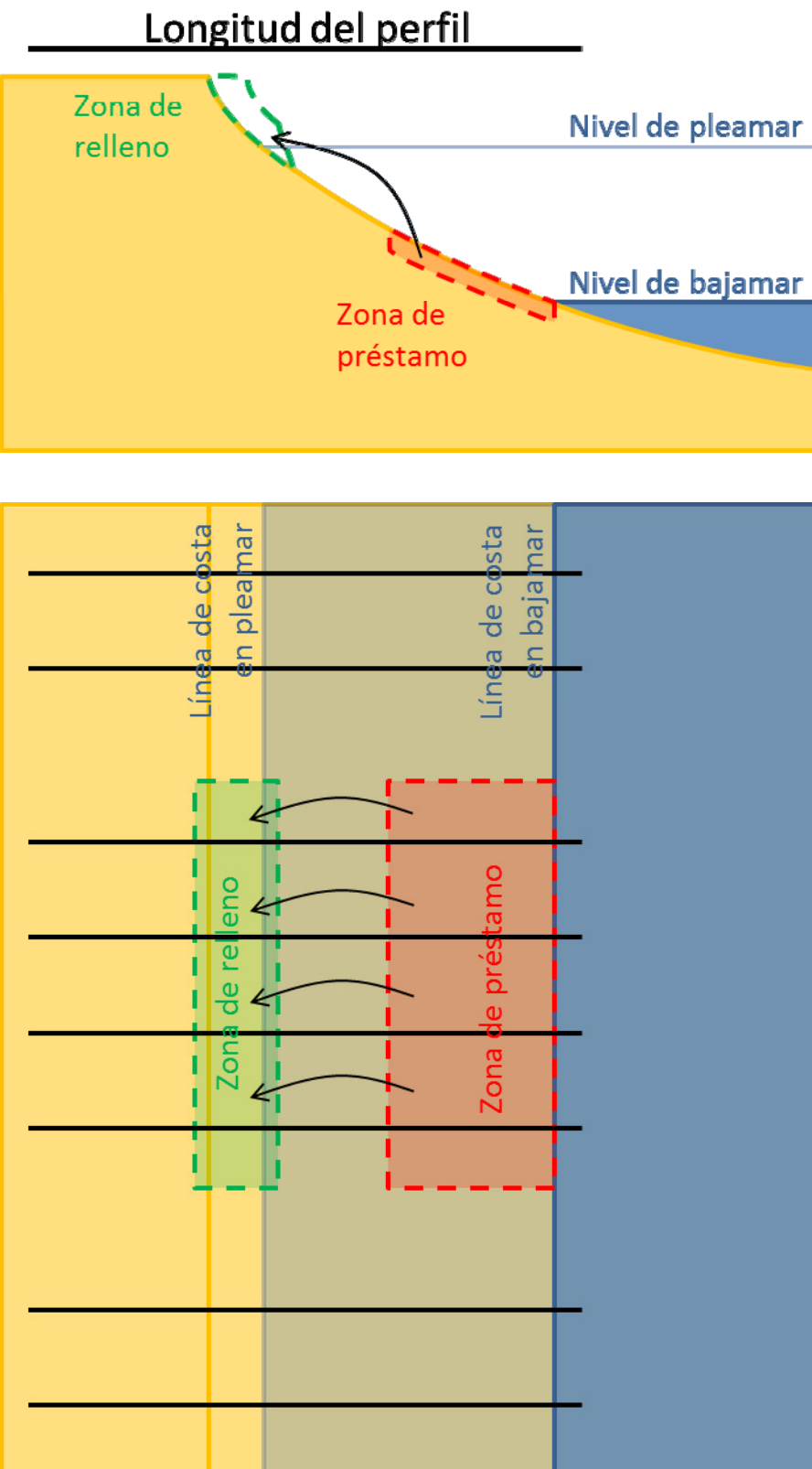


Figura 4. Diagrama de la distribución espacial de los perfiles (líneas negras) mínimos requeridos.
Arriba: Perfil de playa. Abajo: Planta de la playa.



ANEXO I – ESTADILLO DE CAMPO



Estadillo de campo - Perfiles de playa - Distancia Láser

Fecha:		Playa:	
Hora inicio:		Perfil:	
Equipo de Trabajo:			

Dir N (º):	
Cota referencia inicial (m):	
Cota agua final (m):	
Hora final:	

Punto	Distancia (m)	Ángulo (º)
1		
2		
3		
4		
5		
6		
7		
8		
9		
10		
11		
12		
13		
14		
15		
16		
17		
18		
19		
20		
21		
22		
23		
24		
25		
26		
27		

Punto	Distancia (m)	Ángulo (º)
28		
29		
30		
31		
32		
33		
34		
35		
36		
37		
38		
39		
40		
41		
42		
43		
44		
45		
46		
47		
48		
49		
50		
51		
52		
53		
54		

APPENDIX II

FOREDUNE CONCEPTUAL MODEL AND DESIGN CHARACTERISTICS[§]

AII.1. INTRODUCCIÓN

This appendix includes a summary of the most relevant concepts of the work entitled “Relationship between foredune profile morphology and aeolian and marine dynamics: A conceptual model” published by Pellón et al. (2020). This work is a continuation of the research initiated by Laura Ribas de Almeida on foredune morphology and has been developed with her collaboration and contributions. Other publications of this author may be interesting for a detailed design of foredunes. As an example, de Almeida et al. (2019) includes a detailed analysis of the morphology of foredunes, presenting the relations between parameters such as dune height, width, volume, and slope that can be used for engineering foredune restoration projects in combination with the findings presented in this Appendix.

[§] This appendix is based on Pellón, E., de Almeida, L.R., González, M. and Medina, R., 2020. Relationship between foredune profile morphology and aeolian and marine dynamics: A conceptual model.

APPENDIX II

The development and morphology of foredunes are influenced by various factors, including beach characteristics and environmental dynamics. In the short term, foredunes experience morphological changes as erosion due to storm events or recovery during calmer periods when the beach gets wider aeolian drift provides sediment from the dry beach to the foredunes. Over longer timescales, stable conditions are achieved based on wind and marine energy, determining the steady-state location, shape, and size. Aeolian sediment input and marine processes, including wave erosion and accretion during elevated total water level events, play crucial roles in foredune development. This article explores the interplay between wind and marine dynamics and their impact on foredune morphology, providing a conceptual model supported by data correlation.

Foredunes constitute an important sediment reservoir to fight extreme wave events. When the beach is eroded and waves reach the foredune toe, part of the sediment of the dune can be eroded. Additionally, foredunes constitute the first barrier against inland flooding and are the habitat of plants and fauna due to their special environmental conditions. Therefore, it is important to preserve foredunes and contribute to their recovery after eroding episodes. In this sense, the maintenance of a wide dry beach may accelerate dune recovery through the presence of a larger area for the wind to transport the sand to the dune. As a consequence, nature assisted beach enhancement (NABE) techniques can help dune growth and long-term stability by the generation of wider dry beaches. Furthermore, beach scraping can be used as a source of sand for dune nourishment but foredune equilibrium characteristics should be taken into account while performing these engineering works.

This appendix includes the description of the methodology followed for the analysis of foredunes in section AII.2, the findings on the relation between the morphometric parameters of the foredune and the aeolian and marine dynamics in section AII.3, and the long-term conceptual model of foredune morphology in section AII.4.

AII.2. METHODOLOGY

The morphology of foredune profiles was analysed on six beaches along the northern coast of Spain: Puntal de Somo, Valdearenas, Bayas, Doniños, Baldaio, and Traba. The selected beaches are known to be well-preserved and stable. The region experiences mesotidal conditions with semi-diurnal tides and is exposed to NW swells from the North Atlantic Ocean. The most frequent and strong winds come from WSW to WNW. Morphological, wind, and marine data were gathered from specific databases.

Ten morphometric parameters of the beach and foredune were obtained for 193 profiles extracted from a digital elevation model generated by LiDAR surveys. The measurement of the morphological parameters was made considering the foredune toe as a marked increase in the slope between the dry beach and the foredune, and the foredune's crest as the higher point of the first linear ridge at the end of the dry beach (Figure AII.1). Principal component analysis was performed to reduce the dimensionality of the data and identify key morphological parameters. This analysis revealed that foredune volume, foredune toe level and foredune maximum slope are the most important morphological parameters, and the others showed a high correlation with these three or can be obtained as a function of them. Figure AII.1 shows a scheme of these morphometric parameters.

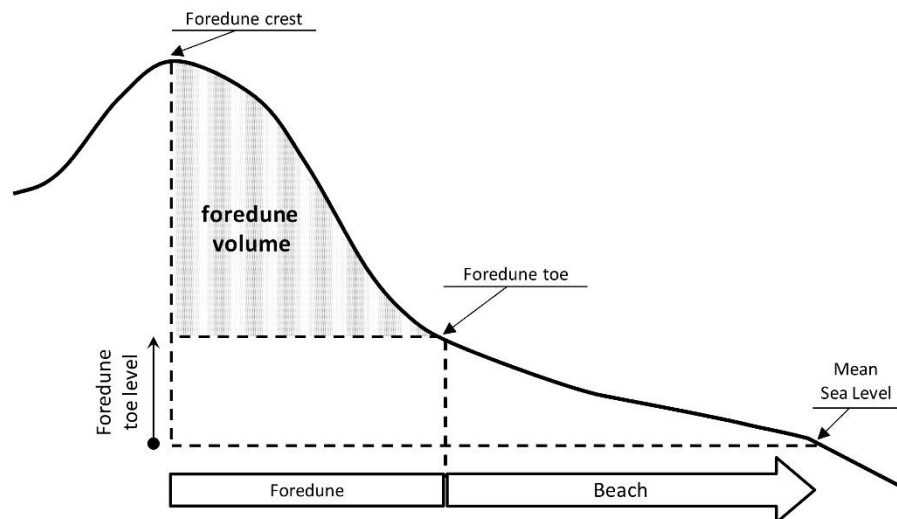


Figure AII.1 Cross-shore profile scheme of the beach and foredune morphometric parameters. Extracted from Pellón et al. (2020).

This study also considers aeolian dynamics using wind data obtained from offshore buoys. The wind data is processed to estimate aeolian drift potential depending on the angle of the shoreline ($DP\alpha$), considering only onshore winds and winds not blocked by topographic features and the sediment grain size information of each beach. Marine dynamics were processed using the Coastal Modeling System (SMC; Quetzalcóatl et al., 2019). The total water level (TWL) time series was calculated based on astronomical tides, storm surges, and wave run-up. The next section relates the morphological parameters with environmental dynamics and statistically analyses their correlation.

APPENDIX II

AII.3. RELATIONSHIP BETWEEN FOREDUNE PROFILE MORPHOLOGY AND AEOLIAN AND MARINE DYNAMICS

This section analyses the relationship between the morphometric parameters of foredunes and the local aeolian and marine dynamics. The results are structured in two sections, the analysis of the foredune location and the foredune volume. In both cases, the study was performed with mean values of morphometric characteristics and dynamics for each beach.

AII.3.1 Foredune location

Regarding the location of foredunes, it is influenced by maximum swash or surge inundation. Wave swash events can scar the foredune and limit the growth of plants, resulting in a relationship between the foredune location and the shape of the beach. The foredune toe, where the dry beach and foredune intersect, is often determined by changes in slope, vegetation, or a predefined level for the entire study area.

In this study, we sought the definition of a total water level (TWL) probability associated with the steady-state position of the foredune. The analysis of a series of return periods of TWL revealed that the foredune toe level relates with the 10-year return period of total water level (TWL_10y), as shown in Figure AII.2. This relation is very useful when rebuilding a foredune in its long-term stability position.

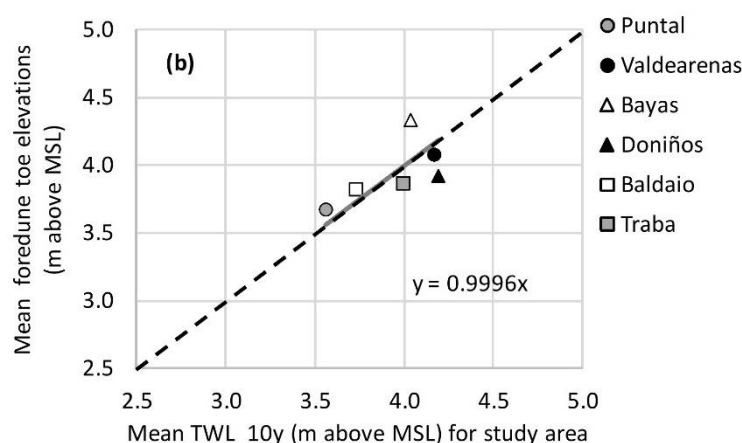


Figure AII.2 Relationship between foredune toe level and the 10-year return period of total water level (TWL_10y). Extracted from Pellón et al. (2020).

AII.3.2 Foredune volume

The volume of foredunes is primarily correlated with aeolian sediment transport. The analysis shows (Figure AII.3) a significant linear regression between aeolian drift potential ($DP\alpha$) and mean foredune volume. However, estimating short-term aeolian sediment transport can be challenging due to various factors such as moisture content, grain size, topography, and vegetation. Actual transport values measured on beaches are often lower than those predicted by transport equations in the short/medium term. Additionally, the overestimation of those equations and the presence of transport-limiting processes can lead to overestimation of dune growth in the long term. In our approach, the empirical relation of Figure AII.3 directly shows the steady-state foredune volume in the long-term, avoiding the integration over the time of overestimated short -term aeolian transport.

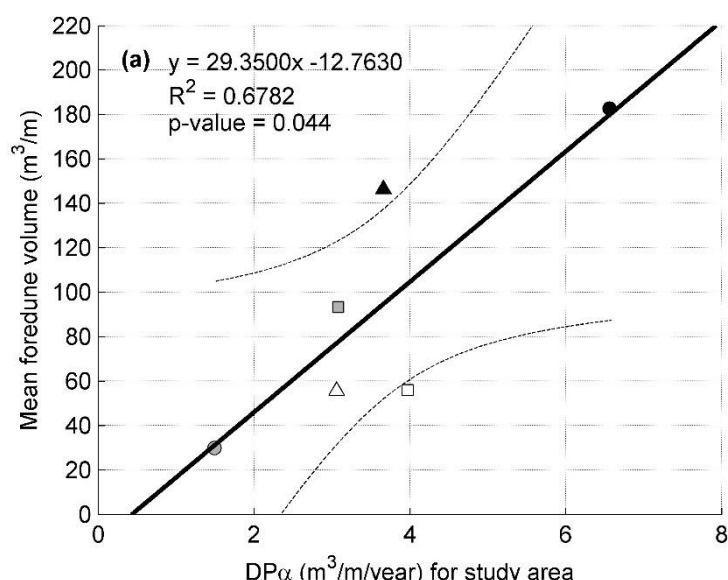


Figure AII.3 Relationship between aeolian drift potential depending on the wind angle in relation to the coastline ($DP\alpha$) and mean foredune volume for each study area.

Extracted from Pellón et al. (2020).

The width of the adjacent beach is considered essential in defining foredune size since it provides sediment for aeolian transport. The critical fetch, which determines the maximum aeolian sediment transport, plays a role in this relationship. If the beach width is shorter than the critical fetch, the amount of sediment transferred to the foredune is reduced. However, if the beach width is longer than the critical fetch, sediment transport rates equal the drift potential, and the beach width is not correlated with foredune volume or accretion. The critical fetch is a complex variable which depends on many factors like

APPENDIX II

wind speed, surface moisture, surface roughness and sediment size. Besides, the dry beach width is a highly variable magnitude that depends on marine dynamics. Therefore, determining the critical fetch and a representative value of long-term dry beach width remain challenging tasks.

Despite the seasonal variation in beach width, assuming foredunes are in their steady-state position, and the previously described relation between the 10-year return period of total water level (TWL_10y) and the position of the foredune, we can assume that the higher the TWL_10y the wider the beach. This means that more fetch will be available for foredune growth. Figure AII.4 shows a positive exponential relationship between TWL_10y and foredune volume, which suggests that higher TWL_10y values result in greater fetch and potential for foredune growth.

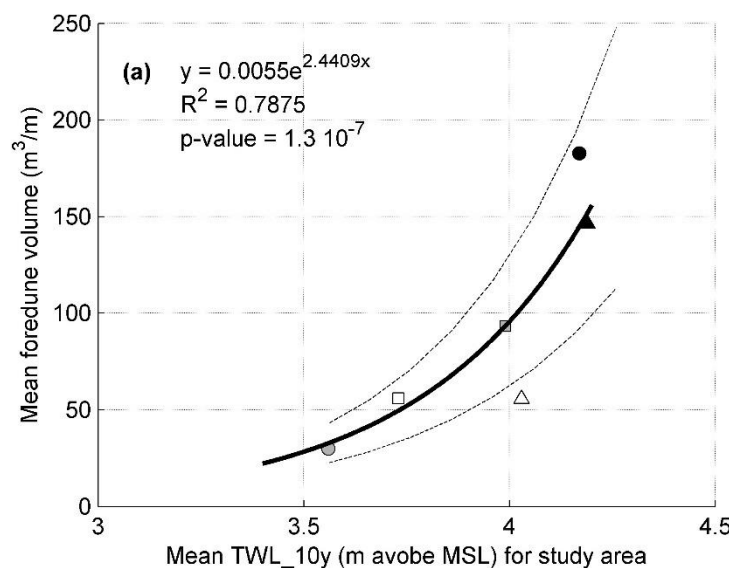


Figure AII.4 Relationship between the 10-year return period of total water level (TWL_10y) and mean foredune volume for each study area. Extracted from Pellón et al. (2020).

Based on the findings, a new conceptual model is proposed, in which foredune location is controlled by marine dynamics and, together with potential wind transport, determines the steady-state size of foredunes.

AII.4. LONG-TERM CONCEPTUAL MODEL OF FOREDUNE MORPHOLOGY

This section presents the long-term conceptual model for the morphology of the foredune. In a beach/foredune system, there is a natural oscillation between erosion and accretion in the short and medium term. During calm periods, the foredune receives sediment from the dry beach, growing and/or migrating towards the sea. During periods of increased marine energy, the foredune is eroded by waves, redistributing sediments along the profile of the dry/submerged beach. After storm-induced erosion, the recovery of the foredune first requires the beach to recover. Once sediments return from submerged areas to the dry beach, the wind is responsible for the recovery of the foredune, depositing sediments on its lee side. In the long term, in the absence of sustained erosion or deposition, the foredune reaches an equilibrium state, whose position and size depend on wind and marine dynamics.

The proposed model considers two main situations regarding the location of the foredune: (i) primarily defined by aeolian dynamics, and (ii) defined by marine dynamics.

AII.4.1. Beach/foredune systems dominated by aeolian dynamics: considering only self-regulation in terms of aeolian sediment drift

In the case of beach/foredune systems dominated by wind dynamics, the foredune grows and migrates towards the sea until reaching a self-regulating point on the beach. As it advances, on a wide beach the foredune receives a maximum supply of sediments due to wind transport (Figure AII.5 from time t_i to t_{i+1}). However, as it progresses beyond a critical point on the beach where sediment supply decreases (critical fetch), its growth and advance slow down due to self-regulation. This is because the sediment supply is no longer at its maximum potential. The size of the foredune in the equilibrium state (t_{i+n}) will be smaller than its potential size due to the limitation of wind transport.

APPENDIX II

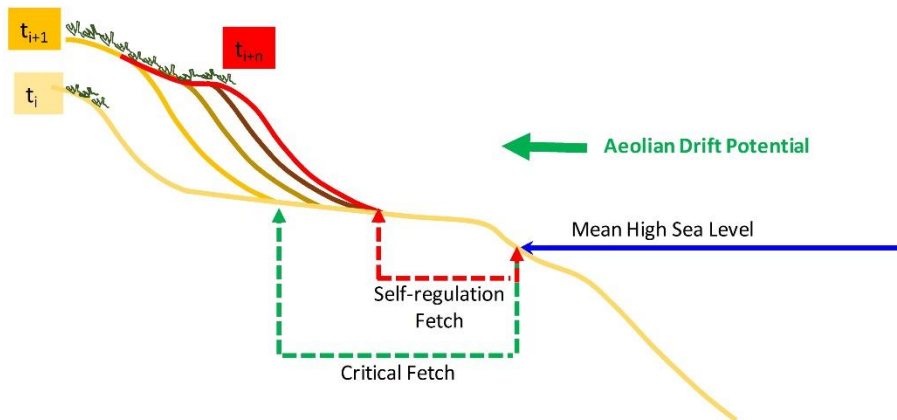


Figure AII.5 Foredune development in a system dominated by aeolian dynamics.
Extracted from Pellón et al. (2020).

AII.4.2. Beach/foredune systems dominated by marine dynamics: considering aeolian drift and marine dynamics

In the case of beach/foredune systems dominated by marine dynamics, the model adds the fact that waves periodically erode the foredunes. The positioning of the foredune in this case depends on the total water level during extreme events (astronomical tide + storm surge + wave runup). If the beach width controlled by marine dynamics is greater than the critical fetch, the foredunes will reach a fully developed state, and their size will be proportional to the aeolian drift potential (Figure AII.6). On the other hand, if marine dynamics do not produce a beach width greater than the critical fetch, the foredune will advance beyond this point, and its size in the equilibrium state will be proportional to both aeolian drift potential and a coefficient reflecting the limitation of fetch (Figure AII.7).

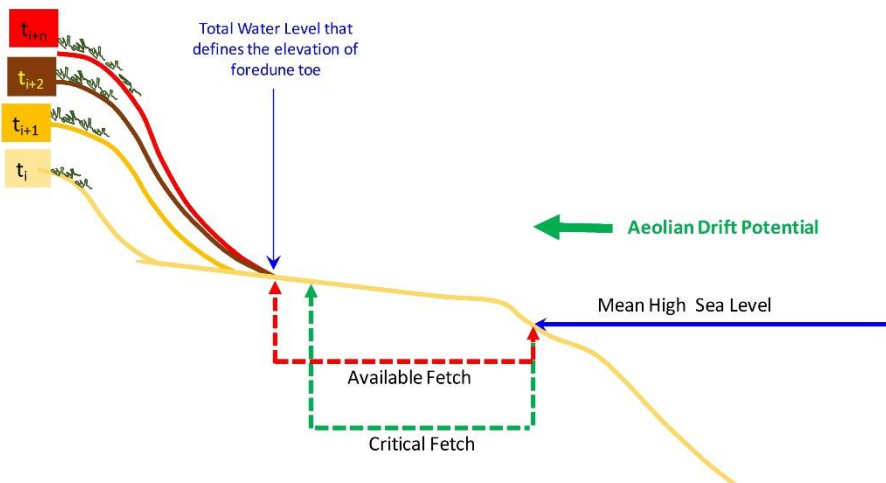


Figure AII.6 Foredune development considering both marine and aeolian dynamics.
Extracted from Pellón et al. (2020).

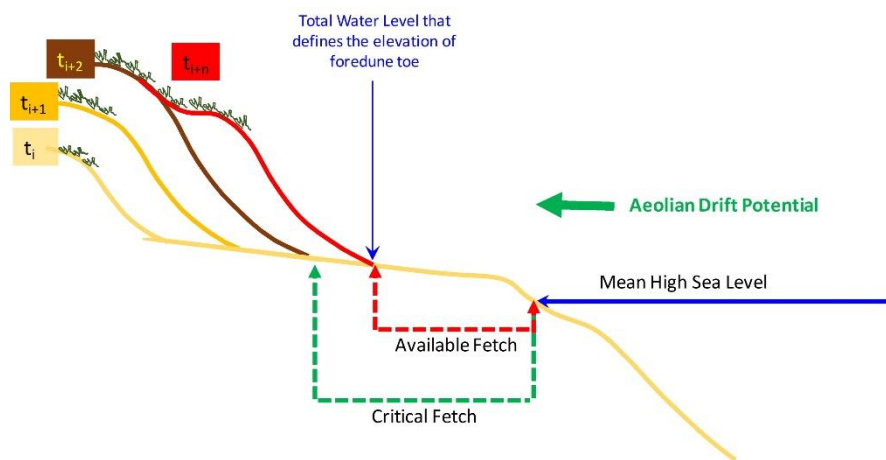


Figure AII.7 Foredune development considering both marine and aeolian dynamics,
but where the marine dynamics are not as energetic as to produce a beach width larger
than the critical fetch. Extracted from Pellón et al. (2020).

In summary, the proposed model describes how the foredune develops and reaches a long-term equilibrium state based on aeolian and marine dynamics. The size and position of the foredune depend on factors such as sediment supply by aeolian transport, beach width, and extreme wave events.